Four-body methods for high-energy ion-atom collisions

Dževad Belkić*

Karolinska Institute, P.O. Box 260, S-171 76 Stockholm, Sweden

Ivan Mančev†

Department of Physics, Faculty of Sciences and Mathematics, P. O. Box 224, 18000 Niš, Serbia

Jocelyn Hanssen‡

Institut de Physique, Université de Metz, Laboratoire de Physique Moléculaire et des Collisions, EA 3941 de l'Institut J. Barriol, FR-CNRS 2843, 1 Boulevard Arago, 57078 Metz Cedex 3, France

(Published 4 January 2008)

The progress in solving problems involving nonrelativistic fast ion (atom)-atom collisions with two actively participating electrons is reviewed. Such processes involve, e.g., (i) scattering between a bare nucleus (projectile) P of charge Z_P and a heliumlike atomic system consisting of two electrons e_1 and e_2 initially bound to the target nucleus T of charge Z_T, i.e., the Z_P-$(Z_T;e_1,e_2)_i$ collisions; (ii) scattering between two hydrogenlike atoms $(Z_P,e_1)_{i_1}$ and $(Z_T,e_2)_{i_2}$, etc. A proper description of these collisional processes requires solutions of four-body problems with four active particles including two nuclei and two electrons. Among various one- as well as two-electron transitions which can occur in such collisions, special attention will be paid to double-electron capture, simultaneous transfer and ionization, simultaneous transfer and excitation, single-electron detachment and single-electron capture. Working within the four-body framework of scattering theory and imposing the proper Coulomb boundary conditions on the entrance and exit channels, the leading quantum-mechanical theories are analyzed. Both static and dynamic interelectron correlations are thoroughly examined. The correct links between scattering states and perturbation potentials are strongly emphasized. Selection of the present illustrations is dictated by the importance of interdisciplinary applications of energetic ion-atom collisions, ranging from thermonuclear fusion to medical accelerators for hadron radiotherapy.

DOI: 10.1103/RevModPhys.80.249 PACS number(s): 03.65.Nk, 11.80.Fv, 34.70.+e, 82.30.Fi

CONTENTS

*Electronic address: Dzevad.Belkic@ki.se
†Electronic address: mancev@pmf.ni.ac.yu
‡Electronic address: jocelyn@univ-metz.fr

 ©2008 The American Physical Society

I. INTRODUCTION

Determination of the interactive dynamics of atomic systems is still among the most fundamental challenges in physics. Since the interaction potentials in atomic systems are exactly known, any discrepancy between experimental measurements and theories can be attributed to inappropriate theoretical models for describing many-particle systems or to unreliable experimental techniques. One of the central questions which arises in scattering problems involving many-electron systems concerns the influence of the electron-electron interaction on the overall dynamics in these collisional phenomena. Since the helium atom (or a heliumlike ion) is the simplest many-electron target where one can assess the importance of electronic correlations, its investigation has attracted most attention from both the theoretical and experimental sides. Collisional processes in which two nuclei and two electrons take part represent pure four-body problems (Belkić, 1997a, 1997b; Belkić and Mančev, 1992, 1993). One of the basic motivations for developing four-body theories to treat ion (atom)-atom collisions is to more thoroughly understand the role of the electron-electron correlation and phase coherences in such important processes. In atomic physics, electronic correlation effects originate from pure Coulombic interactions between active electrons. Phase coherences are interference patterns for competing mechanisms in four-body collisional transitions.

In ion-atom collisions, there are two kinds of electronic correlations: static and dynamic. Static correlations are built into multielectron bound-state wave functions without any reference to collisions. Quantum-mechanical bound states are "prepared" without the presence of an incident beam. Several methods for obtaining bound-state wave functions and the corresponding eigenenergies for two-electron atomic systems have recently been reviewed (Tanner *et al.*, 2000). The dynamic correlations describe interactions between two electrons in the exit channel, if we deal with the Z_P-$(Z_T;e_1,e_2)_i$ collisions, or in the entrance channel, if the $(Z_P,e_1)_{i_1}$-$(Z_T,e_2)_{i_2}$ process is considered. The electronic interactions alone are capable of causing a transition of the entire collisional system from an initial to a final state. Such a dynamical effect automatically possesses both radial and angular correlations through the inclusion of the interelectron Coulomb potential $1/r_{12}$ in the final interaction potential V_f appearing in the post form of the transition amplitude T_{if}^{+}, if the Z_P-$(Z_T;e_1,e_2)_i$ collisions are studied. The same potential $1/r_{12}$ appears in the initial perturbation potential V_i of the prior form of the transition amplitude T_{if}^{-}, if the $(Z_P,e_1)_{i_1}$-$(Z_T,e_2)_{i_2}$ collisions are investigated.

The majority of the theoretical studies that have considered the Z_P-$(Z_T;e_1,e_2)_i$ collisions employed the independent-particle model[1] (IPM) (Hansteen and Mosebekk, 1972; Mukherjee *et al.*, 1973; Biswas *et al.*, 1977; McGuire and Weaver, 1977; Lin, 1979; Theisen and McGuire, 1979; Gayet *et al.*, 1981, 1991; Gayet and Salin, 1987; Gayet, 1989; Olson, 1982; Olson *et al.*, 1986; Brandt, 1983; Ghosh *et al.*, 1985, 1987; Sidorovich *et al.*, 1985; McGuire, 1987, 1992; Stolterfoht, 1990, 1993; Deco and Grün, 1991; Jain *et al.*, 1991; Shingal and Lin, 1991; Martínez *et al.*, 1994, 1997; McCartney, 1997; Zerarka, 1997). The basic feature of all these previous investigations within the IPM and its variants is the preservation of a pure three-body formalism, despite the fact that the studied four-body problems include two active electrons. Within the IPM itself, there are many ways of approximating the wave function of a heliumlike atomic system. An approach in which an active electron of a two-electron atom or ion moves in an effective potential generated by the other nucleus and the passive electron has frequently been used. The term passive electrons is used here in the sense that their interactions with the active electrons do not contribute to the collisional process. Thus, in the IPM, the initial four-body problem is effectively reduced to a three-body problem. The main drawback of the IPM is that the dynamic correlation effects

[1]All acronyms used are defined at the end of the article.

during the collisional phenomenon are completely ignored from the outset.

Hence, if we are to adequately assess the role of electron-electron correlations, we must deal with a four-body problem from the beginning. Guided by this argument, various quantum-mechanical four-body methods have been proposed to study one- and two-electron transitions in scattering of completely stripped projectiles on heliumlike atomic systems or in collisions between two hydrogenlike atoms or ions. In addition to four-body theories, which are the subject of this review, the role of electronic correlations in energetic ion-atom collisions has also been investigated elsewhere (Stolterfoht, 1990, 1993; McGuire, 1992, 1997).

The first formulation and implementation of the four-body continuum distorted-wave (CDW-4B) method for double-electron capture was carried out by Belkić and Mančev (1992, 1993). The CDW-4B method obeys the asymptotic convergence criteria of Dollard (1963, 1964) for Coulomb potentials. These initial computations of Belkić and Mančev (1992, 1993) on the formation of H^- in the H^+-He collisions yielded total cross sections that were in excellent agreement with available experimental data. Subsequently, the CDW-4B method was applied to other collisional systems (Belkić, 1994; Belkić *et al.*, 1994; Gayet *et al.*, 1994a, 1996; Martínez *et al.*, 1999), including double capture into singly and doubly excited final states by multiply charged projectile ions. Further, an adequate description of simultaneous transfer and ionization has been devised using the CDW-4B method (Belkić *et al.*, 1997a, 1997b; Mančev, 1999b, 2001). Studies of transfer ionization by means of the CDW-4B method indicate that dynamic electronic correlations in perturbation potentials are more important than the static ones. The substantial improvement of the CDW-4B method over, e.g., the IPM has been attributed solely to the role of dynamic electron correlation effects.

Throughout this review, emphasis is placed on the adequate solutions of the asymptotic convergence problem (Dollard, 1964; Belkić *et al.*, 1979) by requiring not only the correct asymptotic behaviors of all the scattering wave functions, but also their proper connections with the corresponding perturbation interactions. This strategy proves to be simultaneously fundamental (consistency of theory by reference to the first principles of physics), and practical (stringent scrutiny of theory through its systematic verification against experiment). A striking example which illustrates this issue is a four-body problem with single-electron detachment from H^- by H^+. For this problem, the eikonal Coulomb-Born method has been proposed by Gayet, Janev, and Salin (1973) with the correct asymptotic behaviors of the initial and final scattering states. Yet, the ensuing total cross sections of this method overestimate the corresponding experimental data by some 2-3 orders of magnitude at all impact energies. As shown by Belkić (1997a, 1997b), the reason for this discrepancy was the lack of the proper link between the initial scattering state and the perturbation potential in the entrance channel. When this link has properly been established for the same collisional problem, the modified Coulomb-Born method emerged (Belkić, 1997a, 1997b), exhibiting excellent agreement with the experimental data at all impact energies. This latter approximation is a simplified version of the CDW method for ionization proposed by Belkić (1978), who originally derived the scattering wave for the final state as the product of three full Coulomb functions (later called the C3 function) to satisfy the correct boundary condition for three charged particles in the exit channel. This C3 scattering wave function has repeatedly been rediscovered in subsequent studies (Garibotti and Miraglia, 1980; Brauner, Briggs, and Klar, 1989). Throughout the years, and especially more recently (Gulyás and Fainstein, 1998; Ciappina *et al.*, 2003), it was conclusively established that the most successful theory for heavy-particle ion-atom ionization at high energies is the CDW method of Belkić (1978) regarding both differential and total cross sections. Of late, the CDW method has been exported to neighboring research fields, such as medical physics for a more adequate description of the stopping power of multiply charged ions passing through matter, as encountered in applications to hadron radiotherapy (Belkić, 2007).

The three-body reformulated impulse approximation (RIA-3B) of Belkić (1995, 1996), after resolving a long-standing problem on the inadequacy of the corresponding impulse approximation (IA) for the total cross sections in the H^+-H charge exchange, has been extended to four-body collisions. Cross sections of the four-body reformulated impulse approximation (RIA-4B) of Belkić for transfer ionization (TI) in the H^+-He collisions have been reported in a joint theoretical and experimental study (Mergel *et al.*, 1997). The total cross sections of the RIA-4B for the TI process have indicated a trend of the v^{-11} behavior at sufficiently large values of the impact velocity v. This asymptotic behavior, as the quantum-mechanical counterpart of the corresponding classical double scattering (Thomas, 1927), has been confirmed on the same collision by two subsequent measurements (Schmidt *et al.*, 2002; Schmidt, Jensen, *et al.*, 2005).

As a further exploration of the CDW-4B method, simultaneous transfer and excitation (TE) have also been the subject of studies (Bachau *et al.*, 1992; Gayet and Hanssen, 1992; Gayet *et al.*, 1995; 1997; Ourdane *et al.*, 1999). This process takes place when a target electron is captured by a nonbare projectile, while the initial electronic structure of the latter is excited at the same time. For the process of TE, where a doubly excited (autoionizing) state is formed on the projectile, two modes have been identified and termed the resonant (RTE) and the nonresonant transfer excitation (NTE). In the RTE, excitation of the projectile is due to the dielectronic interaction between the projectile electron and the target electron, which is captured. In the NTE, a target electron is transferred and excitation of the projectile comes from the interaction with the rest of the target. In addition to these two-electron transitions, the CDW-4B method has also been applied to single-electron capture (Belkić *et al.*, 1997; Mančev, 1999a, 2001) in a number of

processes, such as the H^+-He, H^+-Li^+, He^{2+}-He, and Li^{3+}-He collisions. In the CDW-4B method, the electronic continuum intermediate states are included in both channels through the full Coulomb waves. Using this method, we emphasize the pivotal role of the dynamic electron correlations in differential cross sections. In particular, the CDW-4B method predicts two competing double scattering mechanisms leading to a double structure with the Thomas peak of the 1st ($P-e-T$) and 2nd ($P-e-e$) kind, where the former (standard) is a purely high-energy occurrence, whereas the latter (novel) systematically persists at all impact energies (Belkić, 2001, 2004).

In the boundary-corrected four-body first Born approximation (CB1-4B), pure electronic continuum intermediate states are not taken into account. Here the scattering state vectors are given by the product of unperturbed channel states and logarithmic distortion phase factors due to the Coulomb long-range remainders of the perturbation potentials. The CB1-4B method was initially formulated and applied to double-electron capture by Belkić (1993a, 1993b). This method has subsequently been used for describing single-charge exchange in energetic collisions between two hydrogenlike atoms or ions (Mančev, 1995, 1996).

The four-body boundary-corrected continuum intermediate state (BCIS-4B) method of Belkić (1993c) and the four-body Born distorted-wave (BDW-4B) method of Belkić (1994) have been introduced and used first for investigation of double- and then single-electron capture. These two methods, with the correct boundary conditions, can be applied and extended to any number of colliding particles, so that the more generic acronyms BCIS and BDW can be used. Both methods employ the scattering wave functions from the CDW method in one of the two channels, in either the entrance or exit channel, for the initial or final state, depending on whether the prior or post form of the transition amplitudes is used. For the other channel, the BCIS and BDW methods use the corresponding wave functions of the CB1 method. As a result, the distorting potentials that cause the transitions from the initial to final states of the system are different in the BCIS and BDW methods. These latter potentials are the usual electrostatic Coulomb interactions in the BCIS method (shared by the CB1 method), whereas they are the operator-type potentials $\vec{\nabla}\cdot\vec{\nabla}$ in the BDW method (shared by the CDW method). Thus, if one wishes to make these remarks more transparent, the original acronym BDW introduced by Belkić (1994), and subsequently used by Mančev (2003) and Mančev *et al.* (2003), could be relabeled as CDW-CB1. In particular, the notations for the post and prior BDW or, equivalently, CDW-CB1 can further be differentiated by highlighting the use of the boundary-corrected first-order Born initial and final states (BIS and BFS). This has led to yet another equivalent set of acronyms, CDW-BIS and CDW-BFS (Mančev, 2005a, 2005b) for the post and prior versions of the BDW method of Belkić (1994). Using the BCIS and BDW methods, Belkić (1993c, 1994) has shown that double-charge exchange is sensitive to the inclusion of long-range Coulomb effects through electronic continuum states. These latter states play an important role even at those incident energies at which the Thomas double scattering is not apparent. By means of the mentioned hybrid four-body approximations, one can study various mechanisms that can produce the Thomas peaks in the differential cross sections. Even for single-charge exchange with heliumlike targets, these methods deal explicitly with two active electrons from the onset and, therefore, they preserve the four-body nature of the original problem. The post and prior BDW methods (or, equivalently, the CDW-BIS and CDW-BFS methods, respectively) have been employed to compute both differential and total cross sections for single-electron capture in collisions between bare projectiles and heliumlike atoms or ions (Mančev, 2003, 2005a, 2005b; Mančev *et al.*, 2003).

Additionally, there are other hybrid-type approximations with the correct boundary conditions known as the continuum distorted wave eikonal initial state (CDW-EIS) and the continuum distorted wave eikonal final state (CDW-EFS) methods (Crothers and McCann, 1983; Busnengo *et al.*, 1995, 1996; Galassi *et al.*, 2002). The CDW-EIS method was originally introduced by Crothers and McCann (1983) for ionization of hydrogenlike atomic systems by nuclei treated as a pure three-body problem. In the work of Busnengo *et al.* (1996), the CDW-EIS and CDW-EFS methods for single-electron capture from a two-electron target are reduced to a one-electron process. Here, the active captured electron was described by a self-consistent field orbital. The other noncaptured electron is passive, since it is considered as frozen in its initial state during the collision. Therefore, such versions of the CDW-EIS and CDW-EFS methods (Busnengo *et al.*, 1995, 1996; Galassi *et al.*, 2002) belong to the category of three-body approximations. As to pure four-body collisions with two active electrons, the four-body continuum distorted wave eikonal initial state (CDW-EIS-4B) method has also been introduced and applied to double capture from helium by alpha particles (Martínez *et al.*, 1999), but without any success. The CDW-EIS and CDW-EFS methods differ from the CDW-BIS and the CDW-BFS methods, since EIS and EFS are different from BIS and BFS, respectively. Specifically, the difference is in the independent variables in the eikonal phase factors for the two sets of the invoked asymptotic states {EIS, EFS} and {BIS, BFS}.

The dominant feature of most of the quoted quantum-mechanical four-body approximations is that they show systematic agreement with the corresponding experimental data at intermediate and high impact energies. This is striking in view of the fact that the impact parameter versions of the investigated approximations often fail (and do so dramatically in some cases) in their attempts to reproduce experimental data. The first indication on the breakdown of the IPM for double-electron capture has been given by Belkić and Mančev (1992). The clear implication of this is that dynamic correlation effects are of critical importance for two-electron transi-

tions. One of the tasks of the present review is to highlight this latter feature and to assess its overall significance for energetic ion-atom collisions with two actively participating electrons. The major goal of this review is to critically evaluate the efficiency and overall utility of the leading methods within the realm of four-body quantum-mechanical scattering theory. For validation purposes, we shall formulate the necessary theoretical criteria that adequate four-body methods are expected to satisfy. Intermediate and high nonrelativistic energies permit a consistent extension of rigorous pure three-body distorted-wave methods to their pure four-body counterparts without any significant additional approximation. This represents an excellent opportunity to estimate the relevance of the well-known asymptotic convergence problem from formal scattering theory for Coulomb potentials when more than three particles are actively involved. Such an opportunity will presently be seized by building on the past successful experience with the similar challenges encountered in simpler three-body ion-atom rearrangement collisions for which Belkić *et al.* (1979) have conclusively established the critical importance of the correct Coulomb boundary conditions in the most general case with the exact eikonal transition amplitude. Subsequent detailed numerical computations, with dramatic improvements relative to experimental data, expecially for the boundary corrected three-body first-order approximation of this exact eikonal T matrix (Belkić *et al.*, 1986; Belkić, Taylor, and Saini, 1986; Belkić *et al.*, 1987; Belkić and Taylor, 1987; Dewangan and Eichler, 1986), confirmed the validity of this theoretical concept, which was then widely accepted and reviewed in several articles and books on the subject (Bransden and Dewangan, 1988; Bransden and McDowell, 1992; Crothers and Dubé, 1993; Dewangan and Eichler, 1994; Bransden and Joachain, 2003; Belkić, 2001, 2004, 2007).

Atomic units will be used throughout unless otherwise stated.

II. GENERAL THEORY

A. Notation and basic formulas

In the present review we are interested in ion-atom collisions in which two electrons take part. Such processes involve (i) scattering between a bare nucleus (projectile) P of charge Z_P and a heliumlike atomic system consisting of two electrons e_1 and e_2 initially bound to the target nucleus T of charge Z_T, i.e., the Z_P-$(Z_T;e_1,e_2)_i$ collisions, where the parentheses indicate the bound states; (ii) scattering between two hydrogenlike atoms $(Z_P,e_1)_{i_1}$ and $(Z_T,e_2)_{i_2}$, etc. We adopt the quantum-mechanical nonrelativistic spin-independent formalism, which permits consideration of the two electrons as being distinguishable from each other.

Among various processes that can occur in such collisions, special attention will be paid to the following rearrangement collisions

$$Z_P + (Z_T;e_1,e_2)_i \rightarrow \begin{cases} (Z_P;e_1,e_2)_f + Z_T & \text{(double-electron capture)}, \\ (Z_P,e_1)_f + Z_T + e_2 & \text{(transfer ionization)}, \\ (Z_P,e_1)_{f_1} + (Z_T,e_2)_{f_2} & \text{(single-electron capture)}, \\ Z_P + (Z_T,e_2)_f + e_1 & \text{(single-electron ionization/detachment)}, \end{cases}$$

$$(Z_P,e_1)_{i_1} + (Z_T,e_2)_{i_2} \rightarrow \begin{cases} (Z_P;e_1,e_2)_f + Z_T & \text{(single-electron capture)}, \\ (Z_P;e_1,e_2)_f^{**} + Z_T & \text{(transfer excitation)}, \end{cases}$$

where indices i, f, i_1, i_2, f_1, and f_2 represent the collective labels for the set of quantum numbers needed to describe the initial and final bound states, while the double asterisk denotes the doubly excited state.

Let the position vectors of the projectile nucleus, the target nucleus, and electrons $e_{1,2}$ relative to an arbitrary coordinate frame be, respectively, denoted by $\vec{r}_1$, $\vec{r}_2$, $\vec{r}_3$, and $\vec{r}_4$. Then the kinetic energy operator is given by

$$H_0 = -\frac{1}{2M_P}\nabla_{r_1}^2 - \frac{1}{2M_T}\nabla_{r_2}^2 - \frac{1}{2}\nabla_{r_3}^2 - \frac{1}{2}\nabla_{r_4}^2, \quad (1)$$

where M_P and M_T are the masses of the projectile and target, respectively. The position vectors of electrons $e_{1,2}$ relative to Z_P and Z_T are denoted by $\vec{s}_{1,2}$ and $\vec{x}_{1,2}$, respectively. We denote by $\vec{R}$ the position vector of the projectile Z_P relative to Z_T and by r_{12} the interelectron distance.

1. The entrance channel

a. Z_P-$(Z_T;e_1,e_2)_i$ collisions

We first concentrate on the collisions of completely stripped projectiles with heliumlike targets, i.e., the Z_P-$(Z_T;e_1,e_2)_i$ collisions. Introducing $\vec{r}_i$ as a relative vector of Z_P with respect to the center of mass of $(Z_T;e_1,e_2)_i$ we have $\vec{r}_i = \vec{r}_1 - (\vec{r}_3 + \vec{r}_4 + M_T\vec{r}_2)/(M_T+2)$. It is

convenient to express the Hamiltonian H_0 alternatively via a set of independent variables $\{\vec{x}_1,\vec{x}_2,\vec{r}_i\}$

$$H_0 = -\frac{1}{2\mu_i}\nabla^2_{r_i} - \frac{1}{2b}\nabla^2_{x_1} - \frac{1}{2b}\nabla^2_{x_2} - \frac{1}{M_T}\vec{\nabla}_{x_1}\cdot\vec{\nabla}_{x_2}, \tag{2}$$

where $\mu_i = M_P(M_T+2)/(M_P+M_T+2)$ and $b = M_T/(M_T+1)$. The last term in Eq. (2) is the so-called mass polarization term, which can be neglected for heavy particles because $M_T \gg 1$.

The full Hamiltonian of the system under study, in the center-of-mass frame for the whole system, is given by

$$H = H_0 + V, \tag{3}$$

where V represents the total interaction potential operator

$$V = \frac{Z_P Z_T}{R} - \frac{Z_P}{s_1} - \frac{Z_P}{s_2} - \frac{Z_T}{x_1} - \frac{Z_T}{x_2} + \frac{1}{r_{12}}. \tag{4}$$

As usual for rearranging collisions, the complete Hamiltonian from Eq. (3) can further be split into the following form

$$H = H_i + V_i. \tag{5}$$

Here H_i and V_i are the Hamiltonian and the perturbation potential in the entrance channel

$$H_i = H_0 - \frac{Z_T}{x_1} - \frac{Z_T}{x_2} + \frac{1}{r_{12}},$$

$$V_i = \frac{Z_P Z_T}{R} - \frac{Z_P}{s_1} - \frac{Z_P}{s_2}. \tag{6}$$

The unperturbed channel state Φ_i is defined by

$$(H_i - E_i)\Phi_i = 0, \quad \Phi_i = \varphi_i(\vec{x}_1,\vec{x}_2)e^{i\vec{k}_i\cdot\vec{r}_i}. \tag{7}$$

The function $\varphi_i(\vec{x}_1,\vec{x}_2)$ represents the two-electron bound-state wave function of the atomic system $(Z_T;e_1,e_2)_i$, whereas $\vec{k}_i$ is the initial wave vector. This latter wave function satisfies the following eigenproblem

$$(h_i - \epsilon_i)\varphi_i(\vec{x}_1,\vec{x}_2) = 0,$$

$$h_i = -\frac{1}{2b}\nabla^2_{x_1} - \frac{1}{2b}\nabla^2_{x_2} - \frac{Z_T}{x_1} - \frac{Z_T}{x_2} + \frac{1}{r_{12}}, \tag{8}$$

where h_i is the electronic Hamiltonian and ϵ_i is the electronic binding energy. The total energy of the four-body system is given by $E = E_i = k_i^2/(2\mu_i) + \epsilon_i$ and it is conserved during the scattering event.

The wave functions of two-electron atomic systems have been the subject of extensive studies (Bethe and Salpeter, 1977; Tanner *et al.*, 2000). In the case of helium, the variational estimate $\epsilon_i = -2.903\,724\,377\,034\,105$ (Drake, 1988) via a fully correlated Hylleraas wave function, with an explicit allowance for the interelectron coordinate r_{12} (through some 600 expansion terms), could be treated as practically the exact value.

The initial state Φ_i is distorted even at infinity, due to the presence of the asymptotic Coulomb repulsive potential $V_i^\infty = Z_P(Z_T-2)/R$ between the projectile and screened target nucleus. Notice that V_i^∞ is the asymptotic value of the perturbation V_i

$$V_i = \frac{Z_P Z_T}{R} - \frac{Z_P}{s_1} - \frac{Z_P}{s_2} \to \frac{Z_P(Z_T-2)}{R} = V_i^\infty \quad (r_i \to \infty). \tag{9}$$

Bearing in mind the long-range nature of the Coulomb interaction, the Hamiltonian H can be decomposed according to

$$H = H_i^c + V_i^c, \tag{10}$$

$$H_i^c = -\frac{1}{2\mu_i}\nabla^2_{r_i} + \frac{Z_P(Z_T-2)}{r_i} - \frac{1}{2b}\nabla^2_{x_1} - \frac{1}{2b}\nabla^2_{x_2} - \frac{Z_T}{x_1} - \frac{Z_T}{x_2} + \frac{1}{r_{12}}, \tag{11}$$

$$V_i^c = \frac{Z_P Z_T}{R} - \frac{Z_P(Z_T-2)}{r_i} - \frac{Z_P}{s_1} - \frac{Z_P}{s_2}. \tag{12}$$

The potential V_i^c exhibits short-range behavior when $R \to \infty$. The difference $1/R - 1/r_i$ is by a factor δ smaller than $[\vec{R}\cdot(\vec{x}_1+\vec{x}_2)]/R^3$, where $\delta = 1/(M_T+2)$, as can be checked using the Taylor series expansion. Thus, neglecting the terms of the order of $1/M_T$, we have that $r_i \simeq R$, so that V_i^c can be approximated as

$$V_i^c = \frac{2Z_P}{R} - \frac{Z_P}{s_1} - \frac{Z_P}{s_2}. \tag{13}$$

Obviously, V_i^c tends to $\mathcal{O}(1/R^2)$ as $R \to \infty$. It should be emphasized that the perturbation V_i^c depends only on the interaction between electrons and the projectile. The term $2Z_P/R$ in Eq. (13), despite its form, is not related to the internuclear potential, but originates solely from the electron-projectile interaction. The asymptotic tail of the potential $-Z_P/s_1$ is $-Z_P/R$, since $s_1 \to R$ as $R \to \infty$. This can be seen by utilizing a Taylor expansion for Z_P/s_1 around R. The small value of the x_1 coordinate in the entrance channel justifies this development. The same statement also holds true for the potential $-Z_P/s_2$. It is important to note that, unlike the channel perturbation V_i^c, the corresponding perturbation V_i from Eq. (6) contains the internuclear interaction $Z_P Z_T/R$. With the Hamiltonian H_i^c from Eq. (11), the eigenproblem in the entrance channel reads as $(H_i^c - E_i)\Phi_i^c = 0$. This is the counterpart of Eq. (7) when there is a remaining Coulomb potential in the asymptotic region. The solution of the eigenproblem for Φ_i^c is given by

$$\Phi_i^c = \varphi_i(\vec{x}_1,\vec{x}_2)e^{i\vec{k}_i\cdot\vec{r}_i}\mathcal{N}^+(\nu_i)\,{}_1F_1(-i\nu_i,1,ik_i r_i - i\vec{k}_i\cdot\vec{r}_i), \tag{14}$$

where $\mathcal{N}^+(\nu_i) = e^{-\pi\nu_i/2}\Gamma(1+i\nu_i)$ and $\nu_i = Z_P(Z_T-2)/v$. The symbol ${}_1F_1(a,b,z)$ stands for the confluent hypergeometric function. The channel wave function Φ_i^c has the asymptotic form

$$\Phi_i^c(r_i \to \infty) \equiv \Phi_i^+ = \varphi_i(\vec{x}_1,\vec{x}_2)e^{i\vec{k}_i\cdot\vec{r}_i+i\nu_i \ln(k_i r_i-\vec{k}_i\cdot\vec{r}_i)}. \quad (15)$$

Thus the function (14) satisfies the correct Coulomb boundary condition in the entrance channel.

We recall that the wave functions in the attractive Coulomb field $U=-\beta/r$ have the following forms (Landau and Lifshitz, 1977)

$$\Psi_k^{\pm} = N^{\pm}(\nu)e^{i\vec{k}\cdot\vec{r}}\,{}_1F_1(\pm i\nu,1,\pm ikr - i\vec{k}\cdot\vec{r}),$$

with $N^{\pm}(\nu)=e^{\pi\nu/2}\Gamma(1\mp i\nu)$ and $\nu=\mu\beta/k$, where μ is a reduced mass. At $r\to\infty$, this function behaves like

$$\Psi_k^{\pm} \simeq e^{i\vec{k}\cdot\vec{r}\mp i\nu \ln(kr\mp\vec{k}\cdot\vec{r})} + \mathcal{O}(1/r).$$

In the case of a repulsive field $U=\beta/r$, the incoming and outgoing waves are

$$\Psi_k^{\pm} = \mathcal{N}^{\pm}(\nu)e^{i\vec{k}\cdot\vec{r}}\,{}_1F_1(\mp i\nu,1,\pm ikr - i\vec{k}\cdot\vec{r}),$$

where $\mathcal{N}^{\pm}(\nu)=e^{-\pi\nu/2}\Gamma(1\pm i\nu)$ such that the appropriate asymptotic forms read as

$$\Psi_k^{\pm} \simeq e^{i\vec{k}\cdot\vec{r}\pm i\nu \ln(kr\mp\vec{k}\cdot\vec{r})} + \mathcal{O}(1/r). \quad (16)$$

Above, the same symbol $\mathcal{O}(1/r)$ for the remainders of the asymptotes for $\Psi_k^{\pm}$ has two different explicit forms for an attractive $(-\beta/r)$ and repulsive (β/r) potential. The Coulomb wave functions $\Psi_k^{\pm}$ are normalized to a δ function, as in the corresponding plane waves

$$\langle\Psi_{k'}^{\pm}|\Psi_k^{\pm}\rangle = (2\pi)^3\delta(k'-k).$$

The normalization constant is chosen so that the corresponding wave function has unit amplitude.

b. $(Z_P,e_1)_{i_1}$-$(Z_T,e_2)_{i_2}$ collisions

The additive form of the Hamiltonian for this collision in the entrance channel is defined by Eq. (10) with

$$V_i^c = \frac{Z_P Z_T}{R} - \frac{Z_P}{s_2} - \frac{Z_T}{x_1} + \frac{1}{r_{12}} - \frac{(Z_P-1)(Z_T-1)}{r_i} \quad (17)$$

$$\simeq \frac{Z_T+Z_P-1}{R} - \frac{Z_P}{s_2} - \frac{Z_T}{x_1} + \frac{1}{r_{12}}, \quad (18)$$

$$H_i^c = H_0 - \frac{Z_P}{s_1} - \frac{Z_T}{x_2} + \frac{(Z_P-1)(Z_T-1)}{r_i}, \quad (19)$$

$$H_0 = -\frac{1}{2\mu_i}\nabla_{r_i}^2 - \frac{1}{2a}\nabla_{s_1}^2 - \frac{1}{2b}\nabla_{x_2}^2, \quad (20)$$

where $\mu_i=(M_P+1)(M_T+1)/(M_P+M_T+2)$, $a=M_P/(M_P+1)$, and $b=M_T/(M_T+1)$. Here $\vec{r}_i$ is the position vector between the centers of mass of the (Z_T,e_2) and (Z_P,e_1) systems. The set $\{\vec{r}_i,\vec{s}_1,\vec{x}_2\}$ represents the independent coordinates. The asymptotic channel state Φ_i^+ is defined by

$$(H_i^c - E)\Phi_i^+ = 0, \quad \Phi_i^+ = \varphi_P(\vec{s}_1)\varphi_T(\vec{x}_2)e^{i\vec{k}_i\cdot\vec{r}_i+i\nu_i \ln(k_i r_i-\vec{k}_i\cdot\vec{r}_i)}, \quad (21)$$

where $\nu_i=(Z_T-1)(Z_P-1)/v$. The functions $\varphi_P(\vec{s}_1)$ and $\varphi_T(\vec{x}_2)$ are single-electron hydrogenlike states in the entrance channel.

2. The exit channels

a. Double-electron capture

In analogy to the vector $\vec{r}_i$ introduced earlier, we can also consider $\vec{r}_f$ as the position vector of T with respect to the center of mass of the system $(Z_P;e_1,e_2)_f$ via $\vec{r}_f=\vec{r}_2-(\vec{r}_3+\vec{r}_4+M_P\vec{r}_1)/(M_P+2)$. With this, the Hamiltonian H_0 can be written in terms of the independent variables $\{\vec{s}_1,\vec{s}_2,\vec{r}_f\}$ as

$$H_0 = -\frac{1}{2\mu_f}\nabla_{r_f}^2 - \frac{1}{2a}\nabla_{s_1}^2 - \frac{1}{2a}\nabla_{s_2}^2 - \frac{1}{M_P}\vec{\nabla}_{s_1}\cdot\vec{\nabla}_{s_2}, \quad (22)$$

where $\mu_f=M_T(M_P+2)/(M_P+M_T+2)$. The mass polarization term $(1/M_P)\vec{\nabla}_{s_1}\cdot\vec{\nabla}_{s_2}$ can be omitted in accordance with the mass limit $M_P\gg 1$ for heavy particles. It is convenient to express the total Hamiltonian in a separable form, $H=H_f+V_f$, where the channel Hamiltonian H_f and corresponding perturbation V_f are defined via

$$H_f = H_0 - \frac{Z_P}{s_1} - \frac{Z_P}{s_2} + \frac{1}{r_{12}},$$

$$V_f = \frac{Z_P Z_T}{R} - \frac{Z_T}{x_1} - \frac{Z_T}{x_2}. \quad (23)$$

We introduce the unperturbed state Φ_f in the exit channel for double-charge exchange as the solution of the eigenproblem $(H_f-E_f)\Phi_f=0$ which yields

$$\Phi_f = \varphi_f(\vec{s}_1,\vec{s}_2)e^{-i\vec{k}_f\vec{r}_f}, \quad (24)$$

where $\varphi_f(\vec{s}_1,\vec{s}_2)$ is the bound state of the heliumlike atom or ion $(Z_P;e_1,e_2)_f$. This function satisfies the eigenproblem $(h_f-\epsilon_f)\varphi_f(\vec{s}_1,\vec{s}_2)=0$ or, explicitly,

$$\left(-\frac{1}{2a}\nabla_{s_1}^2 - \frac{1}{2a}\nabla_{s_2}^2 - \frac{Z_P}{s_1} - \frac{Z_P}{s_2} + \frac{1}{r_{12}} - \epsilon_f\right)\varphi_f(\vec{s}_1,\vec{s}_2) = 0, \quad (25)$$

where ϵ_f is the binding energy of the final state. Conservation of energy for the entire four-body system requires $E_f=k_f^2/(2\mu_f)+\epsilon_f=E_i=E$, where $\vec{k}_f$ is the final wave vector.

The final state is distorted even at asymptotically large separations due to the presence of an overall repulsive long-range Coulomb interaction between the target nucleus and the screened projectile $V_f^{\infty}=Z_T(Z_P-2)/R$. This suggests that the Hamiltonian should be written in the following additive form

$$H = H_f^c + V_f^c, \quad (26)$$

$$H_f^c = -\frac{1}{2\mu_f}\nabla_{r_f}^2 + \frac{Z_T(Z_P-2)}{r_f} - \frac{1}{2a}\nabla_{s_1}^2 - \frac{1}{2a}\nabla_{s_2}^2 - \frac{Z_P}{s_1} - \frac{Z_P}{s_2} + \frac{1}{r_{12}}, \tag{27}$$

$$V_f^c = \frac{Z_P Z_T}{R} - \frac{Z_T(Z_P-2)}{r_f} - \frac{Z_T}{x_1} - \frac{Z_T}{x_2}. \tag{28}$$

Neglecting the terms of the order of $1/M_P$, we have $\vec{r}_f \simeq -\vec{R}$ or $r_f \simeq R$, so that V_f^c is reduced to

$$V_f^c = \frac{2Z_T}{R} - \frac{Z_T}{x_1} - \frac{Z_T}{x_2}. \tag{29}$$

The potential V_f^c is of a short range, since it tends to $\mathcal{O}(1/R^2)$ when $R\to\infty$. We recall that

$$V_f = \frac{Z_P Z_T}{R} - \frac{Z_T}{x_1} - \frac{Z_T}{x_2} \to \frac{Z_T(Z_P-2)}{R} = V_f^\infty \quad (r_f\to\infty). \tag{30}$$

The solution of the eigenproblem $H_f^c\Phi_f^c = E_f\Phi_f^c$ is

$$\Phi_f^c = \varphi_f(\vec{s}_1,\vec{s}_2)e^{-i\vec{k}_f\vec{r}_f}\mathcal{N}^-(\nu_f)\ {}_1F_1(i\nu_f,1,-ik_fr_f + i\vec{k}_f\cdot\vec{r}_f), \tag{31}$$

where $\mathcal{N}^-(\nu_f) = e^{-\pi\nu_f/2}\Gamma(1-i\nu_f)$ and $\nu_f = Z_T(Z_P-2)/v$. The asymptotic form of Φ_f^c as $r_f\to\infty$ reads as

$$\Phi_f^c(r_f\to\infty) \equiv \Phi_f^- = \varphi_f(\vec{s}_1,\vec{s}_2)e^{-i\vec{k}_f\vec{r}_f - i\nu_f\ln(k_fr_f - \vec{k}_f\vec{r}_f)}. \tag{32}$$

Thus the function (31) obeys the correct boundary condition in the exit channel.

For heavy particle collisions, we have $k_i^2/2\mu_i \gg |\epsilon_f - \epsilon_i|$. In this case, scattering takes place mainly in the forward direction, so that we can write $\hat{\vec{v}}_i \simeq \hat{\vec{v}}_f \equiv \hat{\vec{v}}$, where $\vec{v}_i = \vec{k}_i/\mu_i$, $\vec{v}_f = \vec{k}_f/\mu_f$, and $\hat{\vec{v}}_{i,f} = \vec{v}_{i,f}/v_{i,f}$. It is readily verified for double-electron capture that the following expressions are valid

$$\vec{k}_i\cdot\vec{r}_i + \vec{k}_f\cdot\vec{r}_f = \vec{q}_P\cdot(\vec{s}_1+\vec{s}_2) + \vec{q}_T\cdot(\vec{x}_1+\vec{x}_2) \tag{33}$$

$$= -2\vec{q}_P\cdot\vec{R} - \vec{v}\cdot(\vec{x}_1+\vec{x}_2)$$

$$= 2\vec{q}_T\cdot\vec{R} - \vec{v}\cdot(\vec{s}_1+\vec{s}_2), \tag{34}$$

$$2\vec{q}_P = +\vec{\eta} - v^+\hat{\vec{v}}, \quad 2\vec{q}_T = -\vec{\eta} - v^-\hat{\vec{v}}, \tag{35}$$

$$v^+ = v + \frac{\epsilon_f-\epsilon_i}{v}, \quad v^- = v - \frac{\epsilon_f-\epsilon_i}{v},$$

$$\vec{q}_P + \vec{q}_T = -\vec{v}. \tag{36}$$

The vector of the incident velocity is chosen along the Z axis, i.e., $\hat{\vec{v}} = (0,0,1)$, whereas the vector $\vec{\eta}$ is the transverse momentum transfer, $\vec{\eta} = (\eta\cos\phi_\eta, \eta\sin\phi_\eta, 0)$, so that $\vec{\eta}\cdot\vec{v} = 0$.

b. Single-electron capture

Keeping the same notation as in the case of double-electron capture, we list the quantities that need to be redefined for single-electron capture. Now, in the exit channel we have two hydrogenlike atomic systems, so it is convenient to introduce the vector $\vec{r}_f$ as the position vector between the centers of mass of the $(Z_P,e_1)_{f_1}$ and $(Z_T,e_2)_{f_2}$ systems. The set of the independent Jacobian coordinates $\{\vec{r}_f,\vec{s}_1,\vec{x}_2\}$ can be used; namely, the kinetic energy operator in terms of these coordinates is given by

$$H_0 = -\frac{1}{2\mu_f}\nabla_{r_f}^2 - \frac{1}{2a}\nabla_{s_1}^2 - \frac{1}{2b}\nabla_{x_2}^2, \tag{37}$$

where $\mu_f = (M_T+1)(M_P+1)/(M_P+M_T+2)$. It should be noted that the mass polarization term does not appear when coordinates $\{\vec{r}_f,\vec{s}_1,\vec{x}_2\}$ are employed.

The channel Hamiltonian H_f and perturbation V_f are, respectively, defined by

$$H_f = H_0 - \frac{Z_P}{s_1} - \frac{Z_T}{x_2},$$

$$V_f = \frac{Z_P Z_T}{R} - \frac{Z_T}{x_1} - \frac{Z_P}{s_2} + \frac{1}{r_{12}}. \tag{38}$$

Solving the eigenvalue equation $(H_f - E_f)\Phi_f = 0$, we obtain the unperturbed state Φ_f in the exit channel as

$$\Phi_f = \varphi_P(\vec{s}_1)\varphi_T(\vec{x}_2)e^{-i\vec{k}_f\vec{r}_f}, \tag{39}$$

where $\varphi_P(\vec{s}_1)$ and $\varphi_T(\vec{x}_2)$ are the electron hydrogenlike wave function of the atomic systems $(Z_P,e_1)_{f_1}$ and $(Z_T,e_2)_{f_2}$, respectively. The total energy is given by $E_f = k_f^2/(2\mu_f) + \epsilon_f$, where $\epsilon_f = \epsilon_{f_1} + \epsilon_{f_2}$ with $\epsilon_{f_1} = -Z_P^2/(2n_{f_1}^2)$ and $\epsilon_{f_2} = -Z_T^2/(2n_{f_2}^2)$. The distortion of the unperturbed state Φ_f in the case of single charge exchange is caused by the potential $V_f^\infty = (Z_T-1)(Z_P-1)/R$, which represents the asymptotic form of the perturbation V_f. In this case, the constituent two terms of the separable Hamiltonian $H = H_f^c + V_f^c$ are defined as

$$H_f^c = -\frac{1}{2\mu_f}\nabla_{r_f}^2 + \frac{(Z_T-1)(Z_P-1)}{r_f} - \frac{1}{2a}\nabla_{s_1}^2 - \frac{1}{2b}\nabla_{x_2}^2 - \frac{Z_P}{s_1} - \frac{Z_T}{x_2}, \tag{40}$$

$$V_f^c = \frac{Z_P Z_T}{R} - \frac{(Z_T-1)(Z_P-1)}{r_f} - \frac{Z_P}{s_2} - \frac{Z_T}{x_1} + \frac{1}{r_{12}}. \tag{41}$$

Using $r_f \simeq R$, we obtain the following approximate expression

$$V_f^c \simeq Z_P\left(\frac{1}{R} - \frac{1}{s_2}\right) + (Z_T-1)\left(\frac{1}{R} - \frac{1}{x_1}\right) + \left(\frac{1}{r_{12}} - \frac{1}{x_1}\right). \tag{42}$$

With this, the solution of the eigenvalue equation $H_f^c\Phi_f^c = E_f\Phi_f^c$ is given by

$$\Phi_f^c = \varphi_P(\vec{s}_1)\varphi_T(\vec{x}_2)e^{-i\vec{k}_f\vec{r}_f}\mathcal{N}^-(\nu_f) \times {}_1F_1(i\nu_f,1,-ik_fr_f+i\vec{k}_f\cdot\vec{r}_f), \quad (43)$$

where $\mathcal{N}^-(\nu_f)=e^{-\pi\nu_f/2}\Gamma(1-i\nu_f)$ and $\nu_f=(Z_T-1)(Z_P-1)/v$. The asymptotic form of Φ_f^c as $r_f\to\infty$ is correct since

$$\Phi_f^c(r_f\to\infty)\equiv\Phi_f^- = \varphi_P(\vec{s}_1)\varphi_T(\vec{x}_2)e^{-i\vec{k}_f\vec{r}_f-i\nu_f\ln(k_fr_f-\vec{k}_f\vec{r}_f)}. \quad (44)$$

Employing a similar procedure as in the case of double-electron capture, it can be shown that for heavy scattering aggregates the following relations are valid

$$\vec{k}_i\cdot\vec{r}_i+\vec{k}_f\cdot\vec{r}_f=\vec{\alpha}\cdot\vec{s}_1+\vec{\beta}\cdot\vec{x}_1=-\vec{\alpha}\cdot\vec{R}-\vec{v}\cdot\vec{x}_1, \quad (45)$$

$$\vec{\alpha}=\vec{\eta}-v^-\hat{\vec{v}}, \quad \vec{\beta}=-\vec{\eta}-v^+\hat{\vec{v}}, \quad v^\pm=\frac{v}{2}\pm\frac{\epsilon_i-\epsilon_f}{v},$$

$$\vec{\alpha}+\vec{\beta}=-\vec{v}. \quad (46)$$

c. Transfer ionization

During transfer ionization, one electron (e_1) is captured while the other (e_2) is simultaneously ionized. The unperturbed wave function for this process is given by

$$\Phi_f=\varphi_P(\vec{s}_1)\phi_f, \quad \phi_f=(2\pi)^{-3/2}e^{-i\vec{k}_f\vec{r}_f+i\vec{\kappa}\cdot\vec{x}_2}, \quad (47)$$

where $\vec{\kappa}$ represents the momentum vector of the ejected electron e_2 with respect to its parent nucleus. The wave function which obeys the correct boundary condition has the form

$$\Phi_f^c(r_f\to\infty,x_2\to\infty)\equiv\Phi_f^- = \Phi_f e^{-i\nu_f\ln(k_fr_f-\vec{k}_f\vec{r}_f)+i(Z_T/\kappa)\ln(\kappa x_2+\vec{\kappa}\cdot\vec{x}_2)}, \quad (48)$$

where $\nu_f=(Z_T-1)(Z_P-1)/v$.

The analysis in this section aims to emphasize the need to establish a proper connection between long-range Coulomb distortion effects and the accompanying perturbation potentials. Otherwise, unphysical results could easily be incurred as has been shown by Belkić (1997a, 1997b, 2001, 2004) for ionization (detachment) of H^- by H^+.

B. Perturbation series with the correct boundary conditions

Before proceeding further, it must be emphasized that imposing the proper Coulomb boundary conditions on the entrance and exit channels is of crucial importance for ion-atom collisions. Experience has shown that, if this requirement is disregarded, serious problems may arise, and such models are inadequate for a description of experimental findings.

The dynamics of the entire four-body system are described by means of the Schrödinger equation

$$(H-E)\Psi^\pm=0, \quad (49)$$

where $\Psi^\pm$ are the full scattering states with the outgoing or incoming boundary conditions

$$\Psi^+\to\Phi_i^+ \quad (r_i\to\infty), \quad \Psi^-\to\Phi_f^- \quad (r_f\to\infty). \quad (50)$$

The exact transition amplitude with the correct boundary conditions can be written in the post (+) and prior (−) forms as

$$T_{if}^+=\langle\Phi_f^-|V_f^c|\Psi_i^+\rangle, \quad T_{if}^-=\langle\Psi_f^-|V_i^c|\Phi_i^+\rangle. \quad (51)$$

Both forms are equivalent to each other on the energy shell, i.e., the exact expressions are equal, $T_{if}^+=T_{if}^-$, for transitions for which the total energy is conserved (Belkić, 2004).

Solving a scattering problem in which four bodies take part (two nuclei and two electrons) is extremely difficult. As usual, at intermediate and high impact energies, the perturbation procedure is frequently employed. It is convenient to convert the Schrödinger equation for a four-body problem into the corresponding integral equation such as the Lippmann-Schwinger equations or the associated distorted-wave integral equations.

1. The Lippmann-Schwinger equations for four-body collisions

We introduce the function

$$\Psi_i^+\equiv i\epsilon G^+\Phi_i^+, \quad (52)$$

where Φ_i^+ is the wave function defined by Eqs. (15) and (21). Here ϵ is an infinitesimally small positive number. In addition to the total Green's functions $G^\pm$ in Eq. (52), we also define the initial $G_i^\pm$, the final $G_f^\pm$, and the free Green's functions $G_0^\pm$ as

$$G^\pm=(E-H\pm i\epsilon)^{-1}, \quad G_i^\pm=(E-H_i^c\pm i\epsilon)^{-1}, \quad (53)$$

$$G_f^\pm=(E-H_f^c\pm i\epsilon)^{-1}, \quad G_0^\pm=(E-H_0\pm i\epsilon)^{-1}. \quad (54)$$

These propagators are interrelated by the following Lippmann-Schwinger integral equations for the total Green's functions

$$G^\pm=G_i^\pm+G_i^\pm V_i^cG^\pm, \quad G^\pm=G_f^\pm+G_f^\pm V_f^cG^\pm,$$

$$G^\pm=G_0^\pm+G_0^\pm VG^\pm, \quad (55)$$

as can be checked. For example, if the ansatz $G^\pm=G_i^\pm+G_i^\pm V_i^cG^\pm$ is multiplied from the left by $E-H_i^c\pm i\epsilon$ and simultaneously from the right by $E-H\pm i\epsilon$, it follows that $E-H_i^c\pm i\epsilon=E-H\pm i\epsilon+V_i^c$, in agreement with Eq. (10).

Applying the iteration procedure to Eq. (55), we obtain the following expansions for the total Green's function in terms of G_0^+, G_i^+, and G_f^+

$$G^+=G_0^++G_0^+VG_0^++G_0^+VG_0^+VG_0^+ + G_0^+VG_0^+VG_0^+VG_0^++\cdots, \quad (56)$$

$$G^+ = G_i^+ + G_i^+ V_i^c G_i^+ + G_i^+ V_i^c G_i^+ V_i^c G_i^+ + G_i^+ V_i^c G_i^+ V_i^c G_i^+ V_i^c G_i^+ + \cdots, \tag{57}$$

$$G^+ = G_f^+ + G_f^+ V_f^c G_f^+ + G_f^+ V_f^c G_f^+ V_f^c G_f^+ + G_f^+ V_f^c G_f^+ V_f^c G_f^+ V_f^c G_f^+ + \cdots. \tag{58}$$

Inserting $G^{\pm}$ from Eq. (55) into (52), we have

$$\Psi_i^+ = i\epsilon G^+ \Phi_i^+ = i\epsilon G_i^+ \Phi_i^+ + G_i^+ V_i^c i\epsilon G^+ \Phi_i^+ = i\epsilon G_i^+ \Phi_i^+ + G_i^+ V_i^c \Psi_i^+, \tag{59}$$

where the first term can be written as $i\epsilon G_i^+ \Phi_i^+ = \Phi_i^+$. This can be directly verified if $[i\epsilon/(E - H_i^c + i\epsilon)]\Phi_i^+ = \Phi_i^+$ is multiplied from the left by $E - H_i^c + i\epsilon$. Thus we have $i\epsilon\Phi_i^+ = (E - H_i^c + i\epsilon)\Phi_i^+$, in agreement with Eq. (21). In this way, we obtain the Lippmann-Schwinger equation for the total scattering wave function in the case of a four-body problem

$$\Psi_i^+ = \Phi_i^+ + G_i^+ V_i^c \Psi_i^+. \tag{60}$$

This is an inhomogeneous integral equation, since it contains explicitly the incident wave Φ_i^+. The integral equation (60) can formally be solved as

$$\begin{aligned}
\Psi_i^+ &= \Phi_i^+ + G_i^+ V_i^c \Psi_i^+ \\
&= \Phi_i^+ + G_i^+ V_i^c (\Phi_i^+ + G_i^+ V_i^c \Psi_i^+) \\
&= \Phi_i^+ + G_i^+ V_i^c \Phi_i^+ + G_i^+ V_i^c G_i^+ V_i^c \Psi_i^+ \\
&= \Phi_i^+ + G_i^+ V_i^c \Phi_i^+ + G_i^+ V_i^c G_i^+ V_i^c \Phi_i^+ \\
&\quad + G_i^+ V_i^c G_i^+ V_i^c G_i^+ V_i^c \Psi_i^+ \\
&= (1 + G_i^+ V_i^c + G_i^+ V_i^c G_i^+ V_i^c \\
&\quad + G_i^+ V_i^c G_i^+ V_i^c G_i^+ V_i^c + \cdots)\Phi_i^+ \\
&= \left(1 + \sum_{n=1}^{\infty} (G_i^+ V_i^c)^n\right)\Phi_i^+ = (1 + G^+ V_i^c)\Phi_i^+.
\end{aligned}$$

This is the case because, if we multiply Eq. (57) by V_i^c, we obtain

$$G^+ V_i^c = G_i^+ V_i^c + G_i^+ V_i^c G_i^+ V_i^c + G_i^+ V_i^c G_i^+ V_i^c G_i^+ V_i^c + G_i^+ V_i^c G_i^+ V_i^c G_i^+ V_i^c G_i^+ V_i^c + \cdots = \sum_{n=1}^{\infty} (G_i^+ V_i^c)^n.$$

Hence, the formal solution of the Lippmann-Schwinger equation in terms of the total Green's function G^+ is

$$\Psi_i^+ = \Phi_i^+ + G^+ V_i^c \Phi_i^+ = (1 + G^+ V_i^c)\Phi_i^+. \tag{61}$$

2. The Born expansions with the correct boundary conditions for four-body collisions

Inserting the formal solution (61) into Eq. (51) for the post form of the transition amplitude, it follows that

$$T_{if}^+ = \langle \Phi_f^- | V_f^c | \Psi_i^+ \rangle = \langle \Phi_f^- | V_f^c (1 + G^+ V_i^c) | \Phi_i^+ \rangle. \tag{62}$$

This implies that, by substituting G^+ from Eqs. (56)–(58) into Eq. (62), we can write several different versions of the Born expansions with the correct boundary conditions

$$T_{if}^+ = T_{if}^{(\mathrm{CB1})+} + \langle \Phi_f^- | V_f^c G_0^+ V_i^c | \Phi_i^+ \rangle + \langle \Phi_f^- | V_f^c G_0^+ V G_0 V_i^c | \Phi_i^+ \rangle + \cdots, \tag{63}$$

$$T_{if}^+ = T_{if}^{(\mathrm{CB1})+} + \langle \Phi_f^- | V_f^c G_i^+ V_i^c | \Phi_i^+ \rangle + \langle \Phi_f^- | V_f^c G_i^+ V_i^c G_i^+ V_i^c | \Phi_i^+ \rangle + \cdots, \tag{64}$$

$$T_{if}^+ = T_{if}^{(\mathrm{CB1})+} + \langle \Phi_f^- | V_f^c G_f^+ V_i^c | \Phi_i^+ \rangle + \langle \Phi_f^- | V_f^c G_f^+ V_f^c G_f^+ V_i^c | \Phi_i^+ \rangle + \cdots, \tag{65}$$

$$T_{if}^{(\mathrm{CB1})+} = \langle \Phi_f^- | V_f^c | \Phi_i^+ \rangle. \tag{66}$$

Here $T_{if}^{(\mathrm{CB1})+}$ is the post form of the first Born approximation with the correct boundary conditions for four-body collisions, i.e., the CB1-4B method. As can be seen, the term $T_{if}^{(\mathrm{CB1})+}$ is identical in all versions. In other words, the CB1-4B method can be obtained by replacing the total wave function Ψ_i^+ by the asymptotic channel state Φ_i^+. Two methods for an explicit calculation of the matrix elements in the CB1-4B method for double-charge exchange have been devised and implemented by Belkić (1993a, 1993b).

Likewise, the nth Born approximation with the correct boundary conditions (CBn-4B) may be obtained by keeping the first n terms in the expansion. For example, the four-body second Born approximation with the correct boundary conditions (CB2-4B) can be obtained in this way

$$T_{if;0}^{(\mathrm{CB2})+} = T_{if}^{(\mathrm{CB1})+} + \langle \Phi_f^- | V_f^c G_0^+ V_i^c | \Phi_i^+ \rangle, \tag{67}$$

$$T_{if;i}^{(\mathrm{CB2})+} = T_{if}^{(\mathrm{CB1})+} + \langle \Phi_f^- | V_f^c G_i^+ V_i^c | \Phi_i^+ \rangle, \tag{68}$$

$$T_{if;f}^{(\mathrm{CB2})+} = T_{if}^{(\mathrm{CB1})+} + \langle \Phi_f^- | V_f^c G_f^+ V_i^c | \Phi_i^+ \rangle. \tag{69}$$

Here Eq. (67) in terms of G_0^+ is recognized as an extension of the corresponding three-body second Born approximation with the correct boundary conditions (CB2-3B) of Belkić (1988a, 1991, 2004). Of course, many other versions of the Born expansion can be formulated by utilizing various possible iterative solutions for G^+. In other words, a unique Born series of the transition amplitude T_{if}^+ does not exist.

A similar procedure can be employed for the prior form of the transition amplitude. That is, the time-independent wave function of the whole system in the exit channel is given by the following integral form

$$\Psi_f^- = \Phi_f^- + G_f^- V_f^c \Psi_f^- = (1 + G^- V_f^c)\Phi_f^-. \tag{70}$$

The corresponding prior form of the transition amplitude is

$$T_{if}^- = \langle \Phi_f^- | (1 + G^- V_f^c)^\dagger V_i^c | \Phi_i^+ \rangle. \tag{71}$$

Thus far, explicit computations in the CB1-4B method have been carried out for double-electron capture by Belkić (1993a, 1993b) as well as for single-charge exchange by Mančev (1995, 1996). The CB2-4B method

has not yet been used within the four-body formalism. However, it should be emphasized that much experience has been gained using the CB2-3B method, with its distinct improvement in the description of single-charge exchange, when passing from the first- to the second-order perturbation theory, as demonstrated by Belkić (1991). Guided by this fact, here we recall certain aspects of the basic three-body problem $Z_P+(Z_T,e)\rightarrow(Z_P,e)+Z_T$. If one employs a pure Coulomb potential $V_P=-Z_P/s$ as the perturbation in the entrance channel, together with the unperturbed wave functions Φ_i and Φ_f, where the plane waves describe the relative motion of heavy aggregates, one would obtain the three-body first-order Brinkman-Kramers (BK1-3B) approximation via its transition amplitude $\langle\Phi_f|V_P|\Phi_i\rangle$. By including the second-order term in the Born expansion $\langle\Phi_f|V_TG_0^+V_P|\Phi_i\rangle$ with the free-particle Green's function, one obtains the three-body second-order Brinkman-Kramers approximation (BK2-3B). From the physical viewpoint, the BK2-3B model should be more adequate than the BK1-3B model, due to the addition $V_TG_0^+V_P$. Neither the BK1-3B nor the BK2-3B model obeys the correct boundary conditions. As has been shown by Belkić (1991), the BK2-3B model gives an even poorer description of the corresponding experimental data than the BK1-3B model, which itself is inadequate for differential cross sections of charge exchange in the H^+-H collisions. This shows that inclusion of higher-order terms in a perturbation series can deteriorate the overall description if certain basic principles are disregarded from the outset, as in the Brinkman-Kramers approximation. On the other hand, the CB2-3B method (Belkić, 1988a, 1991; Belkić and Taylor, 1989) yields reliable results relative to the experimental data. Crucially, the CB2-3B method shows a significant improvement over the corresponding boundary-corrected three-body first Born (CB1-3B) method. This success of the CB2-3B method in describing charge-exchange processes has been attributed to the rigorous treatment of the correct boundary conditions, which represent the essential and distinct features of any scattering event (Belkić, 1988a, 1991; Belkić and Taylor 1989). The CB2-3B method for single-electron capture has subsequently been the subject of several investigations (Decker and Eichler, 1989b; Toshima and Igarashi, 1992).

C. The Dodd-Greider distorted-wave series for four-body collisions

In order to solve Eq. (49), we adopt the distorted-wave formalism. We recall the salient features of this theory (Cheshire, 1964; Dodd and Greider, 1966; Greider and Dodd, 1966; Dollard, 1964; Belkić *et al.*, 1979; Crothers and Dubé, 1993).

In the distorted-wave formalism, instead of solving directly the full Schrödinger equation (49) with rigidly determined interactions, one considers a model problem in which the real channel interactions V_i and V_f are replaced by certain distorting potentials W_i and W_f. The following Green's functions are associated with these potentials

$$g_i^+=(E-H_i-W_i+i\epsilon)^{-1},\quad g_f^-=(E-H_f-W_f-i\epsilon)^{-1}, \tag{72}$$

or, equivalently,

$$g_i^+=(1+g_i^+W_i)\mathcal{G}_i^+\equiv\omega^+\mathcal{G}_i^+,$$

$$g_f^-=(1+g_f^-W_f)\mathcal{G}_f^-\equiv\omega^-\mathcal{G}_f^-. \tag{73}$$

Here $\mathcal{G}_i^+$ and $\mathcal{G}_f^-$ are the Green's functions defined by

$$\mathcal{G}_i^+=(E-H_i+i\epsilon)^{-1},\quad \mathcal{G}_f^-=(E-H_f-i\epsilon)^{-1}, \tag{74}$$

where $\omega^\pm$ are the Møller wave operators. Next, instead of $\Psi_{i,f}^\pm=(1+G^\pm V_{i,f}^c)\Phi_{i,f}^\pm$, we introduce the distorted waves

$$\chi_{i,f}^\pm=(1+g_{i,f}^\pm W_{i,f})\Phi_{i,f}=\omega^\pm\Phi_{i,f}. \tag{75}$$

The distorted waves χ_i^+ and χ_f^- satisfy the following equations in the limits $\epsilon\rightarrow0^\pm$

$$(E-H_i-W_i)\chi_i^+=0,\quad (E-H_f-W_f)\chi_f^-=0. \tag{76}$$

The connection of the model problem (76) with the original equation (49) is provided through the condition that $\chi_{i,f}^\pm$ and $\Psi_{i,f}^\pm$ must exhibit the same asymptotic behaviors as $r_{i,f}\rightarrow\infty$

$$\chi_i^+\rightarrow\Psi_i^+\rightarrow\Phi_i^+,\quad r_i\rightarrow\infty, \tag{77}$$

$$\chi_f^-\rightarrow\Psi_f^-\rightarrow\Phi_f^-,\quad r_f\rightarrow\infty. \tag{78}$$

The transition amplitude in its prior form, as defined via

$$T_{if}^-=\langle\Psi_f^-|V_i|\Phi_i\rangle=\langle\Phi_f|(1+G^-V_f)^\dagger V_i|\Phi_i\rangle \equiv\langle\Phi_f|\Omega^{-\dagger}V_i|\Phi_i\rangle, \tag{79}$$

can be expressed in terms of the model quantities in the entrance channel

$$T_{if}^-=\langle\Phi_f|\Omega^{-\dagger}(V_i-W_i)\omega^+ +\Omega^{-\dagger}[1-(V_i-W_i)g_i^+]W_i|\Phi_i\rangle. \tag{80}$$

This relation can be readily verified by employing the definitions for g_i^+ and ω^+ or by an algebraic derivation

$$\begin{aligned}V_i&=V_i(1+g_i^+W_i)-W_i(1+g_i^+W_i)\\&\quad+[1-(V_i-W_i)g_i^+]W_i\\&=(V_i-W_i)\omega^++[1-(V_i-W_i)g_i^+]W_i.\end{aligned}$$

Using the well-known Chew-Goldberger operator identity $1/A-1/B=(1/A)(B-A)(1/B)$ with $1/A=G^+$ and $1/B=g_i^+$, the second term in Eq. (80) becomes $(E+i\epsilon-H_f)(\omega^+-1)=i\epsilon(\omega^+-1)$. We write the transition amplitude T_{if}^- as

$$T_{if}^-=\langle\Phi_f|\Omega^{-\dagger}(V_i-W_i)\omega^+|\Phi_i\rangle+T_{if}^D,$$

$$T_{if}^D=\lim_{\epsilon\rightarrow0}i\epsilon\langle\Phi_f|\omega^+|\Phi_i\rangle=\lim_{\epsilon\rightarrow0}i\epsilon\langle\Phi_f|\chi_i^+\rangle. \tag{81}$$

The contribution of the term T_{if}^D will vanish in the limit $\epsilon\rightarrow0$. The condition

$$\lim_{\epsilon\to 0} i\epsilon\langle\Phi_f|\chi_i^+\rangle = 0 \tag{82}$$

is satisfied by choosing a distorting potential which leads only to elastic scattering in the considered channel and as such does not cause a rearrangement. This can be achieved by choosing the distorting potential in such a way that it depends only on the relative coordinate between the projectile and target.

By a simple transformation, the wave operator Ω^- from Eq. (79) can be rewritten as

$$\Omega^- = [1 + G^-(V_f - W_f)]\omega^-. \tag{83}$$

Then, by employing Eq. (82), we obtain from Eq. (81)

$$\begin{aligned} T_{if}^- &= \langle\Phi_f|\Omega^{-\dagger}(V_i - W_i)\omega^+|\Phi_i\rangle \\ &= \langle\Phi_f|\omega^{-\dagger}[1 + (V_f - W_f^\dagger)G^+](V_i - W_i)\omega^+|\Phi_i\rangle \\ &\equiv \langle\Phi_f|U_{if}^-|\Phi_i\rangle. \end{aligned} \tag{84}$$

We recall that the Hermitian-conjugated relation (83) is given by $\Omega^{-\dagger} = \omega^{-\dagger}[1 + (V_f - W_f^\dagger)G^+]$. Hence, the exact transition amplitude T_{if}^- in the distorted-wave theory reads as

$$T_{if}^- = \langle\chi_f^-|(V_i - W_i) + (V_f - W_f^\dagger)G^+(V_i - W_i)|\chi_i^+\rangle. \tag{85}$$

Similarly, we can obtain the exact post form of the transition amplitude in the distorted-wave theory via

$$T_{if}^+ = \langle\chi_f^-|(V_f - W_f^\dagger) + (V_f - W_f^\dagger)G^+(V_i - W_i)|\chi_i^+\rangle, \tag{86}$$

provided that $\lim_{\epsilon\to 0} i\epsilon\langle\Phi_f|\omega^{-\dagger}|\Phi_i\rangle = 0$. Using

$$\Omega^- = [1 + \Omega^-\mathcal{G}_f^-(V_f - W_f)]\omega^-, \tag{87}$$

the transition operator U_{if}^- introduced in Eq. (84) can be written as the following integral equation

$$U_{if}^- = \omega^{-\dagger}(V_i - W_i)\omega^+ + \omega^{-\dagger}(V_f - W_f^\dagger)\mathcal{G}_f^+ U_{if}^-. \tag{88}$$

This can alternatively be cast into the form

$$U_{if}^-(1 - \mathcal{K}) = \omega^{-\dagger}(V_i - W_i)\omega^+, \quad \mathcal{K} = \omega^{-\dagger}(V_f - W_f^\dagger)\mathcal{G}_f^+, \tag{89}$$

where $\mathcal{K}$ represents the so-called kernel, i.e., the homogeneous term of the integral equation. Since ω^- is given by $\omega^- = 1 + g_f^- W_f$, it follows that the form of $\mathcal{K}$ is independent of the choice of distortion in the initial channel. Expanding U_{if}^- in powers of $\mathcal{K}$, i.e., in an infinite perturbation series, we obtain

$$U_{if}^- = I\left(1 + \sum_{n=1}^{\infty} \mathcal{K}^n\right), \quad I = \omega^{-\dagger}(V_i - W_i)\omega^+, \tag{90}$$

where I is an inhomogeneous term of the integral equation (88). However, this latter expansion diverges in the case of rearrangement collisions due to the existence of disconnected diagrams. These Feynman diagrams would correspond to collisional paths describing three constituents interacting pairwise with each other in the presence of a fourth body as a freely propagating particle. In the impulse space this physical situation is described by means of a delta function in the kernel of the integral equation. The presence of this δ function highlights the conservation of momentum. Such a kernel is said to contain disconnected diagrams. The free motion is mediated via the free-particle Green's resolvent G_0^+, and it leads to the factor $1/(E - E_0 + i\epsilon)$, where $E_0 = k^2/2$. Since in the T matrix we have integration over momentum k in the whole space, it is clear that we may have a situation where $E = E_0$, and this causes divergence of the energy-dependent term $1/(E - E_0 + i\epsilon)$ in the limit $\epsilon \to 0$. The typical kernel $(V_f - W_f^\dagger)G_0^+(V_i - W_i)$ from the iterated transition T operator will not contain any disconnected diagrams if no two-body interaction in the perturbation $V_f - W_f^\dagger$ is repeated in $V_i - W_i$. This can be achieved with the introduction of a virtual intermediate channel x as suggested by Dodd and Greider (1966). The Green's function associated with this virtual channel is given by

$$g_x^\pm = (E - H + V_x \pm i\epsilon)^{-1}, \tag{91}$$

where V_x is an appropriate channel potential. Using

$$G^+ = g_x^+(1 + V_x G^+), \tag{92}$$

we obtain the integral equation

$$\begin{aligned} U_{if}^-(1 - \mathcal{K}_1) = {} & \omega^{-\dagger}(V_i - W_i)\omega^+ + \omega^{-\dagger}(V_f - W_f^\dagger) \\ & \times g_x^+(V_i - W_i)]\omega^+, \end{aligned} \tag{93}$$

where the kernel is now defined by

$$\mathcal{K}_1 = \omega^{-\dagger}(V_f - W_f^\dagger)g_x^+\mathcal{G}_f^+. \tag{94}$$

By employing certain suitably chosen potentials V_x and W_f, the kernel can be freed from disconnected diagrams. An example of such a situation is when the potential V_x does not appear in $V_f - W_f^\dagger$. Inserting Eq. (92) into Eq. (85), we arrive at

$$\begin{aligned} T_{if}^- = {} & \langle\chi_f^-|(V_i - W_i) + (V_f - W_f^\dagger)g_x^+(1 + V_x G^+) \\ & \times (V_i - W_i)|\chi_i^+\rangle. \end{aligned} \tag{95}$$

If we neglect the term with the Green's function G^+, we obtain a first-order approximation for the prior form of the transition amplitude (also denoted by T_{if}^-)

$$T_{if}^- = \langle\chi_f^-|[1 + g_x^-(V_f - W_f)]^\dagger(V_i - W_i)|\chi_i^+\rangle. \tag{96}$$

Introducing an auxiliary distorted wave

$$|\xi_f^-\rangle = [1 + g_x^-(V_f - W_f)]|\chi_f^-\rangle, \tag{97}$$

we have

$$T_{if}^- = \langle\xi_f^-|V_i - W_i|\chi_i^+\rangle. \tag{98}$$

1. Derivation of the distorted waves for the initial states

a. Z_P-$(Z_T;e_1,e_2)_i$ collisions

According to the requirement (77) and the correct asymptotic behavior of Ψ^+, i.e., $\Psi^+ \to \varphi_i(\vec{x}_1,\vec{x}_2)\exp[i\vec{k}_i\cdot\vec{r}_i + i\nu_i \ln(k_i r_i - \vec{k}_i\cdot\vec{r}_i)] \equiv \Phi_i^+(r_i \to \infty)$, the following factorized form for the function χ_i^+ appears to be the most convenient

$$\chi_i^+ = \varphi_i(\vec{x}_1,\vec{x}_2)\psi_i^+, \tag{99}$$

where ψ_i^+ is an unknown function determined by the particular choice of the distorting potential. Inserting Eq. (99) into Eq. (76), we obtain

$$\varphi_i(E-\epsilon_i-H_0-V_i)\psi_i^+ + \frac{1}{b}\sum_{k=1}^{2}\vec{\nabla}_{x_k}\varphi_i\cdot\vec{\nabla}_{x_k}\psi_i^+ + U_i\varphi_i\psi_i^+ + \psi_i^+(\epsilon_i-h_i)\varphi_i = 0, \tag{100}$$

$$U_i = V_i - W_i. \tag{101}$$

The term $(\epsilon_i-h_i)\varphi_i \equiv O_{\varphi_i}(\vec{x}_1,\vec{x}_2)\equiv O_{\varphi_i}$ in Eq. (100) vanishes identically only for the exact eigensolutions $\varphi_i(\vec{x}_1,\vec{x}_2)\equiv\varphi_i$ and ϵ_i of the target Hamiltonian h_i. However, since these are unavailable, the term O_{φ_i} should, in principle, be kept throughout, as suggested by Belkić (1993a) within the CB1-4B method. Explicit computations for double-charge exchange (Belkić, 1993a) and transfer ionization (Belkić *et al.*, 1997a) have shown that the contribution from this term is ~(10–15)%. This correction will be neglected in the present study, so that Eq. (100) becomes

$$\varphi_i\left(\frac{k_i^2}{2\mu_i}-H_0-\frac{Z_PZ_T}{R}+\frac{Z_P}{s_1}+\frac{Z_P}{s_2}\right)\psi_i^+ + \frac{1}{b}\sum_{k=1}^{2}\vec{\nabla}_{x_k}\varphi_i\cdot\vec{\nabla}_{x_k}\psi_i^+ + U_i\varphi_i\psi_i^+ = 0. \tag{102}$$

In general, the presence of the coupling term $\vec{\nabla}_{x_k}\varphi_i\cdot\vec{\nabla}_{x_k}\psi_i^+$ precludes a separation of independent variables in Eq. (102). However, at the same time, there is some flexibility provided by the perturbation potential operator $U_i=V_i-W_i$, which permits a cancellation of the coupling term.

A convenient choice has been made by Belkić and Mančev (1992, 1993) as

$$U_i\chi_i^+ = -\frac{1}{b}\sum_{k=1}^{2}\vec{\nabla}_{x_k}\varphi_i\cdot\vec{\nabla}_{x_k}\psi_i^+. \tag{103}$$

Alternatively, the following choices for U_i can be implemented (Belkić *et al.*, 1997; Mančev, 1999a):

$$U_i\chi_i^+ = Z_P\left(\frac{1}{R}-\frac{1}{s_2}\right)\chi_i^+ - \frac{1}{b}\sum_{k=1}^{2}\vec{\nabla}_{x_k}\varphi_i\cdot\vec{\nabla}_{x_k}\psi_i^+, \tag{104}$$

$$U_i\chi_i^+ = \left[Z_P\left(\frac{1}{R}-\frac{1}{s_2}\right)+\left(\frac{1}{R}-\frac{1}{s_1}\right)\right]\chi_i^+ - \frac{1}{b}\sum_{k=1}^{2}\vec{\nabla}_{x_k}\varphi_i\cdot\vec{\nabla}_{x_k}\psi_i^+. \tag{105}$$

Although other choices are possible, in all cases the requirement that the function χ_i^+ has the correct asymptotic behavior must be satisfied. It is seen that the distorting potentials (103)–(105) contain the term $-(1/b)\Sigma_{k=1}^2\vec{\nabla}_{x_k}\varphi_i\cdot\vec{\nabla}_{x_k}\psi_i^+$, which together with the eikonal approximation $\vec{R}\simeq-\vec{r}_f$ ($M_{P,T}\gg1$), provide an exact solution ψ_i^+ of the differential equation (102). In this case, a separation of the independent variables $\vec{r}_f$, $\vec{s}_1$, and $\vec{s}_2$ is possible, i.e., we can write

$$\psi_i^+ = C_i^+\mathcal{F}_1^+(\vec{s}_1)\mathcal{F}_2^+(\vec{s}_2)\mathcal{F}^+(\vec{r}_f), \tag{106}$$

where C_i^+ is a constant to be determined. We first determine the distorted wave χ_i^+ for the distorting potential (103) in accordance with Belkić and Mančev (1992, 1993). Inserting Eq. (106) into Eq. (102), we obtain

$$\left(\frac{1}{2a}\nabla_{s_k}^2+\frac{Z_P}{s_k}+\frac{p_k^2}{2a}\right)\mathcal{F}_k^+(\vec{s}_k)=0 \quad (k=1,2), \tag{107}$$

$$\left(\frac{1}{2\mu_f}\nabla_{r_f}^2-\frac{Z_PZ_T}{r_f}+\frac{p_f^2}{2\mu_f}\right)\mathcal{F}^+(\vec{r}_f)=0, \tag{108}$$

with the solutions

$$\mathcal{F}_k^+(\vec{s}_k) = N^+(\nu_{P_k})e^{i\vec{p}_k\cdot\vec{s}_k}{}_1F_1(i\nu_{P_k},1,ip_ks_k-i\vec{p}_k\cdot\vec{s}_k), \tag{109}$$

$$\mathcal{F}^+(\vec{r}_f) = \mathcal{N}^+(\nu_{PT})e^{i\vec{p}_f\vec{r}_f}{}_1F_1(-i\nu_{PT},1,ip_fr_f-i\vec{p}_f\cdot\vec{r}_f), \tag{110}$$

where $\mathcal{N}^+(\nu_{PT})=e^{-\pi\nu_{PT}/2}\Gamma(1+i\nu_{PT})$, $\nu_{P_k}=aZ_P/p_k$ $(k=1,2)$ and $\nu_{PT}=Z_PZ_T\mu_f/p_f$. The auxiliary vectors $\vec{p}_1$, $\vec{p}_2$, and $\vec{p}_f$ are determined from the following conditions

$$E-\epsilon_i=\frac{p_1^2}{2a_{P1}}+\frac{p_2^2}{2a_{P2}}+\frac{p_f^2}{2\mu_f}, \tag{111}$$

$$\vec{p}_1\cdot\vec{s}_1+\vec{p}_2\cdot\vec{s}_2+\vec{p}_f\cdot\vec{r}_f=\vec{k}_i\cdot\vec{r}_i, \tag{112}$$

$$C_i^+\exp\left(i\nu_{PT}\ln(p_fr_f-\vec{p}_f\cdot\vec{r}_f-i\sum_{k=1}^{2}\nu_{P_k}\times\ln(p_ks_k-\vec{p}_k\cdot\vec{s}_k)\right)\to\exp[i\nu_i\ln(k_ir_i-\vec{k}_i\cdot\vec{r}_i)],$$

$$r_i\to\infty. \tag{113}$$

Equation (111) is introduced in order to obtain three separable equations from Eq. (102) for the independent variables $\vec{r}_f$, $\vec{s}_1$, and $\vec{s}_2$. Expressions (112) and (113) originate from the requirement that χ_i^+ must satisfy the correct boundary condition (77). It is easily shown that $\vec{p}_k\simeq-\vec{v}$ and $\vec{p}_f\simeq-\vec{k}_i$ for $M_P\gg1$ and $M_T\gg1$, respectively. With these values of the vectors $\vec{p}_1$, $\vec{p}_2$, and $\vec{p}_f$, the energy conservation law is satisfied within the eikonal mass limit, so that $E_i-\epsilon_i=k_i^2/(2\mu_i)$ and, moreover, $C_i^+=\mu_i^{-2i\nu_P}$. The constant C_i^+, which is needed in (113), follows from the limit $(1/\mu_i)(k_ir_i-\vec{k}_i\cdot\vec{r}_i)/(vs_k+\vec{v}\cdot\vec{s}_k)\to1$ as $r_i\to\infty$. Hence, the solution for the function ψ_i^+ is

$$\psi_i^+ = \mu_i^{-2i\nu_P}\mathcal{N}^+(\nu)[N^+(\nu_P)]^2 e^{i\vec{k}_i\cdot\vec{r}_i} \times {}_1F_1(-i\nu,1,ik_ir_f+i\vec{k}_i\cdot\vec{r}_f){}_1F_1(i\nu_P,1,ivs_1+i\vec{v}\cdot\vec{s}_1) \times {}_1F_1(i\nu_P,1,ivs_2+i\vec{v}\cdot\vec{s}_2), \quad (114)$$

where $\nu_K=Z_K/v$ $(K=P,T)$ and $\nu=Z_PZ_T/v$. Now, it is readily checked that the distorted wave $\chi_i^+=\varphi_i\psi_i^+$ has the correct asymptotic behavior (77). It should be noted that the proof of the correctness of the boundary conditions for the continuum distorted-wave methodologies is consistent with the concept of the strong limit from formal scattering theory (Dollard, 1964; Belkić, 2004). This has been shown within the three-body distorted-wave formalism for single-electron capture (Deco *et al.*, 1995). This consistency is not hampered by the presence of the kinetic energy perturbation, as in the three-body symmetric eikonal (SE-3B) approximation, or by the Coulombic behavior of perturbative potentials from the three-body continuum distorted-wave (CDW-3B) method. The same conclusions can be shown to hold true also for the scattering vector χ_i^+ from Eq. (114) which is encountered in double capture treated in the four-body distorted-wave formalism. The role and physical meaning of the strong limit in scattering theory have been analyzed by Belkić (2004).

Proceeding as before, the choice of the distorting potential (104) provides a solution for the distorted wave χ_i^+ in the entrance channel in the following form

$$\chi_i^+ = \mu_i^{i\nu_P}\mathcal{N}^+(\nu_i')N^+(\nu_P)e^{i\vec{k}_i\cdot\vec{r}_i}{}_1F_1(-i\nu_i',1,ik_ir_f+i\vec{k}_i\cdot\vec{r}_f) \times {}_1F_1(i\nu_P,1,ivs_1+i\vec{v}\cdot\vec{s}_1)\varphi_i(\vec{x}_1,\vec{x}_2), \quad (115)$$

where $\nu_i'=Z_P(Z_T-1)/v$. For the distorting potential given by Eq. (105) we obtain the same distorted wave as in Eq. (115), but the following quantities should be redefined accordingly: $\nu_i'\to\nu_i''=[Z_P(Z_T-1)-1]/v$ and $\nu_P\to\nu_P''=(Z_P-1)/v$. The determination of the distorted waves in the exit channel depends on the collisional process considered.

b. $(Z_P,e_1)_{i_1}$-$(Z_T,e_2)_{i_2}$ *collisions*

Imposing the correct boundary condition on the $(Z_P,e_1)_{i_1}$-$(Z_T,e_2)_{i_2}$ collisions via $\chi_i^+\to\Psi_i^+ \to\varphi_P(\vec{s}_1)\varphi_T(\vec{x}_2)e^{i\vec{k}_i\cdot\vec{r}_i+iv_i\ln(k_ir_i-\vec{k}_i\cdot\vec{r}_i)}\equiv\Phi_i^+$, we look for χ_i^+ in a separable form

$$\chi_i^+ = \varphi_P(\vec{s}_1)\varphi_T(\vec{x}_2)\zeta_i^+ \equiv \varphi_{PT}\zeta_i^+. \quad (116)$$

Inserting Eq. (116) into $(E-H_i-W_i)\chi_i^+=0$, we obtain the following equation for ζ_i^+

$$\left(E-\epsilon_i+\frac{1}{2\mu_f}\nabla_{r_f}^2+\frac{1}{2a}\nabla_{s_1}^2+\frac{1}{2a}\nabla_{s_2}^2-\frac{Z_T(Z_P-1)}{r_f}+\frac{Z_P-1}{s_2}\right)\zeta_i^+=0, \quad (117)$$

provided that the distorting potential is given by

$$U_i\chi_i^+ = \left[Z_T\left(\frac{1}{R}-\frac{1}{x_1}\right)-\frac{1}{s_2}+\frac{1}{r_{12}}\right]\chi_i^+ - \frac{1}{a}\vec{\nabla}_{s_2}\varphi_{PT}\cdot\vec{\nabla}_{s_2}\zeta_i^+ - \frac{1}{b}\vec{\nabla}_{x_1}\varphi_{PT}\cdot\vec{\nabla}_{x_1}\zeta_i^+. \quad (118)$$

We can solve Eq. (117) exactly by separation of the independent variables. As the net result for the distorted wave χ_i^+, we have

$$\chi_i^+ = N^+(\nu_P)\mathcal{N}^+(\nu)\varphi_P(\vec{s}_1)\varphi_T(\vec{x}_2)e^{i\vec{k}_i\cdot\vec{r}_i} \times {}_1F_1(-i\nu,1,ik_ir_i-i\vec{k}_i\cdot\vec{r}_i) \times {}_1F_1(i\nu_P,1,ivs_2+i\vec{v}\cdot\vec{s}_2)\varphi_i(\vec{x}_1,\vec{x}_2), \quad (119)$$

where $N^+(\nu_P)=\Gamma(1-i\nu_P)e^{\pi\nu_P/2}$, $\mathcal{N}^+(\nu)=\Gamma(1+i\nu)e^{-\pi\nu/2}$, $\nu=Z_T(Z_P-1)/v$, and $\nu_P=(Z_P-1)/v$.

III. DOUBLE-ELECTRON CAPTURE

A. The CDW-4B method

In order to complete the expression for the transition amplitude in the distorted-wave theory for double-electron capture, we look for the distorted waves in the exit channel. First, we determine the auxiliary distorted wave ξ_f^- defined by Eq. (97). Letting $\epsilon\to0^+$, it can be seen that, according to Eqs. (97) and (91), ξ_f^- is the solution of

$$(E-H+V_x^\dagger)\xi_f^- = (E-H+V_f-W_f+V_x^\dagger)\chi_f^-. \quad (120)$$

Since χ_f^- satisfies the relation (76), Eq. (120) can be reduced to

$$(E-H+V_x^\dagger)\xi_f^- = V_x^\dagger\chi_f^-. \quad (121)$$

Under the assumption

$$V_x^\dagger\chi_f^- = 0, \quad (122)$$

it follows that Eq. (121) becomes solvable analytically. In such a case, we write ξ_f^- in the factored form

$$\xi_f^- = \varphi_f(\vec{s}_1,\vec{s}_2)\psi_f^-, \quad (123)$$

where the unknown function ψ_f^- satisfies the following equation

$$\varphi_f(E-\epsilon_f-H_0-V_f)\psi_f^- + \frac{1}{a}\sum_{k=1}^{2}\vec{\nabla}_{s_k}\varphi_f\cdot\vec{\nabla}_{s_k}\psi_f^- + V_x\varphi_f\psi_f^- = 0. \quad (124)$$

Choosing the potential V_x in the form (Belkić and Mančev, 1992, 1993)

$$V_x = -\frac{1}{a}\sum_{k=1}^{2}\vec{\nabla}_{s_k}\ln\varphi_f\cdot\vec{\nabla}_{s_k}, \quad (125)$$

we have

$$(E-\epsilon_f-H_0-V_f)\psi_f^- = 0,$$

so that the function ψ_f^- finally becomes

$$\psi_f^- = \mu_f^{2i\nu_T}\mathcal{N}^-(\nu)[N^-(\nu_T)]^2 e^{-i\vec{k}_f\vec{r}_f} \times {}_1F_1(i\nu,1,-ik_f r_i - i\vec{k}_f\cdot\vec{r}_i) \times {}_1F_1(-i\nu_T,1,-ivx_1 - i\vec{v}\cdot\vec{x}_1) \times {}_1F_1(-i\nu_T,1,-ivx_2 - i\vec{v}\cdot\vec{x}_2). \quad (126)$$

Employing Eq. (103) for the distorting potential U_i and the corresponding distorted wave for the initial state $\chi_i^+ = \varphi_i\psi_i^+$, where the function ψ_i^+ is determined by Eq. (114), the transition amplitude for double-electron capture within the CDW-4B method acquires the form (Belkić and Mančev, 1992)

$$T_{if}^- = -N^2\int\int\int d\vec{x}_1 d\vec{x}_2 d\vec{r}_i e^{i\vec{k}_i\cdot\vec{r}_i + i\vec{k}_f\vec{r}_i}\mathcal{L}(\vec{r}_i,\vec{r}_f)\varphi_f^*(\vec{s}_1,\vec{s}_2) \times {}_1F_1(i\nu_T,1,ivx_1 + i\vec{v}\cdot\vec{x}_1){}_1F_1(i\nu_T,1,ivx_2 + i\vec{v}\cdot\vec{x}_2) \times\{{}_1F_1(i\nu_P,1,ivs_2 + i\vec{v}\cdot\vec{s}_2)\vec{\nabla}_{x_1}\varphi_i(\vec{x}_1,\vec{x}_2) \cdot\vec{\nabla}_{s_1}{}_1F_1(i\nu_P,1,ivs_1 + i\vec{v}\cdot\vec{s}_1) + {}_1F_1(i\nu_P,1,ivs_1 + i\vec{v}\cdot\vec{s}_1)\vec{\nabla}_{x_2}\varphi_i(\vec{x}_1,\vec{x}_2) \cdot\vec{\nabla}_{s_2}{}_1F_1(i\nu_P,1,ivs_2 + i\vec{v}\cdot\vec{s}_2)\}, \quad (127)$$

where $N = N^+(\nu_P)N^+(\nu_T)$ and

$$\mathcal{L}(\vec{r}_i,\vec{r}_f) = \mu_i^{-2i\nu_P}\mu_f^{-2i\nu_T}[\mathcal{N}^-(\nu)]^2 \times {}_1F_1(-i\nu,1,ik_i r_f + i\vec{k}_i\cdot\vec{r}_f) \times {}_1F_1(-i\nu,1,ik_f r_i + i\vec{k}_f\cdot\vec{r}_i). \quad (128)$$

A considerable simplification of Eq. (128) is obtained in the eikonal approximation

$$\begin{aligned}[\mathcal{N}^-(\nu)]^2\,{}_1F_1(-i\nu,1,ik_i r_f + i\vec{k}_i\cdot\vec{r}_f) &\times {}_1F_1(-i\nu,1,ik_f r_i + i\vec{k}_f\cdot\vec{r}_i)\\ &\simeq (k_i r_f + \vec{k}_i\cdot\vec{r}_f)^{i\nu}(k_f r_i + \vec{k}_f\cdot\vec{r}_i)^{i\nu}\\ &\simeq (\mu_i\mu_f)^{i\nu}[(vR - \vec{v}\cdot\vec{R})(vR + \vec{v}\cdot\vec{R})]^{i\nu}\\ &= (\mu_i\mu_f)^{i\nu}[v^2(R^2 - Z^2)]^{i\nu}\\ &= (\mu_i\mu_f)^{i\nu}(\rho v)^{2i\nu}\\ &\simeq (\mu\rho v)^{2i\nu},\end{aligned}$$

$$\mathcal{L}(\vec{r}_i,\vec{r}_f) \simeq (\mu\rho v)^{2i\nu}, \quad \nu = Z_P Z_T/v, \quad (129)$$

where $\mu = M_P M_T/(M_P + M_T)$. Here $\vec{\rho}$ is the projection of the vector $\vec{R}$ onto the XOY plane perpendicular to the Z axis, i.e., $\vec{\rho} = \vec{R} - \vec{Z}$ with $\vec{\rho}\cdot\vec{Z} = 0$, where the vector $\vec{Z}$ represents the projection of the vector $\vec{R}$ onto the Z axis. The phase factor $(\mu\rho v)^{2i\nu}$, which stems directly from the internuclear potential $V_{PT} = Z_P Z_T/R$, does not influence the total cross section, since

$$Q_{if}^-(a_0^2) = \frac{1}{(2\pi v)^2}\int d\vec{\eta}\,|T_{if}^-(\vec{\eta})|^2 = \int d\vec{\eta}\left|\frac{R_{if}^-(\vec{\eta})}{2\pi v}\right|^2, \quad (130)$$

$$R_{if}^-(\vec{\eta}) = -N^2\int\int\int d\vec{x}_1 d\vec{x}_2 d\vec{r}_i e^{i\vec{q}_{P'}\cdot(\vec{s}_1+\vec{s}_2) + i\vec{q}_{T'}(\vec{x}_1+\vec{x}_2)} \times\varphi_f^*(\vec{s}_1,\vec{s}_2){}_1F_1(i\nu_T,1,ivx_1 + i\vec{v}\cdot\vec{x}_1) \times{}_1F_1(i\nu_T,1,ivx_2 + i\vec{v}\cdot\vec{x}_2) \times\{{}_1F_1(i\nu_P,1,ivs_2 + i\vec{v}\cdot\vec{s}_2)\vec{\nabla}_{x_1}\varphi_i(\vec{x}_1,\vec{x}_2) \cdot\vec{\nabla}_{s_1}{}_1F_1(i\nu_P,1,ivs_1 + i\vec{v}\cdot\vec{s}_1) + {}_1F_1(i\nu_P,1,ivs_1 + i\vec{v}\cdot\vec{s}_1)\vec{\nabla}_{x_2}\varphi_i(\vec{x}_1,\vec{x}_2) \cdot\vec{\nabla}_{s_2}{}_1F_1(i\nu_P,1,ivs_2 + i\vec{v}\cdot\vec{s}_2)\}. \quad (131)$$

It is now obvious from Eq. (130) that the total cross section Q_{if}^- is independent of the internuclear potential $Z_P Z_T/R$, as it should be (Belkić *et al.*, 1979). The basic matrix element R_{if}^- represents the main working expression for calculating the total cross sections. Such a CDW-4B method represents a strict generalization of the CDW-3B method of Cheshire (1964), who originally formulated this latter theory for single-charge exchange within a three-body formalism. As per derivation, which followed the original work of Belkić and Mančev (1992), the result (131) for R_{if}^- in the CDW-4B method represents the rigorous first-order term (96) in the four-body Dodd-Greider perturbation series. This is very important, in view of the absence of any disconnected diagrams in the Dodd-Greider expansion, a feature which precludes divergence of the series. Only nondivergent perturbation series have a chance to provide mathematically meaningful first-order terms that, in turn, could capture the major physical effects. Such is the CDW-4B method which could, therefore, alternatively be called the four-body first-order continuum distorted wave (CDW-4B1) method.

In the same way, we can establish the post form of a first-order of the exact transition amplitude. In this case, we start from the integral equation of Dodd and Greider (1966) in analogy to Eq. (96)

$$T_{if}^+ = \langle\Phi_f|\Omega_f^{-\dagger}(V_f - W_f^\dagger)[1 + g_x^+(V_i - W_i)]\Omega_i^+|\Phi_i\rangle. \quad (132)$$

The derivation of the transition amplitude in the post form is carried out in a fashion similar to its prior counterpart, and the final result is

$$R_{if}^+(\vec{\eta}) = -N^2\int\int\int d\vec{s}_1 d\vec{s}_2 d\vec{r}_f e^{i\vec{q}_{P'}\cdot(\vec{s}_1+\vec{s}_2) + i\vec{q}_{T'}(\vec{x}_1+\vec{x}_2)} \times\varphi_i(\vec{x}_1,\vec{x}_2){}_1F_1(i\nu_P,1,ivs_1 + i\vec{v}\cdot\vec{s}_1) \times{}_1F_1(i\nu_P,1,ivs_2 + i\vec{v}\cdot\vec{s}_2) \times\{{}_1F_1(i\nu_T,1,ivx_2 + i\vec{v}\cdot\vec{x}_2)\vec{\nabla}_{s_1}\varphi_f^*(\vec{s}_1,\vec{s}_2) \cdot\vec{\nabla}_{x_1}{}_1F_1(i\nu_T,1,ivx_1 + i\vec{v}\cdot\vec{x}_1) + {}_1F_1(i\nu_T,1,ivx_1 + i\vec{v}\cdot\vec{x}_1)\vec{\nabla}_{s_2}\varphi_f^*(\vec{s}_1,\vec{s}_2) \cdot\vec{\nabla}_{x_2}{}_1F_1(i\nu_T,1,ivx_2 + i\vec{v}\cdot\vec{x}_2)\}. \quad (133)$$

The transition amplitude as a function of the vector $\vec{\rho}$ can be obtained via

$$a_{if}^{\pm}(\vec{\rho}) = \frac{1}{2\pi v}\rho^{2i\nu}\int d\vec{\eta}\, e^{i\vec{\eta}\vec{\rho}} R_{if}^{\pm}(\vec{\eta}). \tag{134}$$

Using the Parseval relation, i.e., the convolution theorem for the Fourier integral in the total cross section, we have

$$Q_{if}^{\pm}(a_0^2) = \int d\vec{\rho}\,|a_{if}^{\pm}(\vec{\rho})|^2. \tag{135}$$

The differential cross section in the CDW-3B and CDW-4B methods can be calculated directly from the expressions for $T_{if}^{\pm}$ (Pedlow *et al.*, 2005). Alternatively, in an indirect calculation, we carry out first the Fourier integral according to Eq. (134) and then use the following expression for the differential cross section

$$\frac{dQ_{if}^{\pm}}{d\Omega} = \left| i\mu v \int_0^{\infty} d\rho\, \rho^{1+2i\nu} J_{m_i-m_f}(2\mu v\rho \sin[\theta/2]) a_{if}^{\pm}(\rho) \right|^2 \times (a_0^2\ \mathrm{sr}^{-1}\ \mathrm{atom}^{-1}), \tag{136}$$

where θ is the scattering angle in the center-of-mass frame of reference. Here $J_\nu(z)$ is a Bessel function of the first order and the νth kind, whereas m_i and m_f are the magnetic quantum numbers of the initial and final bound state, respectively.

Calculation of the matrix elements for double-electron capture into the ground state $1s^2$ from any heliumlike atom has been carried out by Belkić and Mančev (1992). Their method of calculation provides the total cross sections $Q_{if}^{\pm}$ through four-dimensional integrals that are subsequently computed by utilizing the standard Gauss-Legendre and Gauss-Mehler quadratures (Abramowitz and Stegun, 1956; Press *et al.*, 1992). It can be verified that, in the symmetric resonant case ($i=f$, $Z_P=Z_T$), there is no post-prior discrepancy, i.e., $R_{if}^{-}=R_{if}^{+}$, so that we have $Q_{if}^{-}=Q_{if}^{+}$.

B. The BDW-4B method

The CDW-4B method takes full account of the Coulomb continuum intermediate states of electrons in both the entrance and exit channels. On the other hand, in the CB1-4B method, electrons are treated as being free in the intermediate stage of collision involving double-charge exchange. In other words, the CB1-4B method completely ignores these intermediate ionization electronic continua.

Double ionization dominates over double-charge exchange at high energies. Therefore, to properly describe electron transfer to a final bound state, in the limit of high energies, the electronic continuum intermediate states must be included, and this is fully accomplished in the CDW-4B method. At lower energies, however, charge exchange dominates over ionization. This time, the electronic continuum states represent a drawback, since they overweight the intermediate ionization paths of the studied reaction. Consequently, the CDW-4B method overestimates the corresponding experimental data at lower energies, as was also the case with the CDW-3B method (Belkić *et al.*, 1979).

Models that partially mitigate the overemphasis on continuum intermediate states at lower energies are certain hybrid approximations that combine the CDW-4B method in one channel with the CB1-4B method in the other channel. An example from this hybrid category is the BDW-4B method of Belkić (1994). Specifically, the BDW-4B method exactly coincides with the CDW-4B method in one channel and with the CB1-4B method in the other channel. As such, the BDW-4B method preserves the correct boundary conditions in both scattering channels, since both the CDW-4B and CB1-4B methods do so. Here the wave function given by Eq. (114), from the CDW-4B method, is employed for the entrance channel. We now determine the distorted wave χ_f^- in the exit channel. The boundary condition given by

$$\chi_f^- \underset{r_f\to\infty}{\to} \Psi_f^- \underset{r_f\to\infty}{\to} \Phi_f^- \tag{137}$$

suggests that χ_f^- should be determined in the following factorized form

$$\chi_f^- = \varphi_f(\vec{s}_1,\vec{s}_2)\zeta_f^-. \tag{138}$$

The equation from which we determine ζ_f^- reads as

$$\varphi_f^-(E-\epsilon_f-H_0)\zeta_f^- - W_f\varphi_f\zeta_f^- + \frac{1}{a}\sum_{k=1}^{2}\vec{\nabla}_{s_k}\varphi_f\cdot\vec{\nabla}_{s_k}\zeta_f^- = 0. \tag{139}$$

Here the term $\zeta_f^-(h_f-\epsilon_f)\varphi_f$ is neglected as in the CDW-4B method. The potential W_f is chosen as $W_f = Z_T(Z_P-2)/r_f$ which is the asymptotic form of the perturbation V_f in the exit channel (Belkić, 1994). Obviously, this choice of W_f implies that the function ζ_f^- will be independent of the electronic coordinates, in which case the coupling term $\vec{\nabla}\cdot\vec{\nabla}$ from Eq. (139) will become identical to zero. Consequently, the remaining equation $(E-\epsilon_f-H_0-W_f)\zeta_f^-=0$ can be solved exactly with the result

$$\chi_f^- = \mathcal{N}^-(\nu_f)e^{-i\vec{k}_f\vec{r}_f}\,{}_1F_1(i\nu_f,1,-ik_fr_i - i\vec{k}_f\cdot\vec{r}_i)\varphi_f(\vec{s}_1,\vec{s}_2), \tag{140}$$

where $\mathcal{N}^-(\nu_f)=e^{-\pi\nu_f/2}\Gamma(1-i\nu_f)$ and $\nu_f=Z_T(Z_P-2)/v$. In this way, we obtain a function which is identical to Eq. (31).

If we neglect the term with the total Green's function G^+ in the exact transition amplitude in Eq. (85), we obtain the following expression for the matrix element in the BDW-4B method (e.g., in the prior form)

$$T_{if}^{(\mathrm{BDW})-} = \langle\chi_f^-|V_i - W_i|\chi_i^+\rangle. \tag{141}$$

Inserting Eqs. (140), (103), and (114) into Eq. (141), it follows that

$$T_{if}^{(\mathrm{BDW})-} = -N_P \int\int\int d\vec{x}_1 d\vec{x}_2 d\vec{r}_i e^{i\vec{k}_i\cdot\vec{r}_i + i\vec{k}_f\cdot\vec{r}_f} \times \mathcal{L}_1^-(\vec{r}_i,\vec{r}_f)\varphi_f^*(\vec{s}_1,\vec{s}_2)\{{}_1F_1(i\nu_P,1,ivs_2+i\vec{v}\cdot\vec{s}_2) \times \vec{\nabla}_{x_1}\varphi_i(\vec{x}_1,\vec{x}_2)\cdot\vec{\nabla}_{s_1}\,{}_1F_1(i\nu_P,1,ivs_1+i\vec{v}\cdot\vec{s}_1) + {}_1F_1(i\nu_P,1,ivs_1+i\vec{v}\cdot\vec{s}_1)\vec{\nabla}_{x_2}\varphi_i(\vec{x}_1,\vec{x}_2) \cdot\vec{\nabla}_{s_2}\,{}_1F_1(i\nu_P,1,ivs_2+i\vec{v}\cdot\vec{s}_2)\}, \quad (142)$$

where $N_P=[N^+(\nu_P)]^2$ and $\xi_K=2\nu_K=2Z_K/v$ $(K=P,T)$ and

$$\mathcal{L}_1^-(\vec{r}_i,\vec{r}_f) = \frac{\mathcal{N}_1}{\mu_i^{2i\nu_P}}\,{}_1F_1(-i\nu,1,ik_ir_f+i\vec{k}_i\cdot\vec{r}_f) \times {}_1F_1(-i\nu_f,1,ik_fr_i+i\vec{k}_f\cdot\vec{r}_i),$$

with $\mathcal{N}_1=\mathcal{N}^+(\nu)\mathcal{N}^+(\nu_f)$ and $\nu=Z_PZ_T/v$. Within the eikonal approximation, the following simplification is possible

$$\mathcal{L}_1^-(\vec{r}_i,\vec{r}_f) \simeq \mu_i^{i\nu_i}\mu_f^{i\nu_f}e^{i\nu_f\ln(vR+\vec{v}\cdot\vec{R})}e^{i\nu\ln(vR-\vec{v}\cdot\vec{R})} \simeq \mu^{-i(\xi_P+\xi_T)}(\mu\rho v)^{2i\nu}e^{-i\xi_T\ln(vR+\vec{v}\cdot\vec{R})}. \quad (143)$$

Then the total cross section can be found from Eq. (130), with R_{if}^- replaced by $R_{if}^{(\mathrm{BDW})-}$ where

$$R_{if}^{(\mathrm{BDW})-}(\vec{\eta}) = -N_P\int\int\int d\vec{x}_1 d\vec{x}_2 d\vec{R}\varphi_f^*(\vec{s}_1,\vec{s}_2) \times e^{i\vec{q}_P\cdot(\vec{s}_1+\vec{s}_2)+i\vec{q}_T\cdot(\vec{x}_1+\vec{x}_2)}(vR+\vec{v}\cdot\vec{R})^{-i\xi_T} \times\{{}_1F_1(i\nu_P,1,ivs_2+i\vec{v}\cdot\vec{s}_2)\vec{\nabla}_{x_1}\varphi_i(\vec{x}_1,\vec{x}_2) \cdot\vec{\nabla}_{s_1}\,{}_1F_1(i\nu_P,1,ivs_1+i\vec{v}\cdot\vec{s}_1) + {}_1F_1(i\nu_P,1,ivs_1+i\vec{v}\cdot\vec{s}_1)\vec{\nabla}_{x_2}\varphi_i(\vec{x}_1,\vec{x}_2) \cdot\vec{\nabla}_{s_2}\,{}_1F_1(i\nu_P,1,ivs_2+i\vec{v}\cdot\vec{s}_2)\}. \quad (144)$$

An extension of the analysis to the post version of the formalism can also be accomplished. This time we choose the distorting potential in the form $W_i=Z_P(Z_T-2)/r_i$. This choice in the eikonal approximation gives the distorted waves χ_i^+ as

$$\chi_i^+ = \mathcal{N}^+(\nu_i)e^{i\vec{k}_i\cdot\vec{r}_i}\,{}_1F_1(-i\nu_i,1,ik_ir_f+i\vec{k}_i\cdot\vec{r}_f)\varphi_i(\vec{x}_1,\vec{x}_2). \quad (145)$$

In the exit channel, the potential U_f is chosen as in the CDW-4B method, i.e.,

$$U_f\chi_f^- = -\frac{1}{a}\sum_{k=1}^{2}\vec{\nabla}_{s_k}\varphi_f\cdot\vec{\nabla}_{x_k}\psi_f^-. \quad (146)$$

The distorted wave is given by $\chi_f^-=\varphi_f(\vec{s}_1,\vec{s}_2)\psi_f^-$, where the function ψ_f^- is determined by Eq. (126). The corresponding post form of the transition amplitude is obtained by neglecting the second term in Eq. (86), so that

$$T_{if}^{(\mathrm{BDW})+} = \langle\chi_f^-|V_f-W_f^\dagger|\chi_i^+\rangle = \langle\chi_f^-|U_f^\dagger|\chi_i^+\rangle. \quad (147)$$

Inserting Eqs. (145), (146), and (126) into (147), we have

$$T_{if}^{(\mathrm{BDW})+} = -N_T\int\int\int d\vec{s}_1 d\vec{s}_2 d\vec{r}_f e^{i\vec{k}_i\cdot\vec{r}_i+i\vec{k}_f\cdot\vec{r}_f}\mathcal{L}_2^+(\vec{r}_i,\vec{r}_f) \times\varphi_i(\vec{x}_1,\vec{x}_2)\{{}_1F_1(i\nu_T,1,ivx_2+i\vec{v}\cdot\vec{x}_2) \times\vec{\nabla}_{s_1}\varphi_f^*(\vec{s}_1,\vec{s}_2)\cdot\vec{\nabla}_{x_1}\,{}_1F_1(i\nu_T,1,ivx_1+i\vec{v}\cdot\vec{x}_1) + {}_1F_1(i\nu_T,1,ivx_1+i\vec{v}\cdot\vec{x}_1)\vec{\nabla}_{s_2}\varphi_f^*(\vec{s}_1,\vec{s}_2) \cdot\vec{\nabla}_{x_2}\,{}_1F_1(i\nu_T,1,ivx_2+i\vec{v}\cdot\vec{x}_2)\}, \quad (148)$$

$$\mathcal{L}_2^+(\vec{r}_i,\vec{r}_f) = \frac{\mathcal{N}_2}{\mu_f^{2i\nu_T}}{}_1F_1(-i\nu_i,1,ik_ir_f+i\vec{k}_i\cdot\vec{r}_f) \times{}_1F_1(-i\nu,1,ik_fr_i+i\vec{k}_f\cdot\vec{r}_i),$$

where $N_T=[N^{-*}(\nu_T)]^2$, $\mathcal{N}_2=\mathcal{N}^+(\nu_i)\mathcal{N}^+(\nu)$, and $\nu=Z_PZ_T/v$. The function $\mathcal{L}_2^+(\vec{r}_i,\vec{r}_f)$ can also be expressed in the eikonal approximation via

$$\mathcal{L}_2^+(\vec{r}_i,\vec{r}_f) \simeq \mu_i^{i\nu_i}\mu_f^{i\nu_f}e^{i\nu_i\ln(vR-\vec{v}\cdot\vec{R})}e^{i\nu\ln(vR+\vec{v}\cdot\vec{R})} \simeq \mu^{-i(\xi_P+\xi_T)}(\mu\rho v)^{2i\nu}e^{-i\xi_P\ln(vR-\vec{v}\cdot\vec{R})}. \quad (149)$$

Therefore, the total cross sections are given by

$$Q_{if}^{(\mathrm{BDW})\pm}(a_0^2) = \int d\vec{\eta}\left|\frac{R_{if}^{(\mathrm{BDW})\pm}(\vec{\eta})}{2\pi v}\right|^2, \quad (150)$$

$$R_{if}^{(\mathrm{BDW})+}(\vec{\eta}) = -N_T\int\int\int d\vec{s}_1 d\vec{s}_2 d\vec{R}\varphi_i(\vec{x}_1,\vec{x}_2) \times e^{i\vec{q}_P\cdot(\vec{s}_1+\vec{s}_2)+i\vec{q}_T\cdot(\vec{x}_1+\vec{x}_2)}(vR-\vec{v}\cdot\vec{R})^{-i\xi_P} \times\{{}_1F_1(i\nu_T,1,ivx_2+i\vec{v}\cdot\vec{x}_2)\vec{\nabla}_{s_1}\varphi_f^*(\vec{s}_1,\vec{s}_2) \cdot\vec{\nabla}_{x_1}\,{}_1F_1(i\nu_T,1,ivx_1+i\vec{v}\cdot\vec{x}_1) + {}_1F_1(i\nu_T,1,ivx_1+i\vec{v}\cdot\vec{x}_1)\vec{\nabla}_{s_2}\varphi_f^*(\vec{s}_1,\vec{s}_2) \cdot\vec{\nabla}_{x_2}\,{}_1F_1(i\nu_T,1,ivx_2+i\vec{v}\cdot\vec{x}_2)\}. \quad (151)$$

Notice that $R_{if}^{(\mathrm{BDW})-}$ can be obtained directly from $R_{if}^{(\mathrm{BDW})+}$ by making the transformations $\vec{s}_1\leftrightarrow\vec{s}_2$ and $\vec{x}_1\leftrightarrow\vec{x}_2$ in both Eqs. (144) and (151). This is possible because the vector $\vec{R}$ is invariant under this latter transformation. In such a case, these transformations will map the first of the two terms in $R_{if}^{(\mathrm{BDW})\pm}$ onto the second term, and vice versa. In other words, the contributions to $R_{if}^{(\mathrm{BDW})\pm}$ coming from $\vec{\nabla}_1\cdot\vec{\nabla}_1$ and $\vec{\nabla}_2\cdot\vec{\nabla}_2$ are identical to each other. Hence, these expressions can be rewritten as follows:

$$R_{if}^{(\mathrm{BDW})-}(\vec{\eta}) = -2N_P \int\int\int d\vec{x}_1 d\vec{x}_2 d\vec{R} \times e^{i\vec{q}_P\cdot(\vec{s}_1+\vec{s}_2)+i\vec{q}_T\cdot(\vec{x}_1+\vec{x}_2)} \times (vR+\vec{v}\cdot\vec{R})^{-i\xi_T}\varphi_f^*(\vec{s}_1,\vec{s}_2)F_P(\vec{s}_1,\vec{s}_2), \tag{152}$$

$$R_{if}^{(\mathrm{BDW})+}(\vec{\eta}) = -2N_T \int\int\int d\vec{s}_1 d\vec{s}_2 d\vec{R} \times e^{i\vec{q}_P\cdot(\vec{s}_1+\vec{s}_2)+i\vec{q}_T\cdot(\vec{x}_1+\vec{x}_2)} \times (vR-\vec{v}\cdot\vec{R})^{-i\xi_P}\varphi_i(\vec{x}_1,\vec{x}_2)F_T(\vec{x}_1,\vec{x}_2), \tag{153}$$

$$F_P(\vec{s}_1,\vec{s}_2) = {}_1F_1(i\nu_P,1,ivs_2+i\vec{v}\cdot\vec{s}_2)\vec{\nabla}_{x_1}\varphi_i(\vec{x}_1,\vec{x}_2) \cdot \vec{\nabla}_{s_1}\,{}_1F_1(i\nu_P,1,ivs_1+i\vec{v}\cdot\vec{s}_1), \tag{154}$$

$$F_T(\vec{x}_1,\vec{x}_2) = {}_1F_1(i\nu_T,1,ivx_2+i\vec{v}\cdot\vec{x}_2)\vec{\nabla}_{s_1}\varphi_f^*(\vec{s}_1,\vec{s}_2) \cdot \vec{\nabla}_{x_1}\,{}_1F_1(i\nu_T,1,ivx_1+i\vec{v}\cdot\vec{x}_1). \tag{155}$$

The prior form of the T-matrix element in the BDW-4B method can be physically interpreted in the following manner. The incident particle scatters on each of the three constituents of the target $(Z_T;e_1,e_2)$. In the entrance channel, a collision between the projectile Z_P and target nucleus Z_T results in accumulation of the Coulombic phase factor $\exp[(i/v)Z_PZ_T\ln(vR-\vec{v}\cdot\vec{R})]$. On the other hand, in the exit channel, the target nucleus Z_T interacts with the newly formed atom or ion $(Z_P,2e)_f$ considered as the point charge (Z_P-2), thus accumulating the phase factor $\exp[-(i/v)Z_T(Z_P-2)\ln(vR+\vec{v}\cdot\vec{R})]$ due to the asymptotic residual Coulombic interaction $W_f=Z_T(Z_P-2)/R$. Here no explicit electronic distortion factor is taken into account. In other words, the presence of the two electrons is felt by the target nucleus Z_T solely through the effect of screening the nuclear charge Z_P in the heliumlike atomic system $(Z_P,2e)_f$. In contrast, in the entrance channel, the BDW-4B method allows the projectile to separately distort the nuclear and electronic motions through the additive Coulombic interaction. Thus, the interaction of Z_P with electrons e_1 and e_2 leads to double ionization of the target $(Z_T,2e)_i$. The ionized electrons propagate in the Coulomb field of Z_P in a particular eikonal direction with momenta $\vec{\kappa}_1\approx\vec{\kappa}_2\approx\vec{v}$. Finally, capture of the two electrons occurs from these intermediate ionizing states (capture from continuum), because electrons are traveling with each other, as well as with the projectile, in the same direction, and the attractive potential between Z_P and e_j $(j=1,2)$ is sufficient to bind them together into the new heliumlike atomic system $(Z_P;e_1,e_2)_f$. This is a quantum version of the well-known Thomas classical double scattering. An analogous situation can also be pictured in the case of the post form $R_{if}^{(\mathrm{BDW})+}$ of the transition amplitude. Calculation of the matrix elements $R_{if}^{(\mathrm{BDW})\pm}$ has been done by Belkić (1994). He has shown that the BDW-4B method gives the matrix elements $R_{if}^{(\mathrm{BDW})\pm}$ in terms of four-dimensional real quadratures from 0 to 1, whereas for computations of the total cross sections five-dimensional quadratures are needed. It should be noted that the integrands in the prior and post forms have the functions $[\tau_j/(1-\tau_j)]^{i\nu_{P,T}}$ $(j=1,2)$ which originate from an integral representation of the two confluent hypergeometric functions. These functions possess integrable branch-point singularities at $\tau_{1,2}=0$ and 1, as well as the simple poles at points $\tau_{1,2}=0$. Therefore, Cauchy regularization of the whole integrand should be performed before applying the Gauss-Legendre quadratures (Belkić, 1994).

C. The BCIS-4B method

The BCIS-4B method has been formulated and implemented by Belkić (1993c). This approximation takes full account of the electronic continuum intermediate states in one channel (entrance or exit, depending upon whether the prior or post form of the transition amplitudes is considered). The transition amplitudes in the prior and post versions of the BCIS-4B method without the term $(\rho v)^{2iZ_PZ_T/v}$ are (Belkić, 1993c)

$$R_{if}^{(\mathrm{BCIS})-}(\vec{\eta}) = Z_PN_T \int\int\int d\vec{R}\, d\vec{s}_1 d\vec{s}_2 e^{i\vec{k}_i\cdot\vec{r}_i+i\vec{k}_f\cdot\vec{r}_f} \times (vR-\vec{v}\cdot\vec{R})^{-i\xi_P}\varphi_f^*(\vec{s}_1,\vec{s}_2)\left(\frac{2}{R}-\frac{1}{s_1}-\frac{1}{s_2}\right) \times \varphi_i(\vec{x}_1,\vec{x}_2)\,{}_1F_1(i\nu_T,1,ivx_1+i\vec{v}\cdot\vec{x}_1) \times {}_1F_1(i\nu_T,1,ivx_2+i\vec{v}\cdot\vec{x}_2), \tag{156}$$

$$R_{if}^{(\mathrm{BCIS})+}(\vec{\eta}) = Z_TN_P \int\int\int d\vec{R}\, d\vec{x}_1 d\vec{x}_2 e^{i\vec{k}_i\cdot\vec{r}_i+i\vec{k}_f\cdot\vec{r}_f} \times (vR+\vec{v}\cdot\vec{R})^{-i\xi_T}\varphi_f^*(\vec{s}_1,\vec{s}_2)\left(\frac{2}{R}-\frac{1}{x_1}-\frac{1}{x_2}\right) \times \varphi_i(\vec{x}_1,\vec{x}_2)\,{}_1F_1(i\nu_P,1,ivs_1+i\vec{v}\cdot\vec{s}_1) \times {}_1F_1(i\nu_P,1,ivs_2+i\vec{v}\cdot\vec{s}_2). \tag{157}$$

It should be noted that in $R_{if}^{(\mathrm{BCIS})\pm}$ the electronic continuum intermediate states are included in the same way as in $R_{if}^{(\mathrm{BDW})\mp}$. The essential difference between $R_{if}^{(\mathrm{BDW})\mp}$ and $R_{if}^{(\mathrm{BCIS})\pm}$ lies in the perturbation potentials. In $R_{if}^{(\mathrm{BCIS})\mp}(\vec{\eta})$, these potentials are given by the multiplicative operators $[Z_P(2/R-1/s_1-1/s_2)]$ and $[Z_T(2/R-1/x_1-1/x_2)]$, whereas in the case $R_{if}^{(\mathrm{BDW})\pm}(\vec{\eta})$ we have the typical gradient operator potentials

$$(1/a)\sum_{k=1}^{2}\vec{\nabla}_{s_k}\ln\varphi_f^*(\vec{s}_1,\vec{s}_2)\cdot\vec{\nabla}_{x_k}$$

and

$$(1/b)\sum_{k=1}^{2}\vec{\nabla}_{x_k}\ln\varphi_i(\vec{x}_1,\vec{x}_2)\cdot\vec{\nabla}_{s_k},$$

which are familiar from the CDW-4B method.

Two alternative methods have been developed by Belkić (1993c) for calculation of the required matrix elements. One of these gives the matrix elements $R_{if}^{\pm}(\vec{\eta})$ in terms of a three-dimensional integral over real variables from 0 to 1. The other method provides the basic quantities $R_{if}^{\pm}(\vec{\eta})$ in the form of four-dimensional numerical quadratures over real variables. Both methods have been found to give the same numerical results (Belkić, 1993c).

D. The CB1-4B method

Numerous investigations and comparisons with experiments have confirmed that the CB1-3B method is an accurate theory for rearrangement collisions at intermediate and high impact energies (Belkić, 1988b, 1989b; Belkić *et al.*, 1986; Belkić, Taylor, and Saini, 1986; Belkić *et al.*, 1987; Belkić and Taylor, 1987; Dewangan and Eichler, 1986). Therefore, it is reasonable to extend this approximation to four-body collisions with one or two active electrons. Such an extension for double capture has been done by Belkić (1993b) through the introduction of the CB1-4B method. The transition amplitudes in the CB1-4B method for double-charge exchange within the prior (T_{if}^{-}) and post (T_{if}^{+}) forms are given by

$$T_{if}^{-}=\langle\Phi_f^{-}|V_i^c|\Phi_i^{+}\rangle,\quad T_{if}^{+}=\langle\Phi_f^{-}|V_f^c|\Phi_i^{+}\rangle. \tag{158}$$

Here Φ_i^{+} and Φ_f^{-} are defined by Eqs. (15) and (32), whereas V_i^c and V_f^c are the same as in Eqs. (13) and (29), respectively. Explicitly, the transition amplitudes without the term $(\rho v)^{2iZ_PZ_T/v}$ are (Belkić, 1993b)

$$T_{if}^{\pm}(\vec{\eta})=\int d\vec{R}\,e^{\mp 2i\vec{q}_{P,T}\cdot\vec{R}}(vR+\vec{v}\cdot\vec{R})^{-i\xi}\mathcal{F}^{\pm}(\vec{R}), \tag{159}$$

$$\mathcal{F}^{-}(\vec{R})=Z_P\int\int d\vec{s}_1d\vec{s}_2\varphi_f^{*}(\vec{s}_1,\vec{s}_2)e^{-i\vec{v}\cdot(\vec{s}_1+\vec{s}_2)}\times\left(\frac{2}{R}-\frac{1}{s_1}-\frac{1}{s_2}\right)\varphi_i(\vec{x}_1,\vec{x}_2), \tag{160}$$

$$\mathcal{F}^{+}(\vec{R})=Z_T\int\int d\vec{x}_1d\vec{x}_2\varphi_f^{*}(\vec{s}_1,\vec{s}_2)e^{-i\vec{v}\cdot(\vec{x}_1+\vec{x}_2)}\times\left(\frac{2}{R}-\frac{1}{x_1}-\frac{1}{x_2}\right)\varphi_i(\vec{x}_1,\vec{x}_2). \tag{161}$$

Here, Eq. (33) and $\xi=2(Z_T-Z_P)/v$ are used together with the vectors $\vec{q}_T$ and $\vec{q}_P$ taken from Eq. (35). A complete calculation of the matrix elements $T_{if}^{\pm}(\vec{\eta})$, as a two-dimensional integral, has been performed by Belkić (1993b). The method used is general in the sense that it can be applied to heteronuclear (asymmetric) as well as homonuclear (symmetric) collisions in which double-charge exchange occurs. This has been substantiated for the symmetric He^{2+}-He collision, for which the algorithm of Belkić (1993b) reproduced exactly the results from the corresponding previous study (Belkić, 1993a). This cross-validation is important, since Belkić (1993a) presented a completely different way of calculating the matrix elements. It should be mentioned that a partial-wave analysis of the transition amplitude in the CB1-4B method has also been carried out for double-electron capture in collisions of alpha particles and helium (Gulyás and Szabo, 1994). If the necessary convergence over the partial waves has been achieved, the numerical results of Gulyás and Szabo (1994) would be the same as those obtained without the partial wave analysis. However, this is not the case, possibly due to only 3 partial waves retained in each of several summations, calling for a reinvestigation to clarify the disagreement.

E. Comparison between theories and experiments for double-electron capture

1. Double-electron capture into the ground state

We first analyze the total cross sections in the CDW-4B method for double electron capture from He by fast H^+ and He^{2+} ions

$$H^+ + He(1s^2)\rightarrow H^-(1s^2)+He^{2+}, \tag{162}$$

$$He^{2+}+He(1s^2)\rightarrow He(1s^2)+He^{2+}. \tag{163}$$

In order to investigate the sensitivity of the prior and post forms of the total cross sections to the choice of the ground-state wave functions for He and H^-, we employ four two-electron functions: (i) a one-parameter uncorrelated wave function (Hylleraas, 1929), (ii) a radially correlated two-parameter orbital (Silverman *et al.*, 1960), (iii) a three-parameter function (Green *et al.*, 1954), and (iv) a four-parameter function (Löwdin, 1953). As shown by Belkić and Mančev (1993), the post-prior discrepancy for reaction (162) for all four wave functions is within at most 40% at impact energies where the CDW-4B method is expected to be most adequate ($E\geqslant 100$ keV). In the case of the wave function of Löwdin (1953), the difference between the prior and post cross sections does not exceed 20% at $E\geqslant 100$ keV.

Comparison between the CDW-4B method and the available experimental data for reaction (162) is presented in Fig. 1. Only the prior cross sections obtained with the wave functions of Hylleraas (1929) and Löwdin (1953) are depicted in this figure. The corresponding results computed using the orbitals of Green *et al.* (1954) and Silverman *et al.* (1960) are not displayed in Fig. 1, since they are very close to those generated by means of the wave function of Löwdin (1953). The cross sections of the CDW-4B method are seen to be in excellent agreement with the measurement at impact energies $E\geqslant 100$ keV. The results of the first Born approximation (Gerasimenko, 1961), also given in Fig. 1, are about three orders of magnitude larger than the experimental data. The corresponding results from the three-state two-center close coupling method (Lin, 1979) consider-

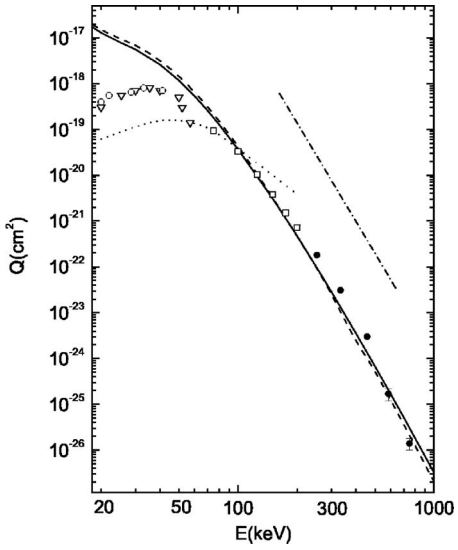

FIG. 1. Total cross sections $Q(\mathrm{cm}^2)$ for double-charge exchange in the collisional reaction $H^+ + He(1s^2) \rightarrow H^-(1s^2) + He^{2+}$. Theory: solid curve: the CDW-4B method (Belkić and Mančev, 1992) [the wave functions of Löwdin (1953)]; dashed curve: the CDW-4B method (Belkić and Mančev, 1992) [the wave functions of Hylleraas (1929)]; dotted curve: the three-state two-center close coupling approximation of Lin (1979), and singly chained curve: the first Born approximation (Gerasimenko, 1961). Experimental data: ● (Schryber, 1967), □ (Toburen and Nakai, 1969), ▽ (Fogel *et al.*, 1958), and ○ (Williams, 1966).

ably underestimate the associated measured values at lower energies ($E \leqslant 45$ keV), with precisely the reversed pattern above 120 keV.

We conclude that, in the case of reaction (162) at impact energies $E \geqslant 100$ keV, the CDW-4B method is relatively weakly dependent upon the choice of the bound-state wave functions of Hylleraas (1929), Löwdin (1953), Green *et al.* (1954), and Silverman *et al.* (1960). Hence, the simplest one-parameter orbital of Hylleraas (1929) can confidently be used in subsequent applications regarding reaction (162). At energies $E \geqslant 100$ keV, where the CDW-4B method is assessed to be the most adequate, the prior and post cross sections are in satisfactory mutual agreement and, furthermore, they provide an adequate interpretation of the existing experimental data on the H^+-He double-charge exchange.

The results of the CDW-4B method (Belkić, 1994; Belkić *et al.*, 1994) for reaction (163) are shown in Table I and Fig. 2. There is no post-prior discrepancy for this reaction, so that $Q_{if}^- = Q_{if}^+ \equiv Q_{if}$. It can be observed from Table I that the dependence of the total cross sections for the He^{2+}-He collisions upon the bound-state wave functions is weak and, therefore, quite similar to that in the H^+-He collisions.

In Fig. 2 we give the total cross sections for process (163) obtained using the CB1-4B, CDW-4B≡CDW-4B1, CDW-4B2, BDW-4B, and BCIS-4B methods. This time the results for total cross sections from the CDW-4B1 method (Belkić, 1994; Belkić *et al.*, 1994) do not reproduce most of the experimental data, except those at the two largest energies 4 and 6 MeV. One of the inadequacies of the CDW-4B1 method is the use of unnormalized total scattering wave functions in both the entrance and exit channels. Of course, the same drawback of the CDW-3B method is also encountered for single-charge exchange (Crothers, 1982), but without significant consequences at impact energies satisfying the usual validity condition (Belkić *et al.*, 1979)

$$\text{incident energy } E \text{ (keV/amu)} \geqslant 80 \max\{|\epsilon_i|, |\epsilon_f|\}, \tag{164}$$

where ϵ_i and ϵ_f are the initial and final orbital energies of the captured electron, respectively.[2] This discrepancy may indicate that the same type of inadequacies invoked in theories of rearrangement collisions could be more serious for double- than for single-charge exchange. Total cross sections for high-energy two-electron transfer are smaller than the corresponding results for one-

TABLE I. The total cross sections $Q_{if}^-(\mathrm{cm}^2) = Q_{if}^+(\mathrm{cm}^2) \equiv Q_{if}(\mathrm{cm}^2)$ for double-charge exchange: $He^{2+} + He(1s^2) \rightarrow He(1s^2) + He^{2+}$ computed by means of the CDW-4B method (Belkić, 1994; Belkić *et al.*, 1994), utilizing the wave functions of Hylleraas (1929), Löwdin (1953), Green *et al.* (1954), and Silverman *et al.* (1960) for both the initial and final states.

	Q_{if} (cm²)			
E (keV)	Hylleraas	Silverman	Green	Löwdin
100	5.31[−16]	6.07[−16]	5.58[−16]	5.49[−16]
200	4.28[−17]	4.50[−17]	4.37[−17]	4.28[−17]
300	8.18[−18]	8.11[−18]	8.19[−18]	7.99[−18]
400	2.25[−18]	2.14[−18]	2.23[−18]	2.17[−18]
500	7.70[−19]	7.08[−19]	7.54[−19]	7.33[−19]
600	3.03[−19]	2.72[−19]	2.95[−19]	2.86[−19]
700	1.33[−19]	1.17[−19]	1.28[−19]	1.25[−19]
800	6.32[−20]	5.44[−20]	6.06[−20]	5.88[−20]
900	3.21[−20]	2.72[−20]	3.06[−20]	2.97[−20]
1000	1.72[−20]	1.44[−20]	1.63[−20]	1.58[−20]
1250	4.34[−21]	3.54[−21]	4.09[−21]	3.98[−21]
1500	1.34[−21]	1.07[−21]	1.26[−21]	1.23[−21]
1750	4.81[−22]	3.79[−22]	4.53[−22]	4.40[−22]
2000	1.93[−22]	1.50[−22]	1.83[−22]	1.78[−22]
2500	4.01[−23]	3.08[−23]	3.92[−23]	3.80[−23]
3000	1.06[−23]	8.11[−24]	1.09[−23]	1.05[−23]
3500	3.37[−24]	2.56[−24]	3.62[−24]	3.74[−24]
4000	1.22[−24]	9.29[−25]	1.39[−24]	1.32[−24]
5000	2.17[−25]	1.65[−25]	2.72[−25]	2.55[−25]
6000	5.10[−26]	3.89[−26]	7.06[−26]	6.51[−26]
7000	1.46[−26]	1.12[−26]	2.21[−26]	2.01[−26]

[2]According to (164), the expected limit of the validity of the CDW-4B method for a He^{2+} projectile is 0.45 MeV, whereas for Li^{3+} impact it is above 2 MeV and for a B^{5+} projectile it is above 9.7 MeV.

electron capture by at least two orders of magnitude. Therefore, it is not surprising that double-charge exchange, a much weaker effect than single-electron transfer, appears to be very sensitive to any, even apparently small, inadequacies of the theory. Nevertheless, this normalization problem is not expected to be the main cause for the lack of agreement between the CDW-4B1 method and experiment below 4 MeV in Fig. 2. This could be inferred from the work of Martínez *et al.* (1999). Their results from the CDW-EIS-4B≡CDW-EIS-4B1 method (which uses the normalized eikonal scattering wave function in the entrance channel) underestimate both the experiments and the CDW-4B1 method for the same process (163) (not shown to avoid clutter).

An alternative reason for the fact that the CDW-4B1 method is satisfactory only at the highest energies (4 and 6 MeV) in Fig. 2 could be the neglect of the second-order contribution from a perturbation series. Indeed, when the first-order contribution from the CDW-4B1 method is augmented by the inclusion of an approximate on-shell second-order term in the transition matrix element (Martínez *et al.*, 1999), the ensuing CDW-4B2 method yields cross sections that agree favorably with most of the available experimental data in Fig. 2, except at 4 and 6 MeV (precisely the reverse pattern relative to the CDW-4B1 method). However, using the four-body continuum distorted wave eikonal initial state method (Martínez *et al.*, 1999), the same procedure of adding an approximate on-shell second-order term to the contribution from the CDW-EIS-4B1 method yields the CDW-EIS–4B2 method, which gave the results that overestimate both the cross sections of the CDW-4B2 method and the experimental data for the process (163). More precisely, Fig. 2 from Martínez *et al.* (1999) shows that throughout the interval 100–6000 keV, $Q_{if}^{(\mathrm{CDW-EIS-4B1})}$ largely underestimates the experimental data. For example, this underestimation is within 2–3 orders of magnitude in the range 100–2000 keV, which is well within the expected validity domain of this method. On the other hand, in the same Fig. 2 from Martínez *et al.* (1999), $Q_{if}^{(\mathrm{CDW-EIS-4B2})}$ is seen to overestimate considerably all the available experimental data in the whole range 100–6000 keV. In particular, at energies 100–1000 keV, the values of the ratio $Q_{if}^{(\mathrm{CDW-EIS-4B2})}/Q_{if}^{(\mathrm{CDW-EIS-4B1})}$ are enormous, ranging from 10^3 to 10^4 (Martínez *et al.*, 1999). Previously, the same on-shell Green's propagator for a second-order contribution has also been used within the IA by Gravielle and Miraglia (1992) for the process (163). They omitted the first-order IA, without showing that this ignored term is indeed negligible. Moreover, such an omission is not supported by the CDW-4B2 method, which contains a significant contribution from the corresponding first-order term provided by the CDW-4B1 method, as seen via the singly chained and dashed curves in Fig. 2. Here it is pertinent to recall that the IA for three- and four-body collisions does not obey the correct boundary conditions. This latter drawback has been rectified by Belkić with the emergence of the RIA-3B and RIA-4B

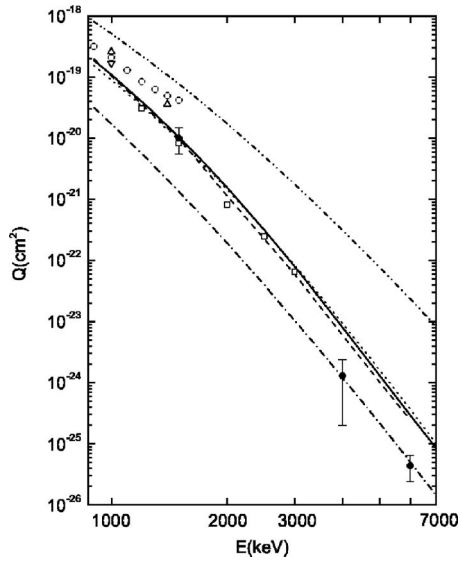

FIG. 2. Total cross sections, as a function of the incident energy E(keV) for reaction (163). The theoretical curves relate only to the transition $1s^2 \rightarrow 1s^2$. Doubly-chained curve: the CB1-4B method (Belkić, 1993a, 1993b); solid curve: the BCIS-4B method (Belkić, 1993c); dotted curve: the BDW-4B method (Belkić, 1994); singly chained curve: the CDW-4B1 method (Belkić, 1994); dashed curve: the CDW-4B2 method (Martínez *et al.*, 1999). All computations are performed by using the one-parameter Hylleraas (1929) orbital for the initial and final states of helium. Experimental data: ○ (Pivovar *et al.*, 1962), △ (McDaniel *et al.*, 1977), ▽ (DuBois, 1987), □ (de Castro Faria *et al.*, 1988), and ● (Schuch *et al.*, 1991).

(Belkić, 1995, 1996; Mergel *et al.*, 1997). Overall, it is physically plausible that the second-order term in a perturbation expansion could play an important role for double- relative to single-electron capture due to the two actively participating electrons in the former process. This is evidenced by large differences between the CDW-4B1 and CDW-4B2 methods, on the one hand, and between the CDW-EIS-4B1 and CDW-EIS-4B2 methods, on the other hand. These initial assessments of the second-order terms in a perturbation series are encouraging. Nevertheless, it would be important to extend such computations by including both on- and off-shell second-order contributions in the CDW-4B2 and CDW-EIS-4B2 methods for the process (163). Furthermore, it would be indispensable to assess the convergence rate in the spectral representation of the Green function from a second-order propagator. This latter spectral representation from Martínez *et al.* (1999) is inconclusive, as it includes only the two hydrogenlike ground states centered on the projectile and target nucleus, without the necessary assessment of the contribution from any of the other, ignored intermediate states.

Further, as can be seen from Fig. 2, the BCIS-4B and BDW-4B methods yield similar values for the displayed total cross sections. These two approximations use normalized scattering wave functions in one channel. The total cross sections from the BCIS-4B and BDW-4B

methods are much smaller than those from the CB1-4B method throughout the energy range under consideration. For example, the difference between the findings of the BDW-4B and CB1-4B methods increases as the impact energy is augmented, reaching two orders of magnitude at 6 MeV. Importantly, the BDW-4B and BCIS-4B methods are in good agreement with most of the available experimental data even without any second-order term from a distorted-wave series. At the two largest energies (4 and 6 MeV), the BDW-4B and BCIS-4B methods overestimate the measurement.

It is also instructive to consider the IPM for reaction (163). According to the IPM, the transition amplitude for double-electron capture is given as a product of the amplitudes for single-electron capture. The differential cross section for double-electron capture in the IPM is given by

$$\frac{dQ_{if}^{(\mathrm{CDW\text{-}IPM})}}{d\Omega} = \left| iv\mu \int_0^\infty d\rho\, \rho^{1+2i\nu} [a_{if}^{(\mathrm{CDW\text{-}3B})}(\rho)]^2 \times J_0(\eta\rho) \right|^2 \left(\frac{a_0^2}{sr}\right), \tag{165}$$

where $a_{if}^{(\mathrm{CDW\text{-}3B})}(\rho)$ is the transition amplitude as a function of ρ in the CDW-3B method (Belkić *et al.*, 1979; Cheshire, 1964) for single-electron capture. The explicit expression for $a_{if}^{(\mathrm{CDW\text{-}3B})}(\rho)$ can be found in the work of Belkić and Salin (1978). The total cross sections $Q_{if}^{(\mathrm{CDW\text{-}IPM})}$ are computed from Eq. (165) by standard integration over ρ in the interval $[0,\infty]$. The results obtained are shown in Table II. These results are in satisfactory agreement with measurements in the energy range 0.9–7 MeV (not shown on Fig. 2 to avoid clutter). Additional computations have been performed in the CDW-IPM using the Hylleraas wave function (Hylleraas, 1929) for the final bound state φ_f and the orbital of the Roothan-Hartree-Fock (RHF) model (Huzinaga, 1961; Roothaan, 1951, 1960) for φ_i, which is expressed in an analytical form (Clementi and Roetti, 1974). These results, denoted by $Q_{if}^{(\mathrm{CDW\text{-}IPM)(ii)}}$, are shown in Table II together with the cross sections $Q_{if}^{(\mathrm{CDW\text{-}IPM)(i)}}$ computed by means of the orbital of Hylleraas (1929) for both the initial and final bound states. It can be seen from this comparison that at lower and intermediate energies 100–1000 keV the results for $Q_{if}^{(\mathrm{CDW\text{-}IPM)(ii)}}$ are smaller than those for $Q_{if}^{(\mathrm{CDW\text{-}IPM)(i)}}$ by a factor $\gamma' = Q_{if}^{(\mathrm{CDW\text{-}IPM)(ii)}} / Q_{if}^{(\mathrm{CDW\text{-}IPM)(i)}}$ ranging in the interval [0.90,0.52] (see the fourth column in Table II). Such a pattern is precisely reversed at higher energies from 1 to 7 MeV at which $\gamma' = 0.90$–1.65. The difference between columns (i) and (ii) from Table II is a well-known consequence of electronic correlations. Radial correlations are abundantly present in the RHF orbital (Clementi and Roetti, 1974), whereas they are ignored in the Hylleraas wave function. The IPM and the related independent-event model (IEM) completely ignore the dynamic correlation effects that make double-charge exchange fundamentally different from single-electron transfer. Nevertheless, both the IPM and IEM can be amended by incorporating static correlations. This has been shown by Crothers and McCarroll (1987) who used the IEM within the CDW method (as denoted by CDW-IEM) to study double-electron capture in the He^{2+}-He collisions. They included static electron correlation effects in the target through the wave function of Pluvinage (1950) with the explicit appearance of the interelectronic r_{12} coordinate. Deco and Grün (1991) used the CDW-IPM with target static correlation effects included by means of the configuration interaction (CI) wave functions.

TABLE II. Theoretical total cross sections $Q_{if}^{(\mathrm{CDW\text{-}IPM})}$ (cm^2) as a function of the incident energy E (keV) for double-charge exchange (163) computed using the CDW-IPM (Belkić *et al.*, 1994). The results in column (i) stem from the orbital of Hylleraas (1929) for both the initial and final bound states of helium, whereas those in column (ii) are based upon the Hylleraas wave function for φ_f and the RHF orbital of Clementi and Roetti (1974) for φ_i. The fourth column is the ratio of the numbers in columns (ii) and (i).

	$Q_{if}^{(\mathrm{CDW\text{-}IPM})}$ (cm^2)		
E (keV)	(i)	(ii)	(ii)/(i)
100	4.75[−14]	2.48[−14]	0.52
200	2.00[−15]	1.36[−15]	0.68
300	2.67[−16]	1.98[−16]	0.74
400	5.78[−17]	4.49[−17]	0.78
500	1.64[−17]	1.32[−17]	0.80
600	5.58[−18]	4.61[−18]	0.83
700	2.15[−18]	1.82[−18]	0.85
800	9.15[−19]	7.91[−19]	0.86
900	4.19[−19]	3.70[−19]	0.88
1000	2.05[−19]	1.84[−19]	0.90
1500	1.08[−20]	1.07[−20]	0.99
2000	1.12[−21]	1.20[−21]	1.07
3000	3.68[−23]	4.50[−23]	1.22
4000	2.81[−24]	3.81[−24]	1.36
5000	3.55[−25]	5.21[−25]	1.47
6000	6.29[−26]	9.84[−26]	1.56
7000	1.42[−26]	2.34[−26]	1.65

2. Double-electron capture into excited states

The prediction of the contributions from excited states requires a convenient description of singly and doubly excited states of a heliumlike atom (ion). One possibility is to describe the final state $\varphi_f(\vec{s}_1,\vec{s}_2)$ by means of configuration interactions. For these CI functions, the procedure to calculate the bound-free form factors as the matrix elements in the CDW-4B method has previously been devised by Belkić and Mančev (1992) in a general manner, which is applicable to both the ground and excited states of heliumlike systems. This can be done by employing a basis set of monoelectronic functions such as Slater-type orbitals (STOs) or hydrogenlike

orbitals with a nuclear charge Z_P (Bachau, 1984; Gayet *et al.*, 1996). Such functions are particularly convenient for describing singly or doubly excited states. When the final state is autoionizing, only the bound component of $\varphi_f(\vec{s}_1,\vec{s}_2)$ is kept, since its decay occurs much after the collision has been completed. The use of these CI wave functions (Bachau, 1984) within the said procedure of Belkić and Mančev (1992) for bound-free form factors facilitates the calculation of the matrix elements for the transition amplitude for double-electron capture into excited states (Gayet *et al.*, 1996). These latter calculations were restricted to singly excited states $(1s,nl)$ with $n \leqslant 3$ and $l \leqslant n-1$ and doubly excited states $(2l,2l')$ with $l,l' \leqslant 1$. Although other singly excited states should be included, this procedure provides a good indication of the contribution from excited states relative to the ground state.

The scattering integrals that appear in the calculation with excited states are of the type considered by Nordsieck (1954). Explicit methods that bypass the cumbersome and implicit differentiation for calculating the most general cases of these scalar and vectorial bound-free form factors were developed in parabolic coordinates (Belkić, 1981, 1983) as well as in spherical ones (Belkić, 1992).

Total cross sections in the CDW-4B method for double-electron capture from He by He^{2+} including several excited states have been reported by Gayet *et al.* (1996). These results are based upon the wave function of Löwdin (1953) for helium in the entrance channel and the CI wave function (Bachau, 1984) for the final state in the exit channel. From the outset, capture into excited states is not expected to play a significant role in process (163), because of the dominance of the ground- to ground-state transition, which is resonant. The explicit computations of Gayet *et al.* (1996) confirm this expectation; the sum from all considered final bound states of helium is very close to the singly chained curve in Fig. 2 from the CDW-4B method for the ground- to ground-state transition alone. For example, at incident energies 1, 2, and 5 MeV, the total cross sections (in cm^2) from the ground- to ground-state transition (with the sum of this contribution and the corresponding yield from the excited states written in parentheses) are $1.48\times10^{-20}(1.97\times10^{-20})$, $1.89\times10^{-22}(2.33\times10^{-22})$, and $3.25\times10^{-25}(3.60\times10^{-25})$, respectively. Moreover, the cross sections due to doubly excited states are smaller than those for singly excited ones, especially at high impact energies (Gayet *et al.*, 1996; Purkait *et al.*, 2006).

The CDW-4B method used by Gayet *et al.* (1996) has also been applied to double-electron capture in the Li^{3+}-He and B^{5+}-He collisions. Here, as anticipated, contributions from the excited states are important (see Figs. 3 and 4). This occurs because the ground- to ground-state transitions for the Li^{3+}-He and B^{5+}-He double-charge exchange are nonresonant and, therefore, excited states could yield a sizable contribution. At smaller impact energies, the main contribution to the total cross section originates from singly excited states, while the ground states $(1s^2)^1S$ provide about 40% of the total cross section. In all cases, the difference be-

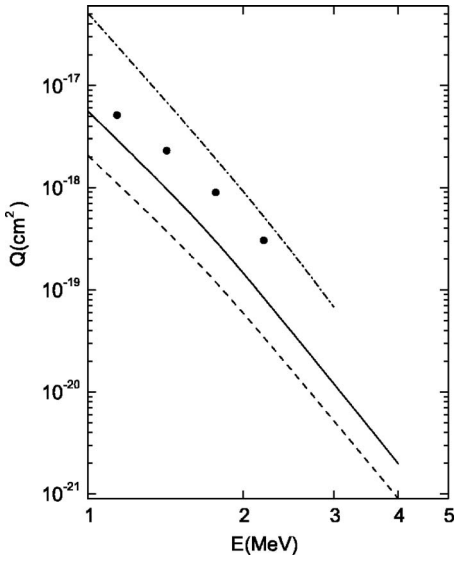

FIG. 3. Total cross sections Q (cm^2) in the CDW-4B method for the reaction $Li^{3+}+He(1s^2)\rightarrow Li^{+}(\Sigma)+He^{2+}$ as a function of the incident energy. The solid curve corresponds to double-electron capture into the ground and all singly excited states, whereas the dashed curve corresponds to double-electron capture into the ground state only (Gayet *et al.*, 1996). The upper singly chained curve corresponds to the results from the CDW-IPM for double-electron capture into all states (Gayet *et al.*, 1994a). Experimental data: ● (Shah and Gilbody, 1985).

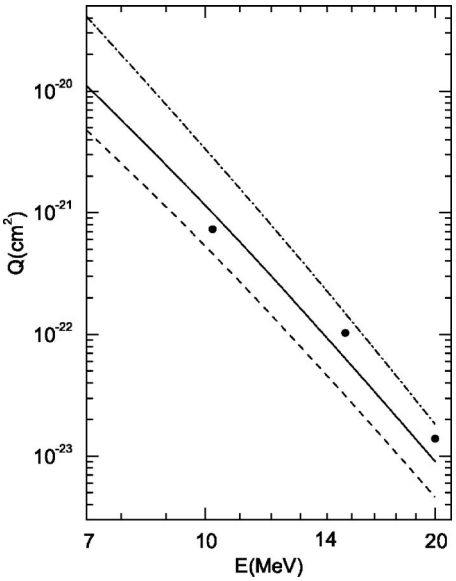

FIG. 4. Total cross sections Q (cm^2) in the CDW-4B method for the reaction $B^{5+}+He(1s^2)\rightarrow B^{3+}(\Sigma)+He^{2+}$ as a function of the incident energy. The solid curve corresponds to double-electron capture into the ground and all singly excited states, whereas the dashed curve corresponds to double-electron capture into the ground state only (Gayet *et al.*, 1996). The upper singly chained curve represents the results from the CDW-IPM for double-electron capture into all states (Gayet *et al.*, 1994a). Experimental data: ● (Hippler *et al.*, 1987).

tween the cross sections for the ground state and the singly excited states diminishes with the increased impact energy. It is clear that the ground-state contribution dominates at very high impact energies. The cross sections for double-excited-state formation are one order of magnitude smaller than the cross sections for single-excited-state formation in the investigated energy range. Furthermore, for the Li^{3+}-He and B^{5+}-He collisions, the contributions from the states $(1s3s)^1S$ and $(1s3p)^1P$ become of the order of (or even significantly larger than) the ones from the states $(1s2s)^1S$ and $(1s2p)^1P$ in the considered energy region (Gayet *et al.*, 1996). The results from the CDW-IPM (Gayet *et al.*, 1994a) are also shown in Figs. 3 and 4. These results correspond to double-electron capture into all final states of the projectile, and they are seen to overestimate the experimental data.

The main goal of this subsection is to assess the contribution of excited states. It is found that they can be important, provided that the investigated transitions are nonresonant when the target is in the ground state. Moreover, the inclusion of excited states into the computation can significantly improve agreement between the CDW-4B method and the experimental data, as in the case of the Li^{3+}-He and B^{5+}-He collisions (Gayet *et al.*, 1994a). However, this is not the case for the He^{2+}-He collisions (Gayet *et al.*, 1994a), since the ground- to ground-state transition in process (163) is dominant due to resonance. Note that for the formation of H^- in the H^+-He double-charge exchange (Belkić and Mančev, 1992, 1993) there are no excited states in the exit channel. Hence, it can be concluded that the CDW-4B1 method provides reliable predictions for double-electron capture at intermediate and high impact energies for the H^+-He, Li^{3+}-He, and B^{5+}-He collisions, but not for the He^{2+}-He collisions, for which an approximate version of the CDW-4B2 method yields good agreement with experiments (see Fig. 2).

It should be noted that the CDW-4B method can also be used with multiparameter highly correlated wave functions, such as those of Byron and Joachain (1966), Joachain and Vanderpoorten (1970), or Tweed (1972) that include a number of CI terms ranging from 12 to 108. These latter orbitals are capable of including most of the radial and angular correlations, despite the fact that they do not explicitly contain the interelectronic coordinate $\vec{r}_{12}$. The wave functions of Joachain and Terao (1991) and Tweed (1972) have been used by Belkić (1997a, 1997b, 2001, 2004, 2007) for single-electron detachment in the H^+-H^- collisions treated within the four-body distorted-wave formalism.

In order to illustrate the validity of the presented distorted-wave approximations, we also analyze the differential cross sections for double-electron capture in collisions between the He^{2+} ions and He atoms for reaction (163) at $E=1.5$ MeV. As stated, for this symmetric and resonant process there is no post-prior discrepancy. The differential cross sections obtained using the BDW-4B method are shown in Fig. 5, where a comparison is made with the CB1-4B and BCIS-4B methods, as

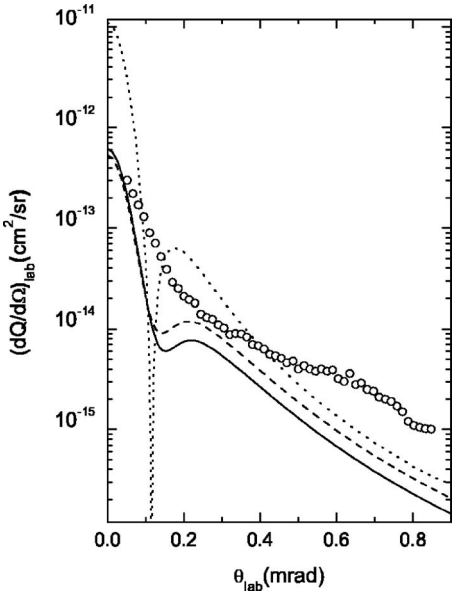

FIG. 5. Differential cross sections $dQ/d\Omega \equiv (dQ/d\Omega)_{\rm lab}$ (cm^2/sr) as a function of the scattering angle $\theta_{\rm lab}$ for reaction (163) at incident energy $E=1.5$ MeV. The computations relate only to the $1s^2 \rightarrow 1s^2$ transition. Theoretical results: (i) solid curve: the BDW-4B method (Belkić *et al.*, 1994); (ii) dashed curve: the BCIS-4B method (Belkić, 1993c); (iii) dotted curve: the CB1-4B method (Belkić, 1993a, 1993b). All computations have been performed using the one-parameter Hylleraas wave function for the initial and final bound states of helium. The computed cross sections are not convolved with the experimental resolution function. Experimental data (including double-electron capture into all bound states of helium): ○ (Schuch *et al.*, 1991).

well as with the existing experimental data (Schuch *et al.*, 1991). The CB1-4B, BDW-4B, and BCIS-4B methods exhibit the proper asymptotic behavior at large interaggregate separations in both the entrance and exit channels. However, unlike the CB1-4B method, the BDW-4B and BCIS-4B methods take full account of the Coulomb continuum intermediate states of both electrons in one channel. Hence, by comparing these two theories with the CB1-4B method, one could learn about the relative importance of the intermediate electronic ionization continua. As seen from Fig. 5, the CB1-4B method exhibits an unphysical and experimentally unobserved dip at $\theta_{\rm lab} \simeq 0.112$ mrad. This extremely sharp dip is due to strong cancellation of the opposite contributions coming from the repulsive $(2Z_K/R)$ and attractive $(-Z_K/\omega_1 - Z_K/\omega_2)$ potentials in Eqs. (160) and (161), where $\omega_j = s_j$ or $\omega_j = x_j$, $j=1,2$ $(K=P,T)$. In a narrow cone near the forward direction, the cross sections in the CB1-4B method greatly overestimate the experimental findings. On the other hand, the BCIS-4B method of Belkić (1993c) provides a substantial improvement over the CB1-4B method. First, in the BCIS-4B method, the dip in the angular distribution disappears and near the dip region the angular distribution exhibits only a minimum at $\theta_{\rm lab} \simeq 0.121$ mrad, followed by a neighboring broader maximum, despite the fact that the same pertur-

bation potential is used as in the CB1-4B method. The behavior of the angular distribution obtained in the BDW-4B method is altogether quite similar to that in the BCIS-4B method.

It should be recalled that the BDW-4B and BCIS-4B methods differ only in the perturbation potentials, such that the former contains the scalar product of the two gradient operators, whereas the latter uses the difference of the Coulomb potentials. As can be seen from Fig. 5, the overall agreement of the BDW-4B and the BCIS-4B methods with the experimental data can be considered fairly good. Nevertheless, at larger scattering angles, despite the proper inclusion of the Rutherford scattering, both the BDW-4B and BCIS-4B methods yield differential cross sections that are considerably lower than the corresponding experimental data (Schuch *et al.*, 1991). Note that the measured findings relate to double-electron capture into all states of He, whereas the considered theories account only for the ground- to ground-state transition ($1s^2 \rightarrow 1s^2$). The main purpose of Fig. 5 is to demonstrate the influence of electronic intermediate ionization continua onto the differential cross sections by direct comparison with the results from the presented four-body theories. None of the theoretical data displayed in Fig. 5 are folded with the experimental resolution function. Using Eq. (165), Belkić *et al.* (1994) computed differential cross sections in the CDW-IPM for reaction (163). Their results are in good agreement with the experimental data at small and intermediate scattering angles (not shown in Fig. 5 to avoid clutter). At larger values of θ, this model underestimates the measurement. The latter theoretical results show some undulations in the angular distribution at larger scattering angles (Belkić *et al.*, 1994).

At sufficiently high impact energies, it should be possible to predict three maxima in the differential double-capture cross section resulting from different higher-order contributions as anticipated by Belkić *et al.* (1994). Applying purely classical arguments, one expects to find the customary Thomas double-scattering peak at the angle $\theta_{\rm lab}^{(1)}=(1/M_P)\sin 60^\circ=(1/M_P)\sqrt{3}/2 \approx 0.118$ mrad$=0.0068^\circ$. This peak corresponds to two consecutive events: (i) one electron is captured through the direct first-order mechanism, and (ii) the other electron is captured through the Thomas double scattering. The next similar structure should occur at the angle $\theta_{\rm lab}^{(2)}=2\theta_{\rm lab}^{(1)}=(2/M_P)\sin 60^\circ=(1/M_P)\sqrt{3}\approx 0.236$ mrad$=0.0136^\circ$. In this case, when both electrons are treated classically, they are supposed to be in the same place at the same time to exhibit the cumulative Thomas double scattering. Each electron first scatters elastically on the projectile through 60° toward its parent nucleus. Subsequent scattering of each electron on the target nucleus is also elastic through the next 60°. The two electrons are then ejected from the target with the velocity of the projectile in the incident beam direction. Then the attractive potential between Z_P and $2e$ suffices to bind these three particles together. These two Thomas peaks have also been analyzed by Martínez *et al.* (1994) within the IPM version of the CDW-EIS method. Their theoretical results for differential cross sections at 400 MeV show the appearance of the structures at $\theta_{\rm lab}^{(1)}$ and $\theta_{\rm lab}^{(2)}$, associated with the mentioned intermediate double-scattering processes.

The third peak can be expected at the angle $\theta_{\rm lab}^{(3)}=(1/M_P)\sqrt{2}\ \sin 45^\circ=(1/M_P)\approx 0.136$ mrad$=0.0078^\circ$, which is situated between $\theta_{\rm lab}^{(1)}$ and $\theta_{\rm lab}^{(2)}$. This time one electron (say, e_1) is first scattered on the projectile through 45° toward the other electron e_2, acquiring velocity $v_1=v\sqrt{2}$. Then, e_1 collides with e_2 elastically and finds itself deflected through another 45° in the incident beam direction with velocity $v_1'=v$. The consequence of such an event on e_2 is manifested in the recoil of this second electron with speed $v_2=v$ through 90° perpendicular to the incident direction. In the final step, e_2 scatters elastically on the target nucleus through another 90° with velocity $v_2'=v$ in the projectile direction. Then both electrons travel in the incident beam direction and are, therefore, captured by the projectile. This event, producing the peak at $\theta_{\rm lab}^{(3)}$, represents a genuine third-order effect. The peak at $\theta_{\rm lab}^{(3)}$ is a pure four-body effect due to dynamic interelectron correlations. Since these latter correlations are absent from the IPM, the peak at $\theta_{\rm lab}^{(3)}$ has not been obtained by Martínez *et al.* (1994) in the mentioned IPM variant of the CDW-EIS method. In order to adequately describe these higher-order phenomena, it would be most appropriate to use the CB2-4B or CB3-4B method. In particular, the CB3-4B method would encounter multidimensional numerical quadratures that could be optimally computed by the Monte Carlo algorithm VEGAS (Belkić, 1995, 1996, 2001, 2004).

New experimental findings are required at higher impact energies to provide a check of these theoretically predicted peaks in the angular distributions. In addition to the experimental results at 1.5 MeV that represent the first measurement of differential cross sections for double-electron capture in the He^{2+}-He collisions, there are also state-selective differential cross sections for the same reaction at energies 0.25–0.75 MeV (Dörner *et al.*, 1998, 2000) obtained using a technique known as COLTRIMS (cold-target recoil-ion-momentum spectroscopy). The same COLTRIMS technique has also been used to measure differential cross sections at impact energies ranging from 0.75 to 1.5 MeV/amu (Dörner, 2005). The COLTRIMS technique offers a unique, albeit indirect, but nevertheless extremely precise way to determine the final state of the projectile, including its scattering angles. Instead of the energy losses and scattering angles of the projectile itself, COLTRIMS determines simultaneously the longitudinal and transverse momenta of the recoil ion (He^{2+}). Since there are only two particles in the final state, the momentum change of the projectile must be compensated exactly by the momentum change of the recoil ion. Thus analyzing the longitudinal momentum (in the beam direction) of the recoil ion is equivalent to the customary translational spectroscopy of the projectile. Moreover, determination

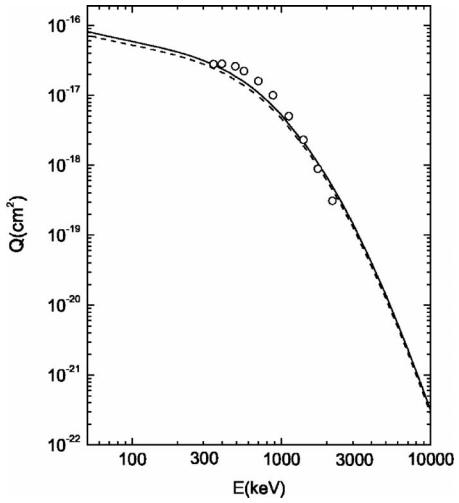

FIG. 6. Total cross sections Q (cm^2) as a function of laboratory incident energy E (keV) for double-charge exchange in the reaction $^7Li^{3+}+{}^4He(1s^2)\rightarrow{}^7Li^{+}+{}^4He^{2+}$. The theoretical curves relate only to the $1s^2\rightarrow 1s^2$ transition. Both the initial and final heliumlike bound states are described by the one-parameter orbital of Hylleraas (1929). The CB1-4B method: the prior Q_{if}^{-} and the post Q_{if}^{+} total cross sections are represented by the dashed and solid curves, respectively (Belkić, 1993b). Experimental data (including double-electron capture into all bound states of Li^+): ○ (Shah and Gilbody, 1985).

of the recoil-ion transverse momentum is equivalent to measuring the scattering angle of the projectile. Although the scattering angle resolution achieved is better than 10^{-5} rad (Dörner *et al.*, 1998, 2000), no structure from the Thomas-type mechanisms has been found. However, higher impact energies than those considered by Dörner *et al.* (1998, 2000) seem to be necessary to detect these Thomas peaks unambiguously in the measurements.

Further, we display the results of Belkić (1993b) obtained by means of the CB1-4B method for the following asymmetric reaction

$$^7Li^{3+}+{}^4He(1s^2)\rightarrow{}^7Li^{+}(1s^2)+{}^4He^{2+}. \tag{166}$$

These results for the total cross sections in both the post and prior versions are depicted in Fig. 6. As can be seen from this figure, the post cross sections are slightly larger than the prior ones. The post-prior discrepancy appears to be somewhat more pronounced at lower than at higher energies. A comparison between the CB1-4B method and the experimental data (Shah and Gilbody, 1985) is also shown in Fig. 6. The results from the CB1-4B method are in satisfactory agreement with the experimental data. Thus, considering only the $1s^2\rightarrow 1s^2$ transition, the CB1–4B method compares more favorably with the measurement than the corresponding CDW-4B method, as evidenced by Figs. 3 and 6. The total cross sections reported by Purkait *et al.* (2006) for process (166) are close to the results from the CB1-4B method and the experimental data from Fig. 6. Nevertheless, this needs to be reassessed by taking into account the final excited states, since they have been neglected by both Belkić (1993c) and Purkait *et al.* (2006). Gayet *et al.* (1994b) have also studied process (166). They used the first-order CDW-EIS-4B method at impact energies 700–5000 keV, but their total cross sections underestimate the experimental data from Fig. 6 by two orders of magnitude [not shown here; see Fig. 2 from Gayet *et al.* (1994b)]. This fact and a similar observation, which we have already made for process (163), indicate that the CDW-EIS-4B method is inadequate for double-electron capture in heavy particle collisions.

IV. SIMULTANEOUS TRANSFER AND IONIZATION

A. The CDW-4B method

In this section we consider a process called transfer ionization, where simultaneous electron capture and ionization take place

$$Z_P+(Z_T;e_1,e_2)_i\rightarrow(Z_P,e_1)_{f_1}+Z_T+e_2(\vec{\kappa}). \tag{167}$$

Here the analysis of the entrance channel is the same as for the corresponding double-electron capture. Therefore, we need to focus only on the exit channel for reaction (167). To this end we first determine the distorted wave ξ_f^- satisfying the following equation (Belkić *et al.*, 1997a)

$$(E-H+V_x-i\epsilon)|\xi_f^-\rangle=-(i\epsilon-V_x)|\chi_f^-\rangle, \tag{168}$$

which is obtained from Eq. (97). Choosing the intermediate channel potential V_x in such a way that the constraint

$$V_x|\chi_f^-\rangle=0 \tag{169}$$

is automatically satisfied, we have in the limit $\epsilon\rightarrow 0^+$

$$(E-H+V_x)|\xi_f^-\rangle=0. \tag{170}$$

Writing ξ_f^- in a factored form similar to the case of χ_i^+,

$$\xi_f^-=\varphi_{f_1}\mathcal{G}_f^-, \tag{171}$$

we arrive at

$$\mathcal{G}_f^-(\epsilon_f-H_0-V_P)\varphi_{f_1}+\varphi_{f_1}(E-\epsilon_f-H_0-V_f)\mathcal{G}_f^- +\frac{1}{a_1}\vec{\nabla}_{s_1}\varphi_{f_1}\cdot\vec{\nabla}_{x_1}\mathcal{G}_f^-+V_x\xi_f^-=0, \tag{172}$$

where $a_1=M_P/(M_P+1)$. This equation can be solved without any further approximation if the model potential V_x is chosen according to (Belkić *et al.*, 1997a)

$$V_x=Z_P\left(\frac{1}{R}-\frac{1}{s_2}\right)-\left(\frac{1}{x_1}-\frac{1}{r_{12}}\right)-\frac{1}{a_1}\vec{\nabla}_{s_1}\varphi_{f_1}\cdot\vec{\nabla}_{x_1}\circ\frac{1}{\varphi_{f_1}}. \tag{173}$$

Hence, using the mass limit $M_{P,T}\gg 1$, Eq. (172) is reduced to

$$\left(E-\epsilon_f-H_0+\frac{Z_T-1}{x_1}+\frac{Z_T}{x_2}-\frac{Z_P(Z_T-1)}{r_i}\right)\mathcal{G}_f^-=0, \tag{174}$$

where the independent variables are separated, and this permits the exact solution. The possible nodes of φ_{f_1} would render V_x singular in Eq. (173). In order to bypass this difficulty, we introduce the symbol $\circ$ in Eq. (173) to indicate that V_x acts only on those functions that contain φ_{f_1} in the factored form, as exemplified by Eq. (171). In other words, symbol $\circ$ determines the domain of the definition of operator V_x, which is allowed to act only on a subspace of the complete Hilbert space containing wave functions with a factored hydrogenlike bound state φ_{f_1}. This will be the case if we seek $\mathcal{G}_f^-$ in a factored form, such as

$$\mathcal{G}_f^-=C_f^-\varphi_{\vec{q}_1}^-(\vec{x}_1)\varphi_{\vec{q}_2}^-(\vec{x}_2)\varphi_{\vec{q}_i}^-(\vec{r}_i), \tag{175}$$

$$\varphi_{\vec{q}_1}^-(\vec{x}_1)=\Gamma(1+i\nu_T')e^{\pi\nu_T'/2+i\vec{q}_1\cdot\vec{x}_1}\times{}_1F_1(-i\nu_T',1,-iq_1x_1-i\vec{q}_1\cdot\vec{x}_1), \tag{176}$$

$$\varphi_{\vec{q}_2}^-(\vec{x}_2)=\Gamma(1+i\zeta')e^{\pi\zeta'/2+i\vec{q}_2\cdot\vec{x}_2}\times{}_1F_1(-i\zeta',1,-iq_2x_2-i\vec{q}_2\cdot\vec{x}_2), \tag{177}$$

$$\varphi_{\vec{q}_i}^-(\vec{r}_i)=\Gamma(1-i\nu'')e^{-\pi\nu''/2+i\vec{q}_i\cdot\vec{r}_i}\times{}_1F_1(i\nu'',1,-iq_ir_i-i\vec{q}_i\cdot\vec{r}_i), \tag{178}$$

where C_f^- is a constant, $\nu_T'=(Z_T-1)a_1/q_1$, $\zeta'=Z_Ta_2/q_2$, $\nu''=Z_P(Z_T-1)\mu_i/q_i$, and $a_2=a_1=M_P/(M_P+1)$. The unknown vectors $\vec{q}_1$, $\vec{q}_2$, and $\vec{q}_i$ can be determined by imposing the required simultaneous constraints

$$E-\epsilon_f=\frac{q_1^2}{2a_1}+\frac{q_2^2}{2a_2}+\frac{q_i^2}{2\mu_i}, \tag{179}$$

$$\vec{q}_1\cdot\vec{x}_1+\vec{q}_2\cdot\vec{x}_2+\vec{q}_i\cdot\vec{r}_i=-\vec{k}_f\cdot\vec{r}_f+\vec{\kappa}\cdot\vec{x}_2. \tag{180}$$

Then, Eqs. (179) and (180) together with the relation $\vec{r}_f=-a\vec{r}_i-b(\vec{x}_1+\vec{x}_2)/\mu_f$, where $a=M_P/(M_P+2)$, $b=M_T/(M_T+2)$, as well as the mass limit $M_{P,T}\gg1$, lead to

$$\vec{q}_1=\frac{a}{\mu_f}\vec{k}_f\simeq\frac{1}{\mu_f}\vec{k}_f\simeq\vec{v},$$

$$\vec{q}_2=\frac{a}{\mu_f}\vec{k}_f+\vec{\kappa}\simeq\frac{1}{\mu_f}\vec{k}_f+\vec{\kappa}\simeq\vec{p},\quad \vec{q}_i=a\vec{k}_f\simeq\vec{k}_f, \tag{181}$$

where

$$\vec{p}=\vec{v}+\vec{\kappa}. \tag{182}$$

In this way, the distorted wave $\xi_f^-=\varphi_{f_1}\mathcal{G}_f^-$ is obtained as

$$\xi_f^-=N^-(\zeta)N^-(\nu_T)\mathcal{N}^-(\nu)\phi_f\varphi_P(\vec{s}_1)\times{}_1F_1(-i\zeta,1,-ipx_2-i\vec{p}\cdot\vec{x}_2)\times{}_1F_1(-i\nu_T,1,-ivx_1-i\vec{v}\cdot\vec{x}_1)\times{}_1F_1(i\nu,1,-ik_fr_i-i\vec{k}_f\cdot\vec{r}_i),\quad \nu=Z_P\nu_T, \tag{183}$$

where the function ϕ_f is defined by Eq. (47) and $N^-(\zeta)=\Gamma(1+i\zeta)e^{\pi\zeta/2}$, $N^-(\nu_T)=\Gamma(1+i\nu_T)e^{\pi\nu_T/2}$, and $\zeta=Z_T/p$ with $\nu_T=(Z_T-1)/v$. Using Eqs. (104), (115), and (183), the expression for the prior form of the transition amplitude $T_{if}^-=\langle\xi_f^-|U_i|\chi_i^+\rangle$ becomes

$$\begin{aligned}T_{if}^-&=N_{PT}\int\int\int d\vec{R}\,d\vec{s}_1d\vec{s}_2e^{i\vec{\alpha}\cdot\vec{s}_1+i\vec{\beta}\cdot\vec{x}_1-i\vec{\kappa}\cdot\vec{x}_2}\\&\quad\times R_\nu(\vec{r}_i,\vec{r}_f)\varphi_P^*(\vec{s}_1){}_1F_1(i\nu_T,1,ivx_1+i\vec{v}\cdot\vec{x}_1)\\&\quad\times{}_1F_1(i\zeta,1,ipx_2+i\vec{p}\cdot\vec{x}_2)[Z_P(1/R-1/s_2)\\&\quad\times{}_1F_1(i\nu_P,1,ivs_1+i\vec{v}\cdot\vec{s}_1)\varphi_i(\vec{x}_1,\vec{x}_2)\\&\quad-\vec{\nabla}_{x_1}\varphi_i(\vec{x}_1,\vec{x}_2)\cdot\vec{\nabla}_{s_1}{}_1F_1(i\nu_P,1,ivs_1+i\vec{v}\cdot\vec{s}_1)\\&\quad-{}_1F_1(i\nu_P,1,ivs_1+i\vec{v}\cdot\vec{s}_1)O_{\varphi_i}(\vec{x}_1,\vec{x}_2)]\\&\equiv T_{if;\nu}^-(\vec{\eta}),\end{aligned} \tag{184}$$

where the auxiliary function $O_{\varphi_i}(\vec{x}_1,\vec{x}_2)$ is given by $(\epsilon_i-h_i)\varphi_i\equiv O_{\varphi_i}(\vec{x}_1,\vec{x}_2)\equiv O_{\varphi_i}$ and

$$R_\nu(\vec{r}_i,\vec{r}_f)=\mathcal{N}^{-*}(\nu)\mathcal{N}^+(\nu){}_1F_1(-i\nu,1,ik_fr_i+i\vec{k}_f\cdot\vec{r}_i)\times{}_1F_1(-i\nu,1,ik_ir_f+i\vec{k}_i\cdot\vec{r}_f), \tag{185}$$

$$\vec{\alpha}=\vec{\eta}-\left(\frac{v}{2}-\frac{\epsilon_i-\epsilon_f-E_\kappa}{v}\right)\hat{\vec{v}},$$

$$\vec{\beta}=-\vec{\eta}-\left(\frac{v}{2}+\frac{\epsilon_i-\epsilon_f-E_\kappa}{v}\right)\hat{\vec{v}}, \tag{186}$$

with $N_{PT}=(2\pi)^{-3/2}N^+(\nu_P)N^{-*}(\nu_T)N^{-*}(\zeta)$ and $E_\kappa=\kappa^2/2$. In Eq. (184), we used the relation $\vec{k}_i\cdot\vec{r}_i+\vec{k}_f\cdot\vec{r}_f=\vec{\alpha}\cdot\vec{s}_1+\vec{\beta}\cdot\vec{x}_1$. The difference $\epsilon_i-(\epsilon_f+E_\kappa)\equiv\tilde{Q}$ from Eqs. (186) between the initial and final electronic energies is also known as the inelasticity factor, or the $\tilde{Q}$ factor (this is more commonly known as the Q factor, but we use the label $\tilde{Q}$ instead, in order to avoid confusion with cross sections that are presently denoted by Q). This observable is of key importance for translational spectroscopy, which through measurement of the inelasticity factor determines the energy gain or loss of the scattered projectiles.

By analogy, the post form of the transition amplitude T_{if}^+ can be derived with the final result (Belkić *et al.*, 1997a)

$$\begin{aligned}T_{if}^+&=N_{PT}\int\int\int d\vec{R}\,d\vec{x}_1d\vec{x}_2e^{i\vec{\alpha}\cdot\vec{s}_1+i\vec{\beta}\cdot\vec{x}_1-i\vec{\kappa}\cdot\vec{x}_2}\\&\quad\times R_\nu(\vec{r}_i,\vec{r}_f)\varphi_i(\vec{x}_1,\vec{x}_2){}_1F_1(i\nu_P,1,ivs_1+i\vec{v}\cdot\vec{s}_1)\\&\quad\times{}_1F_1(i\zeta,1,ipx_2+i\vec{p}\cdot\vec{x}_2)\{[Z_P(1/R-1/s_2)\\&\quad+(1/r_{12}-1/x_1)]{}_1F_1(i\nu_T,1,ivx_1+i\vec{v}\cdot\vec{x}_1)\varphi_f^*(\vec{s}_1)\\&\quad-\vec{\nabla}_{s_1}\varphi_f^*(\vec{s}_1)\cdot\vec{\nabla}_{x_1}{}_1F_1(i\nu_T,1,ivx_1+i\vec{v}\cdot\vec{x}_1)\}\end{aligned}$$

$$\equiv T^{+}_{if;\nu}(\vec{\eta}). \tag{187}$$

Here an important simplification can be made, similarly to Eq. (129), for double-electron capture, by using the following eikonal approximation

$$R_{\nu}(\vec{r}_i,\vec{r}_f) \simeq (\mu\rho v)^{2i\nu}. \tag{188}$$

As before, it can be shown that the phase factor $(\mu\rho v)^{2i\nu}=(\mu\rho v)^{2iZ_P(Z_T-1)/v}$ does not contribute to the total cross sections $Q^{\pm}_{if}$. The triple-differential cross sections for simultaneous transfer and ionization can be obtained from

$$Q^{\pm}_{if}(\vec{\kappa}) \equiv \frac{d^3Q^{\pm}_{if}}{d\vec{\kappa}} = \int d\vec{\eta}\left|\frac{T^{\pm}_{if;\nu}(\vec{\eta})}{2\pi v}\right|^2 = \int d\vec{\eta}\left|\frac{T^{\pm}_{if;0}(\vec{\eta})}{2\pi v}\right|^2$$
$$= \int d\vec{\eta}|\mathcal{T}_{if}(\vec{\eta})|^2, \tag{189}$$

$$\mathcal{T}^{\pm}_{if}(\vec{\eta}) = \frac{T^{\pm}_{if;0}(\vec{\eta})}{2\pi v}, \tag{190}$$

so that the corresponding total cross sections are given by

$$Q^{\pm}_{if} = \int d\vec{\kappa} Q^{\pm}_{if}(\vec{\kappa}). \tag{191}$$

In the above derivation of the transition amplitudes in the CDW-4B method, the ionized electron e_2 is described by the Coulomb wave

$$\varphi^{-}_{\vec{\kappa}}(\vec{x}_2) \equiv N^{-}(\zeta)\phi_{\vec{\kappa}}(\vec{x}_2)\,{}_1F_1(-i\zeta,1,-ipx_2-i\vec{p}\cdot\vec{x}_2),$$

$$\phi_{\vec{\kappa}}(\vec{x}_2) = (2\pi)^{-3/2}e^{i\vec{\kappa}\cdot\vec{x}_2},$$

where $\vec{p}=\vec{\kappa}+\vec{v}$, as in Eq. (182). Even though the appropriate starting ansatz in the undistorted scattering state Φ_f is given by the plane wave $\phi_{\vec{\kappa}}(\vec{x}_2)$ centered on T, the present four-body analysis establishes a distortion of $\phi_{\vec{\kappa}}(\vec{x}_2)$ via function $N^{-}(\zeta)\,{}_1F_1(-i\zeta,1,-ipx_2-i\vec{p}\cdot\vec{x}_2)$. This is a function of the composite electron momentum $\vec{\kappa}+\vec{v}\equiv\vec{p}$, and not merely of $\vec{\kappa}$, which one would expect in the corresponding standard first Born approximation. The presence of the vector $\vec{v}$ in the momentum of the ejected electron has physical meaning, which points to the possibility of a description of the so-called electron capture to continuum (ECC) with a characteristic cusp in the emission spectra as has been observed experimentally in the TI process for the He^{2+}–He collisions (Sarkadi *et al.*, 2001). Different choices have been made in the literature for the wave function of the final state of the emitted electron. For example, in the case of ionization of helium by ion impact, this function has been defined as the product of the e-P continuum state with the e–residual-target continuum state (Fainstein *et al.*, 1987, 1988). As such, the fields of P and T act simultaneously on the electron ejected from helium (the two-center problem), as in the study of Belkić (1978) in the first application of the CDW-3B method to ionization of atomic hydrogen by protons. Note that the final-state wave function of the electron ejected from helium can contain explicitly the interelectron distance (Pedlow *et al.*, 2005). Overall, multiple continua represent the main difficulty in the TI process, since a proper description of the final state for the ejected electron requires the simultaneous influence of the Coulomb potentials due to the projectile, target, and captured electron to be taken into account.

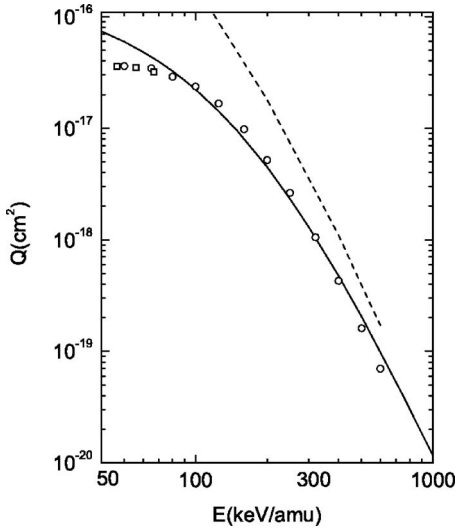

FIG. 7. Total cross sections $Q(\mathrm{cm}^2)$ as a function of the laboratory incident energy $E(\mathrm{keV/amu})$ for transfer ionization $^4He^{2+}+{}^4He(1s^2)\rightarrow{}^4He^{+}(1s)+{}^4He^{2+}+e$. The solid curve represents the post total cross section of the CDW-4B method (Belkić *et al.*, 1997a). The dashed curve represents the post cross sections of the CDW-IEM (Dunseath and Crothers, 1991). Experimental data: □ (Shah *et al.*, 1989) and ○ (Shah and Gilbody, 1985).

The presented prior and post forms T^{-}_{if} and T^{+}_{if} have a common perturbation $V_P(R,s_2)=Z_P(1/R-1/s_2)$. Of course, considered outside the T matrix, the potential $V_{P_2}=-Z_P/s_2$ represents the direct Coulomb interaction between e_2 and Z_P. Its asymptotic value $V^{\infty}_{P_2}(R)$ at large distances s_2 is given by $-Z_P/R$, since $s_2\rightarrow R$ as $R\rightarrow\infty$. Hence, the term $V_P(R,s_2)$ is precisely the difference between the asymptotic and finite values of the same potential, $V_P(R,s_2)=V^{\infty}_{P_2}(R)-V_{P_2}(s_2)$. As such, $V_P(R,s_2)$ is a short-range interaction, in accordance with the correct boundary condition. However, when placed in the T matrices (184) or (187), the potential V_{P_2} plays the role of a perturbation, which causes the capture of the electron e_1. This could occur only through some kind of underlying correlation between e_2 and e_1. For example, a part of the energy received by the electron e_2 in its collision with Z_P could be sufficient to accomplish transfer of e_1 to the projectile. The post form T^{+}_{if} contains an additional term

$$\Delta V_{12} = \frac{1}{r_{12}} - \frac{1}{x_1}, \tag{192}$$

which is completely absent from T^{-}_{if}. Through ΔV_{12} the dielectronic interaction $1/r_{12}$ appears explicitly in Eq.

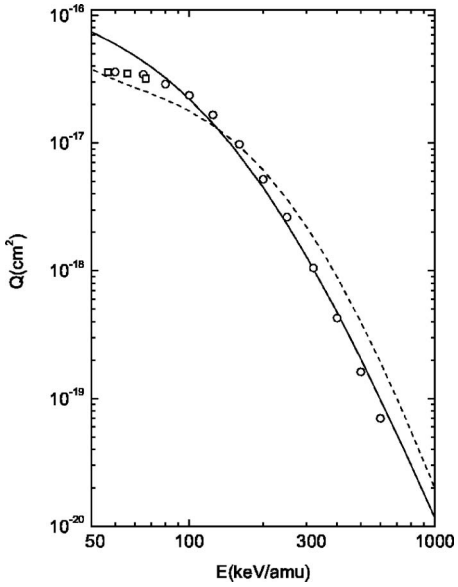

FIG. 8. Total cross sections $Q(\mathrm{cm}^2)$ as a function of laboratory incident energy E (keV/amu) for transfer ionization $^4\mathrm{He}^{2+}+{}^4\mathrm{He}(1s^2)\rightarrow{}^4\mathrm{He}^+(1s)+{}^4\mathrm{He}^{2+}+e$. The solid and dashed curves correspond, respectively, to the post and prior cross sections of the CDW-4B method (Belkić *et al.*, 1997a). Experimental data: □ (Shah *et al.*, 1989) and ○ (Shah and Gilbody, 1985).

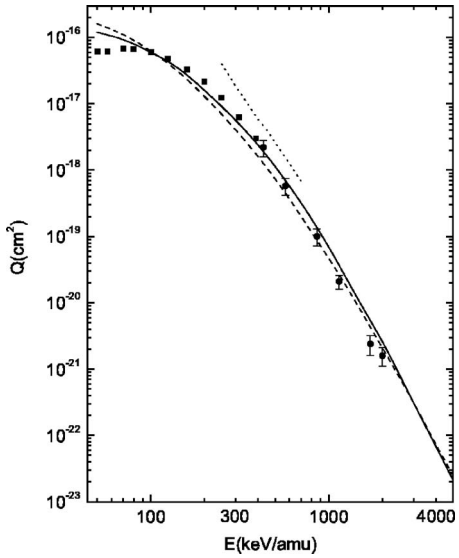

FIG. 9. Total cross sections Q (cm^2) as a function of the laboratory incident energy E (keV/amu) for the reaction $\mathrm{Li}^{3+}+\mathrm{He}\rightarrow\mathrm{Li}^{2+}+\mathrm{He}^{2+}+e$. The solid and dashed curves represent, respectively, the prior Q_{if}^{-} and post Q_{if}^{+} cross sections of the CDW-4B method (Mančev, 2001) with the complete perturbation potentials. The dotted curve represents a quantum field method of the second order (Bhattacharyya *et al.*, 1988). Experimental data: ■ (Shah and Gilbody, 1985) and ● (Woitke *et al.*, 1998).

(187). In combination with the initial and final distorted functions on both centers Z_P and Z_T, this dielectronic interaction describes the Thomas P-e-e scattering. Due to the perturbation ΔV_{12}, the cross section in the post form should be more adequate than its prior counterpart. The calculation of the matrix elements for TI has been carried out by Belkić *et al.* (1997a). The total cross sections in the CDW-4B method for transfer ionization are given in terms of seven-dimensional integrals over the real variables. The number of integration points is gradually and systematically increased until convergence to two decimal places has been reached (Belkić *et al.*, 1997a).

B. Comparison between theories and experiments for transfer ionization

To illustrate the validity of the CDW-4B method of Belkić *et al.* (1997a) for the TI process, we examine the total cross sections for the following symmetric reaction

$$\mathrm{He}^{2+}+\mathrm{He}(1s^2)\rightarrow\mathrm{He}^+(1s)+\mathrm{He}^{2+}+e. \tag{193}$$

We also review asymmetric transfer ionization which has subsequently been studied by Mančev (2001) for the reaction

$$\mathrm{Li}^{3+}+\mathrm{He}(1s^2)\rightarrow\mathrm{Li}^{2+}(1s)+\mathrm{He}^{2+}+e. \tag{194}$$

The results for process (193) in the energy interval from 50 to 1000 keV/amu are displayed in Figs. 7 and 8. In Fig. 7, a comparison is made between the CDW-4B method (Belkić *et al.*, 1997a) and CDW-IEM (Dunseath and Crothers, 1991). From a numerical point of view the CDW-IEM also encounters similar seven-dimensional quadratures when dealing with the total cross sections for a TI process. The main difference between the CDW-IEM and CDW-4B method is in the electron correlation treatment. The CDW-IEM includes the static-electron correlations (SEC) in the target using the bound-state wave function of Pluvinage (1950)

$$\varphi_i(\vec{x}_1,\vec{x}_2)=c(k)\frac{Z_T^3}{\pi}e^{-Z_T(x_1+x_2)}e^{-ikr_{12}}\times{}_1F_1(1-i\eta',2,2ikr_{12}), \tag{195}$$

where $r_{12}=|\vec{x}_1-\vec{x}_2|$, $\eta'=1/(2k)$, and $c(k)$ is the normalization constant, with k being a nonlinear variational parameter. The corresponding lowest binding energy $\epsilon_{i,\mathrm{Pluv}}=-2.878$ for the ground state ^1S of helium is obtained for $k=0.41$, in which case $c(k)=0.603\,366$. The wave function (195) contains two entirely uncorrelated hydrogenlike wave functions with the unscreened charge Z_T multiplied with a corrective r_{12}-dependent term of the form $\exp(-ikr_{12})\,{}_1F_1(1-i\eta',2,2ikr_{12})$. Another wave function of helium (Rodriguez and Gasaneo, 2005) might also be useful here, with the continuum wave function for the e-e interaction replaced by a simpler ansatz, which seems equally adequate as that of Pluvinage.

In the CDW-IEM (Dunseath and Crothers, 1991), dynamic electron correlations (DEC) are completely neglected, whereas the CDW-4B method explicitly includes the DEC through the dielectronic interaction $1/r_{12}$ in the transition T operator. It should be noted that the SEC can also be fully included in the CDW-4B

method using the corresponding wave function, but it is ignored in the present illustrations with the purpose of providing an unambiguous assessment of the DEC alone. The relative role of the SEC and DEC is otherwise apparent from the two curves associated with the CDW-IEM and CDW-4B method displayed in Fig. 7. A comparison of these two theories with the experimental data in Fig. 7 clearly shows that the CDW-4B method represents a substantial improvement over the CDW-IEM. It can be concluded that the DEC plays a more important role than the SEC for TI in process (193).

Further, we evaluate the post-prior discrepancy which arises from the unequal perturbation potentials used in the T matrices (184) and (187). In Fig. 8, we display the prior (Q_{if}^{-}) and post (Q_{if}^{+}) cross sections of the CDW-4B method (Belkić *et al.*, 1997a). The prior results in this figure do not include the correction O_{φ_i}, which has been shown by Belkić *et al.* (1997a) to be negligibly small. The comparison in Fig. 8 reveals that the post-prior discrepancy is significant throughout the energy range 50–1000 keV/amu. The post cross sections are larger by nearly 50% than the prior results at lower energies, with precisely the opposite pattern at higher energies. Such a considerable difference can be attributed to the role of the dielectronic repulsion $1/r_{12}$. We recall that the difference between Q_{if}^{-} and Q_{if}^{+} is due solely to the potential $\Delta V_{12}=1/r_{12}-1/x_1$, which is present in the post and absent from the prior cross sections. Also in Fig. 8 the theoretical cross sections are compared with the experimental data for reaction (193). It can be seen from Fig. 8 that, in contrast to the prior variant Q_{if}^{-}, the post version Q_{if}^{+} of the CDW-4B method is in good agreement with the measurements at impact energies $E \geqslant 80$ keV/amu. At lower energies, the results for Q_{if}^{+} are larger than the experimental values, as expected, since the CDW-4B method is a high-energy approximation. The superiority of the post over the prior version can be attributed to the electron-electron interaction $1/r_{12}$ in the perturbation U_f of the former variant.

The post and prior total cross sections for TI in reaction (194), derived with the full perturbations are plotted in Fig. 9, where the experimental findings (Shah and Gilbody, 1985; Woitke *et al.*, 1998) are also displayed. The CDW-4B method used by Mančev (2001) is found to be in good agreement with the experimental data. The post cross sections lie below the prior ones at impact energies between 100 and 3000 keV/amu, with the reverse behavior above 3000 keV/amu. These computations have been performed for electron transfer to the ground state. Comparison between the CDW-4B method and measurements especially at lower impact energies needs to be reassessed by including a contribution from all excited states. The theoretical results of Bhattacharyya *et al.* (1988) are also depicted in Fig. 9. Their cross sections have been obtained using a relativistically covariant field approach via the second-order Feynman diagrams. As can be seen from Fig. 9, the results from Bhattacharyya *et al.* (1988) greatly overestimate the experimental data.

As shown by Mančev (2001), the prior total cross sections computed with and without the term $V_P(R,s_2)$ differ from each other by a considerable amount which can reach 67% at 50–5000 keV/amu. The potential $-Z_P/s_2$ from $V_P(R,s_2)$ can cause capture of electron e_1 through the e_1-e_2 correlation. This points to a potential role of the SEC in the process (194). As shown above, the CDW-4B method is in good accordance with the experimental data on TI for the He^{2+}-He and Li^{3+}-He collisions. Regarding the total cross sections for the TI in the H^+-He collisions at higher impact energies (not shown), the CDW-4B method overestimates some of the measured data (Mergel *et al.*, 1997; Schmidt *et al.*, 2002; Schmidt, Jensen, *et al.*, 2005; Schmidt, Fardi, *et al.*, 2005), whereas at intermediate energies satisfactory agreement is found with the experimental findings of Shah and Gilbody (1985).

Over the last five years, there has been increasing interest in studying the TI in the $H^+ + He \rightarrow H + He^{2+} + e$ collisions (Tolmanov and McGuire, 2000; Mergel *et al.*, 2001; Popov *et al.*, 2002; Schmidt *et al.*, 2002; Schmidt, Fardi, *et al.*, 2005; Schmidt, Jensen, *et al.*, 2005; Schmidt-Böcking, Mergel, Dörner, *et al.*, 2003; Schmidt-Böcking, Mergel, Schmidt, *et al.*, 2003; Schmidt-Böcking *et al.*, 2005; Godunov *et al.*, 2004, 2005; Schöffler *et al.*, 2005). One of the motivations for these investigations has been the fact that multiple-differential cross sections for fragmentation processes can provide valuable information on the nature of electronic correlations in atomic systems. When protons are used as projectiles, a hydrogen atom is formed in the exit channel. In this case, due to the absence of postcollisional Coulomb interactions with the scattered projectile, target correlation effects are expected to be manifested in a more straightforward manner.

For high impact energies, two qualitatively different TI mechanisms contribute to the total cross sections by a comparable amount (Schmidt, Jensen, *et al.*, 2005). These are the so-called kinematic TI (KTI) and the Thomas TI (TTI) processes. As usual, the Thomas process can be understood as two consecutive binary collisions, first by the projectile with one of the target electrons and second between this latter electron and either the target nucleus (the Thomas P-e-T scattering) or another target electron (the Thomas P-e-e scattering). The P-e-e mechanism was first identified in the experiments of Pálinkás *et al.* (1989, 1990) by a coincident detection of the atomic hydrogen and analysis of the energy and angular distributions of emitted electrons for scattering of 1 MeV protons on helium. These authors (Pálinkás *et al.*, 1989, 1990) found a peak in the doubly differential cross section $d^2Q_{if}/dE_e d\Omega_e$ at $\theta_e=90°$ and $E_e=600$ keV. In such a P-e-e mechanism, the projectile-electron potential is accompanied by the electron-electron interaction, leaving one of the electrons with a velocity which is nearly the same as that of the projectile. Since the projectile is much more massive than the electron, it continues to move at almost the same velocity as before the collision. The other electron is emitted into the con-

tinuum with a momentum magnitude equal to that of the projectile, but at an angle of 90° with respect to the direction of the projectile (Briggs and Taulbjerg, 1979; Horsdal-Pedersen *et al.*, 1986).

Electron capture can proceed via different reaction channels called kinematic capture and *P-e-T* capture. Kinematic capture (also known as the Brinkman-Kramers or the first Born approximation mechanism) is mediated by the projectile-electron interaction in the field of the target ion. In order for the TI to take place, capture (either kinematic or *P-e-T*) must be accompanied by an additional process such as shake-off or an independent ionization of the second electron by the projectile. In the shake-off process, one electron is removed from the atom by the projectile, whereas the other electron has a finite probability of ending up in the continuum. This mechanism becomes important for small values of Z_P/v. Hence, the sudden removal of one electron can lead to the emission of a second electron into the continuum. For a transition of the second electron to one of the excited states, a shake-up process can occur. Calculations of the probability of these shake processes can be carried out by using the so-called sudden approximation (Shi and Lin, 2002).

In order to distinguish these different reaction channels in an experiment, the projectile momentum transfer (both transverse and longitudinal components) must be measured with an extremely high resolution to within 0.3 a.u., which is about 10^{-5} of the actual projectile momentum. This is not feasible with standard techniques such as translational spectroscopy or the like, but it is achievable by COLTRIMS. Any momentum change of the projectile must be compensated by summing the momenta of the recoiling ion and emitted electrons. Measuring the impact projectile position on the detector (with a typical resolution less than 0.1 mm), as well as the time of flight of the fragments (from the moment of fragmentation up to the instant when the detector is hit), it becomes possible to determine the particle momenta after fragmentation.

Moreover, COLTRIMS can distinguish between the two TI mechanisms mentioned above, KTI and TTI, by measuring the longitudinal recoil ion momentum for each of the TI events (Mergel *et al.*, 1997; Schmidt *et al.*, 2002; Schmidt, Jensen, *et al.*, 2005; Schmidt, Fardi, *et al.*, 2005). Namely, for the KTI mechanism, the expected longitudinal recoil ion momentum, which is determined by energy- and momentum-conservation laws, is given by $p_{\parallel}=-v/2-\tilde{Q}/v$. In the case of the TTI mechanism, the helium nucleus takes no part in the collision, so that the expected longitudinal recoil-ion momentum for this mechanism is zero. In principle, the Thomas *P-e-e* mechanism could occur with two initially unbound electrons. In other words, this process can proceed even with the two electrons at rest prior to scattering. With this latter assumption, the recoil momentum becomes zero, since the target nucleus does not participate in the process and, moreover, the same nucleus is at rest before the collision.

Schmidt, Jensen, *et al.* (2005) have investigated experimentally the TI process in the H^+-He collisions in the earlier inaccessible high-energy range 1.4–5.8 MeV. They found that for the highest energy (5.8 MeV), the TTI mechanism yields the dominant contribution to the total TI cross section. On the other hand, at the lower end of the energy range considered by Schmidt, Jensen, *et al.* (2005), it has been found that the KTI mechanism is the dominant pathway of the total TI.

Whenever the KTI and TTI processes can be separated (Mergel *et al.*, 1997; Schmidt *et al.*, 2002; Schmidt, Jensen, *et al.*, 2005; Schmidt, Fardi, *et al.*, 2005), it is possible to extract the quantity $P_S=Q_{KTI}/(Q_{SC}+Q_{KTI})<1$, where Q_{SC} denotes the cross section for single capture (SC). By definition, P_S can be interpreted as the probability for the shake-off of the second electron after the first electron has been captured by the projectile via the KTI. The Thomas *P-e-e* part is excluded here since the continuum electron is obviously not shaken off in this process. Schmidt, Jensen, *et al.* (2005) have investigated the shake-off probability P_S as a function of the projectile velocity, and they found a rather weak decrease over the energy range of their measurements, 1.4–5.8 MeV. At higher velocities they approached the expected shake-off limit of 1.63% which is also found in the ratio of double and single ionization of He by photons or protons (Shi and Lin, 2002).

In the experiment of Mergel *et al.* (1997), a velocity dependence $Q\sim v^{-7.4\pm1}$ of the total cross section for the Thomas *P-e-e* double scattering was found in a rather limited interval of $E=0.3$–1.4 MeV. Schmidt *et al.* (2002) carried out a measurement on the TI process in the H^+-He collisions at higher energies 2.5–4.5 MeV and subsequently for an extended energy interval 1.4–5.8 MeV (Schmidt, Jensen, *et al.*, 2005). In the latter experiment, the total cross section for the TI process has been estimated to exhibit the asymptotic behavior $Q\sim v^{-10.78\pm0.27}$. This velocity dependence is in agreement with the corresponding prediction of the classical model of Thomas (1927) for the expected asymptotic v^{-11} behavior, which has also been predicted by the peaking approximation of the BK2 model (Briggs and Taulbjerg, 1979). However, these latter two models are valid at $v\gg v_e$ and as such they are not suitable for a quantitative comparison with the experimental data of Schmidt *et al.* (2002), Schmidt, Jensen, *et al.* (2005), and Schmidt, Fardi, *et al.* (2005). On the other hand, a detailed quantum-mechanical computation of the cross sections for the TI by using the RIA-4B of Belkić (1995, 1996) shows excellent agreement with the experimental data of Mergel *et al.* (1997) as well as Schmidt *et al.* (2002), Schmidt, Jensen, *et al.* (2005), and Schmidt, Fardi, *et al.* (2005). The RIA-4B also predicts the v^{-11} behavior at sufficiently high energies (Belkić, 2004).

The differential cross sections for TI in the $H^+ + He \rightarrow H + He^{2+} + e$ collisions have been measured by means of COLTRIMS (Mergel *et al.*, 2001; Schmidt-Böcking, Mergel, Dörner, *et al.*, 2003; Schmidt-Böcking, Mergel, Schmidt, *et al.*, 2003) at the impact energies ranging from

0.15 to 1.4 MeV. The azimuthal scattering angle θ of the hydrogen atom was as small as 0.1–0.5 mrad. These scattering angles are about 100 times smaller than those from earlier experiments of this type. The experiments (Mergel *et al.*, 2001; Schmidt-Böcking, Mergel, Dörner, *et al.*, 2003; Schmidt-Böcking, Mergel, Schmidt, *et al.*, 2003) found that (i) the ejected electron is predominantly emitted into the backward direction and always opposite to the scattered hydrogen atom; (ii) the captured electron, the recoil He^{2+} ion, and the ejected electron always share comparable momenta; (iii) the direction of the maximum ejection is insensitive to the impact energy, but contains some dependence upon the momentum transfer. Furthermore, from the final-state momentum pattern of H, He^{2+}, and e_2 it is possible to reveal a part of the initial momentum wave function, which is dominated by the non-s^2 contributions (Schmidt-Böcking, Mergel, Dörner, *et al.*, 2003; Schmidt-Böcking, Mergel, Schmidt, *et al.*, 2003). On the basis of these experimental data, it has been contemplated (Schmidt-Böcking, Mergel, Dörner, *et al.*, 2003; Schmidt-Böcking, Mergel, Schmidt, *et al.*, 2003) that the reaction $H^+ + He \rightarrow H + He^{2+} + e$ in the range of extremely small scattering angles θ can be used for obtaining information on the structure of the wave function in the momentum representation. However, this latter idea has become a subject of some controversy (Popov *et al.*, 2002; Vinitsky *et al.*, 2005). In particular, the theoretical analysis by Popov *et al.* (2002) has questioned the consistency of the hypothesis of Schmidt-Böcking, Mergel, Dörner, *et al.* (2003) and Schmidt-Böcking, Mergel, Schmidt, *et al.* (2003) and, therefore, this theme needs further clarification.

The most recent development and refinement within COLTRIMS provide a coincident multifragment imaging technique for eV and sub-eV fragment detection (Schmidt-Böcking *et al.*, 2005). In the experiments by Godunov *et al.* (2005) and Schöffler *et al.* (2005), transfer ionization $H^+ + He \rightarrow H + He^{2+} + e$ has been examined at a single proton energy (630 keV) by detecting the ionized electron perpendicularly to the direction of incidence. These authors proposed a simple theoretical model which could explain qualitatively certain observed effects in the measured triple-differential cross sections for TI in the H^+-He collisions. They pointed out that the TI process offers a unique opportunity to study radial and angular correlations in the helium target. Specifically, angular electron correlations in the ground state of helium yield a broad peak in the electron emission spectra in the backward direction relative to the incoming beam. As discussed, the TI event proceeds through different channels, such as the KTI and TTI. It is known that these mechanisms are sensitive to the collision energy. However, the experimentally observed features (Godunov *et al.*, 2005) are virtually insensitive to the collision energy. This prompted Godunov *et al.* (2005) to assume that the target correlation plays the leading role. They further argued that the fully differential cross sections for TI in the H^+-He collisions can be used as a sensitive probe for the target correlation whenever post-collisional effects are either nonexistent or negligibly small. Such conjectures necessitate further theoretical studies to clarify more fully the role of these correlation effects in differential cross sections for the TI process.

In addition to simultaneous transfer and ionization in collisions by protons and other heavier nuclei with a heliumlike target, the TI process can also occur when positrons are used as projectiles. In this case, formation of positronium takes place with one of the two electrons, while the other electron from the target is ionized (Nath and Sinha, 2000). It should be pointed out that in ion-atom collisions various processes of interest can occur, for example, simultaneous double capture and ionization in the He^{2+}-Ar collisions (Fregenal *et al.*, 2000). A proper description of such a process necessitates five-body models which are not the subject of the present review.

V. SINGLE-ELECTRON DETACHMENT

A. The ECB-4B and the MCB-4B methods

Among ionizing four-body collisions, it is also important to illustrate processes with strong static interelectron correlations. To this end, we shall review total cross sections for single-electron detachment, $H^+ + H^- \rightarrow H^+ + H + e$. This process has been studied in the four-body eikonal Coulomb-Born (ECB-4B) method (Gayet, Janev, and Salin, 1973), the four-body modified Coulomb-Born (MCB-4B) method (Belkić, 1997a, 1997b, 2001, 2004, 2007), etc. Since the three-body versions of these methods will not be discussed, the shorter acronyms ECB and MCB will be used hereafter for ECB-4B and MCB-4B, respectively. The T matrices in the prior versions of the ECB and the MCB methods for single-electron detachment from H^- by H^+ read as

$$T_{if}^{(\mathrm{X})-} = \langle \chi_f^- | V_i^{(\mathrm{X})} | \chi_i^+ \rangle$$
$$= \tilde{N}^{-*}(\zeta) \int\int\int d\vec{s}_1\, d\vec{x}_1 d\vec{x}_2 e^{i\vec{q}\cdot\vec{s}_1 - i(\vec{\kappa}+\vec{q})\cdot\vec{x}_1} \varphi_f^*(\vec{x}_2)$$
$$\times {}_1F_1(i\zeta, 1, ips_1 + i\vec{p}\cdot\vec{s}_1)(vs_1 + \vec{v}\cdot\vec{s}_1)^{-i\nu_P}$$
$$\times V_i^{(\mathrm{X})} \varphi_i(\vec{x}_1, \vec{x}_2); \quad (\mathrm{X} = \mathrm{ECB} \text{ or } \mathrm{X} = \mathrm{MCB}),$$

$$V_i^{(\mathrm{ECB})} = -\frac{1}{s_1} + V_P(R, s_2),$$

$$V_i^{(\mathrm{MCB})} = [V_P(R, s_2) + u_i] + \frac{\nu_P}{s_1} \frac{1 + i(\vec{v}s_1 + v\vec{s}_1)\cdot\vec{\nabla}_{x_1}}{vs_1 + \vec{v}\cdot\vec{s}_1},$$

with $\tilde{N}^-(\zeta) = (2\pi)^{-3/2}\Gamma(1+i\zeta)e^{\pi\zeta/2}$, $\zeta = 1/p$, $V_P(R, s_2) = 1/R - 1/s_2$, $u_i\varphi_i = (h_i - \epsilon_i)\varphi_i \equiv O_{\varphi_i}$, $\vec{q} = \vec{k}_f - \vec{k}_i = \vec{\eta} + \vec{v}(\epsilon_i - \epsilon_f - E_\kappa)/v^2$, $E_\kappa = \kappa^2/2$, $\vec{\eta}\cdot\vec{v} = 0$, $\nu_P = 1/v$, and $\vec{p} = \vec{\kappa} - \vec{v}$, where h_i is the target Hamiltonian. Here, the T-matrix elements $T_{if}^{(\mathrm{ECB})-}$ and $T_{if}^{(\mathrm{MCB})-}$ are written succinctly via the joint expression $T_{if}^{(\mathrm{X})-}$ (X=ECB, MCB) to highlight the similarity between the ECB and MCB methods. As seen, the only difference between the

ECB and the MCB methods is in the perturbation potentials $V_i^{(\mathrm{ECB})}$ and $V_i^{(\mathrm{MCB})}$. Otherwise, both methods have the same initial and final distorted wave functions $\chi_i^+ = \varphi_i(\vec{x}_1,\vec{x}_2)e^{i\vec{k}_i\cdot\vec{r}_i}(vs_1+\vec{v}\cdot\vec{s}_1)^{-i\nu_P}$, and $\chi_f^- = \tilde{N}^-(\zeta)e^{i\vec{k}_f\cdot\vec{r}_i+i\vec{\kappa}\cdot\vec{x}_1}\varphi_f(\vec{x}_2)\,{}_1F_1(-i\zeta,1,-ips_1-i\vec{p}\cdot\vec{s}_1)$. These functions possess the correct asymptotic behaviors. However, the initial perturbation in the ECB method is incorrect, since $V_i^{(\mathrm{ECB})}$ is unrelated to χ_i^+. In sharp contrast, the above expression for $V_i^{(\mathrm{MCB})}$ is correct, since it follows directly and uniquely from the application of the full Schrödinger operator $H-E_i$ to χ_i^+, as per definition of a generic perturbation. Here, H and E_i are the total Hamiltonian and the energy of the whole system in the initial state, respectively. In computations, $V_P(R,s_2)$ is ignored in $V_i^{(\mathrm{ECB})}$ as well as in $V_i^{(\mathrm{MCB})}$ and, additionally, O_{φ_i} is neglected in $T_{if}^{(\mathrm{MCB})-}$.

B. Comparison between theories and experiments for single-electron detachment

Total cross sections $Q_{if}^{(\mathrm{ECB})-}$, computed by Gayet, Janev, and Salin (1973) using the 2-parameter radially correlated CI wave function of Silverman *et al.* (1960) for $H^-(1s^2)$, overestimate the experimental data by some 2–3 orders of magnitude (see Fig. 10). Moreover, $Q_{if}^{(\mathrm{ECB})-}$ saturates to a constant value at high energies, at variance with the proper Bethe asymptotic limit, $(1/E)\ln(E)$. As shown by Belkić (2001, 2004, 2007), this fundamental failure of the ECB method remains incurable by enhancing the angular correlations in the target CI wave function via the inclusion of a larger number (N=3–61) of variational parameters. As to the MCB method, it can be seen from Fig. 10 that the cross sections $Q_{if}^{(\mathrm{MCB})-}$ exhibit a remarkably good convergence with the increasing number (2–61) of the variational parameters in the target CI wave function. Crucially, the converged results for N=61 in the MCB method are in excellent agreement with the experimental data at all energies. Further, with the increasing impact energy E, the cross sections $Q_{if}^{(\mathrm{MCB})-}$ possess the required Bethe limit. Overall, this brief analysis and the illustration in Fig. 10 illuminate the critical role of the proper connection between the perturbation potentials and the corresponding scattering states. Also for an excellent quantitative agreement between the MCB method and the experiments, a high degree of static interelectron correlation (especially angular) is necessary to be included into the CI wave function of the target, $H^-(^1S)$.

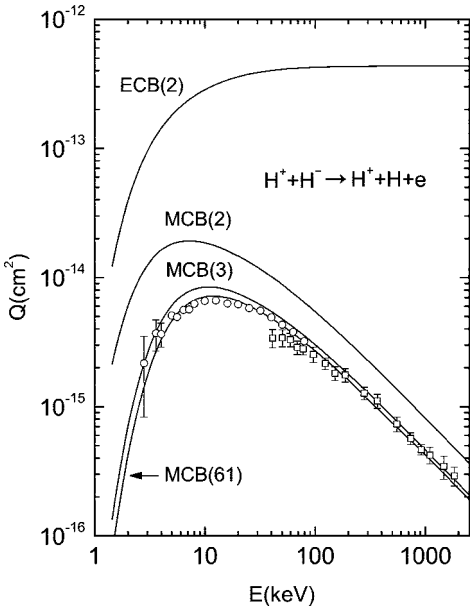

FIG. 10. Total cross sections Q (cm^2) for single-electron detachment from $H^-(1s^2)$ by H^+. Impact energy E (keV) is in the laboratory reference system. Theories (in the prior versions), with only H($1s$) in the exit channel: the ECB method (Gayet, Janev, and Salin, 1973) and the MCB method (Belkić, 1997a, 1997b). Integers N with the acronyms ECB and the MCB represent the numbers of variational parameters in the target CI wave functions, which are taken from Silverman *et al.* (1960) for N=2 as well as N=3 and from Joachain and Terao (1991) for N=61. Experimental data, with all the final states H(Σ) in the exit channel: □ (Peart *et al.*, 1970) and ○ (Melchert *et al.*, 1999). The original data of Peart *et al.* (1970) are for electron impact, and here they are scaled to the equivalent proton impact energy. The ECB and MCB methods share the same properly behaving scattering wave functions, but differ sharply in their initial perturbation potentials $V_i^{(\mathrm{ECB})}$ and $V_i^{(\mathrm{MCB})}$, where the former is incorrect, whereas the latter is correct (see the text). More details are given by Belkić (2007).

$$T_{if}^- = N_{PT}\int\int\int d\vec{R}\,d\vec{x}_1 d\vec{x}_2 e^{i\vec{\alpha}\cdot\vec{s}_1+i\vec{\beta}\cdot\vec{x}_1}\varphi_{f_1}^*(\vec{s}_1)\varphi_{f_2}^*(\vec{x}_2)$$
$$\times\,{}_1F_1(i\nu_T,1,ivx_1+i\vec{v}\cdot\vec{x}_1)$$
$$\times[V_P(R,s_2)\varphi_i(\vec{x}_1,\vec{x}_2)\,{}_1F_1(i\nu_P,1,ivs_1+i\vec{v}\cdot\vec{s}_1)$$
$$-\vec{\nabla}_{x_1}\varphi_i(\vec{x}_1,\vec{x}_2)\cdot\vec{\nabla}_{s_1}\,{}_1F_1(i\nu_P,1,ivs_1+i\vec{v}\cdot\vec{s}_1)], \tag{196}$$

$$T_{if}^+ = N_{PT}\int\int\int d\vec{R}\,d\vec{x}_1 d\vec{x}_2 e^{i\vec{\alpha}\cdot\vec{s}_1+i\vec{\beta}\cdot\vec{x}_1}\varphi_i(\vec{x}_1,\vec{x}_2)\varphi_{f_2}^*(\vec{x}_2)$$
$$\times\,{}_1F_1(i\nu_P,1,ivs_1+i\vec{v}\cdot\vec{s}_1)\{[V_P(R,s_2)+\Delta V_{12}]$$
$$\times\varphi_{f_1}^*(\vec{s}_1)\,{}_1F_1(i\nu_T,1,ivx_1+i\vec{v}\cdot\vec{x}_1)-\vec{\nabla}_{s_1}\varphi_{f_1}^*(\vec{s}_1)$$
$$\cdot\vec{\nabla}_{x_1}\,{}_1F_1(i\nu_T,1,ivx_1+i\vec{v}\cdot\vec{x}_1)\}, \tag{197}$$

$$V_P(R,s_2)=Z_P\left(\frac{1}{R}-\frac{1}{s_2}\right),\quad \Delta V_{12}=\left(\frac{1}{r_{12}}-\frac{1}{x_1}\right), \tag{198}$$

where $N_{PT}=N^+(\nu_P)N^{-*}(\nu_T)$, $N^-(\nu_T)=\Gamma(1+i\nu_T)e^{\pi\nu_T/2}$, $N^+(\nu_P)=\Gamma(1-i\nu_P)e^{\pi\nu_P/2}$, $\nu_P=Z_P/v$, and $\nu_T=(Z_T-1)/v$.

VI. SINGLE-ELECTRON CAPTURE

A. The CDW-4B method

The transition amplitudes within the CDW-4B method for single-electron capture in the prior and post versions without $(\mu\rho v)^{2iZ_P(Z_T-1)/v}$ are (Belkić *et al.*, 1997)

The two momentum transfers $\vec{\alpha}$ and $\vec{\beta}$ in Eqs. (196) and (197) are defined in Eq. (46). After analytical calculation using the Nordsieck technique, the expressions for these two transition amplitudes can be reduced to a three-dimensional integral, which must be evaluated numerically, e.g., by means of the standard Gauss-Legendre quadratures as in the initial study (Belkić *et al.*, 1997) and in a related subsequent work (Mančev, 1999a).

First, we consider single capture from helium by fast protons, i.e.,

$$H^+ + He(1s^2) \to H(1s) + He^+(1s). \tag{199}$$

Here, for the initial bound-state wave function $\varphi_i(\vec{x}_1,\vec{x}_2)$, we employ the CI orbital $(1s1s')$ of Silverman *et al.* (1960)

$$\varphi_i(\vec{x}_1,\vec{x}_2) = \frac{\mathcal{N}}{\pi}(e^{-ax_1-bx_2} + e^{-bx_1-ax_2}),$$

$$\mathcal{N}^{-2} = 2[(ab)^{-3} + (a/2+b/2)^{-6}].$$

Despite its simplicity, this open-shell orbital of the helium ground-state wave function includes radial correlations to a large extent, within approximately 95%. The explicit computations for process (199) include only the ground–to–ground-state transition of the captured electron. The contribution from excited states of hydrogen is taken into account approximately via the n^{-3} scaling law of Oppenheimer (1928) with an overall multiplicative factor 1.202.

1. The Thomas double scattering at all energies

Differential cross sections in the CDW-4B method for the process (199) without the term $(\mu\rho v)^{2iZ_P(Z_T-1)/v}$ are shown in Fig. 11 highlighting the two Thomas peaks of the 1st and 2nd kind, which are mediated by the double scatterings H^+-e-He^{2+} and H^+-e-e, respectively (Belkić, 2001, 2004). It can be seen that the Thomas peak for the H^+-e-e mechanism is systematically and clearly present at all impact energies and without any splitting. At sufficiently high energies, this latter peak is located at the Thomas critical angle, $\theta_{c.m.}\approx 0.027$ deg. At lower energies, e.g. 30, 50, and 100 keV (not shown), the Thomas critical angles for the H^+-e-e peak are near 0.040, 0.035, and 0.031 deg, respectively. On the other hand, the Thomas peak for the H^+-e-He^{2+} mechanism appears clearly only at sufficiently high energies in the CDW-4B method, where it is always split in the middle, but this has not been confirmed experimentally. To check these predictions of the CDW-4B theory, especially for the H^+-e-e mechanism, it would be important to have the experimental data on $dQ/d\Omega$ for process (199) with the two separate contributions from the Thomas double scattering of the 1st and 2nd kind. At present, such measured data are unavailable.

2. Total cross sections

Computations of the post and prior total cross sections have been carried out at incident energies ranging from 20 to 20 000 keV (Belkić *et al.*, 1997). The total cross sections (the post version) as a function of impact energy are displayed in Fig. 12. The solid curve obtained by means of the CDW-4B method corresponds to the case where the complete perturbation $V_f = V_P(R,s_2) + \Delta V_{12} - \vec{\nabla}_{s_1} \ln \varphi_f^*(\vec{s}_1)\cdot\vec{\nabla}_{x_1}$ is used. A comparison with a number of experimental data is also shown in Fig. 12. As can be seen from this figure, the CDW-4B method (Belkić *et al.*, 1997) is in excellent agreement with the available experimental findings. It should be emphasized that this comparison extends over three orders of magnitude of the impact energy, 20–20 000 keV, for which the cross sections vary within 12 orders of magnitude, 10^{-27}–10^{-15} cm^2. With such a stringent test, the CDW-4B method is seen in Fig. 12 to establish its reliability at energies $E \geqslant 70$ keV in accordance with Eq. (164).

In order to determine the relative importance of the dynamic correlations, the post total cross sections in the

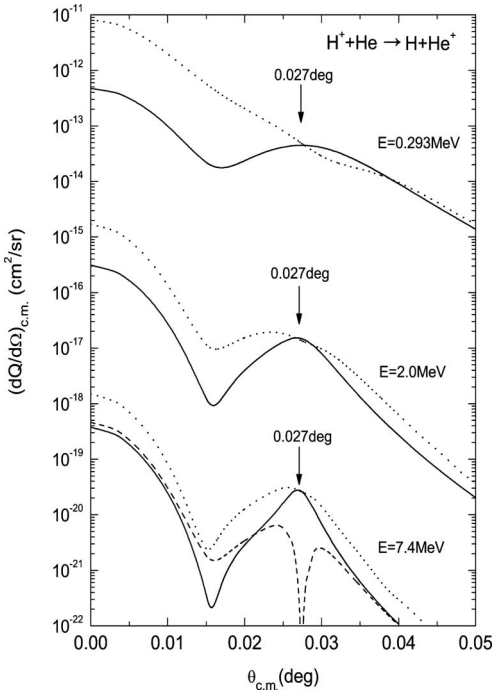

FIG. 11. Differential cross sections $(dQ/d\Omega)_{c.m.}$ at proton energies 0.293, 2, and 7.4 MeV in the post version of the CDW-4B method for single-electron capture from $He(1s^2)$ by H^+ (Belkić, 2001, 2004). Dotted curves: the results from the full perturbation V_f summing the contributions from (i) $-\vec{\nabla}_{s_1} \ln \varphi_f^*(\vec{s}_1)\cdot\vec{\nabla}_{x_1}$,(ii) $\Delta V_{12}=1/r_{12}-1/x_1$, and (iii) $V_P(R,s_2)=1/R-1/s_2$. Dashed and solid curves: the separate contributions from (i) and (ii), respectively. To avoid clutter, the contribution from (i) is shown only at 7.4 MeV. Perturbations (i) and (ii) yield the Thomas double scatterings of the 1st and 2nd kind, H^+-e-He^{2+} (at sufficiently high energies) and H^+-e-e (at all energies). The critical Thomas angle is indicated by the arrow at $\theta_{c.m.}=0.027$ deg. The H^+-e-He^{2+} and the H^+-e-e peaks always appear with and without splitting, respectively. A dip in the Thomas peak is unphysical, as it has never been detected experimentally.

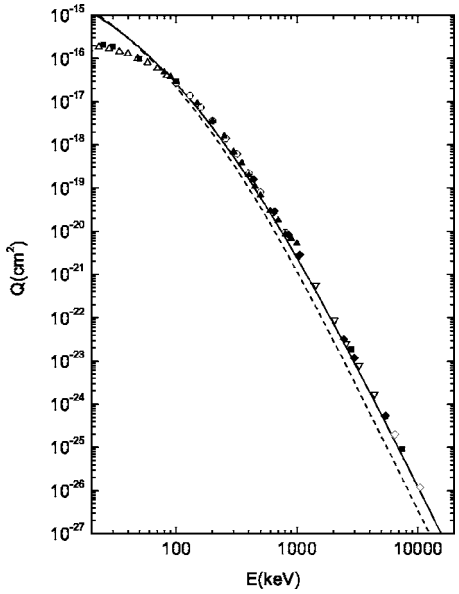

FIG. 12. Total cross sections Q (cm^2) for single-electron capture from helium by protons as a function of laboratory impact energy obtained by means of CDW-4B method (Belkić *et al.*, 1997). The wave function of Silverman *et al.* (1960) is used for the initial bound state. The solid and dashed curves correspond to the cases where the potential ΔV_{12} is included and excluded from the complete perturbation V_f, respectively. Experimental data: ▽ (Schryber, 1967), △ (Shah *et al.*, 1989), ○ (Shah and Gilbody, 1985), ● (Horsdal-Pedersen *et al.*, 1983), ◇ (Berkner *et al.*, 1965), ▲ (Williams, 1967), ▼ (Martin *et al.*, 1981), and ◆ (Welsh *et al.*, 1967).

CDW-4B method used without the potential ΔV_{12} from the complete perturbation V_f are plotted in Fig. 12 (dashed curve). It can be observed from this figure that dynamic electron correlations are essential, since exclusion of the relevant term ΔV_{12} yields the results that significantly underestimate the experimental data at all energies above 100 keV. These theoretical findings provide evidence for the importance of the dynamic correlations, especially at high impact energies.

The difference between the post and prior results with the complete perturbations V_i and V_f is small, such that this post-prior discrepancy does not exceed 15% (Belkić *et al.*, 1997). However, keeping only the scalar product of the gradient operators in the following way

$$V_i \approx -\vec{\nabla}_{x_1} \ln \varphi_i(\vec{x}_1,\vec{x}_2) \cdot \vec{\nabla}_{s_1}, \quad V_f \approx -\vec{\nabla}_{s_1} \ln \varphi_f^*(\vec{s}_1) \cdot \vec{\nabla}_{x_1}, \tag{200}$$

a very large post-prior discrepancy has been reported (Belkić *et al.*, 1997). It should be noted that all earlier computations by the CDW method before the work of Belkić *et al.* (1997) were based exclusively upon the approximation (200).

The CDW-4B method has also been applied to other processes, such as the He^{2+}-He and H^+-Li^+ collisions, with the main purpose of determining whether electronic correlations remain important (Mančev, 1999a). Here the total cross sections obtained for the He^{2+}-He collisions by means of the one-parameter wave function (Hylleraas, 1929) and the two-parameter radially correlated function (Silverman *et al.*, 1960) are very close to each other. Although the Hylleraas wave function is less accurate, it includes some crude radial correlations through the presence of the Slater-screened effective charge of the target nucleus (e.g., $Z_T^{\text{eff}}=1.6875$ for $Z_T=2$). The prior form (196) does not contain the interelectronic term $1/r_{12}$, which accounts for the dynamic correlations. As a result, the prior amplitude and, accordingly, the prior cross sections are expected to be more sensitive to the accuracy of the initial wave function than the corresponding results from the post form. This has indeed been verified by Mančev (1999a) to be the case. Nevertheless, this latter effect is less important for the Li^+ target due to the higher nuclear charge.

When the term $Z_P(1/R-1/s_2)$ is neglected in the prior form, earlier results (Belkić and Janev, 1973; Belkić and Gayet, 1977; Gayet *et al.*, 1981) were reproduced exactly for capture into the ground state in terms of the wave function of Hylleraas (1929) and Silverman *et al.* (1960). More recently (Belkić *et al.*, 1997; Mančev, 1999a), the prior total cross sections have been computed with the complete perturbation potential. Here, the difference between the contributions from the usual gradient operators $-\vec{\nabla}\cdot\vec{\nabla}$ and its sum with the term $Z_P(1/R-1/s_2)$ does not exceed 15% above 30 keV/amu. The term $Z_P(1/R-1/s_2)$ also has a similar influence on the results obtained in the case of the post formalism. As stated, the potential $-Z_P/s_2$ has the asymptotic value $-Z_P/R$ at large distances between Z_P and e_2. A relatively small contribution from the term $Z_P(1/R-1/s_2)$ suggests that for single-electron capture at intermediate and high energies, the potential $-Z_P/s_2$ is nearly canceled by Z_P/R. Therefore, ignoring the two terms $Z_P(1/R-1/s_2)$ does not represent a severe additional approximation, and this is what has previously been done (Belkić and Janev, 1973; Belkić and Gayet, 1977; Gayet *et al.*, 1981).

The post total cross sections derived with the full perturbation according to Eq. (197), as well as without the terms $1/r_{12}-1/x_1$, are displayed in Fig. 13, where the existing experimental data are also plotted for SC in the He^{2+}-He collisions. The CDW-4B method with the complete perturbation (solid curve in Fig. 13) is in good agreement with the available measurements above 150 keV/amu. Neglect of the relevant term for the dynamic electron correlation $\Delta V_{12}=1/r_{12}-1/x_1$ from Eq. (197) leads to the results that are shown with the dotted curve in Fig. 13, and they are seen to underestimate the experimental findings. Similar to the case of the H^+-He collisions, the difference between these two curves for the He^{2+}-He scattering becomes more significant at higher impact energies. This reaffirms the importance of dynamic electron correlations for single capture, especially at higher impact energies. In the same figure, comparison is made between the results from the CDW-4B method and the CDW-IEM (with the wave function of Pluvinage) for the target as obtained by Mančev (1999a)

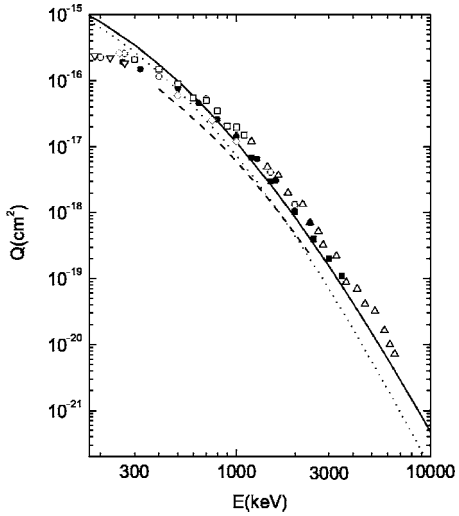

FIG. 13. Total cross sections Q (cm^2) as a function of laboratory incident energy E (keV) for the reaction $^4He^{2+}+{}^4He(1s^2)\rightarrow{}^4He^+(\Sigma)+{}^4He^+(1s)$. The solid and dotted curves represent the post cross sections Q_{if}^+ of the CDW-4B method (Mančev, 1999a) with the complete perturbation potential and without the potential $(1/r_{12}-1/x_1)$, respectively. The results of the CDW-4B method are obtained using the wave function of Hylleraas (1929) for the ground state of the helium target atom. The dashed curve represents the results of the CDW-IEM of Dunseath and Crothers (1991) based upon the Pluvinage wave function with the corresponding theoretical binding energy. Experimental data: ○ (DuBois, 1987), ▽ (Shah *et al.*, 1989), ◇ (Mergel *et al.*, 1995), ● (Shah and Gilbody, 1985), □ (Pivovar *et al.*, 1961), △ (Hvelplund *et al.*, 1976), and ■ (de Castro Faria *et al.*, 1988).

and Dunseath and Crothers (1991), respectively. The formulation of Dunseath and Crothers (1991) ignores dynamic correlations altogether, and this may be one of the reasons for its less favorable agreement with the experimental data, as is clear from Fig. 13. Moreover, this might also indicate that dynamic electronic correlations in the perturbation potentials that cause the transition are more important than the static ones in the target bound-state wave function.

The discrepancy between the post and prior cross sections in the CDW-4B method depends essentially on the choice of the ground-state wave function of helium. This discrepancy is larger for the wave function of Hylleraas (1929) than for the one of Silverman *et al.* (1960). In the case of the wave functions of Hylleraas (1929) and Silverman *et al.* (1960) the post-prior discrepancy does not exceed 20% and 5%, respectively, for the He^{2+}-He collisions at energies considered in Fig. 13. For instance, at impact energies 600, 6000, and 10 000 keV, the post-prior discrepancy for the Hylleraas wave function is 6.2%, 10.8%, and 17.9%, respectively, whereas at the same energies for the orbital of Silverman *et al.* (1960) the discrepancy is 2.2%, 1.2%, and 4.9%, respectively. Of course, the post-prior discrepancy would not exist if the exact wave function were known for helium.

The total cross sections from the CDW-4B method for the reaction

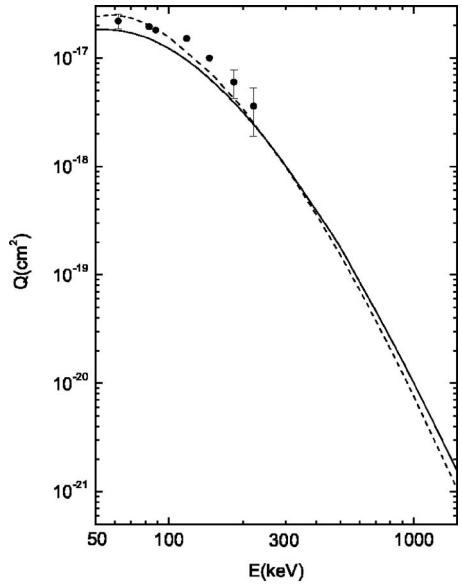

FIG. 14. Total cross sections Q (cm^2) as a function of laboratory incident energy E (keV) for the reaction $H^++{}^7Li^+(1s^2)\rightarrow H(\Sigma)+{}^7Li^{2+}(1s)$. The solid curve represents the post cross sections Q_{if}^+ from the CDW-4B method with the complete perturbation potential. The dashed curve represents the results from the CDW-4B method obtained without the term $(1/r_{12}-1/x_1)$ in Eq. (197). Experimental data: ● (Sewell *et al.*, 1980).

$$H^+ + {}^7Li^+(1s^2) \rightarrow H(\Sigma) + {}^7Li^{2+}(1s) \tag{201}$$

are shown in Fig. 14, together with the experimental findings of Sewell *et al.* (1980). Unfortunately, their measured data have been reported only up to 250 keV. As can be seen, the CDW-4B method (Mančev, 1999a) slightly underestimates these experimental data.

The classical trajectory Monte Carlo (CTMC) model has been used by Wetmore and Olson (1988) to describe the reaction (201), along with a classical model for helium with two active electrons. The CTMC approach treats all participants in a collision (i.e., the projectile, the target nucleus, and the two target electrons) as classical point particles that interact through Coulomb potentials and move according to Newton's law. However, such a helium model removes the electron-electron force and allows each electron to interact with the target nucleus independently through a separate Coulomb potential. Hence, this version of the CTMC model cannot provide any information on electron correlation effects.

Charge-exchange reaction (201) has also been considered theoretically by Ford *et al.* (1982), where the total cross sections were computed at impact energies 50–250 keV by means of the perturbative "one-and-a-half-centered expansion" (POHCE) approximation. Here the single-particle model was adopted for the target described through a local, exponentially screened potential of the type $V_T=-2/r-\exp(-3.3954r)/r$. We note that there is good agreement between the results of the CDW-4B and POHCE methods. In contrast, the cross sections of the CTMC model exhibit a different trend via a peak around 175 keV (not shown). However,

such a peak is not present in the corresponding results of the CDW-4B and POHCE methods, or in the experimental data.

Next, we consider single-electron capture from helium by the Li^{3+} ion

$$Li^{3+} + He \rightarrow Li^{2+} + He^{+}. \quad (202)$$

This process has been treated previously using various theoretical approximations (Belkić *et al.*, 1979; Suzuki *et al.*, 1984; Saha *et al.*, 1985; Belkić, 1989a; Gravielle and Miraglia, 1995; Busnengo *et al.*, 1996). All these studies consider the process (202) as an equivalent three-body problem ignoring correlation effects from the outset. The contribution from the electron-electron interaction via the DEC within the CDW-4B method for the Li^{3+}-He collisions has been examined by Mančev (2001).

The post and prior total cross sections of the CDW-4B method obtained using the one-parameter orbital of Hylleraas (1929) and the two-parameter wave function of Silverman *et al.* (1960) are close, as in the previously considered systems. Specifically, in the case of the post form, the difference between the results for these two wave functions is less than 7%, whereas for the prior form the post-prior discrepancy is within 16% (Mančev 2001). As mentioned, the prior cross sections are more sensitive to the accuracy of the initial-state wave function than the post ones. This is due to the fact that the expression for the prior amplitude, Eq. (196), does not contain the interelectron term $1/r_{12}$, which explicitly accounts for dynamic correlations.

The theoretical post total cross sections obtained with the CDW-4B method for single-electron capture to the ground state in the Li^{3+}-He collisions are displayed in Fig. 15 (solid curve) together with the experimental data (Shah and Gilbody 1985; Woitke *et al.*, 1998). As can be seen from this figure, the computed cross sections are in satisfactory agreement with the experimentally measured data. The solid curve from the CDW-4B method lies slightly below the experimental findings, because these theoretical results include only capture into the ground state, while the contribution from excited states is roughly taken into account by an overall multiplying factor 1.202 from the rule of Oppenheimer (1928). When the relevant term for dynamic correlations ΔV_{12} is ignored in Eq. (197), the resulting cross sections are found to greatly underestimate the experimental data (see the dashed curve in Fig. 15). This provides direct evidence that dynamic correlations play an important role for electron capture in the ground state, especially at higher impact energies.

By increasing the charge of the projectile, the contribution from capture into excited states becomes more important. This has been examined by Mančev (2001) via the extension of the CDW-4B method to encompass capture to the final excited states

$$Li^{3+} + He(1s^2) \rightarrow Li^{2+}(n_f \ell_f) + He^{+}(1s), \quad (203)$$

where the values of the quantum numbers $n_f \ell_f$ were restricted to $1s$, $2s$, $2p$, $3s$, $3p$, and $3d$. As an illustration, Mančev (2001) gave the results at energies 60, 800, and

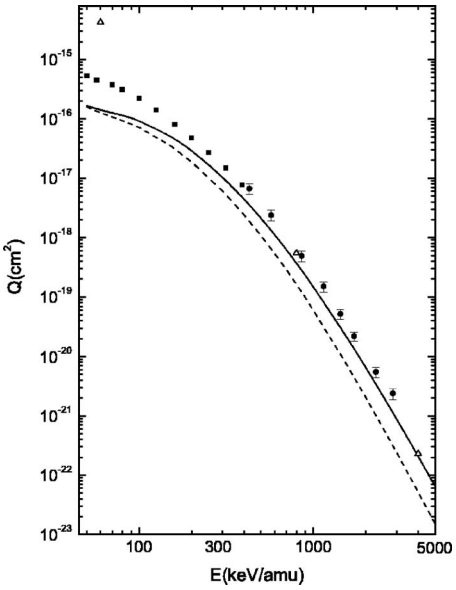

FIG. 15. Total cross sections Q (cm^2) as a function of laboratory incident energy E (keV/amu) for the reaction $Li^{3+}+He \rightarrow Li^{2+}+He^{+}$. The solid and dashed curves represent the post cross sections Q_{if}^{+} of the CDW-4B method (Mančev, 2001) with the complete perturbation potential and without the potential $(1/r_{12}-1/x_1)$, respectively. The symbol △ refers to the post total cross sections Q_{Σ}^{+} obtained from Eq. (204), whereas the two curves correspond to capture into the ground state and the contribution from exited states is accounted by 1.202 as an overall multiplying factor. The results are obtained using the orbital of Hylleraas (1929) for the ground state of the helium target atom. Experimental data: ■ (Shah and Gilbody, 1985) and ● (Woitke *et al.*, 1998).

4000 keV/amu. The total cross sections $Q_{\Sigma}^{\pm}$ are obtained via the $(n_f)^{-3}$ scaling law (Oppenheimer 1928)

$$Q_{\Sigma}^{\pm} = Q_1^{\pm} + Q_2^{\pm} + 2.081 Q_3^{\pm}. \quad (204)$$

Here $Q_{n_f}^{\pm} = \Sigma_{\ell_f m_f} Q_{n_f \ell_f m_f}^{\pm}$, where $Q_{n_f \ell_f m_f}^{\pm}$ are the state-selective partial cross sections for capture into the state determined by the quantum numbers n_f, ℓ_f, and m_f. The results obtained by Mančev (2001) show that the electronic correlations remain important for the included excited states. The contribution from the term ΔV_{12} to the total cross section for excited states retains a similar trend relative to that for capture into the ground state. This can be demonstrated if we compare the post total cross sections computed with and without the term ΔV_{12} and denote the corresponding results by Q_{nl}^{+} and $\overline{Q}_{12}^{+}$. Then, for the $1s$, $2s$, and $3s$ states at 4000 keV/amu, the following values are obtained: $Q_{nl}^{+}/\overline{Q}_{12}^{+}=4.05$, 4.10, and 4.10, respectively. These ratios at 800 keV/amu become 2.28, 2.24, and 2.21, whereas at 60 keV/amu they are 1.10, 1.66, and 1.48, respectively. The ratios for $Q_{n\ell}^{+}/\overline{Q}_{12}^{+}$ also exhibit similar behavior for other excited states (Mančev 2001). The values of the total cross sections Q_{Σ}^{+} computed using Eq. (204) are shown in Fig. 15. As expected, the contribution from excited states becomes less important as the impact energy increases. However,

at lower energies, the theoretical total cross sections Q_Σ^+ (triangles) notably overestimate the experimental data. An evaluation of the contribution from the perturbation term $V_P(R,s_2)$ has been done by Mančev (2001) for the Li^{3+}-He collisions. The conclusion was that this contribution is significant (up to 40%).

B. The CDW-BFS (prior BDW-4B) and the CDW-BIS (post BDW-4B) methods

In this section, we consider certain distorted-wave methods that include continuum intermediate states of the captured electron only in one channel (Belkić, 1994; Mančev, 2003, 2005a, 2005b; Mančev *et al.*, 2003). We choose the perturbation potential and the distorted wave of the initial state in the same manner as in the CDW-4B method

$$U_i = Z_P\left(\frac{1}{R}-\frac{1}{s_2}\right)-\sum_{k=1}^{2}\vec{\nabla}_{x_k}\ln\varphi_i\cdot\vec{\nabla}_{x_k}, \tag{205}$$

$$\chi_i^+ = N^+(\nu_P)\mathcal{N}^+(\nu)e^{i\vec{k}_i\cdot\vec{r}_i}\varphi_i(\vec{x}_1,\vec{x}_2)\,{}_1F_1(i\nu_P,1,ivs_1+i\vec{v}\cdot\vec{s}_1)$$
$$\times{}_1F_1(-i\nu,1,ik_ir_i-i\vec{k}_i\cdot\vec{r}_i). \tag{206}$$

Further, for the final state, we use the wave function (44) from the CB1-4B method

$$\Phi_f^- = \varphi_P(\vec{s}_1)\varphi_T(\vec{x}_2)e^{-i\vec{k}_f\cdot\vec{r}_f-i\nu_f\ln(k_fr_f-\vec{k}_f\cdot\vec{r}_f)}, \tag{207}$$

where $\nu=Z_P(Z_T-1)/v$, $\nu_P=Z_P/v$, and $\nu_f=(Z_P-1)(Z_T-1)/v$. With this choice, the prior form of the transition amplitude can be written as (Belkić, 1994; Mančev, 2003)

$$T_{if}^- = \langle\Phi_f^-|U_i|\chi_i^+\rangle. \tag{208}$$

This represents the CDW-BFS method. The explicit expression for the transition amplitude in the CDW-BFS method is (Mančev, 2003; Mančev *et al.*, 2003)

$$T_{if}^- = N^+(\nu_P)\int\int\int d\vec{x}_1d\vec{x}_2d\vec{R}\,e^{i\vec{\alpha}\cdot\vec{s}_1+i\vec{\beta}\cdot\vec{x}_1}$$
$$\times\mathcal{L}(R)\varphi_P^*(\vec{s}_1)\varphi_T^*(\vec{x}_2)$$
$$\times[V_P(R,s_2)\varphi_i(\vec{x}_1,\vec{x}_2)\,{}_1F_1(i\nu_P,1,ivs_1+i\vec{v}\cdot\vec{s}_1)$$
$$-\vec{\nabla}_{x_1}\varphi_i(\vec{x}_1,\vec{x}_2)\cdot\vec{\nabla}_{s_1}\,{}_1F_1(i\nu_P,1,ivs_1+i\vec{v}\cdot\vec{s}_1)]. \tag{209}$$

The function $\mathcal{L}(R)$ is

$$\mathcal{L}(R) = [\mathcal{N}^+(\nu_f)]^*\mathcal{N}^+(\nu)\,{}_1F_1(-i\nu_f,1,ik_fr_i+i\vec{k}_f\cdot\vec{r}_i)$$
$$\times{}_1F_1(-i\nu,1,ik_ir_i-i\vec{k}_i\cdot\vec{r}_i)$$
$$\simeq(k_fr_i+\vec{k}_f\cdot\vec{r}_i)^{i\nu_f}(k_ir_i-\vec{k}_i\cdot\vec{r}_i)^{i\nu}\quad(r_i\to\infty).$$

Replacement of Coulomb scattering waves for the relative motion of heavy particles by their asymptotic forms has been done previously (McCarroll and Salin, 1967; Gayet, 1972; Belkić *et al.*, 1979; Belkić, 2001). Here we resort to the well-known eikonal hypothesis, which assumes that the momentum k_i acquires large values. For heavy-particle collisions, the reduced mass of the whole system in the entrance channel is very large ($\mu_i\gg1$) and, hence, k_i is large even at very small incident velocities v_i (say, of the order of 0.01 a.u.). Due to their large mass, heavy projectiles are only slightly deflected from their initial direction and, therefore, scattering takes place predominantly in a narrow forward cone, which implies that $\hat{\vec{k}}_i\simeq\hat{\vec{k}}_f$. Thus, in the mass limit $M_{P,T}\gg1$, for the initial and final heavy-particle velocities $\vec{v}_i\simeq\vec{k}_i/\mu_i$ and $\vec{v}_f\simeq\vec{k}_f/\mu_f$, we can write $\vec{v}_i\simeq\vec{v}_f\equiv\vec{v}$. This mass limit also justifies the replacement of $\vec{r}_i$ by $\vec{R}$. Hence, such an eikonal hypothesis permits a consistent reduction of the function $\mathcal{L}(R)$ to the following simplified form

$$\mathcal{L}(R)\simeq(vR-\vec{v}\cdot\vec{R})^{iZ_P(Z_T-1)/v}(vR+\vec{v}\cdot\vec{R})^{i(Z_P-1)(Z_T-1)/v}$$
$$=\rho^{2iZ_P(Z_T-1)/v}(vR+\vec{v}\cdot\vec{R})^{-i\xi},$$

where $\xi=(Z_T-1)/v$. Here the unimportant phase factors of the unit moduli are ignored. The factor $\rho^{2iZ_P(Z_T-1)/v}$ has no influence on the total cross sections and may be omitted (Belkić *et al.*, 1986).

Further, we can formulate the post form of the transition amplitude using the wave function of the initial state from the CB1-4B method

$$\Phi_i^c(r_i\to\infty)\equiv\Phi_i^+=\varphi_i(\vec{x}_1,\vec{x}_2)e^{i\vec{k}_i\cdot\vec{r}_i+i\nu_i\ln(k_ir_i-\vec{k}_i\cdot\vec{r}_i)}.$$

On the other hand, χ_f^- and U_f will retain the same forms as in the CDW-4B method

$$U_f=\left[Z_P\left(\frac{1}{R}-\frac{1}{s_2}\right)-\left(\frac{1}{x_1}-\frac{1}{r_{12}}\right)\right]$$
$$-\vec{\nabla}_{s_1}\ln\varphi_{PT}(\vec{s}_1,\vec{x}_2)\cdot\vec{\nabla}_{s_1}$$
$$-\vec{\nabla}_{x_2}\ln\varphi_{PT}(\vec{s}_1,\vec{x}_2)\cdot\vec{\nabla}_{x_2},$$

$$\chi_f^- = \varphi_{PT}(\vec{s}_1,\vec{x}_2)e^{-i\vec{k}_f\cdot\vec{r}_f}\mathcal{N}^-(\nu)N^-(\nu_T)$$
$$\times{}_1F_1(-i\nu_T,1,-ivx_1-i\vec{v}\cdot\vec{x}_1)$$
$$\times{}_1F_1(i\nu,1,-ik_fr_f+i\vec{k}_f\cdot\vec{r}_f),$$

where $\varphi_{PT}(\vec{s}_1,\vec{x}_2)=\varphi_P(\vec{s}_1)\varphi_T(\vec{x}_2)$. Hence, the post form of the transition amplitude in the CDW-BIS method is (Belkić, 1994; Mančev, 2005a, 2005b)

$$T_{if}^+ = \langle\chi_f^-|U_f|\Phi_i^+\rangle, \tag{210}$$

with the following expression for the matrix elements

$$T_{if}^+ = [N^-(\nu_T)]^*\int\int\int d\vec{x}_1d\vec{x}_2d\vec{R}\,e^{i\vec{k}_i\cdot\vec{r}_i+i\vec{k}_f\cdot\vec{r}_f}\varphi_i(\vec{x}_1,\vec{x}_2)\mathcal{R}$$
$$\times\{{}_1F_1(i\nu_T,1,ivx_1+i\vec{v}\cdot\vec{x}_1)[V_P(R,s_2)+\Delta V_{12}]$$
$$\times\varphi_P^*(\vec{s}_1)\varphi_T^*(\vec{x}_2)-\varphi_T^*(\vec{x}_2)\vec{\nabla}_{s_1}\varphi_P^*(\vec{s}_1)$$
$$\cdot\vec{\nabla}_{x_1}\,{}_1F_1(i\nu_T,1,ivx_1+i\vec{v}\cdot\vec{x}_1)\}, \tag{211}$$

$$\mathcal{R} = [\mathcal{N}^-(\nu)]^* \mathcal{N}^+(\nu_i)\, {}_1F_1(-i\nu, 1, ik_f r_f - i\vec{k}_f \cdot \vec{r}_f)$$
$$\times {}_1F_1(-i\nu_i, 1, ik_i r_i - i\vec{k}_i \cdot \vec{r}_i)$$
$$\simeq (vR + \vec{v} \cdot \vec{R})^{i\nu} (vR - \vec{v} \cdot \vec{R})^{i\nu_i}$$
$$= (\rho v)^{2i\nu_i} (vR + \vec{v} \cdot \vec{R})^{-i\xi},$$

where $V_P(R,s_2) = Z_P(1/R - 1/s_2)$, $\Delta V_{12} = 1/r_{12} - 1/x_1$, $\nu_i = Z_P(Z_T - 2)/v$, and $\xi = \nu_i - \nu = -Z_P/v$.

It should be noted that calculation of the angular distributions $dQ_{if}/d\Omega$ becomes particularly convenient in the CDW-BIS method, when the two-electron target is neutral as in the case with helium ($Z_T = 2$). In this case, the function $\mathcal{R}$ is reduced to $\mathcal{R} = (vR + \vec{v} \cdot \vec{R})^{-i\xi}$ without any overall multiplying ρ term. Hence, the same algorithm within the CDW-BIS method permits obtaining both total cross sections (Z_T, Z_P arbitrary) and differential cross sections (for any Z_P and $Z_T = 2$), as previously pointed out by Belkić (1994). The CDW-BIS method contains the term ΔV_{12} which carries information on dynamic correlations. After the analytical calculation outlined by Mančev (2005b), the expression for T_{if} can be written in terms of a five-dimensional integral.

The matrix elements of the CDW-BFS method can be reduced to a two-dimensional integral using a similar technique. Details can be found in the work of Mančev (2003). As mentioned earlier, the CDW-BIS and CDW-BFS methods (Mančev 2003, 2005a, 2005b) are, respectively, the same as the post and prior BDW-4B methods of Belkić (1994), after the appropriate adaptation to single-electron capture. It should be reemphasized that introducing these hybrid-type second-order approximations was motivated mainly by the idea of approximating the exact wave function in one of the channels by a simple analytical function that can provide an adequate description of the principal interaction region. Importantly, the CDW-BIS and CDW-BFS methods preserve the correct boundary conditions in both channels.

In order to illustrate the adequacy of the CDW-BIS and CDW-BFS methods, we consider several collisional processes. The results obtained by the CDW-BFS method for the total cross sections in the case of the rearrangement process

$$^4He^{2+} + {}^4He(1s^2) \rightarrow {}^4He^+(\Sigma) + {}^4He^+(1s) \qquad (212)$$

are shown in Fig. 16 at energies between 100 keV and 10 MeV. Explicit computations are carried out only for capture to the ground state ($1s$). The symbol Σ in $He^+(\Sigma)$ means that the results obtained in this way are multiplied additionally by a factor of 1.202 in order to include roughly a contribution from all excited states; namely, the total cross sections are obtained via $Q_\Sigma \simeq Q_{1s,1s}\Sigma_{n=1}^{\infty} n^{-3} \approx 1.202 Q_{1s,1s}$. In Fig. 16, the results of the CDW-BFS method are compared with those from the CDW-4B method (Mančev, 1999a). We recall that the distorting potential U_i is the same in the prior CDW-4B and CDW-BFS methods. Both approximations satisfy the correct boundary conditions in the entrance and exit channels. However, unlike the CDW-4B method, the CDW-BFS method takes full account of the Coulomb continuum intermediate state of the captured electron only in the entrance channel. Hence, by comparing these two theories, we can learn about the relative importance of the intermediate ionization electron continua. As can be seen from Fig. 16, the CDW-BFS method provides similar cross sections as the CDW-4B method at higher impact energies. However, at lower energies, the results from the CDW-BFS method are smaller than the corresponding results of the CDW-4B method. This illustrates the remarkable sensitivity of second-order theories for single-charge exchange to the role of the electronic ionization continua. Also included in Fig. 16 are the experimental data for comparison with the theory. The CDW-BFS method is found to be in good agreement with the majority of measurements throughout the energy range of overlap. The total cross sections measured by Hvelplund *et al.* (1976) overestimate the theoretical results.

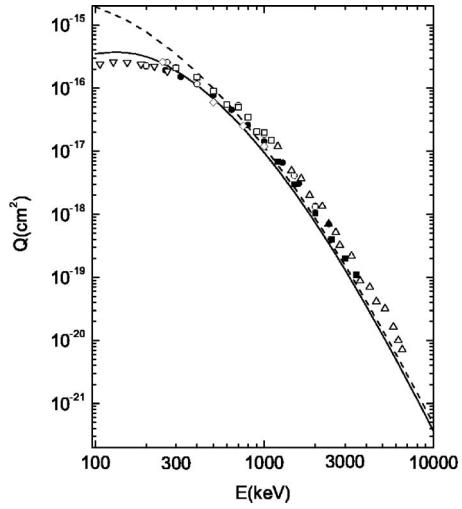

FIG. 16. Total cross sections Q (cm^2) as a function of laboratory incident energy E (keV) for the reaction $^4He^{2+} + {}^4He(1s^2) \rightarrow {}^4He^+(\Sigma) + {}^4He^+(1s)$. The solid curve represents the cross sections Q of the CDW-BFS method (Mančev, 2003). The dashed curve represents the results of the prior form of the CDW-4B method (Mančev, 1999a). Experimental data: ○ (DuBois, 1987), ▽ (Shah *et al.*, 1989), ◇ (Mergel *et al.*, 1995), ● (Shah and Gilbody, 1985), □ (Pivovar *et al.*, 1961), △ (Hvelplund *et al.*, 1976), and ■ (de Castro Faria *et al.*, 1988).

According to the CDW-BIS method, the following approximation is utilized for the distortion of the initial scattering state in the entrance channel (Mančev 2005a, 2005b)

$$F_i = \mathcal{N}^+(\nu_i) e^{i\vec{k}_i \cdot \vec{r}_i}\, {}_1F_1(-i\nu_i, 1, ik_i r_i - i\vec{k}_i \cdot \vec{r}_i)$$
$$\simeq \exp[i\vec{k}_i \cdot \vec{r}_i + i\nu_i \ln(k_i r_i - \vec{k}_i \cdot \vec{r}_i)]$$
$$\simeq e^{i\vec{k}_i \cdot \vec{r}_i} (vR - \vec{v} \cdot \vec{R})^{-i\nu_i}.$$

A similar eikonal approximation is chosen in the exit channel within the CDW-BFS method (Mančev, 2003; Mančev *et al.*, 2003)

$$F_f = \mathcal{N}^+(\nu_f)e^{-i\vec{k}_f\vec{r}_f}\,{}_1F_1(i\nu_f,1,-ik_fr_f+i\vec{k}_f\cdot\vec{r}_f)$$
$$\simeq \exp[-i\vec{k}_f\cdot\vec{r}_f - i\nu_f\ln(k_fr_f-\vec{k}_f\cdot\vec{r}_f)]$$
$$\simeq e^{-i\vec{k}_f\vec{r}_f}(vR+\vec{v}\cdot\vec{R})^{-i\nu_f}.$$

In these expressions for the $\vec{R}$-dependent eikonal phases from both F_i and F_f, the unimportant phases of the unit moduli are ignored. The factor F_f comes from the long-range Coulomb repulsion between the screened positively charged nuclei (Z_P-1) and (Z_T-1) in the exit channel, whereas F_i originates from repulsion between a bare projectile Z_P and the screened target nucleus (Z_T-2) in the entrance channel. We recall that an eikonal phase is a good approximation to the full continuum wave function only when the third argument of the confluent hypergeometric function involved is sufficiently large. This is justified for heavy particle collisions even at quite low impact energies, due to large values of reduced masses.

The high-energy behavior of the cross sections in the CDW-BFS method for the $1s$-n_fl_f capture is given by the asymptote $Q_{if}\sim v^{-11-2l_f}$. Thus, for capture into the excited states with $l_f>0$, at very high energies, the CDW-BFS method does not give the correct v^{-11} behavior. Nevertheless, this deficiency in the asymptotic region is not of crucial importance at intermediate and some high energies, prior to the onset of the Thomas double-scattering mechanism. A similar deficiency in the asymptotic velocity dependence has also been found in the case of other one-channel distorted-wave models, such as the target continuum distorted-wave (TCDW) method (Dubé, 1983; Crothers and Dunseath, 1987), the CDW-EIS and CDW-EFS methods (Busnengo *et al.*, 1995, 1996). The TCDW method, which is designed for asymmetric collisions $(Z_T \gg Z_P)$, uses the wave function of the CDW-3B method in the final state and the undistorted channel wave function in the initial state of the system. Therefore, the TCDW method is inadequate, as it neglects the correct boundary condition in the entrance channel.

The CDW-BFS method also gives good results for other collisions, such as single-electron capture in the H^+-He and H^+-Li^+ collisions (Mančev, 2003). The results of computations for the H^+-He collisions in an energy interval from 40 keV to 15 MeV are shown in Fig. 17, where we compare the CDW-BFS method with experimental data. As can be seen, the CDW-BFS method is found to be consistently in excellent agreement with the available experimental data for the total cross sections from intermediate to high nonrelativistic energies. Experimental data do not relate to the process $H^+ + {}^4He(1s^2) \rightarrow H(\Sigma) + {}^4He^+(1s)$, but rather to $H^+ + {}^4He(1s^2) \rightarrow H(\Sigma) + {}^4He^+$ collisions, where the last symbol $^4He^+$ indicates that no information is available on the postcollisional state of the target remainder $^4He^+$. This means that, if a strict comparison with measurement is desired, the theory has to allow for all possible contributions arising from transitions of the noncaptured electron e_2 in He^+. In practice, however, only excitation and ionization of the He^+ ion can play a nonnegligible role at high impact energies. In the same figure, a comparison with the theoretical results of Winter (1991) is given. The computation of the cross sections given by Winter (1991) was carried out at proton energies 50, 100, and 200 keV by means of the close coupling (CC) approximation using a basis of about 50 Sturmian functions. The full two-electron interaction was included. The agreement between the results from the CDW-BFS and CC methods is quite good. The cross sections from the CDW-4B method obtained by Belkić *et al.* (1997) (not shown in Fig. 17 to avoid clutter, but displayed earlier in Fig. 12) are also in good agreement with the findings of the CDW-BFS method. Further, it is found that the interaction $V_P(R,s_2)$ contributes about 9–30% to the total cross section (dashed curve in Fig. 17).

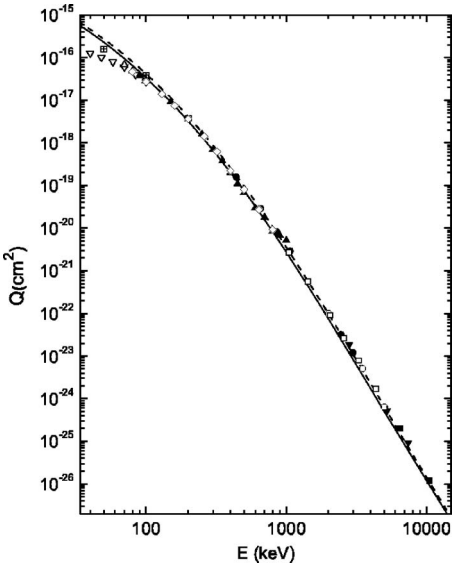

FIG. 17. Total cross sections Q (cm^2) as a function of laboratory energy E (keV) for the reaction $H^+ + {}^4He(1s^2) \rightarrow H(\Sigma) + {}^4He^+$. The solid curve represents the results from the CDW-BFS method with the full perturbation potential (Mančev, 2003). The dashed curve represents the results of the CDW-BFS method obtained without the potential $V_P(R,s_2) = Z_P(1/R - 1/s_2)$. Experimental data: ▽ (Shah *et al.*, 1989), ■ (Berkner *et al.*, 1965), ○ (Schwab *et al.*, 1987), ● (Welsh *et al.*, 1967), □ (Schryber, 1967), ◇ (Shah and Gilbody, 1985), ▲ (Allison, 1958), ▼ (Horsdal-Pedersen *et al.*, 1983), and △ (Rudd *et al.*, 1983). Theory (CC): ⊞ (Winter, 1991).

As to total cross sections in the CDW-BIS method, computations have been performed by Mančev (2005b) in the energy interval [20,10000] keV. A comparison between the CDW-BIS method and numerous experimental data reveals good agreement. The CDW-BIS method provides very similar cross sections as the CDW-BFS method at higher impact energies. However, at lower energies, the results of the CDW-BIS method are smaller than the corresponding results of the CDW-BFS method. Moreover, the CDW-BIS method shows better

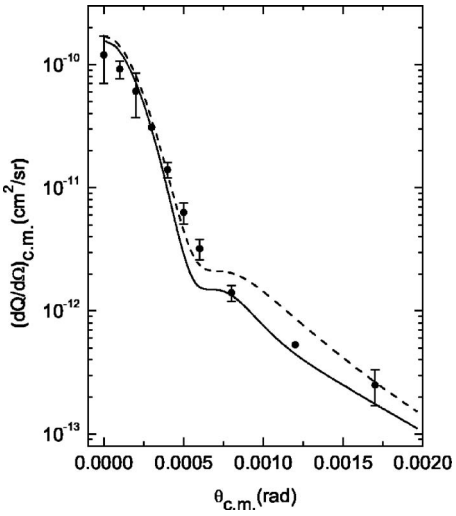

FIG. 18. Differential cross sections $(dQ/d\Omega)_{\mathrm{c.m.}}$ (cm^2/sr) as a function of the scattering angle $\theta_{\mathrm{c.m.}}$ (rad) for single-electron capture in the H$^+$-He collisions at a proton impact energy of 100 keV. Cross sections and scattering angles are in the center-of-mass system. Solid curve: the results of the CDW-BFS method with the full perturbation potential (Mančev *et al.*, 2003). Dashed curve: the results of the CDW-BFS method obtained without the potential $V_P(R,s_2)=Z_P(1/R-1/s_2)$. Experimental data: ● (Martin *et al.*, 1981).

agreement with measurements than the CDW-BFS method (Mančev, 2005b).

A more refined test of the validity of theoretical models is provided by differential cross sections (DCS). The DCS data from the CDW-BFS method for the H$^+$-He

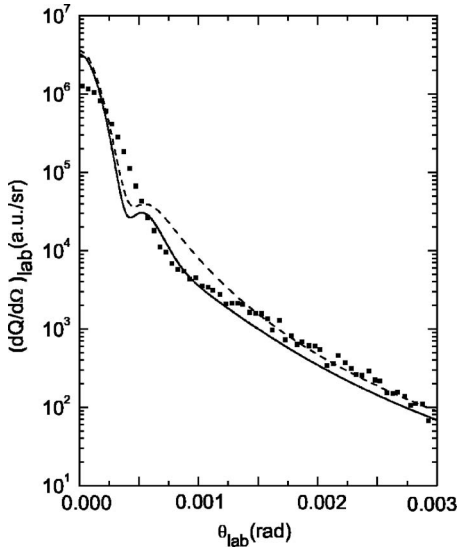

FIG. 19. Differential cross sections $(dQ/d\Omega)_{\mathrm{lab}}$ (a.u./sr) for single-electron capture in the H$^+$-He collisions as a function of the scattering angle θ_{lab} (rad) at a proton impact energy of 150 keV. Solid curve: the results of the CDW-BFS method with the full perturbation potential (Mančev *et al.*, 2003). Dashed curve: the results of the CDW-BFS method obtained without the potential $V_P(R,s_2)=Z_P(1/R-1/s_2)$. Experimental data: ■ (Mergel *et al.*, 2001).

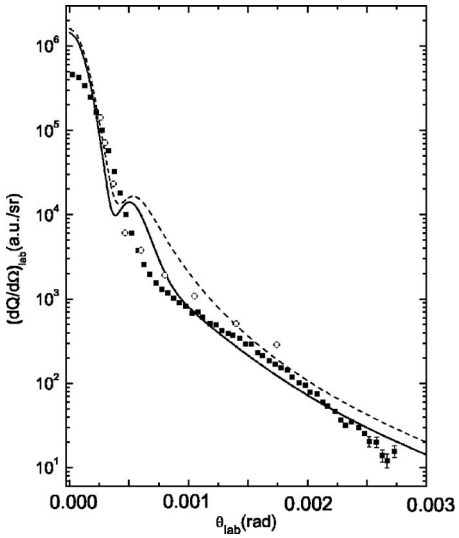

FIG. 20. The same as in Fig. 19, except for 200 keV. The additional symbols denoted by ○ represent the experimental data of Loftager (2002).

collisions at 100 keV are depicted in Fig. 18, together with the experimental data of Martin *et al.* (1981). It is seen from this figure that there is a very good agreement between the theory and the measurements. Bross *et al.* (1994) have also measured differential cross sections for single-electron capture in the H$^+$-He collisions at 100 keV, and their results are very close to those of Martin *et al.* (1981).

In Figs. 19–21, more DCS data are presented at proton energies 150, 200, and 300 keV. A comparison is made between the theory (Mančev *et al.*, 2003) and the measurements of Mergel *et al.* (2001). Figures 19 and 20 reveal good agreement between theory and experiment at 150 and 200 keV. At 300 keV also satisfactory agreement is obtained as shown in Fig. 21. Here at larger scattering angles the experimental data overestimate the theoretical results, but otherwise both theory and experiment exhibit quite similar behavior.

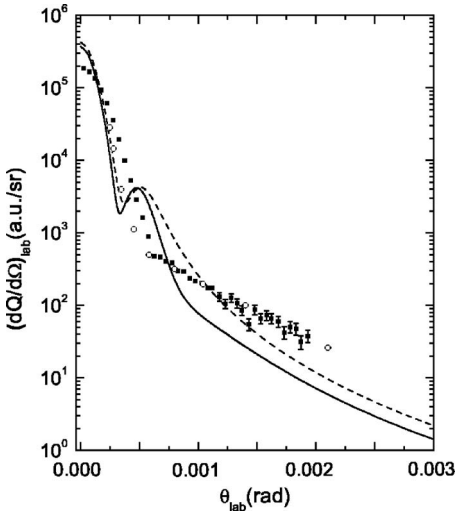

FIG. 21. The same as in Fig. 20, except for 300 keV.

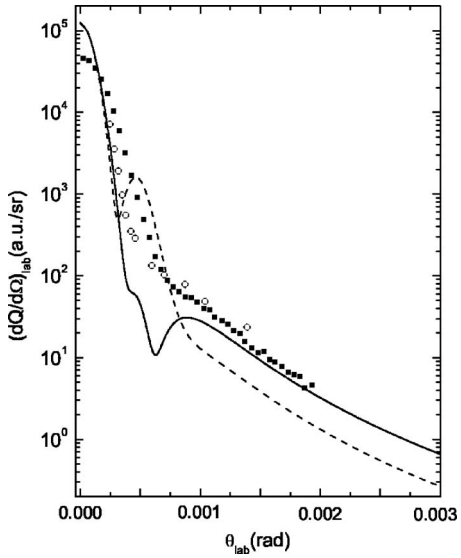

FIG. 22. Differential cross sections $(dQ/d\Omega)_{\rm lab}$ (a.u./sr) for single-electron capture in the H^+-He collisions as a function of the scattering angle $\theta_{\rm lab}$ (rad) at 400 keV. Cross sections and scattering angles are in the laboratory system. Solid curve: the results of the CDW-BIS method (Mančev, 2005a, 2005b). Dashed curve: the CDW-BFS method (Mančev, 2003; Mančev *et al.*, 2003). Experimental data: ■ (Mergel *et al.*, 2001) and ○ (Loftager, 2002).

The results from the CDW-BIS method for differential cross sections at 400 and 630 keV for the process (199) are depicted in Figs. 22 and 23. These figures show that, at smaller scattering angles, the CDW-BIS and CDW-BFS methods give similar results and, moreover,

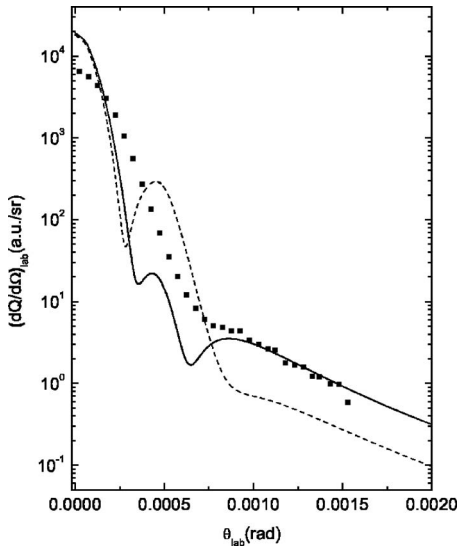

FIG. 23. Differential cross sections $(dQ/d\Omega)_{\rm lab}$ (a.u./sr) for single-electron capture in the H^+-He collisions as a function of the scattering angle $\theta_{\rm lab}$ (rad) at a proton impact energy of 630 keV. Cross sections and scattering angles are in the laboratory system. Solid curve: the results of the CDW-BIS method (Mančev, 2005a, 2005b). Dashed curve: the results of the CDW-BFS method (Mančev, 2003; Mančev *et al.*, 2003). Experimental data: ■ (Mergel *et al.*, 2001).

these are in satisfactory agreement with the experimental data. In Fig. 22, two sets of experimental findings (Loftager, 2002; Mergel *et al.*, 2001) are displayed. Mergel *et al.* (2001) measured the differential cross sections using COLTRIMS. Different behaviors are obtained in the CDW-BIS and CDW-BFS methods around the Thomas peak region. When the impact energy increases, the CDW-BIS method shows the Thomas peak at the same angle as the CDW-BFS method. However, the presently considered impact energies are not sufficiently large for the quoted experiments to detect the Thomas peak in an unambiguous way. The CDW-BIS method exhibits an unphysical and experimentally unobserved dip located after the Thomas peak region. This additional peak is due to a mutual cancellation among the individual terms in the perturbation potential U_f. At larger scattering angles, the CDW-BIS method shows good accordance with the experimental data. This can be attributed to the inclusion of the interaction potential ΔV_{12} which describes dynamic electron correlations. We recall that the differential cross sections in the CDW-BFS method are obtained after performing a two-dimensional numerical integration. This is advantageous relative to the CDW-4B method, in which a five-dimensional quadrature is required for the same purpose when Eq. (136) is used. Thus far, differential cross sections have not become available in the CDW-4B method. The DCS data for the H^+-He collisions at intermediate and high impact energies have been reported by Abufager *et al.* (2005) as well as by Adivi and Bolorizadeh (2004). Abufager *et al.* (2005) used an improved version of the three-body CDW-EIS method, taking particular care of the representation of the bound and continuum target states. Their method gives a good description of single-electron capture in the H^+-He collisions at intermediate and high energies, when an appropriate representation of the target potential is employed. Adivi and Bolorizadeh (2004) used a second-order model which ignores the correct boundary conditions and has logarithmic divergence. Therefore, regarding atomic collisions, their method is theoretically unfounded (Dollard, 1964; Belkić *et al.*, 1979) for the same reasons that have been criticized in the divergent strong potential Born approximation (Bransden and Dewangan, 1988; Crothers and Dubé, 1993; Dewangan and Eichler, 1994; Belkić, 2001, 2004, 2007). Regarding the Thomas double scattering, despite considerable theoretical interest, there are only a few experimental investigations of electron capture in fast H^+-He collisions. The Thomas peak in the DCS at $\theta_{\rm lab}=$ 0.47 mrad has been observed by Horsdal-Pedersen *et al.* (1983) at impact energies 2.82, 5.42, and 7.4 MeV. Using the COLTRIMS technique, Fischer *et al.* (2006) have reported their DCS data for electron capture at 7.5 and 12.5 MeV in the H^+-He collisions. In their experiment, the Thomas peak is clearly separated. Moreover, the angle at which the dip occurs between the kinematic and Thomas single-capture processes is determined with a higher precision than in the study of Horsdal-Pedersen *et al.* (1983).

C. Electron capture by hydrogenlike projectiles

In this section, we consider single-electron capture in two types of collisions, such as collisions between hydrogenlike projectiles and hydrogenlike targets as well as multielectron targets

$$(Z_P,e_1)+(Z_T,e_2)\rightarrow(Z_P;e_1,e_2)+Z_T, \tag{213}$$

$$(Z_P,e_1)+(Z_T,e_2;\{e_3,e_4,\ldots,e_{N+2}\}) \rightarrow(Z_P;e_1,e_2)+(Z_T;\{e_3,e_4,\ldots,e_{N+2}\}), \tag{214}$$

where $\{e_3,e_4,\ldots,e_{N+2}\}$ denotes N noncaptured electrons. In the case of a multielectron target, we introduce the following assumptions. All N noncaptured electrons are considered as passive such that their interactions with the active electrons e_1 and e_2 do not contribute to the capture process. We also suppose that the passive electrons occupy the same orbitals before and after the collisions (Belkić *et al.*, 1979). The final state of the target is ignored in such a frozen-core approximation. In this model, the passive electrons do not participate individually in capture of the active electron and this permits the use of an effective local target potential V_T. The transition amplitudes in the ensuing first Born approximation with the correct boundary conditions can be written in either the post or prior form as follows

$$T_{if}^{+}(\vec{\eta})=\int\int\int d\vec{s}_1 d\vec{s}_2 d\vec{R}\,\Phi_f^{-*}[V_T(x_1)+V_T(x_2)-2V_T(R)]\Phi_i^{+}, \tag{215}$$

$$T_{if}^{-}(\vec{\eta})=\int\int\int d\vec{s}_1 d\vec{x}_2 d\vec{R}\,\Phi_f^{-*}\left(V_T(x_1)-V_T(R)+\frac{Z_P-1}{R}-\frac{Z_P}{s_2}+\frac{1}{r_{12}}\right)\Phi_i^{+}, \tag{216}$$

$$\Phi_f^{-}=\psi_f(\vec{s}_1,\vec{s}_2)\exp\left(-i\vec{k}_f\cdot\vec{r}_f-i\frac{Z_P-2}{v}\int_Z^{\infty}dZ'V_T(R')\right), \tag{217}$$

$$\Phi_i^{+}=\psi_P(\vec{s}_1)\psi_i^T(\vec{x}_2)\exp\left(i\vec{k}_i\cdot\vec{r}_i-i\frac{Z_P-1}{v}\ln(vR-\vec{v}\cdot\vec{R})-i\frac{Z_P-1}{v}\int_{-\infty}^{Z}dZ'V_T(R')\right), \tag{218}$$

where $\psi_f(\vec{s}_1,\vec{s}_2)$ is the bound-state wave function of the atomic system $(Z_P;e_1,e_2)$, whose binding energy is ϵ_f. The hydrogenlike wave function of the (Z_P,e_1) system is denoted as $\psi_P(\vec{s}_1)$, and the corresponding binding energy is ϵ_P. The initial orbital $\psi_i^T(\vec{x}_2)$ of the active electron in the multielectron target satisfies the following equation

$$[-\tfrac{1}{2}\nabla_x^2-V_T(x)-\epsilon_i^T]\psi_i^T(\vec{x})=0. \tag{219}$$

The post and prior amplitudes (215) and (216) are identical to each other on the energy shell if (i) $\psi_i^T(\vec{x})$ is a solution of the eigenvalue problem (219) for a selected model potential $V_T(x)$ and (ii) the final bound-state wave function $\psi_f(\vec{s}_1,\vec{s}_2)$ is exact. Whenever at least one of these two conditions is not satisfied, there will be a post-prior discrepancy.

For a given central field $V_T(x)$, Eq. (219) can be solved numerically. Certain realistically screened potentials for a neutral target atom are appealing, such as those of Green, Sellin, and Zachor (GSZ) (Green *et al.*, 1969) or Herman and Skillman (1963) (HS), since they exhibit two correct asymptotic behaviors $(-Z_T/x)$ and $(-1/x)$ at small and large values of x, respectively. Nevertheless, these atomic model potentials are not practical within the present distorted-wave formalism, since they preclude analytical calculation of the Coulomb phase integrals. However, the standard analytical calculation of the whole T matrix, e.g., within the CDW method, can be reestablished by choosing a pure Coulomb potential $V_T(x)=-Z_T^{\rm eff}/x$ for a multielectron target, where $Z_T^{\rm eff}$ is an effective nuclear charge. We proceed in this way and choose the value of $Z_T^{\rm eff}$ following Belkić *et al.* (1979). This is done by requiring that the energy due to $V_T(x)=-Z_T^{\rm eff}/x$, for an electron occupying the orbital of the principal quantum number n_i, be equal to the RHF two-parameter orbital energy $\epsilon_i^{\rm RHF}$ (Clementi and Roetti, 1974), i.e., $Z_T^{\rm eff}=n_i(-2\epsilon_i^{\rm RHF})^{1/2}$. For the initial state of the active electron in a multielectron target, we employ the RHF wave function given as a linear combination of the normalized STOs via

$$\psi_i^{\rm RHF}(\vec{r})=\sum_{k=1}^{N_i}C_k\chi_{n_k l_i m_i}^{(\alpha_k)}(\vec{r}), \tag{220}$$

$$\chi_{n_k l_i m_i}(\vec{r})=\sqrt{\frac{(2\alpha_k)^{1+2n_k}}{(2n_k)!}}r^{n_k-1}e^{-\alpha_k r}Y_{l_i,m_i}(\hat{\vec{r}}), \tag{221}$$

where C_k and α_k are the parameters obtained variationally by Clementi and Roetti (1974) and n_k is the orbital number.

Consistent treatments of electron capture from a multielectron target by a bare projectile have been performed on ion-atom collisions (Bachau *et al.*, 1988; Belkić, 1989a; Decker and Eichler, 1989a; Belkić and Mančev, 1990; Dewangan and Eichler, 1994). A direct comparison between, e.g., the GSZ and RHF models shows that total cross sections are only slightly sensitive to the choice of the target potential. For example, the magnitude of the difference between the two sets of charge exchange total cross sections using the GSZ and RHF models for the H^+-C and He^{2+}-Li collisions does not exceed 15% at intermediate and high energies within the CB1-3B method (Belkić and Mančev, 1990). A test computation (Belkić, 1989b) of the H^+-He charge exchange demonstrated that the HS potential for the target yields total cross sections that differ from the RHF model by at most 12%. Assuming that a similar conclusion would also hold true for the problems considered in the present study and bearing in mind the advantages of analytical calculations, we consider a model with the Coulomb potential V_T and the target

STOs. As mentioned, the related effective charge $Z_T^{\rm eff}$ will be determined following Belkić *et al.* (1979). A direct consequence of these simplifications is a reduction of the complicated multielectron process (214) to a more manageable four-body problem

$$(Z_P,e_1)+(Z_T^{\rm eff},e_2)\rightarrow(Z_P;e_1,e_2)+Z_T^{\rm eff}. \tag{222}$$

Under these circumstances, the transition amplitudes (215) and (216) become (Mančev, 1996)

$$T_{if}^{+}(\vec{\eta})=Z_T^{\rm eff}\int\int\int d\vec{s}_1 d\vec{s}_2 d\vec{R}\,(\rho v)^{2i\nu_f}\times e^{-i\vec{v}\cdot\vec{s}_2+i\vec{\beta}\cdot\vec{R}}\psi_f^{*}(\vec{s}_1,\vec{s}_2)\left(\frac{2}{R}-\frac{1}{x_1}-\frac{1}{x_2}\right)\times\psi_P(\vec{s}_1)\psi_i^{\rm RHF}(\vec{x}_2)(vR-\vec{v}\cdot\vec{R})^{i\xi}, \tag{223}$$

$$T_{if}^{-}(\vec{\eta})=\int\int\int d\vec{s}_1 d\vec{x}_2 d\vec{R}\,(\rho v)^{2i\nu_f}e^{-i\vec{v}\cdot\vec{s}_2+i\vec{\beta}\cdot\vec{R}}\psi_f^{*}(\vec{s}_1,\vec{s}_2)\times\left(\frac{Z_T^{\rm eff}+Z_P-1}{R}-\frac{Z_T^{\rm eff}}{x_1}-\frac{Z_P}{s_2}+\frac{1}{r_{12}}\right)\times\psi_P(\vec{s}_1)\psi_i^{\rm RHF}(\vec{x}_2)(vR-\vec{v}\cdot\vec{R})^{i\xi}, \tag{224}$$

where $\xi=(Z_T^{\rm eff}-Z_P+1)/v$ and $\nu_f=Z_T^{\rm eff}(Z_P-2)/v$. Here the usual eikonal approximation is also employed, and furthermore

$$\vec{k}_i\cdot\vec{r}_i+\vec{k}_f\cdot\vec{r}_f=-\vec{v}\cdot\vec{s}_2+\vec{\beta}\cdot\vec{R},\quad \vec{\beta}=-\vec{\eta}-\beta_z\hat{\vec{v}},$$

$$\beta_z=v/2+\Delta\epsilon/v,\quad \Delta\epsilon=\epsilon_P+\epsilon_i^{\rm RHF}-\epsilon_f.$$

Using the Nordsieck technique, Mančev (1996) calculated the matrix elements of the post form T_{if}^{+} in terms of two-dimensional real integrals. Evaluation of the prior form of the transition amplitude is more difficult only from a numerical point of view; namely, the term $1/r_{12}$ in the perturbation potential from Eq. (224) requires an additional three-dimensional integral in T_{if}^{-} which must be carried out numerically. Therefore, the prior matrix elements T_{if}^{-} from Eq. (224) can be reduced to a five-dimensional quadrature. Following the procedure of Belkić (1993c) for evaluating matrix elements of this type, Mančev (1996) presented another method of calculation which yields the basic post matrix element T_{if}^{+} in the form of a one-dimensional integral over the real variable belonging to the interval [0,1].

D. Comparison between theories and experiments for single-electron capture

In this section, we use two and three examples for the processes (213) and (214), respectively. They are given by the following rearrangement collisions

$$\mathrm{H}+\mathrm{H}\rightarrow\mathrm{H}^-+\mathrm{H}^+, \tag{225}$$

$$^4\mathrm{He}^+ + \mathrm{H}\rightarrow{}^4\mathrm{He}+\mathrm{H}^+, \tag{226}$$

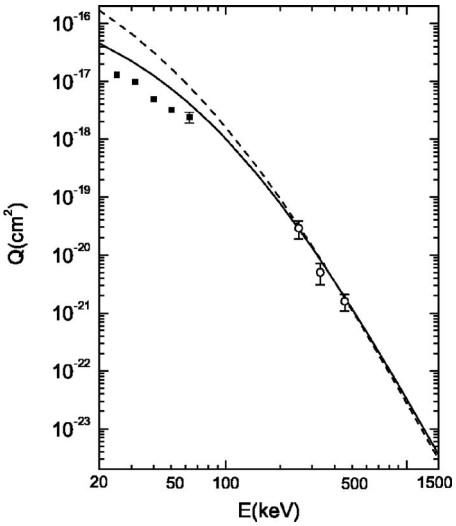

FIG. 24. Total cross sections Q (cm^2) for single-electron capture in the collisional reaction $\mathrm{H}+\mathrm{H}\rightarrow\mathrm{H}^-+\mathrm{H}^+$ as a function of incident energy. Solid curve: the CB1-4B method (Mančev, 1995); dashed curve: the first Born approximation (Mapleton, 1960, 1965). Experimental data: ● (McClure, 1968) and ○ (Schryber, 1967).

$$^4\mathrm{He}^+ + {}^4\mathrm{He}\rightarrow{}^4\mathrm{He}+{}^4\mathrm{He}^+, \tag{227}$$

$$\mathrm{H}+{}^4\mathrm{He}\rightarrow\mathrm{H}^-+{}^4\mathrm{He}^+, \tag{228}$$

$$^7\mathrm{Li}^{2+}+{}^4\mathrm{He}\rightarrow{}^7\mathrm{Li}^+ + {}^4\mathrm{He}^+. \tag{229}$$

The results obtained from the CB1-4B method for the total cross sections for reaction (225) are shown in Fig. 24 (Mančev, 1995). The wave function for the negative hydrogen ion is described by means of the 2-parameter orbital of Silverman *et al.* (1960). Comparison of these theoretical results with the experiment is limited to the data of McClure (1968). His results are the only experimental data available for (225), and they are at the restricted impact energies $E\leqslant 63$ keV. However, in the same figure, the experimental results of Schryber (1967) for the reaction $\mathrm{H}+\mathrm{H}_2\rightarrow\mathrm{H}^-+\mathrm{H}_2^+$ are also plotted. Here the values for the experimentally determined cross sections are divided by 2; namely, we assumed that the hydrogen molecule could be treated as two isolated H atoms (the Bragg sum rule). It can be seen in Fig. 24 that the agreement between the CB1-4B method and the experimental data is good. The theoretical curve of Mapleton (1960, 1965) in the first Born approximation is also displayed in Fig. 24. The difference between the CB1-4B method (Mančev, 1995) and the first Born approximation used by Mapleton (1960, 1965) is in the Coulomb phase factors. These phases are completely ignored by Mapleton (1960, 1965). Such a comparison should provide valuable information on the importance of the correct boundary conditions for the problem under study. Figure 24 shows that the CB1-4B method employed by Mančev (1995) yields a significant improvement over the cross sections given by Mapleton (1960, 1965) when compared with experiments. As expected, Fig. 24 dem-

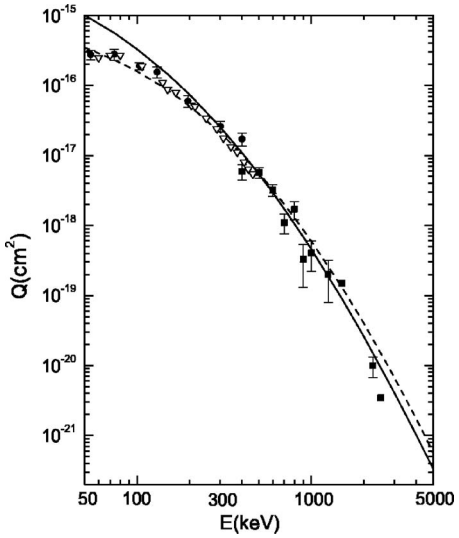

FIG. 25. Total cross sections Q (cm^2) for single-charge exchange in the reaction $^4He^+ + H \rightarrow {}^4He + H^+$ as a function of incident energy. Dashed curve: the CB1-4B method (Mančev, 1995). Solid curve: the CDW-4B method (Mančev, 2007). Both computations refer to the post forms carried out using the two-parameter wave function of Silverman *et al.* (1960) for helium. Experimental data: ● (Olson *et al.*, 1977), ■ (Hvelplund and Andersen, 1982), and ▽ (Shah and Gilbody, 1995).

onstrates that the logarithmic phase factors play a more prominent role at lower than at higher impact energies.

In Fig. 25, the theoretical results of Mančev (1996, 2007) from the CB1-4B and CDW-4B methods for process (226) are compared with the experimental data of Olson *et al.* (1977). The dashed and solid curves refer, respectively, to the CB1-4B and CDW-4B methods with the wave function of Silverman *et al.* (1960) for helium. The wave function of Löwdin (1953) for helium yields very similar cross sections (Mančev, 1996). The agreement between the CB1-4B as well as CDW-4B methods and the experimental data can be considered as satisfactory.

The cross sections for charge exchange in the reaction (227) are depicted in Fig. 26. Despite the fact that there are many experimental data for the reaction (227), theoretical studies are scarce, because of the difficulties which arise in treating collision systems that are more complex than a three-body problem. The CB1-4B method extended to the reaction (227) by Mančev (1996, 2007) provides the first quantum-mechanical description of this problem. The CB1-4B and CDW-4B methods are seen in Fig. 26 to be in satisfactory agreement with the available measurements. At lower impact energies, the CB1-4B and CDW-4B methods overestimate the experimental findings, as anticipated.

The results of computations using the CB1–4B method (Mančev, 1996) for the formation of the $H^-(1s^2)$ ions in the H-He collisions, i.e., for process (228), are plotted in Fig. 27. The ground state of the H^- ion is described by the two-parameter wave function of Silverman *et al.* (1960). It should be noted that the two-electron orbital of Silverman *et al.* (1960) gives a bound energy for $H^-(1s^2)$ below −0.5 a.u. (ϵ_f = −0.513 328 9 a.u.) which ensures a stable bound state of the H^- ion. In Fig. 27, the cross sections from the CB1-4B method are compared with the experimental

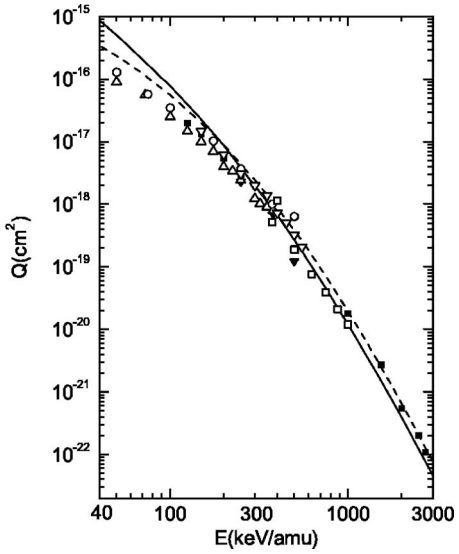

FIG. 26. Total cross sections Q (cm^2) as a function of laboratory incident energy for symmetric single-charge exchange $^4He^+ + {}^4He \rightarrow {}^4He + {}^4He^+$. Dashed curve: the CB1-4B method (Mančev, 1996, 2007). Solid curve: the CDW-4B method (Mančev, 2007). Both computations refer to the post forms carried out using the two-parameter wave function of Silverman *et al.* (1960) for helium in the exit channel and the RHF wave function for helium in the entrance channel. Experimental data: ■ (Forest *et al.*, 1995), □ (de Castro Faria *et al.*, 1988) ○ (DuBois, 1989), ▽ (Atan *et al.*, 1991), ▼ (Itoh *et al.*, 1980), and △ (Pivovar *et al.*, 1961).

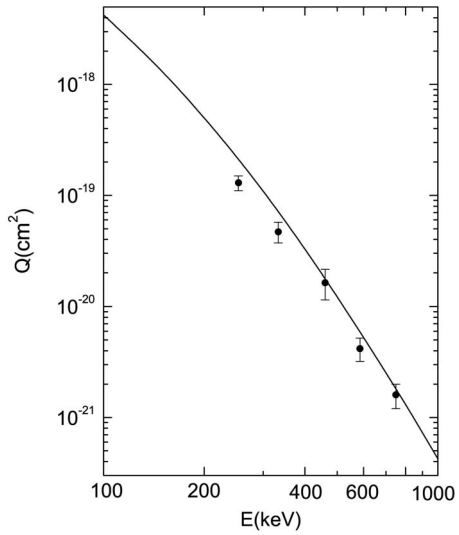

FIG. 27. Total cross sections Q (cm^2) as a function of laboratory incident energy E (keV) for single-charge exchange $H + {}^4He \rightarrow H^- + {}^4He^+$. The solid curve is due to the post version of the CB1-4B method as computed by Mančev (1996) using the two-parameter wave function of Silverman *et al.* (1960) for the negative hydrogen ion $H^-(1s^2)$ in the exit channel and the RHF wave function for target helium in the entrance channel. Experimental data: ● (Schryber, 1967).

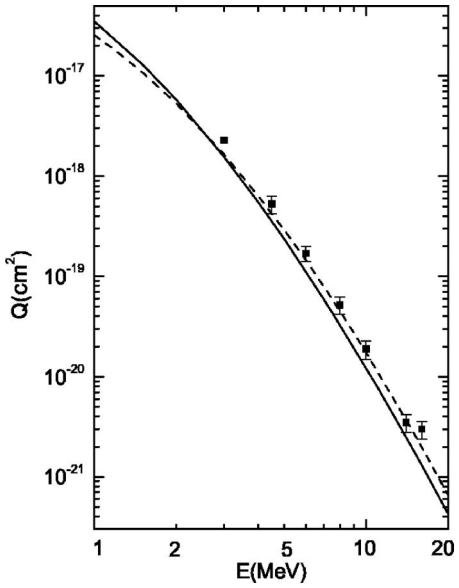

FIG. 28. Total cross sections Q (cm^2) as a function of laboratory incident energy for asymmetric single-charge exchange $^7Li^{2+}+{}^4He \rightarrow {}^7Li^{+}+{}^4He^{+}$. Dashed curve: the CB1-4B method (Mančev, 1995). Solid curve: the CDW-4B method (Mančev, 2007). Both computations refer to the post forms carried out using the two-parameter wave function of Silverman *et al.* (1960) for the heliumlike ion $Li^{+}(1s^2)$ in the exit channel and the RHF wave function for target helium in the entrance channel. Experimental data: ■ (Woitke *et al.*, 1998).

data of Schryber (1967). Agreement between the theory and the measurement is quite good.

The total cross sections from the CB1-4B (Mančev, 1995) and CDW-4B (Mančev, 2007) methods for single-electron capture in the process (229) are given in Fig. 28. A comparison between these theoretical results and the experimental data of Woitke *et al.* (1998) shows satisfactory agreement.

VII. SIMULTANEOUS TRANSFER AND EXCITIATION

In the second part of this review, we consider resonant collisions involving, e.g., two hydrogenlike atomic systems

$$(Z_P,e_1)_{i_1}+(Z_T,e_2)_{i_2}\rightarrow (Z_P;e_1,e_2)_f^{**}+Z_T. \tag{230}$$

This is a simultaneous transfer and excitation, the TE process, where a doubly excited (autoionizing) state is produced in the projectile after capture of the target electron. Here two processes interfere through the so-called resonant and nonresonant modes, i.e., the RTE and NTE modes, respectively. The RTE mode occurs via capture of the target electron and excitation of the projectile electron by means of the interaction $1/r_{12}$ between the two electrons. The NTE mode appears when the target electron is transferred by its interaction with the projectile nucleus, whereas the excitation of the heliumlike projectile comes from the interaction of the projectile electron with the target nucleus (Gayet *et al.*, 1997). Reaction (230) is the prototype as the simplest example of a TE. Of course, the TE can also occur in more complicated colliding particles, involving, e.g., a multielectron target. An example is the first experiment on TE by Tanis *et al.* (1982) who measured the total cross sections for the S^{13+}-Ar collision system.

The doubly excited state of the projectile in the exit channel of (230) relaxes either by radiative decay via x-rays emission (TEX) or through the Auger mechanism (TEA), thus providing two different and complementary experimental approaches for understanding the TE process (Itoh *et al.*, 1985; Justiniano *et al.*, 1987). The first experimental evidence of the resonant TEX mode (RTEX) was reported by Tanis *et al.* (1982). A similar measurement of the TE via the RTEX mode was subsequently made on a molecular target by Schulz *et al.* (1987). In the theoretical studies by Brandt (1983) and Feagin *et al.* (1984), the RTE and NTE were first considered as two independent modes. However, the basic features of the CDW-4B method could obviously provide a more adequate description of the TE by a natural introduction of the critical interference effects between the RTE and NTE modes (Bachau *et al.*, 1992; Gayet and Hanssen, 1992). Furthermore, the CDW-4B method can be of help in interpreting the experiment of Justiniano *et al.* (1987). Here a very asymmetric collisional system S^{15+}-H was investigated, where the state $(S^{14+})^{**}$ formed in the exit channel decays via the radiative emission lines $K\alpha$-$K\alpha$ and $K\alpha$-$K\beta$ which are dominated by the RTEX mode. The CDW-4B method has been found (Bachau *et al.*, 1992) to be in good agreement with the experimental data of Justiniano *et al.* (1987), as well as with the results of Brandt (1983). Furthermore, it has been reported (Bachau *et al.*, 1992) that the interference between the RTE and NTE modes can be important if the TE process occurs as the result of a nearly symmetrical collisional system such as He^{+}-H or He^{+}-He. These two latter collisions involving the TE process have been studied experimentally (Itoh *et al.*, 1985) and theoretically (Gayet *et al.*, 1995, 1997; Ourdane *et al.*, 1999). The latter two theoretical studies used the CDW-4B method. Here the TE process is observed experimentally through the TEA mode. Agreement between the experimental data obtained using the 0° electron spectroscopy technique and the theoretical cross sections computed by the CDW-4B method for the TEA mode is not satisfactory. These theoretical total cross sections showed that some autoionizing states largely underestimate the corresponding experimental data of Itoh *et al.* (1985). Such a discrepancy could be due to competition between direct and indirect TE. The direct TE is the customary TE, which we have already defined. The indirect TE is a process in which forward emitted electrons are generated through two intermediate channels: (a) direct target ionization, and (b) simultaneous capture of the target electron and ionization of the projectile electron. The direct and indirect TE cannot be distinguished if the electron ejected from the target is not detected by a coincident measurement. Subsequently, Ourdane *et al.* (1999) revisited this problem using the CDW-4B

method, but this time with a more consistent description of the final autoionizing state, by including the adjacent continuum components in addition to the discrete ones. Specifically, the final state used by Ourdane *et al.* (1999) is described within the atomic resonant structures from the formalism of Fano (1961).

A. The CDW-4B method for the TE process

As mentioned, the main feature of the CDW-4B method of key relevance for the TE process is preservation of the phase relation between the NTE and RTE modes. The prior transition amplitude for the basic TE process (230) in the CDW-4B method can be written as (Gayet and Hanssen, 1992)

$$T_{if}^{-} = N_{if}^{-} \int\int\int d\vec{R}\, d\vec{r}_1 d\vec{r}_2 e^{i\vec{k}_i\cdot\vec{r}_i + i\vec{k}_f\cdot\vec{r}_f} (\mu v\rho)^{2i\nu} \times \varphi_f^*(\vec{s}_1,\vec{s}_2)\, {}_1F_1(i\nu_T;1;ivx_2 + i\vec{v}\cdot\vec{x}_2) \times \left\{ \left(\frac{1}{r_{12}} - \frac{1}{s_2} + \frac{Z_T}{R} - \frac{Z_T}{x_1} \right) \varphi_P(\vec{s}_1)\varphi_T(\vec{x}_2) \times {}_1F_1(i\nu_P;1;ivs_2 + i\vec{v}\cdot\vec{s}_2) - \varphi_P(\vec{s}_1) \times \vec{\nabla}_{x_2}\varphi_T(\vec{x}_2)\cdot\vec{\nabla}_{s_2}\, {}_1F_1(i\nu_P;1;ivs_2 + i\vec{v}\cdot\vec{s}_2) \right\}, \quad (231)$$

where $N_{if}^{-} = \Gamma(1-i\nu_P)\Gamma(1-i\nu_T)e^{\pi(\nu_P+\nu_T)/2}$, $\nu_P = (Z_P-1)/v$, $\nu_T = Z_T/v$, $\nu = Z_T(Z_P-1)/v$. Here the phase factor $(\mu v\rho)^{2i\nu}$ stems from the eikonal approximation to the relative motion of the heavy particles. As before, this phase can be omitted for the computation of the total cross sections (Belkić *et al.*, 1979). Moreover, such an omission is not limited to total cross sections alone, since it can be made whenever the integration over $\vec{\eta}$ has been carried out. This applies also to cross sections that are differential in the energy and/or angle or ejected electrons generated by either direct or indirect ionization. Since only the electron e_2 is transferred, one has the usual kinematic relation

$$\vec{k}_i\cdot\vec{r}_i + \vec{k}_f\cdot\vec{r}_f \simeq -\vec{\eta}\cdot\vec{\rho} - \left(\frac{1}{2} + \frac{\epsilon_i - \epsilon_f}{v^2}\right)\vec{v}\cdot\vec{R} - \vec{v}\cdot\vec{s}_2. \quad (232)$$

Here $\epsilon_i = \epsilon_P + \epsilon_T$, where ϵ_P and ϵ_T are the initial electronic energies of the bound states in the hydrogenlike systems $(Z_P,e_1)_{i_1}$ and $(Z_T,e_2)_{i_2}$, respectively. Likewise, ϵ_f is the final electronic energy of the doubly excited state of the system $(Z_P;e_1,e_2)_f^{**}$. Moreover, in Eq. (231) for T_{if}^{-}, the level of approximation made for the excitation process is similar to the usual first Born approximation, which is well known to give good results for the excitation process at high impact velocities. More importantly, the transition amplitude for TE from Eq. (231) contains a coherent contribution from both the RTE and NTE modes.

B. Comparison between theories and experiments

The type of deexcitation (radiative or Auger) occurring after the formation of an autoionizing state via the TE process depends on the ratio between Z_P and Z_T. Specifically, there are two limiting cases: (i) if $Z_P/Z_T \gg 1$, the process is radiative via the TEX mode, and (ii) if $Z_P/Z_T \simeq 1$, the deexcitation is an Auger process via the TEA mode.

1. The TEX mode for radiative decays of asymmetric systems

a. The model of Brandt for the RTEX mode

The first model for the RTEX mode was proposed by Brandt (1983) along the lines of the dielectronic recombination (DR) process (McLaughlin and Hahn, 1982). In the DR process, a free electron moving with momentum $\vec{p}$ with respect to an ion of nuclear charge Z_P is captured

$$(Z_P,e_1)_i + e_2 \rightarrow (Z_P;e_1,e_2)_f, \quad (233)$$

where i and f are the usual quantum numbers of the initial and final bound states in the entrance and exit channels, respectively. The energy conservation for this process gives $p^2/2 + \epsilon_i = \epsilon_f$, where ϵ_i and ϵ_f are the initial and final electronic binding energies, respectively. Therefore, the DR process is resonant whenever

$$p = \sqrt{2(\epsilon_f - \epsilon_i)} \equiv p_r. \quad (234)$$

The difference between the DR process and the RTEX mode of the TE collision is that the electron e_2 captured by the projectile $(Z_P,e_1)_i$ is not free, but rather it is bound to the target with binding energy ϵ_T. The model of Brandt (1983) is especially adapted to the case where $\epsilon_T \ll \epsilon_i$, i.e., for highly asymmetric collisions ($Z_P \gg Z_T$). In such an approximation, ϵ_T can be neglected so that the influence of the target is manifested merely through the momentum distribution $|\tilde{\varphi}_i(\vec{k})|^2$, where $\tilde{\varphi}_i(\vec{k})$ is the wave function in the momentum space representation. Here $\vec{k}$ is the electron momentum in the target frame. In fact, in the projectile frame, the quasifree electron e_2 has an energy distribution that exhibits a very large peak. Following McLaughlin and Hahn (1982), the cross section for the RTEX mode can be written as the standard convolution

$$Q_{\mathrm{RTEX}} = \int d\vec{k}\, Q_{\mathrm{DR}}(p)|\tilde{\varphi}_i(\vec{k})|^2, \quad (235)$$

where $Q_{\mathrm{DR}}(p)$ is the cross section for the DR process, whereas $\vec{p}$ is the electron momentum in the projectile frame

$$\vec{p} = \vec{k} - \vec{v}. \quad (236)$$

Here $\vec{v}$ is the impact velocity in the laboratory frame whose origin is placed at the target, which is presumed to be at rest.

While $Q_{\mathrm{DR}}(p)$ is strongly peaked around $p = p_r$, the distribution $|\tilde{\varphi}_i(\vec{k})|^2$ is much broader, with a maximum at

some $k=k_{\max}$. For a collision occurring at a high impact energy, we have $v \gg k_{\max}$, in which case Eq. (236) gives

$$p \simeq \sqrt{v^2 - 2vk_z}, \tag{237}$$

where k_z is the projection of the momentum $\vec{k}$ onto the velocity $\vec{v}$ which is itself along the Z axis. In this case, Eq. (235) becomes

$$Q_{\mathrm{RTEX}} \simeq \int_{-\infty}^{+\infty} dk_z P_i(k_z) Q_{\mathrm{DR}}(p), \tag{238}$$

where $P_i(k_z)$ is the Compton profile of the target

$$P_i(k_z) = \int_{-\infty}^{+\infty} dk_x \int_{-\infty}^{+\infty} dk_y |\tilde{\varphi}_i(\vec{k})|^2. \tag{239}$$

It is well known that $Q_{\mathrm{DR}}(p)$ is a sharp and narrow function of width Γ around p_r, whereas $P_i(k_z)$ is a much more slowly varying function. Such a circumstance justifies the usage of the standard mean-value theorem (Prudnikov *et al.*, 1981) [also termed the impulse approximation by Brandt (1983)], in which case the cross section Q_{RTEX} acquires the form

$$Q_{\mathrm{RTEX}} \simeq \frac{1}{v} P_i(k_{z_r}) \int_{\epsilon_r - \Delta\epsilon_r/2}^{\epsilon_r + \Delta\epsilon_r/2} d\varepsilon \, Q_{\mathrm{DR}}(\varepsilon), \tag{240}$$

where k_{z_r} is the value of k_z at resonance as in Eq. (234), and $\Delta\epsilon_r$ is an interval around ϵ_r. The cross section Q_{DR} depends upon ε via $\varepsilon = p^2/2$, where p is given by Eq. (237). The above integration over the whole resonance width Γ should not depend upon $\Delta\epsilon_r$. This will be the case if the parameter $\Delta\epsilon_r$ is taken to be sufficiently large relative to the resonance width ($\Delta\epsilon_r \gg \Gamma$). The model of Brandt (1983) is expected to be successful in predicting both the magnitude and the shape of the RTEX cross section for collisions between multiply charged ions and light atoms or molecules. This is indeed the case, as illustrated in Figs. 29 and 30. The limitation of this approximation is the relationship (237), which entails the condition $v \gg k_{\max}$. Overall, the model of Brandt (1983) is restricted to asymmetric collisions ($Z_P \gg Z_T$) and, as such, cannot treat the nonresonant TEX (NTEX) mode.

b. A model for the NTEX modes

In this mode, excitation is produced by interactions between the projectile electron and target nucleus. Simultaneously, capture is due to interactions between the target electron and projectile nucleus. These two processes can be considered as being independent of each other, provided that the interaction between the two active electrons does not play a significant role in the dynamics of the collision. In this case the IPM applies, so that the total cross section for the NTEX mode has been defined by Brandt (1983) via

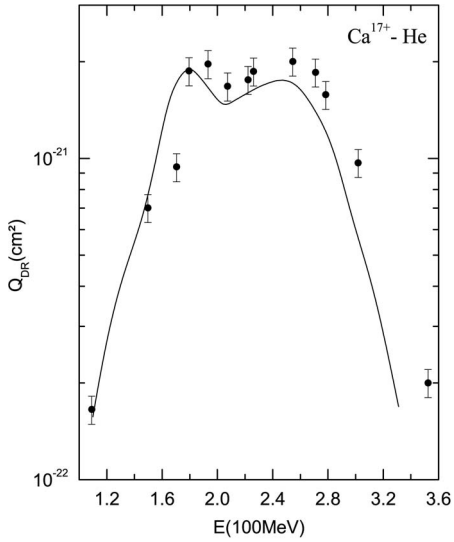

FIG. 29. The Ca^{17+}-He collisional system. Shown are the RTEX peaks for these asymmetric collisions ($Z_P \gg Z_T$). Theoretical curve (McLaughlin and Hahn, 1982) and experimental data (circles) (Tanis *et al.*, 1982).

$$Q_{\mathrm{NTEX}}^{\mathrm{IPM}} \equiv Q_{\text{exc-cap}} = 2\pi \int_0^{\infty} P_{\mathrm{exc}}(b) P_{\mathrm{cap}}(b) b \, db. \tag{241}$$

Here b is the impact parameter, whereas $P_{\mathrm{exc}}(b)$ and $P_{\mathrm{cap}}(b)$ are the excitation and capture probabilities, respectively. A refinement of this model, still within the IPM for the NTEX, has been made by Hahn (1989), and Hahn and Ramadan (1989). This is achieved by considering that formation of a doubly excited state (say, d) is followed by a stabilizing radiative decay of d with the so-called fluorescence yield denoted by $\omega(d)$. Then the total cross section for the NTEX mode becomes

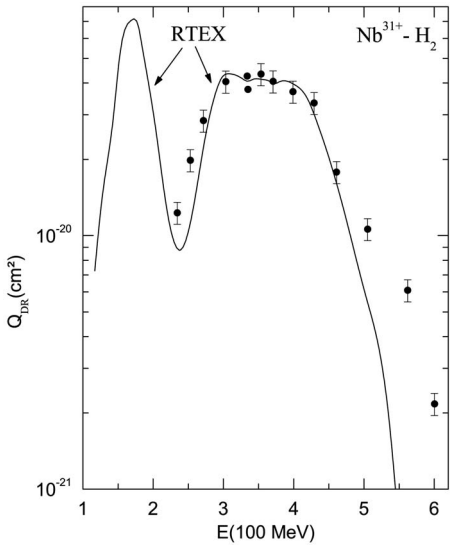

FIG. 30. The Nb^{31+}-H_2 collisional system. Shown are the RTEX peaks for these asymmetric collisions ($Z_P \gg Z_T$). Theoretical curve (McLaughlin and Hahn, 1982) and experimental data (circles) (Tanis *et al.*, 1982).

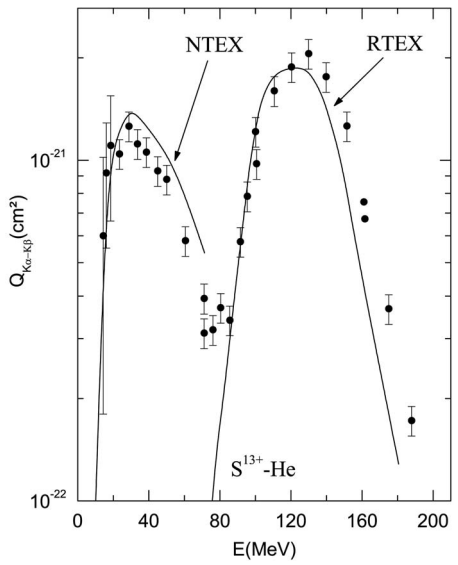

FIG. 31. The RTEX and NTEX cross sections for the collisional S^{13+}-He system. Theoretical curves (Hahn, 1989) and experimental data (circles) (Tanis, 1987). The results shown by the curve NTEX are multiplied by 3.

$$Q_{\mathrm{NTEX}}^{\mathrm{IPM}} = \sum_d \omega(d) Q_{\mathrm{NTE}}^{\mathrm{IPM}}(d), \tag{242}$$

$$Q_{\mathrm{NTE}}^{\mathrm{IPM}}(d) = \frac{1}{2\pi v^2} \int_{q_{\min}}^{q_{\max}} q\, dq \int d\vec{k}\, P_i(k_z) \times |C(\vec{k})|^2 |F(\vec{q}-\vec{k})|^2, \tag{243}$$

where $\vec{q}$ is the transfer momentum $\vec{q}=\vec{k}_i-\vec{k}_f$ with $q_{\min}=\Delta\epsilon_{if}/v \equiv (\epsilon_i-\epsilon_f)/v$ and $q_{\max}=k_i+k_f \simeq \infty$. Here $|C(\vec{k})|^2$ and $|F(\vec{q}-\vec{k})|^2$ are capture and excitation probabilities, respectively, whereas $P_i(k_z)$ is the Compton profile from Eq. (239). Since $|C(\vec{k})|^2$ decreases rapidly and $|F(\vec{q}-\vec{k})|^2$ increases with energy, it follows that the product of these two probabilities should give a peak. Such a peak would occur at an energy which is lower than the one from the RTEX mode. Moreover, if the Compton profile is not too large, the NTEX and RTEX peaks are expected to be very well separated. Indeed, this is shown in Fig. 31 for the case of the S^{13+}-He system, for which the two peaks are seen as being distinctly separated.

C. The CDW-4B method for the TEX modes

For simplicity, we consider the prototype reaction (230), assuming that both hydrogenlike atomic systems in the entrance channel are in their ground states ($i_1=i_2=1s$). For such a process, the transition amplitude in the CDW-4B method is given by Eq. (231) for arbitrary charges Z_P and Z_T. In Eq. (231), the autoionizing state $\varphi_f(\vec{s}_1,\vec{s}_2)$ can be defined within the well-known Feshbach formalism (Feshbach, 1962). In this formalism of resonant scattering, a doubly excited state can be described using a set of hydrogenlike basis functions centered on Z_P (Bachau, 1984). Such a basis set should be adequate for heliumlike doubly excited autoionizing states. The formalism of Feshbach consists of discarding the lowest orbitals which could lead to an eigenstate below the investigated doubly excited state. Surely, one such discarded basis function could be the ground state of the projectile $(Z_P,e_1)_{i_1}$ if i_1 is chosen to be the lowest state of this hydrogenlike system in the TE process (230). Indeed, the illustrations for this latter process will be given only for the ground states ($i_1=1s, i_2=1s$) of the colliding hydrogenlike atoms. Thus, whenever the wave function $\varphi_P(\vec{s}_1)$ describes the ground state of the $(Z_P,e_1)_{i_1}$ system, this function will be absent from the CI basis set comprised of the purely hydrogenlike orbitals with the nuclear charge Z_P employed to construct $\varphi_f(\vec{s}_1,\vec{s}_2)$. As such, the overlap between the ground state $\varphi_P(\vec{s}_1)$ and $\varphi_f(\vec{s}_1,\vec{s}_2)$, as the integral over $\vec{s}_1$, will be equal to zero. This implies that the interaction $Z_T/R-1/s_2$ and the $\vec{\nabla}\cdot\vec{\nabla}$ potential operator will not contribute at all to the matrix element T_{if}^- in Eq. (231). Under these simplifying conditions, Eq. (231) is reduced to (Bachau *et al.*, 1992)

$$\begin{aligned} T_{if}^- &= N_{if}^- \int\int\int d\vec{R}\, d\vec{r}_1 d\vec{r}_2 \exp(i\vec{k}_i\cdot\vec{r}_i + i\vec{k}_f\cdot\vec{r}_f) \\ &\times {}_1F_1(i\nu_T;1;ivx_2+i\vec{v}\cdot\vec{x}_2)\varphi_f^*(\vec{s}_1,\vec{s}_2)\left(\frac{1}{r_{12}}-\frac{Z_T}{x_1}\right) \\ &\times \varphi_P(\vec{s}_1)\varphi_T(\vec{x}_2)\,{}_1F_1(i\nu_P;1;ivs_2+i\vec{v}\cdot\vec{s}_2) \\ &\equiv T_{if,12}^- + T_{if,1}^-. \end{aligned} \tag{244}$$

As mentioned, the phase $(\mu v\rho)^{2i\nu}$ is ignored whenever T_{if}^- is not used for cross sections that are differential in the angles of the scattered projectile. The matrix elements $T_{if,12}^-$ and $T_{if,1}^-$ denote the part of T_{if}^- associated with perturbations $1/r_{12}$ and $-Z_T/x_1$, respectively. The remaining integrals in Eq. (244) are of the same type as those encountered previously by Belkić and Mančev (1992) for double-charge exchange in the CDW-4B method. As discussed, for calculating such integrals, the Nordsieck technique can be used to reduce the transition amplitude to a triple quadrature which is subsequently evaluated numerically following the procedure of Belkić and Mančev (1992). The same technique has also been applied by Bachau *et al.* (1992) to T_{if}^- from Eq. (244).

D. The CDW-4B method for the TE process in asymmetric collisions

Here the results obtained by means of the CDW-4B method are compared with the corresponding data from collisional experiments on the TE process with a molecular target H_2 (Justiniano *et al.*, 1987; Schulz *et al.*, 1987). As usual, it is assumed that the molecule H_2 can be considered as two independent H atoms. Thus, an example of the equivalent four-body collisional system is (Bachau *et al.*, 1992)

$$S^{15+}(1s) + H(1s) \rightarrow S^{14+}(nl,n'l') + H^{+}. \quad (245)$$

The experimental data just mentioned show that the deexcitation of the autoionizing state $(nl,n'l')$ gives spectra with radiative decay lines $K\alpha$-$K\alpha$, $K\alpha$-$K\beta$, and $K\beta$-$K\beta$. The computations within the CDW-4B method include the $K\alpha$-$K\alpha$ and $K\alpha$-$K\beta$ lines at impact energies ranging between 80 and 160 MeV by covering most of the lowest resonances $(LL,LM,LN,\ldots)$. This energy range corresponds to a peak in the RTEX mode, as expected from Eq. (234).

1. The $K\alpha$-$K\alpha$ emission line from S^{14+}

The $K\alpha$-$K\alpha$ emission line is produced by three doubly excited states $(2s^2)^1S$, $(2p^2)^1D$, and $(2p^2)^1S$. The wave functions of these latter states are obtained using the code of Bachau (1984). The configuration $(2p^2)$ appears to be the major component among these three states. The $(2p^2)$ state can decay radiatively through the following two electric-dipole transitions

$$(2p^2) \xrightarrow{\text{Ly } \alpha} (1s,2p) \xrightarrow{\text{Ly } \alpha} (1s^2). \quad (246)$$

Since the experiments of Schulz *et al.* (1987) and Justiniano *et al.* (1987) were performed with unpolarized colliding aggregates, there is a probability of 1/4 to find the S^{15+}-H system in a definite singlet state. Therefore, a factor of 1/2 $(2\times 1/4)$ must be introduced in the calculations of the cross sections for the $K\alpha$-$K\alpha$ line emission in addition to the fluorescence yield $\omega(d)$, which includes some cascade contributions. Here the extra multiplying factor of 2 written inside the small parentheses stems from using the Bragg sum rule to convert the theoretical results on the S^{15+}-H system to the corresponding experimental data on the S^{15+}-H_2 system for the purpose of comparison. The contribution of cascades from higher doubly excited states $(KLM,KLN,\ldots)$ has been ignored in these computations. Both contributions from the RTEX and NTEX modes have been coherently included in the CDW-4B method through the first and second terms $T^{-}_{if,12}$ and $T^{-}_{if,1}$ in the full transition amplitude T^{-}_{if} from Eq. (244). However, it is expected that for a highly asymmetric collision with $Z_P \gg Z_T$, such as the process (245), the contribution from the NTEX mode becomes totally negligible relative to the RTEX mode.

The total cross sections for the reaction (245) are illustrated in Fig. 32 by comparing theory and experiment. The results for the RTEX mode treated by Brandt (1983) within the IPM are shown by the dashed curve. The cross sections of a more complete description by the CDW-4B method used by Bachau *et al.* (1992) are shown by a solid curve. These two methods compare favorably to each other, as well as to the experimental data of Justiniano *et al.* (1987). The agreement between the cross sections $Q^{\mathrm{IPM}}_{\mathrm{RTEX}}$ (Brandt, 1983) and $Q^{\mathrm{CDW\text{-}4B}}_{\mathrm{RTEX+NTEX}}$ (Bachau *et al.*, 1992) is good, as anticipated, due to the very small influence of NTEX on the process (245). In particular, the two theories are seen in Fig. 32 to be in nearly perfect accordance on the left wing of the resonance peak. On the right wing of the same peak, toward its high-energy tail, there is a discrepancy between the IPM and CDW-4B method. At these higher energies, the IPM is in better agreement with the experimental result than the CDW-4B method. This may be because the IPM includes some cascade effects, whereas the CDW-4B method does not. Such a conjecture is plausible, since Justiniano *et al.* (1987) have shown that cascade-based contributions to the TE process are important at high impact energies.

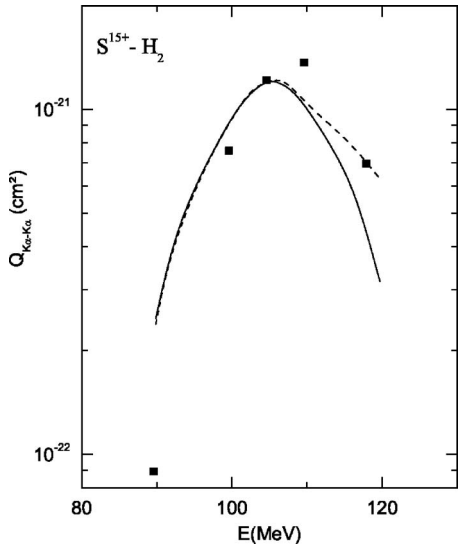

FIG. 32. Total cross sections for production of the $K\alpha$-$K\alpha$ lines from S^{14+}. Dashed curve: the DR model (Justiniano *et al.*, 1987). Solid curve: the CDW-4B method (Bachau *et al.*, 1992). Solid squares: experimental data (Justiniano *et al.*, 1987).

In Fig. 33, we present the state-selective total cross sections for the TE process studied using the CDW-4B

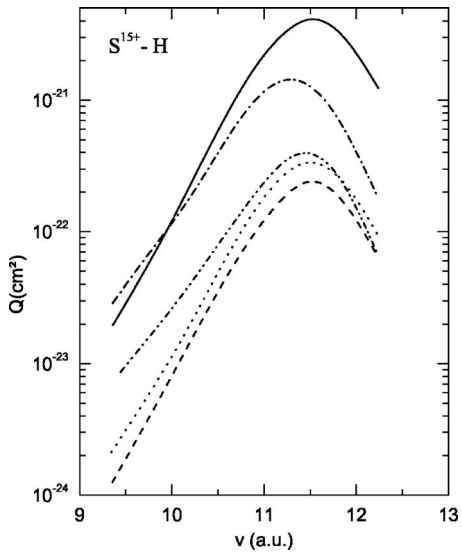

FIG. 33. State-selective total excitation cross sections in the CDW-4B method for the S^{15+}-H system (Bachau *et al.*, 1992). $(2s^2)\ ^1S$: singly chained curve; $(2p^2)\ ^1S$: doubly chained curve; $(2p^2)\ ^1D_0$: solid curve; $(2p^2)\ ^1D_{+1}$: dotted curve; $(2p^2)\ ^1D_{-1}$: dashed curve.

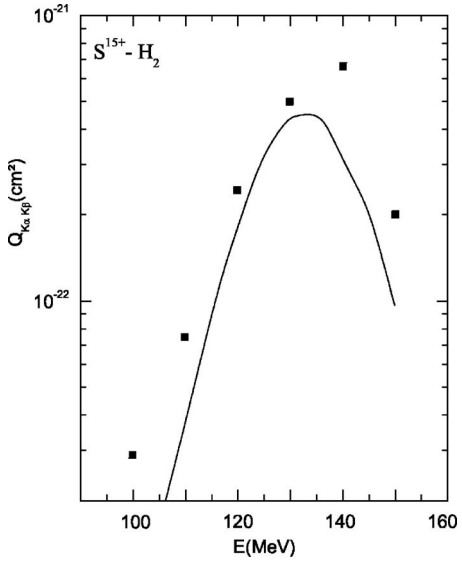

FIG. 34. Total cross sections for production of the $K\alpha$-$K\beta$ lines from S^{14+}. The solid curve represents the CDW-4B method (Bachau *et al.*, 1992), and solid squares are the experimental data (Justiniano *et al.*, 1987).

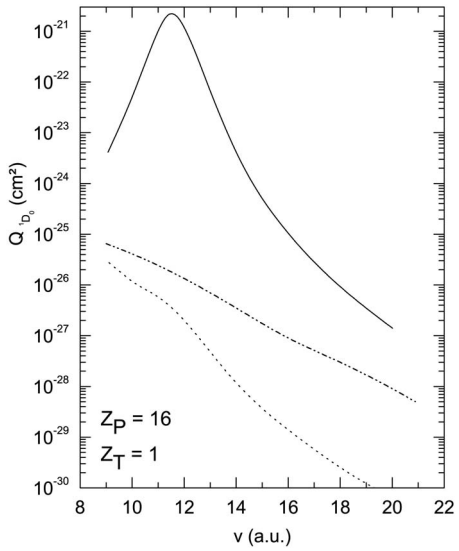

FIG. 35. Total cross sections in the CDW-4B method for excitation of the $(2p^2)\ ^1D_0$ state of S^{14+} in a collision of S^{15+} with atomic hydrogen target (Z_T=1) (Bachau *et al.*, 1992). Dotted curve: $Q_{1D_0}^{\mathrm{NTEX}}$; dashed curve: $Q_{1D_0}^{\mathrm{RTEX}}$; solid curve: $Q_{1D_0}^{\mathrm{TEX}}$; doubly-chained curve: CDW-IPM (Gayet and Hanssen, 1994). In this process, the RTEX and TEX total cross cross sections practically coincide with each other, due to a totally negligible influence of the NTEX mode, $Q_{1D_0}^{\mathrm{TEX}} \simeq Q_{1D_0}^{\mathrm{RTEX}}$ (solid and dashed curves indistinguishable). Here we set $1D_0 \equiv {}^1D_0$.

method for substates $(\lambda_0\lambda_0')\ ^{2S+1}L_M$, where M is the projection of the total momentum L. We observe that the substate $(2p^2)\ ^1D_0$ is dominant at $v>10$ a.u. ($E>80$ MeV).

2. The $K\alpha$-$K\beta$ emission lines from S^{14+}

The $K\alpha$-$K\beta$ emission in the process (245) is produced by five important configurations of the autoionizing state: $(2s3s)\ ^1S$, $(2p3p)\ ^1P$, $(2p3p)\ ^1D$, $(2s3d)\ ^1D$, and $(2p3p)\ ^1S$. Following the preceding case, the cascades (*KLN, KLO,*….) have been ignored. In Fig. 34, the results of the CDW-4B method are displayed together with the experimental data of Justiniano *et al.* (1987). Here we observe satisfactory agreement up to about 130 MeV. The maximum of the experimentally detected $K\alpha$-$K\beta$ peak is located at an impact energy around 140 MeV. This peak corresponds to the RTEX mode induced by the *KLM* cascade transition. Both this peak and its high-energy slope are underestimated by the CDW-4B method due to the neglect of all cascade contributions.

Regarding the $K\alpha$-$K\alpha$ and $K\alpha$-$K\beta$ emission lines, which are due primarily to the RTEX mode with the NTEX mode being negligible, it can generally be concluded that there is good agreement between the CDW-4B method and the experimental data. This provides motivation for extending the study to encompass interference effects between the RTEX and NTEX modes.

E. Influence of the target charge Z_T on the interference between the RTEX and NTEX modes

In this section, we analyze the dependence of the cross sections upon the interference effects between the RTEX and NTEX modes. This will be discussed for different charges of the target nucleus in the process

$$S^{15+}(1s) + (Z_T, e_2)_i \rightarrow S^{14+}[(2p^2)\ ^1D_0] + Z_T, \qquad (247)$$

where i=1s. Here the state $(2p^2)\ ^1D_0$ is chosen for the analysis, because this transition gives the largest cross section, as is clear from Fig. 33 (solid curve). Furthermore, for each value of the selected Z_T, computations have been made in the energy range corresponding to the peak in the RTEX mode. Another restriction in the computations is the standard condition for the validity of the CDW method at those impact energies that satisfy the inequality (164). As such, the lower limit of the validity of the CDW method is satisfied at an impact energy higher than 78 MeV (v=9.9 a.u.) for $Z_T \leqslant 7$, 128 MeV (v=12.7 a.u.) for Z_T=10, and 328 MeV (v=20.2 a.u.) for Z_T=16.

The cross sections for the process (247) treated by the CDW-4B method are presented in Figs. 35 and 36 for Z_T=1 and 10, respectively (Bachau *et al.*, 1992). The results for the RTEX, NTEX, and TEX modes are shown by the dashed, dotted, and solid curves, respectively. The total process includes the RTEX and NTEX nodes. Recall that, according to Eq. (244), the RTEX and NTEX modes are described by the terms $T_{if,12}^{-}$ and $T_{if,1}^{-}$, respectively. Computations have been carried out for Z_T=1, 4, 10, and 16 (Bachau *et al.*, 1992). The results obtained show that the location of the maximum of the RTEX peak shifts to larger v with Z_T increased, as also implied by Eq. (234). For example, this latter peak moves from

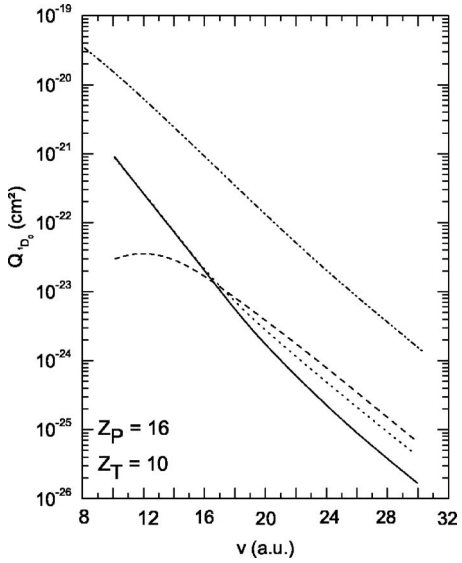

FIG. 36. The same as in Fig. 35, except for Z_T=10.

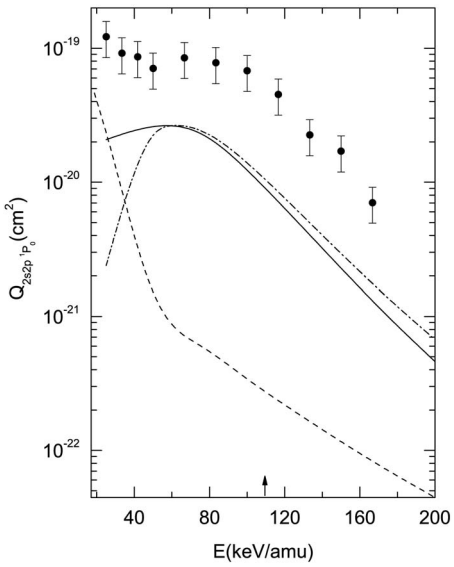

FIG. 37. The total cross section in the CDW-4B method for the RTEA, NTEA, and TEA modes of the collision $He^+(1s)+H(1s)\rightarrow He(2s2p\ ^1P_0)+H^+$ (Gayet *et al.*, 1995, 1997). Singly-chained curve: Q_{RTEA}. Dashed curve: Q_{NTEA}. Solid curve: Q_{TEA}. The solid circles are the experimental data (Zouros *et al.*, 1988) with an error of 30%. According to (164), the CDW-4B method should be valid above 110 keV/amu, as indicated by the vertical arrow on the abscissa.

v=11.5 a.u. for Z_T=1 (Fig. 35) to v=12.6 a.u. for Z_T=16 (not shown here; see Bachau *et al.*, 1992). It can be seen in Fig. 35 for Z_T=1 that at the energies within the RTEX peak ($8\leqslant v\leqslant 20$ a.u.) we have $Q_{NTEX}\ll Q_{RTEX}$. As a consequence, the interference between these two modes is totally negligible and there is no difference between the pure RTEX and TEX cross sections, so that the corresponding curves in Fig. 35 coincide. Figure 35 also confirms that the good agreement between the DR model (without NTEX) and the CDW-4B method, as seen earlier in Fig. 32 is not coincidental. For Z_T=4 (not shown), although Q_{NTEX} is much smaller (by two orders of magnitude) than Q_{RTEX}, a destructive interference effect (to within 15%) on the cross sections has been observed (Bachau *et al.*, 1992).

When Z_T increases, the contribution of the NTEX mode to the total cross section also increases, because its amplitude appears roughly proportional to Z_T, as is clear from $T_{if,1}^{-}$ in Eq. (244). As such, the cross section for the NTEX mode becomes dominant for Z_T=10 (Fig. 36) and Z_T=16 (Bachau *et al.*, 1992). In these cases, the shape of the RTEX peak is seen to disappear altogether. Thus, for production of the $(2p^2)\ ^1D_0$ state, the RTEX and NTEX modes may lead to a destructive interference. Overall, for the asymmetric case $Z_P\gg Z_T$, the TEX process is essentially dominated by the RTEX mode. However, for $Z_P\simeq Z_T$ interference effects can become important.

F. The TEA mode for nearly symmetrical systems: Auger decay

In the preceding section, the doubly excited state $(S^{14+})^{**}$ produced by a TE process via a collision between S^{15+} and H led to a radiative decay. Alternatively, the same TE process could also be completed when this doubly excited state decays through the Auger mechanism, i.e., via the TEA mode. This possibility has been investigated by Gayet *et al.* (1995, 1997) using the CDW-4B method for a He^+ projectile on a He or H target. The total cross sections obtained from the CDW-4B method are not in quantitative agreement with the experimental data of Itoh *et al.* (1985) and Zouros *et al.* (1988), as seen in Figs. 37 and 38 for the He^+-H collisions. Nevertheless, these theoretical results show in Figs. 37 and 38 that the interference between the RTEA and NTEA modes can be important (Gayet *et al.*, 1995, 1997). However, the experimental data for the produc-

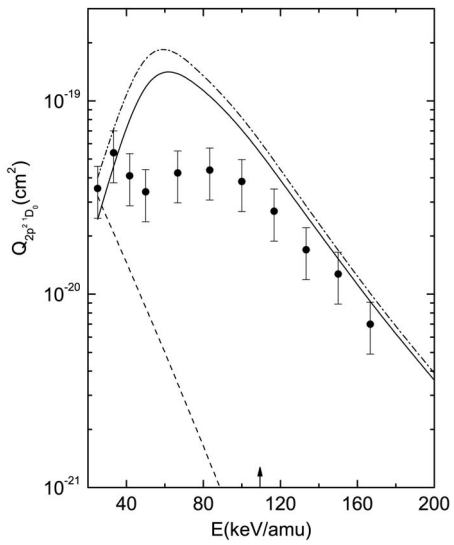

FIG. 38. The same as in Fig. 37, except for the collision $He^+(1s)+H(1s)\rightarrow He(2p^2\ ^1D_0)+H^+$.

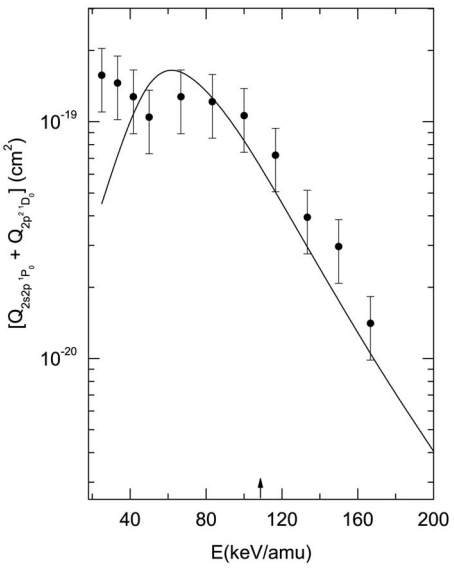

FIG. 39. The same as in Fig. 37, except for the collision $He^+(1s)+H(1s)\rightarrow He(2p^2\ ^1D_0+2s2p\ ^1P_0)+H^+$.

tion of the $(2s2p)\ ^1P_0$ state are seen in Fig. 37 as being largely underestimated by the CDW-4B method. This is not understood at present. By contrast, a reasonable agreement between the CDW-4B method and the experimental data is obtained in the case of the production of the $(2p^2)\ ^1D_0$ state (Fig. 38).

It should be noted that the experimental total cross sections correspond to the integrated contribution of the two constituent overlapping peaks in the energy spectrum of the emitted electron (Zouros *et al.*, 1988). The integrated sum of such two measured peaks yields good agreement between theory and experiment (Fig. 39). Nevertheless, such a comparison might be questionable, because the $(2p^2)\ ^1D_0$ cross section is smaller than the $(2s2p)\ ^1P_0$ cross section in the measurement, whereas the reverse is true for the theory (solid curve in Figs. 37 and 38). A similar remark is also relevant to the He target for the $(2s^2)\ ^1S$, as well as for the $(2s2p)\ ^3P_0$ states and their sum (Gayet *et al.*, 1995, 1997). The experimental data of Itoh *et al.* (1985) and Zouros *et al.* (1988) were obtained using the technique of zero-degree electron spectroscopy, by which the TEA mode and the channel of direct ionization (DI) were not separated (for simplicity, the DI channel will hereafter encompass both earlier mentioned mechanisms for ejection of electrons, such as direct target ionization, as well as simultaneous capture of the target electron and ionization of the projectile electron). In other words, these experimentally determined cross sections do not correspond to the TEA alone, since they always contain an admixture from the DI channel. This situation does not match the computations of Gayet *et al.* (1995, 1997), who employed the CDW-4B method with doubly excited states that include only discrete orbitals. This assumes that all ejected electrons are produced exclusively by autoionizing decays, i.e., via the Auger effect. However, the emitted electrons that are measured can be either Auger electrons or electrons ionized via the DI channel. Therefore, in order to properly interpret the experiments by Itoh *et al.* (1985) and Zouros *et al.* (1988), an improved model is needed using a more adequate doubly excited state description, which takes into account the adjacent continuum orbitals in addition to the discrete ones.

This latter task has been undertaken by Ourdane *et al.* (1999) who treated the TE process by means of the CDW-4B method improved by including the DI channel within the theory of Fano (1961) for a description of atomic resonant structures. Ourdane *et al.* (1999) have investigated a nearly symmetrical four-body system by supposing that each line of the electron spectrum could be associated with a single isolated resonance. The additional continuum orbitals chosen by Ourdane *et al.* (1999) were discretized via a basis set of the STOs, following the procedure of Macías *et al.* (1988), whereas pure discrete orbitals were the same as those from Gayet *et al.* (1995, 1997). Following this procedure, coherence effects between bound and continuum orbitals were included to a presumably sufficient extent. With this amelioration, it is reasonable to expect that the improved computation of Ourdane *et al.* (1999) should give more adequate cross sections than those of Gayet *et al.* (1995, 1997). We return to this point later on. In particular, it would be important to see whether the CDW-4B method improved for the DI channel could reproduce the asymmetric shape profiles in the spectra due to the $(2s2p)\ ^3P$ doubly excited states. Such asymmetries have been observed experimentally in the measurements of Itoh *et al.* (1985).

Specifically, it was suggested by Itoh *et al.* (1985) that these asymmetric line shapes stem from an interference between the TE and ECC. It should also be mentioned that the role of the DI channel has been assessed for double-excitation processes studied experimentally by Bordenave-Montesquieu *et al.* (1982), as well as by van der Straten and Morgenstern (1986). An important conclusion from these experiments is that the role of interference among resonances with different origins can significantly alter the overall shape of the recorded spectral profiles.

G. The CDW-4B method for the TEA modes

We now return to the transition amplitude defined by Eq. (231), but without the term $(\mu v\rho)^{2i\nu}$. As mentioned, this is justified whenever integration over the transverse momentum transfer η is performed, as in the total cross sections and the angular or energy distributions of ejected electrons (Belkić, 1978). Here the main focus will be on the establishment of the wave function $\varphi_f(\vec{s}_1,\vec{s}_2)$ for doubly excited states.

1. Description of the final state

An isolated autoionizing state can be conceived as a superposition of certain bound and continuum states of an electron (Fano, 1961). In this case, the final-state wave function $\varphi_f(\vec{s}_1,\vec{s}_2)\equiv\varphi_f(E_e,\vec{s}_1,\vec{s}_2)$ becomes depen-

dent on the electron energy E_e near the autoionizing threshold energy $\epsilon_f \equiv E_S$, which is needed to describe the complete TE process. Then the final state can be written as

$$\varphi_f(E_e,\vec{s}_1,\vec{s}_2) = \alpha(E_e)\Bigg(\Psi_S(E_S,\vec{s}_1,\vec{s}_2) + \mathcal{P}\int dE_e' \Psi_C(E_e',\vec{s}_1,\vec{s}_2)\frac{1}{E_S - E_e'}V(E_e')\Bigg) + \beta(E_e)\Psi_C(E_S,\vec{s}_1,\vec{s}_2), \quad (248)$$

where $\mathcal{P}$ denotes the Cauchy principal value of the integral. Here $\Psi_S(E_S,\vec{s}_1,\vec{s}_2)$ is the bound component of the resonant part of the autoionizing state with the corresponding energy E_S, which can be computed as in the work of Bachau (1984). Likewise $\Psi_C(E_e,\vec{s}_1,\vec{s}_2)$ is the adjacent continuum component. In Eq. (248), the function $V(E_e)$ represents the coupling between the bound and continuum components

$$V(E_e) = \left\langle \Psi_S(E_S,\vec{s}_1,\vec{s}_2)\left|\frac{1}{r_{12}}\right|\Psi_C(E_e,\vec{s}_1,\vec{s}_2)\right\rangle,$$

$$\alpha(E_e) = \frac{1}{\pi V(E_e)\sqrt{\epsilon_S^2+1}}, \quad \beta(E_e) = \frac{\epsilon_S}{\sqrt{\epsilon_S^2+1}},$$

$$\epsilon_S = 2\frac{E_e - E_S}{\Gamma_S}, \quad \Gamma_S = 2\pi|V(E_S)|^2, \quad (249)$$

where Γ_S is the width of the autoionizing state of energy E_S. The normalization of the continuum component $\Psi_C(E_e,\vec{s}_1,\vec{s}_2)$ is achieved on the energy scale, with the accompanying static exchange approximation. Let the function $\Psi_C(E_e,\vec{s}_1,\vec{s}_2)$ be represented via

$$\Psi_C(E_e,\vec{s}_1,\vec{s}_2) = \mathcal{A}[\varphi_{1s}(\vec{s}_1)\varphi_{LM}^A(\vec{s}_2)], \quad (250)$$

where $\mathcal{A}$ is the usual antisymmetrization operator. Here $\varphi_{1s}(\vec{s}_1)$ is the discrete orbital for the bound electron in the $He^+(1s)$ ion with binding energy E_{1s}. Likewise, $\varphi_{LM}^A(\vec{s}_2)$ is the continuum orbital for the Auger electron with the corresponding energy $E_S - E_{1s}$. For the (L,M) configuration of an autoionizing state, the continuum orbital is given by

$$\varphi_{LM}^A(\vec{s}_2) = \chi_{LM}^A(s_2)Y_L^M(\hat{\vec{s}}_2), \quad (251)$$

where $\chi_{LM}^A(s_2)$ is the radial continuum wave function and $Y_L^M(\hat{\vec{s}}_2)$ is the usual spherical harmonic.

The radial function χ_{LM}^A can be described by a linear combination of STOs

$$\chi_{LM}^A(s_2) = \chi_j(s_2) = \sum_{i=0}^{N_C} b_i^j S_i^j(s_2),$$

$$S_i^j(s_2) = s_2^{n_i-1}\exp(-\alpha_i^{[k_j]}s_2), \quad j=(L,M), \quad (252)$$

where N_C is the total number of the retained continuum orbitals, and n_i is the orbital number. Here the expansion coefficients b_i^j are determined by a variational procedure, through a single diagonalization, which yields both bound states and discretized continuum states. This can be achieved, e.g., by the algorithm of Macías *et al.* (1988). Briefly, in this latter code, the damping coefficients $\alpha_i^{[k_j]}$ are chosen as a geometrical sequence

$$\alpha_i^{[k_j]} = \alpha_0^{[k_j]}\beta^{i+\mu}, \quad i=0,\ldots,N_C, \quad j=(L,M), \quad (253)$$

where $[k_j]$, α_0, β, and μ are parameters which are fixed for each studied system. Within the static exchange approximation, the continuum wave function $\chi_j(s_2)$, constructed with a set of STOs from Eq. (252), represents a preparatory step for the subsequent diagonalization which gives the (N_C+1) eigenfunctions $\Psi_C(E_k,\vec{s}_1,\vec{s}_2)$ and the corresponding energies E_k. If the condition $E_k=0$ is imposed for, e.g., the double-ionization threshold of He, then the states with $E_k>-2$ a.u. will lie in the first continuum range. The nonlinear parameter μ allows us to determine a sequence $\{\alpha_i^{[k_j]}\}$ such that one of the eigenenergies (say, E_m) matches the energy E_S of the autoionizing state. This procedure of Macías *et al.* (1988) also permits an advantageous and convenient normalization for $\Psi_C(E_m,\vec{s}_1,\vec{s}_2)$ via $N=(2/|E_{m-1}-E_{m+1}|)^{1/2}$. Moreover, at $E_m=E_S$, the principal value integral can be evaluated as

$$\mathcal{P}\int dE_e' \Psi_C(E_e',\vec{s}_1,\vec{s}_2)\frac{1}{E_S - E_e'}V(E_e') = \sum_{k\neq m}\bar{\Psi}_C(E_k,\vec{s}_1,\vec{s}_2)\frac{1}{E_m - E_k}\overline{V}(E_k), \quad (254)$$

$$\overline{V}(E_e) = \left\langle \Psi_S(E_S,\vec{s}_1,\vec{s}_2)\left|\frac{1}{r_{12}}\right|\bar{\Psi}_C(E_e,\vec{s}_1,\vec{s}_2)\right\rangle. \quad (255)$$

The bar over Ψ_C indicates a continuum state normalized to unity. Then finally, for E_e close to E_S, an isolated doubly excited state can be written as

$$\varphi_f(E_e,\vec{s}_1,\vec{s}_2) = \alpha(E_e)\Bigg(\Psi_S(E_S,\vec{s}_1,\vec{s}_2) + \sum_{k\neq m}\bar{\Psi}_C(E_k,\vec{s}_1,\vec{s}_2)\frac{1}{E_m - E_k}\overline{V}(E_k)\Bigg) + \beta(E_e)\Psi_C(E_S,\vec{s}_1,\vec{s}_2), \quad E_m = E_S. \quad (256)$$

2. Cross sections for the TEA mode

The ionization transition amplitude $T_{if}^- \equiv T_{if}^-(E_e,\theta_e,\varphi_e,\vec{\eta})$ is given by Eq. (231) for an ejected electron of energy E_e in the direction (θ_e,φ_e) at a fixed impact energy E. Note that when the doubly excited state wave function is described by Eqs. (248) and (256), with the ansatz (250), the interaction $Z_T/R - 1/s_2$ and the $\vec{\nabla}\cdot\vec{\nabla}$ potential operator give nonzero contributions. In such a case, Eq. (231) must be used because the simplified form (244) does not hold any longer. For the present purpose, E_e needs to be close to the resonance energy E_S. Then,

the energy distribution of the emitted electron $Q_{if}^{-}(E_e,\theta_e,\varphi_e)\equiv Q_{if}(E_e,\theta_e,\varphi_e)$ can be written in terms of $T_{if}^{-}(E_e,\theta_e,\varphi_e,\vec{\eta})$ as

$$Q_{if}(E_e,\theta_e,\varphi_e)=\frac{d^2Q_{if}}{d\Omega_e dE_e}=\int d\vec{\eta}\left|\frac{T_{if}^{-}(E_e,\theta_e,\varphi_e,\vec{\eta})}{2\pi v}\right|^2. \quad (257)$$

Here, for convenience, we write $Q_{if}(E_e,\theta_e,\varphi_e)$ as a double rather than a triple differential cross sections, but the third differential is implicitly present via $d\Omega_e\equiv[\sin(\theta_e)]d\theta_e\,d\varphi_e$. The so-called total cross section for the TEA process, $Q_{if}(E_S)$, in the case of an asymmetric profile resonance of total width Γ_S, is defined by

$$Q_{if}(E_S)=\int d\Omega_e\int_0^\infty dE_e[Q_{if}(E_e,\theta_e,\varphi_e)-Q_C(E_e,\theta_e,\varphi_e)],\quad \Omega_e=(\theta_e,\varphi_e), \quad (258)$$

where $Q_C(E_e,\theta_e,\varphi_e)$ is the ionization background determined by interpolation of the smooth electron spectrum which appears close to the resonance. It is clear that Eq. (258) will give a non-negligible total cross section only for values of energy E_e located within the narrow range $[E_S-\Gamma_S,E_S+\Gamma_S]$. As mentioned earlier, the cross sections reported by Itoh *et al.* (1985) have been measured using zero-degree electron spectroscopy. This implies that $Q_{if}(E_e,\theta_e,\varphi_e)$ must be calculated with $\theta_e=0°$ and $\varphi_e=0°$. As a consequence, the projectile is left in an s state after autoionization, so that the nonzero contribution from the continuum will stem only from the case with $M=0$. Thus, with $\theta_e=0°$, $\varphi_e=0°$, and $M=0$, a simpler notation $Q_{if}(E_e,\theta_e=0°,\varphi_e=0°)\equiv Q'_{if}(E_e)$ and $Q_C(E_e,\theta_e=0°,\varphi_e=0°)\equiv Q'_C(E_e)$ appears more convenient. Under these conditions, Eq. (258) is reduced to

$$Q_{if}(E_S)=\frac{4\pi}{2L+1}\int_0^\infty dE_e[Q'_{if}(E_e)-Q'_C(E_e)], \quad (259)$$

where L is the total angular momentum of the considered autoionizing state.

H. Applications of the CDW-4B method improved by the Feshbach resonance formalism

The concept discussed in the preceding section of a more realistic description of the TEA process by means of the CDW-4B method, improved within the Feshbach formalism for resonances, has been tested by Ourdane *et al.* (1999) against the experimental data of Itoh *et al.* (1985) for the collision

$$^3\mathrm{He}^+(1s)+{}^4\mathrm{He}(1s^2)\rightarrow{}^3\mathrm{He}^{**}(nl,n'l')+{}^4\mathrm{He}^+(1s). \quad (260)$$

The following four doubly excited states of $^3\mathrm{He}(nl,n'l')$ have been included in the computations: $(2s^2)\,{}^1S$, $(2s2p)\,{}^3P$, $(2p^2)\,{}^1D$, and $(2s2p)\,{}^1P$. Since the collisional system (260) is a five-body problem, an additional approximation has been made to account for the presence of the spectator electron in the target. The simplest way to proceed is to introduce the Slater screening of He. This amounts first to using $Z_T^{\mathrm{eff}}=1.6875$ instead of the bare nuclear charge $Z_T=2$ for the helium target. Further, in the interaction potential $Z_T(1/R-1/x_1)$ in Eq. (231), Z_T is replaced by an effective charge Z_{NTE}. In the computations of Gayet *et al.* (1995), Z_{NTE} was taken to be equal to either 1 or 1.6875. The parameters for the bound orbitals $\Psi_S(E_S,\vec{s}_1,\vec{s}_2)$ of the doubly excited state of $\mathrm{He}^{**}(nl,n'l')$ have been given by Gayet *et al.* (1995). The latter parameters (resonant energies and their widths) compare favorably with the corresponding theoretical results of Bhatia and Temkin (1975). Writing these latter parameters in parentheses, we have, e.g., for the autoionizing state $^3P^o$, $E_S(\mathrm{a.u.})=-0.6834(-0.6929)$, $\Gamma(\mathrm{eV})=0.036(0.0363)$, whereas for the $^1D^e$ state, $E_S=-0.6918(-0.7028)$ and $\Gamma(\mathrm{eV})=0.081(0.0729)$, where the superscripts o and e stand for odd and even parity of the state, respectively. Overall, relatively good agreement (to within 1%) exists between the computations of Ourdane *et al.* (1999) and Bhatia and Temkin (1975). The continuum orbitals of the final state $\Psi_C(E_e,\vec{s}_1,\vec{s}_2)$ have been discretized by the procedure of Macías *et al.* (1988). The ensuing parameters appearing in the configuration $j=(L,0)$ for a given index $i(i=0,\ldots,N_C)$ that have been used in the computations of Ourdane *et al.* (1999) were $\alpha_i=2\beta^{-i/2+\mu}$ ($n_i=L+1$, i even) and $\alpha_i=2\beta^{-(i-1)/2+\mu}$ ($n_i=L+2$, i odd) with $\beta=1.6$. The transition amplitude from Eq. (231) contains two different terms defined by the Coulomb interaction via the electrostatic potentials and by the gradient-gradient $(\vec{\nabla}\cdot\vec{\nabla})$ potential operator, which is the typical dynamic coupling occurring in the standard CDW method. This latter interaction term contains a contribution from the continuum component $\Psi_C(E_e,\vec{s}_1,\vec{s}_2)$ which describes the ECC channel. Thus the ECC effect is included in the CDW-4B method by the $\vec{\nabla}\cdot\vec{\nabla}$ interaction potential operator which couples the continuum state $\Psi_C(E_e,\vec{s}_1,\vec{s}_2)$ with the initial distorted-wave function in the integral over $\vec{s}_2$ in Eq. (231). The matrix elements with the $\vec{\nabla}\cdot\vec{\nabla}$ term cause numerical instabilities in the computations from Ourdane *et al.* (1999), especially regarding convergence of the discretized continuum states $\Psi_C(E_e,\vec{s}_1,\vec{s}_2)$. Ourdane *et al.* (1999) have estimated that the contribution from the ECC process (via the said $\vec{\nabla}\cdot\vec{\nabla}$ term) is very small and, as such, it was neglected.

I. Comparison between theories and experiments for electron spectra close to Auger peaks

1. Electron energy spectrum lines

We first discuss the energy distributions of emitted electrons in the TE process (260). The theoretical electron spectra from the CDW-4B method (Ourdane *et al.*, 1999) are plotted and compared with the corresponding experimental data (Itoh *et al.*, 1985) in Figs. 40–42 in the

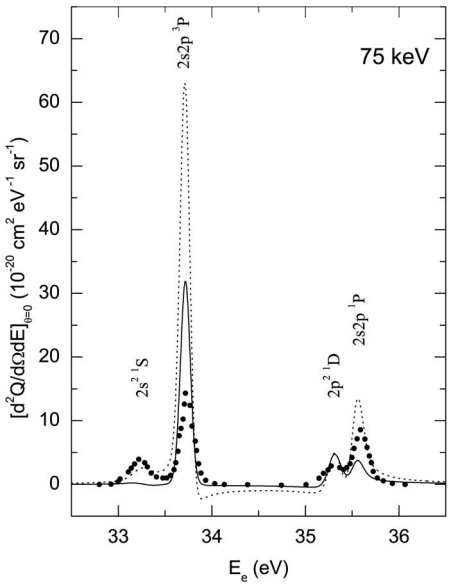

FIG. 40. Zero-degree electron energy spectra at an impact energy E of 75 keV for the collision $^3\mathrm{He}^+(1s)+{}^4\mathrm{He}(1s^2)\rightarrow{}^3\mathrm{He}(2l2l'\ ^{2S+1}L)+{}^4\mathrm{He}^+(1s)$ (Ourdane *et al.*, 1999). The $(2l2l')\ ^{2S+1}L$ states are $(2s^2)\ ^1S$, $(2s2p)\ ^3P$, $(2p^2)\ ^1D$, and $(2s2p)\ ^1P$. The CDW-4B method: solid curve, $Z_{\mathrm{NTE}}=1$; dotted curve, $Z_{\mathrm{NTE}}=1.6875$. Solid circles are the experimental data of Itoh *et al.* (1985).

energy range 32–42 eV at three impact energies of the $^3\mathrm{He}^+$ ion: 75, 100, and 500 keV. For a comparison between the experiment and the CDW-4B method, the theoretical data have been convoluted using a Gaussian function of a width equal to the experimental resolution of the spectrometer (about 0.2 eV). The limitation of the validity of the standard CDW method for the $^3\mathrm{He}^+$ ion in the case of reaction (260) is estimated using Eq. (164) to be about 330 keV (110 keV/amu). Although the impact energies 75 and 100 keV, considered in Figs. 40 and 41, are below the validity limit of the CDW method according to (164), qualitative agreement between the theoretical and experimental results is still obtained consistently. Further, in Figs. 40–42, the results for the two effective charges mentioned earlier ($Z_{\mathrm{NTE}}=1$ and 1.6875) are shown. It is seen that the choice of this effective charge can significantly influence the outcomes of the computations in the CDW-4B method at $E=75$ and 100 keV (Figs. 40 and 41). In this method, the initial and final states from the entrance and exit reaction channels are strongly coupled. As mentioned, this latter coupling, which is mediated with the $\vec{\nabla}\cdot\vec{\nabla}$ interaction potential operator in Eq. (231), is responsible for an enhanced influence of the continuum intermediate states at lower impact energies. As a consequence, the total cross sections from the CDW-4B method systematically overestimate experimental data at lower energies, i.e., below the usual Massey maximum. This overestimation also occurs in differential cross sections as is clear from Figs. 40 and 41. However, at high impact energies, e.g., 500 keV, good agreement between the theoretical and experimental spectra is obtained, as shown in Fig. 42. Moreover, it can be seen in Fig. 42 that at high impact energies the influence of the choice of the effective charge Z_{NTE} is negligible. Nevertheless, the version of the CDW-4B method used by Ourdane *et al.* (1999) has a limitation: it considers each line as an isolated resonance, i.e., it ignores overlapping resonances altogether. Therefore, the continuum of a given excited state has no simple relationship in magnitude and phase with the continuum adjacent to a doubly excited state. This can lead to certain problems in the interference between transition amplitudes of any two consecutive autoionizing states. However, neither interferences between the transition amplitudes of contiguous doubly excited states nor the effects due to postcollisional interaction (PCI) were evaluated by Ourdane *et al.* (1999) in the CDW-4B method. This is

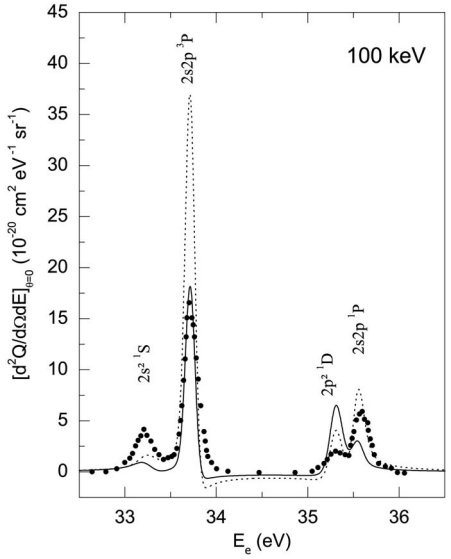

FIG. 41. The same as in Fig. 40, except for 100 keV.

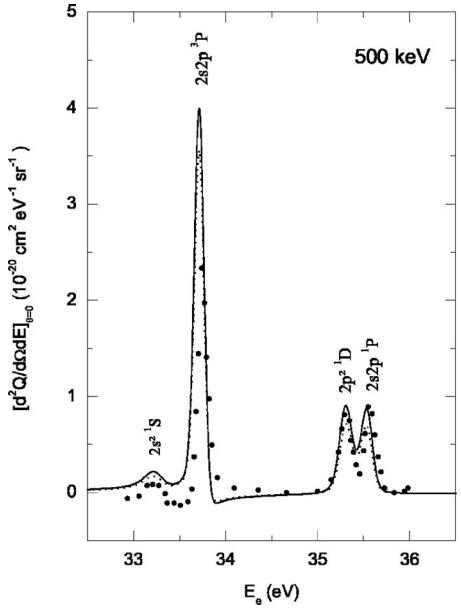

FIG. 42. The same as in Fig. 40, except for 500 keV.

the case because the theoretical spectra given in this latter study are pure sums of contributions from each line superimposed on top of its own background. The background contribution has been subtracted from theoretical cross sections using Eq. (259). This has been done because the corresponding experimental data were reported by Itoh *et al.* (1985) with the background subtracted, as well. Of course such a subtraction may lead to unphysical, i.e., negative cross sections in some parts of the spectrum. Indeed, this can be seen in Figs. 40–42 in both the experiment and the theory. Although overall good agreement between theory and experiment is obtained in Figs. 40–42, it should be noted that the computed lineshapes (especially the ^3P lineshape) are very sensitive to the width which is used in the convolution. Moreover, there is a slight shift between the theoretical and experimental resonant energies in Figs. 40–42.

2. Total cross section for the TEA mode

Next, we turn our attention to the total cross sections for the TE reaction (260). In Figs. 43–46, the corresponding results of Ourdane *et al.* (1999) from the CDW-4B method are compared with the experimental data (Itoh *et al.*, 1985) for the following doubly excited states of helium: $(2s2p)\,^1P$, $(2p^2)\,^1D$, $(2s^2)\,^1S$ and $(2s2p)\,^3P$. In these cases, for each doubly excited state, the cross sections in the CDW-4B method have been obtained by numerical integration of the theoretical profiles over a sufficiently wide energy range around the resonance energy E_S. It is clear from Eq. (256) that the final wave function, for an energy E_e around the autoionizing energy E_S, exhibits its dependence upon E_e only in the coefficients $\alpha(E_e)$ and $\beta(E_e)$. Therefore, the general form of $Q'_{if}(E_e)$ can be simplified as

$$Q'_{if}(E_e) = \alpha^2(E_e)Q_d(E_S) + \alpha(E_e)\beta(E_e)Q_x(E_S) + \beta^2(E_e)Q_c(E_S), \tag{261}$$

where $Q_c(E_S)$ is the local continuum contribution (background) and $Q_d(E_S)$ is the total cross section both from the discrete component $\Psi_S(E_S,\vec{s}_1,\vec{s}_2)$ and from the resonant continuum defined by the principal value integral in Eq. (254). Moreover, $Q_x(E_S)$ is a cross section defined from the product of the transition amplitudes from $Q_c(E_S)$ and $Q_d(E_S)$. It can be shown that the TEA total cross section $Q_{if}(E_S)$ given by Eq. (259) may be written as

$$Q_{if}(E_S) = \frac{4\pi}{2L+1}\left(Q_d(E_S) - \frac{1}{2}\Gamma_S \pi Q_c(E_S)\right). \tag{262}$$

This formula hints at the following two important facts: (i) The term $[4\pi/(2L+1)]Q_d(E_S)$ which defines the total TEA cross section is not equivalent to the cross section Q_{TE} from Gayet *et al.* (1997), who employed only the discrete orbitals. As mentioned, $Q_d(E_S)$ contains the same discrete orbitals as those from Gayet *et al.* (1997) and the resonant continuum components. (ii) One could argue that the term $\Gamma_S \pi Q_c(E_S)/2$ could accidentally cancel the contribution from the resonant continuum in $Q_d(E_S)$ due to the principal value integral. In such a case, $Q_{if}(E_S)$ from Eq. (262) would coincide with Q_{TE} from Gayet *et al.* (1997). However, explicit computations show that such a fortuitous and delicate cancellation does not occur. Therefore, the improvement of the CDW-4B method employed by Ourdane *et al.* (1999) over the corresponding computations from Gayet *et al.* (1997) is genuine. Hence, it is important to examine the results from Ourdane *et al.* (1999) obtained by a numerical integration of Eq. (259). For the $(2s2p)^1P_0$ state, the result from the CDW-4B method without the coupling between the doubly excited state and the continuum (Gayet *et al.*, 1997) is much smaller than the experimental data, as seen in Fig. 43. However, the results of Ourdane *et al.* (1999) show good agreement with the measured cross sections of Itoh *et al.* (1985), even in the low-energy range $E<110$ keV/amu, i.e., below the validity limit for the standard CDW method. In this range, better agreement is obtained with $Z_{\mathrm{NTE}}=1.6875$, which illustrates a previously mentioned feature, i.e., the increasing influence of the spectator electron in the target at smaller impact energies. On the other hand, $Z_{\mathrm{NTE}}=1$ gives better agreement with experiment above 110 keV/amu, where the standard CDW method is expected to be most adequate.

In the case of the $(2p^2)^1D_0$ state, the theoretical results are seen in Fig. 44 to overestimate the measured cross section below 110 keV/amu. Moreover, the CDW-4B method for $Z_{\mathrm{NTE}}=1$ does not reproduce the experimentally observed dip at 70 keV/amu, but merely an oscillation appears at 50 keV/amu for $Z_{\mathrm{NTE}}=1.6875$. However, above 110 keV/amu, the CDW-4B method for both values of Z_{NTE} (Ourdane *et al.*, 1999) and the measurement (Itoh *et al.*, 1985) are in good agreement within the experimental uncertainty. In Fig. 44 at $E>60$ keV the overall influence of the coupling between the discrete component and adjacent continuum is such that the resulting cross sections are lowered, and this improves the agreement with the experiment, relative to the case when the said coupling is ignored (Gayet *et al.*, 1997).

In an isolated resonance approach, the two above-mentioned states ($^1P_0$ and $^1D_0$) have been studied separately. The sum of the two theoretical cross sections for the states $^1P_0$ and $^1D_0$ is in good agreement with the corresponding sum of the experimental data above 110 keV/amu (not shown here, but the situation is similar to Fig. 39 for the He^+-H collisions). Nevertheless, this theoretical sum is still unable to reproduce the oscillation from the experimental sum in the range 25–100 keV/amu. Such oscillatory structures might be due to the interference between the two states $^1P_0$ and $^1D_0$, as argued by van der Straten and Morgenstern (1986), who also pointed out that the dip in the cross sections for the production of the $^1D_0$ state could be the consequence of the effect of the PCI on the state $^1P_0$. As already mentioned, the CDW-4B method does not take the PCI into account. It is also possible that the discussed oscillatory structure may stem from a combined

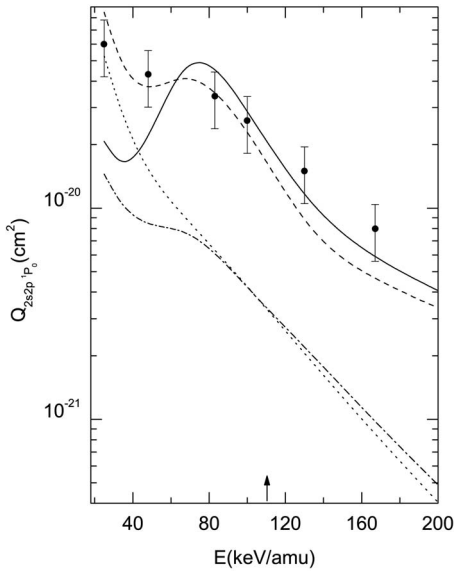

FIG. 43. Total cross sections for the collision ^{3}He$^+$($1s$) + ^{4}He($1s^2$) → ^{3}He($2s2p\ ^1P_0$) + ^{4}He$^+$($1s$). The results of the CDW-4B method (Ourdane *et al.*, 1999): solid curve, Z_{NTE}=1; dashed curve, Z_{NTE}=1.6875. The results of the CDW-4B method (Gayet *et al.*, 1995, 1997): singly-chained curve, Z_{NTE} =1; dotted curve, Z_{NTE}=1.6875. Experimental data of Itoh *et al.* (1985): solid circles.

effect of both the discrete-continuum coupling and PCI interferences between the two investigated states.

Similar remarks to those above could also be made for the ^1S state (Fig. 45). In the range 110–200 keV/amu, the results of the CDW-4B method used by Ourdane *et al.* (1999) are in much better agreement with experiment than the ones from Gayet *et al.* (1997). Below the limit of the validity for the CDW-4B method, as represented by the arrow, the theoretical results of Ourdane *et al.* (1999) largely underestimate the experimental data, which do not exhibit any oscillatory structure. Since the ^1S state is

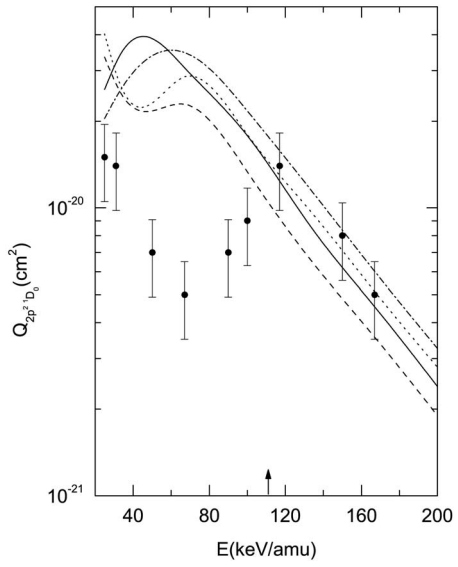

FIG. 44. The same as in Fig. 43, except for ^{3}He($2p^2\ ^1D_0$).

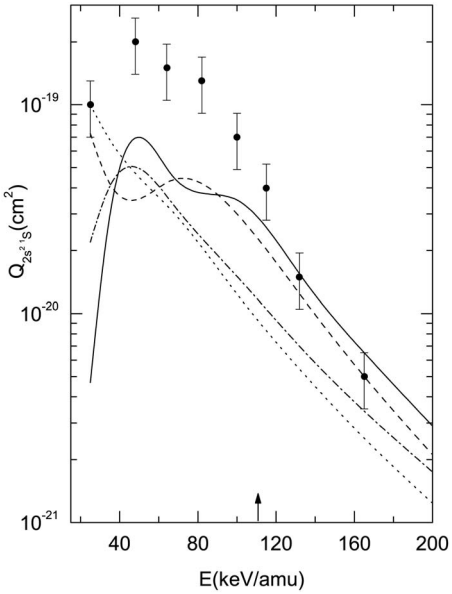

FIG. 45. The same as in Fig. 43, except for ^{3}He($2s^2\ ^1S$).

well separated in energy from the ^3P state, the interference between the two states is expected to be negligible. Therefore, the oscillation in theoretical cross sections is likely to be the result of the discrete-continuum coupling.

Finally, the situation for the $^3P_0$ state (Fig. 46) is comparable to that for the ^{1}S state (Fig. 45). As can be seen from Fig. 46, the CDW-4B method employed by Ourdane *et al.* (1999) represents a major improvement in the high-energy range over the results of Gayet *et al.* (1997). In addition, at energies smaller than 110 keV/amu, the discrepancy between the cross sections given by Ourdane *et al.* (1999) and the experimental data is not so pronounced.

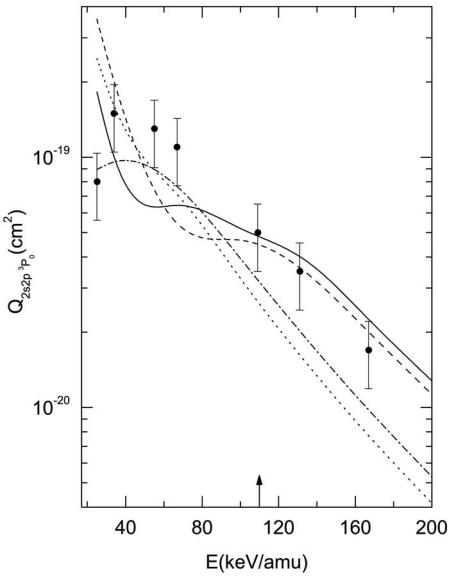

FIG. 46. The same as in Fig. 43, except for ^{3}He($2s2p\ ^3P_0$).

Overall, the study of the TE process in the He^+-He collisions carried out by Ourdane *et al.* (1999) has shown that the adjacent continuum of a low-lying doubly excited state plays a significant role. This collisional system appears particularly interesting in two respects: (i) the target and the projectile nuclear charges are the same, and this results in interference between competing contributions from the resonant and nonresonant modes; and (ii) the influence of the electron continuum is strong, because the final states of helium under consideration decay mainly through autoionization.

In the applicable energy range (above 110 keV/amu), the CDW-4B method appears to give reliable predictions for the TEA processes, provided that in the transition amplitude the wave function of the final doubly excited state includes both the discrete and adjacent continuum components. For this case, the theoretical electron energy spectra near resonances (as well as the integrated energy profiles) are in better agreement with the experimental data (Itoh *et al.*, 1985) than the previous CDW-4B method obtained with the discrete components only (Gayet *et al.*, 1995, 1997). In fact, the results from the CDW-4B method (Ourdane *et al.*, 1999) depart from the experimental spectra only at impact energies where the standard CDW method for single-electron capture does not apply (below 110 keV/amu in this case). However, at higher collision energies, the CDW-4B method successfully reproduces the experimental electron spectra. Furthermore, the good agreement of the integrated energy profiles with experimentally measured cross sections for the TEA process is a significant improvement over all previous predictions, which considered the coupling with the adjacent continuum as a PCI effect. Nevertheless, it should be kept in mind that both variants of the CDW-4B method shown in Figs. 43–46 are limited to the framework of isolated resonances alone. This could advantageously be overcome by using the Padé-based resonant scattering theory which treats both isolated and overlapping resonances on the same footing (Belkić, 2005). In addition, the continuum-continuum terms (due to the $\vec{\nabla}\cdot\vec{\nabla}$ interaction operator), which Ourdane *et al.* (1999) viewed as negligible, have caused convergence difficulties in the Feshbach-Fano spectral representation of autoionizing states. These additional approximations introduced by Ourdane *et al.* (1999) into the CDW-4B method should not seriously affect their main conclusions. Finally, it should be pointed out that the concept of a pure transfer and excitation process considered as a simple postcollisional Auger decay of the discrete component of a given doubly excited state might be misleading. In fact, it has been argued (Ourdane *et al.*, 1999) that this concept makes sense only in the limit of a negligible autoionization width Γ_S. Of course, one may introduce a so-called transfer-excitation total cross section by integrating an electron energy profile, after removal of the ionization background as seen in Eq. (259). However, in so doing one must also remember that a hidden contribution from the continuum is necessarily included in the final result, unless $\Gamma_S=0$.

VIII. CONCLUSIONS

A thorough overview of the current status and a critical assessment of the existing quantum-mechanical four-body theories for energetic ion-atom collisions are presented. A proper description of these collisions with two active electrons, such as the Z_P-$(Z_T;e_1,e_2)_i$ and the $(Z_P,e_1)_{i_1}$-$(Z_T,e_2)_{i_2}$ scatterings, requires solution of the pertinent four-body problems. We have considered a number of inelastic collisions, and special attention has been focused on double-electron capture, transfer ionization, transfer excitation, single-electron detachment, and single-electron capture. We have limited the scope of this review to intermediate and high nonrelativistic impact energies. A quantum-mechanical treatment has been adopted to set the formal theoretical framework for a description of four-body rearrangement collisions. After establishing the basic notation, we presented a derivation of the Lippmann-Schwinger equations, the Born as well as Dodd-Greider perturbation expansions with the correct boundary conditions, and the leading distorted-wave methods for four-body collisions. Subsequently, the particular one- and two-electron transitions in scatterings of completely stripped projectiles on heliumlike atomic systems or in collisions between two hydrogenlike atoms (ions) were analyzed. The heliumlike atom (ion) is the simplest many-electron system where one can investigate the importance of electron correlation effects. The studies reviewed here for He as a target indicate that dynamic electronic correlations in the perturbation potentials are much more important than the static ones stemming from the target bound-state wave function. A substantial improvement of most of the four-body methods over, e.g., the corresponding IPM has been attributed exclusively to the role of dynamic electron correlation effects. The main drawback of the IPM, as well as other related models, is in effectively reducing the initial four-body problem to the associated three-body problem. In this procedure, dynamic electron-electron correlations are completely ignored from the outset. All four-body theories reviewed here are seen to naturally incorporate the usual static as well as dynamic correlation effects of active electrons. In particular, the static interelectron correlations are shown to be very important for ionizing collisions, involving H^- as a target, such as single-electron detachment from H^- by H^+. Moreover, for these latter collisions, an even stronger emphasis is placed onto the proper connection between the distorted wave functions and the corresponding perturbations, as illustrated within the MCB method, which agrees excellently with the available experimental data from the threshold through the Massey maximum to the Bethe region of high energies. By contrast, ignoring the said connection, as done in the ECB method, leads to utterly unphysical total cross sections which overestimate the experimental data by 2–3 orders of magnitude, and tend to a constant value at high impact energies

instead of reaching the correct Bethe asymptotic limit.

In the present work, particular emphasis is placed on the critical importance of preserving the proper Coulomb boundary conditions in both formal four-body theory and computational practice. This is guided by common past experience, which has shown that whenever such conditions, as the most basic requirements from the formal scattering theory, are overlooked, severe fundamental problems arise. As a consequence, models with incorrect boundary conditions are seen as inadequate for describing experimental findings. The total scattering wave functions of the four-body theories presented here satisfy the correct boundary conditions for both the initial and final asymptotic states. In addition to long-range Coulomb distortions of plane waves for relative motion of two charged heavy aggregates, we account for intermediate ionization continua of electrons in both the entrance and exit channels for the CDW-4B method or in either the entrance or exit channel for asymmetric distorted-wave treatments, as in the BCIS-4B, BDW-4B, CDW-BIS, and CDW-BFS methods. We recall that in the CB1-4B method electronic continuum intermediate states are not taken into account.

Double-electron capture in the collisional systems considered here has been studied by means of the CB1-4B, CDW-4B, BDW-4B, and BCIS-4B methods. Unlike its success in single-electron capture at intermediate and a wide range of high energies (up to the onset of the Thomas double scattering), the CB1–4B method, as the prototype of the first-order theories, is satisfactory for double-electron capture only at intermediate energies, and in a limited region of high energies. By contrast, as the prototype of the second-order theories, the CDW-4B method, which is excellent for one-electron capture, continues to be successful for the majority of double-electron capture processes, as well. This is particularly true for two-electron capture from He by H^+, for which it is sufficient to include only the ground-to-ground state transition, due to the absence of the excited states of H^- in the exit channel. Moreover, using the CDW-4B method for double-electron capture in the Z_P-He collisions with $Z_P \geqslant 3$, it is found that the contribution from excited states can be important compared to the contribution from the ground state. As such, including excited states into the computations can improve agreement between the CDW-4B method and experimental data. Regarding double-electron capture in the He^{2+}-He($1s^2$) collisions, excited states are expected to play a minor role due to the dominance of the resonant $1s^2 \rightarrow 1s^2$ transition. The CDW-4B method confirms this anticipation, but it fails to reproduce the majority of the available experimental data at high energies that are well within the domain of the validity of this theory for the He^{2+}-He($1s^2$) collisions. This has apparently been ameliorated in the past by using a crude approximation to the Green function from the second-order propagator of a perturbation expansion, which is not of the Dodd-Greider type. Nevertheless, improved agreement of this "augmented" CDW-4B method for the two-electron transfer in the He^{2+}-He($1s^2$) collisions should be taken with caution, since the approximate Green function is merely off-shell and, moreover, only two hydrogenlike ground states centered on the projectile and target nucleus are taken into account from the sum over the discrete and continuous parts of the whole spectrum. More systematic work is needed for this particular colliding system, first by treating the on- and off-shell contributions on the same footing, and second by assessing the convergence rate in the spectral representation of the Green function from the second-order term of a chosen perturbation series. As to the BCIS-4B, BDW-4B, and CDW-EIS-4B methods, they have been applied to double-electron capture in the He^{2+}-He collisions. At moderately high energies, relatively good agreement with experiments is found using the BCIS-4B and the BDW-4B methods, whereas the CDW-EIS-4B method fails much more severely than the CDW-4B method for this collision. This is unexpected given the success of the CDW-EIS method for single-electron capture at a wide range of intermediate and high energies. As an attempt to rescue this unsatisfactory situation, the "augmented" CDW-EIS-4B method has been used in the past by including approximately a second-order term in a perturbation expansion, in precisely the same manner as done in the "augmented" CDW-4B method. However, this has not met with success and, therefore, further studies are needed to clarify the hidden drawbacks of the CDW-EIS-4B method for double-electron capture. Such studies are needed in view of a similar inadequacy of the CDW-EIS-4B method for double-electron capture in the Li^{3+}-He collisions. No such inadequacies are present in the BDW-4B method, which differs from the CDW-EIS-4B method only in the independent variables of the Coulomb logarithmic phase factors. The present work has also been concerned with analyzing the role of continuum intermediate states. The net effect of these latter states is observed to be striking in the case of the symmetric resonant double-charge transfer in the He^{2+}-He collisions at high energies. We have also concluded that for double-charge exchange the four-body methods presented here are weakly dependent upon the choice of bound-state wave functions. By implication, the static correlations of two electrons bound to the target do not play a significant role in double-electron capture.

Simultaneous electron transfer and ionization in the He^{2+}-He and Li^{3+}-He collisions have also been studied with the CDW-4B method. The theoretical results for the total cross sections for these processes show good agreement with the available experimental data at intermediate and high impact energies. A number of recent measurements of the differential and total cross sections for transfer ionization in fast H^+-He collisions require additional theoretical considerations to achieve full agreement between theory and experiment.

Single-electron capture has been the subject of investigations since the early days of quantum mechanics, and interest in this fundamentally important process has remained steady. In this review, single-charge exchange in collisions between completely stripped projectiles and

heliumlike atoms (ions) has been studied. Using the CDW-4B, CDW-BFS, and CDW-BIS methods, we have analyzed cross sections for single-electron capture in different processes (H^+-He, He^{2+}-He, H^+-Li^+, and Li^{3+}-He). The CDW-4B method provides evidence that dynamic correlations play an important role for electron capture, especially at higher impact energies for total and differential cross sections. For differential cross sections, the dynamic interelectron correlations lead to the Thomas peak of the 2nd kind, which is mediated by the $Z_P-e_1-e_2$ double scattering. In the CDW-4B method, the Thomas peak of the 2nd kind appears at all impact energies without any splitting at the critical Thomas angle. Remarkably, at high energies, the strength of the Thomas $Z_P-e_1-e_2$ peak remains very significant and comparable to that of the Thomas double scattering of the 1st kind ($Z_P-e_1-Z_T$). The Thomas $Z_P-e_1-Z_T$ peak, which is appreciable only at sufficiently high energies, is always split into two subpeaks at the Thomas critical angle, but the ensuing dip is unphysical, as it has never been observed experimentally. To test these findings of the CDW-4B method for single-electron capture involving heliumlike targets, there is a need for experimental data that could provide two clearly separated contributions from the Thomas double scatterings of the 1st and the 2nd kind. We have found that dynamic interelectron correlations also remain important for capture into excited states, as demonstrated in the Li^{3+}-He collisions. It should be noted that the four-body CDW-BIS and CDW-BFS methods are convenient for computations of differential cross sections, and in the H^+-He collisions good agreement between these two methods and the measurements is found at a number of impact energies. Electron transfer in collisions between two hydrogenlike atoms (ions) has been investigated by means of the CB1-4B and CDW-4B methods. As shown, the CB1-4B and CDW-4B methods can be adapted to investigate single-electron capture from multielectron targets with hydrogenlike projectiles. To this end, the initial state of the target active electron is described by the Roothan-Hartree-Fock wave function, which reduces the original multielectron problem to a purely four-body problem. We can say that all quantum-mechanical boundary-correct four-body theories presented here are adequate for a description of single-electron capture in ion-atom collisions and show systematic agreement with experimental data at intermediate and high impact energies.

We also reviewed a class of resonant collisions with a focus on simultaneous transfer and excitation. In transfer excitation, two modes have been highlighted: resonant and nonresonant transfer excitation. The interference between these two modes can be important, especially for nearly symmetric collisional systems (He^+-H or He^+-He). Doubly excited states, which are produced on the projectile after capture of the target electron, can be relaxed either by radiative decay or through the Auger mechanism. These modes and contributions are coherently included in the CDW-4B method. This is essential to preserve the importance of the interference phase. For highly asymmetric collisions ($Z_P \gg Z_T$), such as the S^{15+}-H scattering, the radiative decay in transfer excitation is dominated by the resonant mode relative to the corresponding nonresonant contribution. The influence of the target charge Z_T on the interference between these resonant and nonresonant radiative decays within transfer excitation has also been assessed. It is found that whenever $Z_P \simeq Z_T$, these latter interference effects can become important. Further, the CDW-4B method for transfer excitation in the He^+-He collisions has shown that the adjacent continuum of a low-lying doubly excited state can play a significant role. Moreover, within the region of its validity, the CDW-4B method gives reliable predictions for transfer excitation via emission of Auger electrons. This is possible, provided that the transition amplitude in the CDW-4B method includes the wave function of the final doubly excited state with both discrete and adjacent continuum components. For this case, the theoretical electron energy spectra near resonances (as well as the integrated energy profiles) are in better agreement with the corresponding measurements than the associated predictions of the CDW-4B method based upon the discrete components alone. The CDW-4B method for transfer-excitation is limited to isolated resonances because of the adapted Feshbach-Fano formalism. In reality, the corresponding experimental data contain both isolated and overlapping resonances. An improved version of the CDW-4B method is desired by treating both isolated and overlapping resonances on the same footing. This is feasible by using the Padé-based resonant scattering theory which has been shown to be remarkably successful for spetroscopy.

Finally, we can conclude that most of the presently analyzed quantum-mechanical four-body methods are capable of providing adequate results for single- and double-electron transitions at intermediate and high energies. Interest in these methods remains steady, and further progress is expected in their extension to pure five-body scattering problems, without resorting to the customary frozen-core approximation, to adequately describe the existing coincident experiments with three active electrons.

In addition to its fundamental importance within few-body quantum mechanics, the collisional problems reviewed here also find significant applications in other neighboring research fields such as astrophysics, thermonuclear fusion, plasma physics and medical physics, through particle transport phenomena. This is the case because the cross sections for the presently studied scattering problems are indispensable as entry data for accurate and reliable Monte Carlo simulations of the passage of energetic multiply charged light ions through matter including organic tissue. Such energetic ions deposit nearly the total impact energy at the end of their range via the Bragg peak, and they are neutralized by single-or multiple-electron capture. Therefore, the stopping power must be determined accurately for the most appropriate modeling of the passage of these ions through matter. Such databases are provided by cross sections from the quantum-mechanical methods studied

in this review. This represents an added value of paramount importance for such methods that go beyond atomic physics, where they were originally established. The most prominent example is radiotherapy by energetic light ions such as H^+, $He^{2+}, \ldots, C^{6+}$. Here, reliable energy deposition by beam particles in tissue is predicted by judicious intertwining of powerful Monte Carlo simulation algorithms with atomic physics databases for cross sections of processes reviewed in the present work, as well as in the related previous overviews on extensively studied three-body collisions.

Overall, fast heavy particle collisions are topical again as greatly stimulated by the recent favorable settlement of the International Thermonuclear Reactor. Likewise, high-energy multiply charged ion beams, as a powerful part of hadron therapy, are increasingly in demand, and this motivates construction of medical accelerators worldwide. In these and other important practical applications, augmented projectile charge enhances significantly the probability for two-electron transitions. This, in turn, influences substantially the overall energy balance as well as stability of ion plasma, and alters considerably the energy deposition of ion beams in the traversed matter. Such a critical conclusion demands a thorough revision and update of the customary procedures and stopping power data bases in particle transport physics. This is deemed necessary because the atomic physics input into the existing major Monte Carlo algorithms for simulations of the passage of multiply charged ions through matter is currently based primarily on interactions leading to one-electron transitions, e.g., single ionization, single excitation, etc.

ACKNOWLEDGMENTS

A number of our colleagues, experts in energetic ion-atom collisions, are thanked for their critical reading of the original manuscript and for their helpful comments. Dž.B. is grateful to the Royal Swedish Academy of Sciences for the Nobel Foundation research grants over a period of three years on the theory of high-energy ion-atom collisions. He also wishes to express his gratitude to the King Gustav the 5th Fund in Stockholm for support. I.M. acknowledges support by MNZŽS Project No. 141029A. J.H. thanks the Service for International Relations at the Paul Verlaine University, Metz, France, for support.

LIST OF ACRONYMS

BCIS-4B	Four-body continuum intermediate state with the correct boundary conditions
BDW-4B	Four-body Born distorted wave
BK1-3B	Three-body first-order Brinkman Kramers
BK2-3B	Three-body second-order Brinkman Kramers
CB1-3B	Three-body first Born with the correct boundary conditions (alternative acronym used in the literature, B1B)
CB1-4B	Four-body first Born with the correct boundary conditions
CB2-3B	Three-body second Born with the correct boundary conditions (alternative acronym used in the literature, B2B)
CB2-4B	Four-body second Born with the correct boundary conditions
CB3-4B	Four-body third Born with the correct boundary conditions
CBn-4B	Four-body *n*th Born with the correct boundary conditions
CC	Close coupling
CDW-3B	Three-body continuum distorted wave
CDW-4B	Four-body continuum distorted wave
CDW-4B1	Four-body first-order continuum distorted wave
CDW-4B2	Four-body second-order continuum distorted wave
CDW-BIS	Continuum distorted wave, Born initial state
CDW-BFS	Continuum distorted wave, Born final state
CDW-CB1	Continuum distorted wave, boundary-corrected first Born
CDW-EIS	Continuum distorted wave, eikonal initial state
CDW-EIS-4B1	Four-body first-order continuum distorted wave, eikonal initial state
CDW-EIS-4B2	Four-body second-order continuum distorted wave, eikonal initial state
CDW-EFS	Continuum distorted wave, eikonal final state
CDW-IEM	Continuum distorted wave-independent event model
CDW-IPM	Continuum distorted wave, impact parameter model
CI	Configuration interaction
COLTRIMS	Cold-target recoil-ion momentum spectroscopy
CTMC	Classical trajectory Monte Carlo
DCS	Differential cross section
DEC	Dynamical electron correlations
DI	Direct ionization
DR	Dielectronic recombination
ECB-4B	Four-body eikonal Coulomb-Born
ECC	Electron capture to continuum
GSZ	Green-Sellin-Zachor
HS	Herman-Skillman
IA	Impulse approximation
IEM	Independent-event model
IPM	Independent-particle model
KTI	Kinematic transfer ionization
MCB-4B	Four-body modified Coulomb-Born
NTE	Nonresonant transfer excitation
NTEX	Nonresonant transfer excitation via x rays (radiative decays)
PCI	Postcollisional interaction

POHCE	Perturbative one-and-a-half-centered expansion
RIA-3B	Three-body reformulated impulse approximation
RIA-4B	Four-body reformulated impulse approximation
RHF	Roothaan-Hartree-Fock
RTE	Resonant transfer excitation
RTEX	Resonant transfer excitation via x rays (radiative decays)
SC	Single capture
SEC	Static electron correlations
SE-3B	Three-body symmetric eikonal
STO	Slater-type orbital
TE	Transfer and excitation
TEA	Transfer excitation via Auger mechanism
TEX	Transfer excitation via x rays (radiative decays)
TI	Transfer ionization
TCDW	Target continuum distorted wave
TTI	Thomas transfer ionization

REFERENCES

Abramowitz, M., and I. Stegun, 1956, Eds., *Handbook of Mathematical Functions* (Dover, New York).

Abufager, P., P. Fainstein, A. Martínez, and R. Rivarola, 2005, J. Phys. B **38**, 11.

Adivi, E. G., and M. A. Bolorizadeh, 2004, J. Phys. B **37**, 3321.

Allison, S., 1958, Rev. Mod. Phys. **30**, 1137.

Atan, H., W. Steckelmacher, and M. Lukas, 1991, J. Phys. B **24**, 2559.

Bachau, H., 1984, J. Phys. B **17**, 1771.

Bachau, H., G. Deco, and A. Salin, 1988, J. Phys. B **21**, 1403.

Bachau, H., R. Gayet, J. Hanssen, and A. Zerarka, 1992, J. Phys. B **25**, 839.

Belkić, Dž., 1978, J. Phys. B **11**, 3529.

Belkić, Dž., 1981, J. Phys. B **14**, 1907.

Belkić, Dž., 1983, J. Phys. B **16**, 2773.

Belkić, Dž., 1988a, Europhys. Lett. **7**, 323.

Belkić, Dž., 1988b, Phys. Rev. A **37**, 55.

Belkić, Dž., 1989a, Phys. Scr. **40**, 610.

Belkić, Dž., 1989b, Phys. Scr. **T28**, 106.

Belkić, Dž., 1991, Phys. Rev. A **43**, 4751.

Belkić, Dž., 1992, Phys. Scr. **45**, 9.

Belkić, Dž., 1993a, Phys. Rev. A **47**, 189.

Belkić, Dž., 1993b, J. Phys. B **26**, 497.

Belkić, Dž., 1993c, Phys. Rev. A **47**, 3824.

Belkić, Dž., 1994, Nucl. Instrum. Methods Phys. Res. B **86**, 62.

Belkić, Dž., 1995, Nucl. Instrum. Methods Phys. Res. B **99**, 218.

Belkić, Dž., 1996, Phys. Scr. **53**, 414.

Belkić, Dž., 1997a, Nucl. Instrum. Methods Phys. Res. B **124**, 365.

Belkić, Dž., 1997b, J. Phys. B **30**, 1731.

Belkić, Dž., 2001, J. Comput. Methods Sci. Eng. **1**, 1.

Belkić, Dž., 2004, *Principles of Quantum Scattering Theory* (Institute of Physics, Bristol).

Belkić, Dž., 2005, *Quantum-Mechanical Signal Processing and Spectral Analysis* (Institute of Physics, Bristol).

Belkić, Dž., 2007, *Quantum Theory of High-Energy Ion-Atom Collisions* (Taylor & Francis, London).

Belkić, Dž., and R. Gayet, 1977, J. Phys. B **10**, 1923.

Belkić, Dž., R. Gayet, J. Hanssen, I. Mančev, and A. Nuñez, 1997, Phys. Rev. A **56**, 3675.

Belkić, Dž., R. Gayet, J. Hanssen, and A. Salin, 1986, J. Phys. B **19**, 2945.

Belkić, Dž., R. Gayet, and A. Salin, 1979, Phys. Rep. **56**, 279.

Belkić, Dž., and R. Janev, 1973, J. Phys. B **6**, 1020.

Belkić, Dž., and I. Mančev, 1990, Phys. Scr. **42**, 285.

Belkić, Dž., and I. Mančev, 1992, Phys. Scr. **45**, 35.

Belkić, Dž., and I. Mančev, 1993, Phys. Scr. **46**, 18.

Belkić, Dž., I. Mančev, and V. Mergel, 1997a, Phys. Rev. A **55**, 378.

Belkić, Dž., I. Mančev, and V. Mergel, 1997b, Hyperfine Interact. **108**, 141.

Belkić, Dž., I. Mančev, and M. Mudrinić, 1994, Phys. Rev. A **49**, 3646.

Belkić, Dž., and A. Salin, 1978, J. Phys. B **11**, 3905.

Belkić, Dž., and H. Taylor, 1987, Phys. Rev. A **35**, 1991.

Belkić, Dž., and H. Taylor, 1989, Phys. Rev. A **39**, 6134.

Belkić, Dž., H. Taylor, and S. Saini, 1986, Z. Phys. D: At., Mol. Clusters **3**, 59.

Belkić, Dž., H. Taylor, and S. Saini, 1987, Phys. Rev. A **36**, 1601.

Berkner, K., S. Kaplan, G. Paulikas, and R. Pyle, 1965, Phys. Rev. **140**, A729.

Bethe, H., and E. Salpeter, 1977, *Quantum Mechanics of One- and Two Electron Atoms* (Plenum, New York).

Bhattacharyya, S., K. Rinn, E. Salzborn, and L. Chatterjee, 1988, J. Phys. B **21**, 111.

Bhatia, A. K., and A. Temkin, 1975, Phys. Rev. A **11**, 2018.

Biswas, S., K. Bhadra, and D. Basu, 1977, Phys. Rev. A **15**, 1900.

Bordenave-Montesquieu, A., A. Gleizes, and P. Benoit-Cattin, 1982, Phys. Rev. A **25**, 245.

Brandt, D., 1983, Phys. Rev. A **27**, 1314.

Bransden, B. H., and D. P. Dewangan, 1988, Adv. At. Mol. Phys. **25**, 343.

Bransden, B. H., and M. R. C. McDowell, 1992, *Charge Exchange and the Theory of Ion-Atom Collisions* (Clarendon Press, Oxford).

Bransden, B. H., and C. J. Joachain, 2003, *Physics of Atoms and Molecules*, 2nd ed. (Prentice Hall, New York).

Brauner, M., J. S. Briggs, and H. Klar, 1989, J. Phys. B **22**, 2265.

Briggs, J., and K. Taulbjerg, 1979, J. Phys. B **12**, 2565.

Bross, S. W., S. Bonham, A. Gaus, J. Peacher, T. Vajnai, M. Schulz, and H. Schmidt-Böcking, 1994, Phys. Rev. A **50**, 337.

Busnengo, H. F., A. Martínez, and R. Rivarola, 1995, Phys. Scr. **51**, 190.

Busnengo, H. F., A. Martínez, and R. Rivarola, 1996, J. Phys. B **29**, 4193.

Byron, F. W., and C. J. Joachain, 1966, Phys. Rev. Lett. **16**, 1139.

Cheshire, I. M., 1964, Proc. Phys. Soc. London **84**, 89.

Ciappina, M. F., W. R. Cravero, and C. R. Garibotti, 2003, J. Phys. B **36**, 3775.

Clementi, E., and C. Roetti, 1974, At. Data Nucl. Data Tables **14**, 177.

Crothers, D. S. F., 1982, J. Phys. B **15**, 2061.

Crothers, D. S. F., and L. J. Dubé, 1993, Adv. At., Mol., Opt. Phys. **30**, 287.

Crothers, D. S. F., and K. M. Dunseath, 1987, J. Phys. B **20**, 4115.

Crothers, D. S. F., and J. F. McCann, 1983, J. Phys. B **16**, 3229.
Crothers, D. S. F., and R. McCarroll, 1987, J. Phys. B **20**, 2835.
Decker, F., and J. Eichler, 1989a, Phys. Rev. A **39**, 1530.
Decker, F., and J. Eichler, 1989b, J. Phys. B **22**, L95.
de Castro Faria, N., F. Freire, and A. G. Pinho, 1988, Phys. Rev. A **37**, 280.
Deco, G., and N. Grün, 1991, Z. Phys. D: At., Mol. Clusters **18**, 339.
Deco, G., J. Maidagan, O. Fojón, and R. Rivarola, 1995, Phys. Scr. **51**, 334.
Dewangan, D., and J. Eichler, 1986, J. Phys. B **19**, 2939.
Dewangan, D., and J. Eichler, 1994, Phys. Rep. **247**, 59.
Dodd, L. R., and K. R. Greider, 1966, Phys. Rev. **146**, 675.
Dollard, J. D., 1963, Ph.D. thesis (University of Michigan).
Dollard, J. D., 1964, J. Math. Phys. **5**, 729.
Dörner, R., 2005, private communication.
Dörner, R., V. Mergel, O. Jagutzki, L. Spielberger, J. Ullrich, R. Moshammer, and H. Schmidt-Böcking, 2000, Phys. Rep. **330**, 95.
Dörner, R., V. Mergel, L. Spielberger, O. Jagutzki, H. Schmidt-Böcking, and J. Ullrich, 1998, Phys. Rev. A **57**, 312.
Drake, G., 1988, Nucl. Instrum. Methods Phys. Res. B **31**, 7.
Dubé, L. J., 1983, J. Phys. B **16**, 1783.
DuBois, R. D., 1987, Phys. Rev. A **36**, 2585.
DuBois, R. D., 1989, Phys. Rev. A **39**, 4440.
Dunseath, K. M., and D. S. F. Crothers, 1991, J. Phys. B **24**, 5003.
Fainstein, P., V. Ponce, and R. Rivarola, 1987, Phys. Rev. A **36**, 3639.
Fainstein, P., V. Ponce, and R. Rivarola, 1988, J. Phys. B **21**, 2989.
Fano, U., 1961, Phys. Rev. **124**, 1866.
Feagin, J. M., J. S. Briggs, and T. M. Reeves, 1984, J. Phys. B **17**, 1057.
Feshbach, H., 1962, Ann. Phys. (N.Y.) **19**, 287.
Fischer, D., K. Stochkel, H. Cederquist, H. Zettergren, P. Reinhed, R. Schuch, A. Kallberg, A. Simonsson, and H. T. Schmidt, 2006, Phys. Rev. A **73**, 052713.
Fogel, Ya. M., R. V. Mitin, V. Kozlov, and N. S. Romashko, 1958, Zh. Eksp. Teor. Fiz. **35**, 565 [Sov. Phys. JETP **8**, 390 (1959)].
Ford, A., J. Reading, and R. Becker, 1982, J. Phys. B **15**, 3257.
Forest, J. L., J. A. Tanis, S. M. Ferguson, R. R. Haar, K. Lifrieri, and V. L. Plano, 1995, Phys. Rev. A **52**, 350.
Fregenal, D., J. Fiol, G. Bernardi, S. Suárez, P. Focke, A. González, A. Muthig, T. Jalowy, K. Groeneveld, and H. Luna, 2000, Phys. Rev. A **62**, 012703.
Galassi, M., P. Abufager, A. Martínez, R. Rivarola, and P. D. Fainstein, 2002, J. Phys. B **35**, 1727.
Garibotti, C. R., and J. E. Miraglia, 1980, Phys. Rev. A **21**, 572.
Gayet, R., 1972, J. Phys. B **5**, 483.
Gayet, R., 1989, J. Phys. (Paris), Colloq. **50**, C1-53.
Gayet, R., and J. Hanssen, 1992, J. Phys. B **25**, 825.
Gayet, R. and J. Hanssen, 1994, Nucl. Instrum. Methods Phys. Res. B **86**, 52.
Gayet, R., R. Janev, and A. Salin, 1973, J. Phys. B **6**, 993.
Gayet, R., J. Hanssen, and L. Jacqui, 1995, J. Phys. B **28**, 2193 [J. Phys. B **30**, 1619 (1997) (corrigenda)].
Gayet, R., J. Hanssen, L. Jacqui, A. Martínez, and R. Rivarola, 1996, Phys. Scr. **53**, 549.
Gayet, R., J. Hanssen, L. Jacqui, and M. Ourdane, 1997, J. Phys. B **30**, 2209.
Gayet, R., J. Hanssen, A. Martínez, and R. Rivarola, 1991, Z. Phys. D: At., Mol. Clusters **18**, 345.
Gayet, R., J. Hanssen, A. Martínez, and R. Rivarola, 1994a, Nucl. Instrum. Methods Phys. Res. B **86**, 158.
Gayet, R., J. Hanssen, A. Martínez, and R. Rivarola, 1994b, Comments At. Mol. Phys. **30**, 231.
Gayet, R., R. Rivarola, and A. Salin, 1981, J. Phys. B **14**, 2421.
Gayet, R., and A. Salin, 1987, J. Phys. B **20**, L571.
Gerasimenko, V., 1961, Zh. Eksp. Teor. Fiz. **41**, 1104 [Sov. Phys. JETP **14**, 789 (1962)].
Ghosh, M., C. Mandal, and S. Mukharjee, 1985, J. Phys. B **18**, 3797.
Ghosh, M., C. Mandal, and S. Mukharjee, 1987, Phys. Rev. A **35**, 5259.
Godunov, A., C. Whelan, and H. Walters, 2004, J. Phys. B **37**, L201.
Godunov, A., C. Whelan, H. Walters, V. Schipakov, M. Schöffler, V. Mergel, R. Dörner, O. Jagutzki, L. Schmidt, J. Titze, and H. Schmidt-Böcking, 2005, Phys. Rev. A **71**, 052712.
Gravielle, M. S., and J. Miraglia, 1992, Phys. Rev. A **45**, 2965.
Gravielle, M. S., and J. Miraglia, 1995, Phys. Rev. A **51**, 2131.
Green, L., M. Mulder, M. Lewis, and J. Woll, 1954, Phys. Rev. **93**, 757.
Green, A. E., D. Sellin, and A. Zachor, 1969, Phys. Rev. **184**, 1.
Greider, K., and L. R. Dodd, 1966, Phys. Rev. **146**, 671.
Gulyás, L., and Gy. Szabo, 1994, Z. Phys. D: At., Mol. Clusters **29**, 115.
Gulyás, L., and P. D. Fainstein, 1998, J. Phys. B **31**, 3297.
Hahn, Y., 1989, Phys. Rev. A **40**, 2950.
Hahn, Y., and H. Ramadan, 1989, Phys. Rev. A **40**, 6206.
Hansteen, J. M., and O. Mosebekk, 1972, Phys. Rev. Lett. **29**, 1361.
Herman, F., and S. Skillman, 1963, *Atomic Structure Calculations* (Prentice-Hall, Englewood Cliffs, NJ).
Hippler, R., S. Datz, P. Miller, P. Pepmiller, and P. Dittner, 1987, Phys. Rev. A **35**, 585.
Horsdal-Pedersen, E., C. Cocke, and M. Stockli, 1983, Phys. Rev. Lett. **50**, 1910.
Horsdal-Pedersen, E., B. Jensen, and K. Nielsen, 1986, Phys. Rev. Lett. **57**, 1414.
Huzinaga, S., 1961, Phys. Rev. **122**, 131.
Hvelplund, P., and A., Andersen, 1982, Phys. Scr. **26**, 375.
Hvelplund, P., J. Heinemeier, E. Horsdal-Pedersen, and F. Simpson, 1976, J. Phys. B **9**, 491.
Hylleraas, E., 1929, Z. Phys. **54**, 347.
Itoh, A., M. Asari, and F. Fukuzawa, 1980, J. Phys. Soc. Jpn. **48**, 943.
Itoh, A., T. Zouros, D. Schneider, U. Stettner, W. Zeitz, and N. Stolterfoht, 1985, J. Phys. B **18**, 4581.
Jain, A., R. Shingal, and T. Zouros, 1991, Phys. Rev. A **43**, 1621.
Joachain, C. J., and R. Vanderpoorten, 1970, Physica (Amsterdam) **46**, 333.
Joachain, C. J., and M. Terao, 1991, private communication.
Justiniano, E., R. Schuch, M. Schulz, S. Reusch, P. Mokler, D. McLaughlin, and Y. Hahn, 1987, in *Proceedings of the XVth International Conference on the Physics of Electronic and Atomic Collisions, Brighton*, edited by H. B. Gilbody *et al.* (North-Holland, Amsterdam), p. 477.
Landau, L., and E. Lifshitz, 1977, *Quantum Mechanics*, 3rd ed. (Pergamon, London).
Lin, C. D., 1979, Phys. Rev. A **19**, 1510.
Loftager, P., 2002, private communication.
Löwdin, P., 1953, Phys. Rev. **90**, 120.

Macías, A., F. Martín, A. Riera, and N. Yáñez, 1988, Int. J. Quantum Chem. **33**, 279.
Mančev, I., 1995, Phys. Scr. **51**, 762.
Mančev, I., 1996, Phys. Rev. A **54**, 423.
Mančev, I., 1999a, Phys. Rev. A **60**, 351.
Mančev, I., 1999b, Nucl. Instrum. Methods Phys. Res. B **154**, 291.
Mančev, I., 2001, Phys. Rev. A **64**, 012708.
Mančev, I., 2003, J. Phys. B **36**, 93.
Mančev, I., 2005a, J. Comput. Methods Sci. Eng. **5**, 73.
Mančev, I., 2005b, Europhys. Lett. **69**, 200.
Mančev, I., 2007, Phys. Rev. A **75**, 052716.
Mančev, I., V. Mergel, and L. Schmidt, 2003, J. Phys. B **36**, 2733.
Mapleton, R., 1960, Phys. Rev. **117**, 479.
Mapleton, R., 1965, Proc. Phys. Soc. London **85**, 841.
Martin, P. J., K. Arnett, D. Blankenship, T. Kvale, J. Peacher, I. Redd, V. Sutcliffe, J. T. Park, C. D. Lin, and J. McGuire, 1981, Phys. Rev. A **23**, 2858.
Martínez, A., R. Gayet, J. Hanssen, and R. Rivarola, 1994, J. Phys. B **27**, L375.
Martínez, A., H. Busnengo, R. Gayet, J. Hanssen, and R. Rivarola, 1997, Nucl. Instrum. Methods Phys. Res. B **132**, 344.
Martínez, A., R. Rivarola, R. Gayet, and J. Hanssen, 1999, Phys. Scr. **T80**, 124.
McCarroll, R., and A. Salin, 1967, Proc. Phys. Soc. London **90**, 63.
McCartney, M., 1997, J. Phys. B **30**, L155.
McClure, G., 1968, Phys. Rev. **166**, 22.
McDaniel, E., M. Flannery, H. Ellis, F. Eisele, and W. Pope, 1977, U.S. Army Missile Research and Development Command Technical Report, No. H, **1**, 78.
McGuire, J., 1987, Phys. Rev. A **36**, 1114.
McGuire, J., 1992, Adv. At., Mol., Opt. Phys. **29**, 217.
McGuire, J., 1997, *Electron Correlation Dynamics in Atomic Collisions* (Cambridge University Press, Cambridge, England).
McGuire, J. H., and L. Weaver, 1977, Phys. Rev. A **16**, 41.
McLaughlin, D. J., and Y. Hahn, 1982, Phys. Lett. **88**, 394.
Melchert, F., S. Krüdener, K. Huber, and E. Salzborn, 1999, J. Phys. B **39**, L139.
Mergel, V., R. Dörner, M. Achler, Kh. Khayyat, S. Lencinas, J. Euler, O. Jagutzki, S. Nüttgens, M. Unverzagt, L. Spielberger, W. Wu, R. Ali, J. Ullrich, H. Cederquist, A. Salin, C. Wood, R. Olson, Dž. Belkić, C. Cocke, and H. Schmidt-Böcking, 1997, Phys. Rev. Lett. **79**, 387.
Mergel, V., R. Dörner, Kh. Khayyat, M. Achler, T. Weber, O. Jagutzki, H. Lüdde, C. Cocke, and H. Schmidt-Böcking, 2001, Phys. Rev. Lett. **86**, 2257.
Mergel, V., R. Dörner, J. Ullrich, O. Jagutzki, S. Lencinas, S. Nüttgens, L. Spielberger, M. Unverzagt, C. Cocke, R. Olson, M. Schulz, U. Buck, E. Zanger, W. Theisinger, M. Isser, S. Geis, and H. Schmidt-Böcking, 1995, Phys. Rev. Lett. **74**, 2200.
Mukherjee, S. C., K. Roy, and N. Sil, 1973, J. Phys. B **6**, 467.
Nath, B., and C. Sinha, 2000, Phys. Rev. A **61**, 062705.
Nordsieck, A., 1954, Phys. Rev. **93**, 785.
Olson, R. E., 1982, J. Phys. B **15**, L163.
Olson, R. E., A. Salop, R. Phaneuf, and F. Mayer, 1977, Phys. Rev. A **16**, 1867.
Olson, R. E., A. Wetmore, and M. McKenzie, 1986, J. Phys. B **19**, L629.
Oppenheimer, J. R., 1928, Phys. Rev. **31**, 349.
Ourdane, M., H. Bachau, R. Gayet, and J. Hanssen, 1999, J. Phys. B **32**, 2041.
Pálinkás, J., R. Schuch, H. Cederquist, and O. Gustafsson, 1989, Phys. Rev. Lett. **63**, 2464.
Pálinkás, J., R. Schuch, H. Cederquist, and O. Gustafsson, 1990, Phys. Scr. **42**, 175.
Peart, B., D. Walton, and K. Dolder, 1970, J. Phys. B **3**, 1346.
Pedlow, R. T., S. F. C. O'Rourke, and D. S. F. Crothers, 2005, Phys. Rev. A **72**, 062719.
Pivovar, L. I., V. M. Tubaev, and M. T. Novikov, 1961, Zh. Eksp. Teor. Fiz. **41**, 26 [Sov. Phys. JETP **14**, 20 (1962)].
Pivovar, L. I., M. T. Novikov, and V. M. Tubaev, 1962, Zh. Eksp. Teor. Fiz. **42**, 1490 [Sov. Phys. JETP **15**, 1035 (1962)].
Pluvinage, P., 1950, Ann. Phys. (Paris) **5**, 145.
Popov, Yu., O. Chuluunbaatar, S. I. Vinitsky, L. Ancarani, C. Dal Cappello, and P. S. Vinitsky, 2002, J. Exp. Theor. Phys. **95**, 620.
Press, W., S. Teukolsky, W. Vetterling, and B. Flannery, 1992, *Numerical Recipes in Fortran 77: The Art of Scientific Computing* (Cambridge University Press, Cambridge, England), Vol. 1.
Prudnikov, A. P., Yu. Britchkov, and O. Marietchev, 1981, *Integrals and Series* (Nauka, Moscow), Vol. 1.
Purkait, M., S. Sounda, A. Dhara, and C. Mandal, 2006, Phys. Rev. A **74**, 042723.
Rodriguez, K. V., and G. Gasaneo, 2005, J. Phys. B **38**, L259.
Roothaan, C. C. J., 1951, Rev. Mod. Phys. **23**, 69.
Roothaan, C. C. J., 1960, Rev. Mod. Phys. **32**, 179.
Rudd, M. E., R. D. DuBois, L. H. Toburen, C. Ratcliffe, and T. Goffe, 1983, Phys. Rev. A **28**, 3244.
Saha, G., S. Datta, and S. Mukherjee, 1985, Phys. Rev. A **31**, 3633.
Sarkadi, L., L. Lugosi, K. Tökési, L. Gulyás, and Á. Kövér, 2001, J. Phys. B **34**, 4901.
Schmidt, H. T., A. Fardi, J. Jensen, P. Reinhed, R. Schuch, K. Støchkel, H. Zettergren, H. Cederquist, and C. Cocke, 2005, Nucl. Instrum. Methods Phys. Res. B **233**, 43.
Schmidt, H. T., A. Fardi, R. Schuch, S. Schwartz, H. Zettergren, H. Cederquist, L. Bagge, H. Danared, A. Källberg, J. Jensen, K. Rensfelt, V. Mergel, L. Schmidt, C. Cocke, and H. Schmidt-Böcking, 2002, Phys. Rev. Lett. **89**, 163201.
Schmidt, H. T., J. Jensen, P. Reinhed, R. Schuch, K. Støchkel, H. Zettergren, H. Cederquist, L. Bagge, H. Danared, A. Källberg, H. Schmidt-Böcking, and L. Cocke, 2005, Phys. Rev. A **72**, 012713.
Schmidt-Böcking, H., V. Mergel, R. Dörner, C. Cocke, O. Jagutzki, L. Schmidt, T. Weber, H. Lüdde, E. Weigold, J. Barakdar, H. Cederquist, H. Schmidt, R. Schuch, and A. S. Kheifets, 2003, Europhys. Lett. **62**, 477.
Schmidt-Böcking, H., V. Mergel, L. Schmidt, R. Dörner, O. Jagutzki, K. Ullmann, T. Weber, H. Lüdde, E. Weigold, and A. Kheifets, 2003, Radiat. Phys. Chem. **68**, 41.
Schmidt-Böcking, H., M. Schöffler, T. Janke, A. Czasch, V. Mergel, L. Schmidt, R. Dörner, O. Jagutzki, M. Hattass, T. Weber, E. Weigold, H. T. Schmidt, R. Schuch, H. Cederquist, Y. Demkov, C. Whelan, A. Godunov, and J. Walters, 2005, Nucl. Instrum. Methods Phys. Res. B **233**, 3.
Schöffler, M., A. Godunov, C. Whelan, H. Walters, V. Schipakov, V. Mergel, R. Dörner, O. Jagutzki, L. Schmidt, J. Titze, E. Weigold, and H. Schmidt-Böcking, 2005, J. Phys. B **38**, L123.
Schryber, U., 1967, Helv. Phys. Acta **40**, 1023.
Schuch, R., E. Justiniano, H. Vogt, G. Deco, and N. Grün,

1991, J. Phys. B **24**, L133.
Schulz, M., E. Justiniano, R. Schuch, P. Mokler, and S. Reusch, 1987, Phys. Rev. Lett. **58**, 1734.
Schwab, W., G. Baptista, E. Justiniano, R. Schuch, H. Vogt, and E. Weber, 1987, J. Phys. B **20**, 2825.
Sewell, E. C., G. Angel, K. Dunn, and H. Gilbody, 1980, J. Phys. B **13**, 2269.
Shah, M. B., and H. Gilbody, 1985, J. Phys. B **18**, 899.
Shah, M. B., and H. B. Gilbody, 1995, private communication.
Shah, M. B., P. McCallion, and H. Gilbody, 1989, J. Phys. B **22**, 3037.
Shingal, R., and C. D. Lin, 1991, J. Phys. B **24**, 251.
Shi, T. Y., and C. D. Lin, 2002, Phys. Rev. Lett. **89**, 163202.
Sidorovich, V., V. Nikolaev, and J. McGuire, 1985, Phys. Rev. A **31**, 2193.
Silverman, J., O. Platas, and F. A. Matsen, 1960, J. Chem. Phys. **32**, 1402.
Stolterfoht, N., 1990, Phys. Scr. **42**, 192.
Stolterfoht, N., 1993, Phys. Rev. A **48**, 2980.
Suzuki, H., Y. Kajikawa, N. Toshima, H. Ryufuku, and T. Watanabe, 1984, Phys. Rev. A **29**, 525.
Tanis, J., 1987, Nucl. Instrum. Methods Phys. Res. A **262**, 52.
Tanis, J., E. Bernstein, W. Graham, M. Clark, S. Shafroth, B. Johnson, K. Jones, and M. Meron, 1982, Phys. Rev. Lett. **49**, 1325.
Tanner, G., K. Richter, and J. M. Rost, 2000, Rev. Mod. Phys. **72**, 497.
Theisen, T., and J. H. McGuire, 1979, Phys. Rev. A **20**, 1406.
Thomas, L., 1927, Proc. R. Soc. London, Ser. A **114**, 561.
Toburen, L. H., and M. Y. Nakai, 1969, Phys. Rev. **177**, 191.
Tolmanov, S. G., and J. McGuire, 2000, Phys. Rev. A **62**, 032711.
Toshima, N., and A. Igarashi, 1992, Phys. Rev. A **45**, 6313.
Tweed, R. J., 1972, J. Phys. B **5**, 810.
van der Straten, P., and R. Morgenstern, 1986, J. Phys. B **19**, 1361.
Vinitsky, P. S., Yu. Popov, and O. Chuluunbaatar, 2005, Phys. Rev. A **71**, 012706.
Welsh, L. M., K. Berkner, S. Kaplan, and R. Pyle, 1967, Phys. Rev. **158**, 85.
Wetmore, A. E., and R. Olson, 1988, Phys. Rev. A **38**, 5563.
Williams, J. F., 1966, Phys. Rev. **150**, 7.
Williams, J. F., 1967, Phys. Rev. **157**, 97.
Winter, T., 1991, Phys. Rev. A **44**, 4353.
Woitke, O., P. Závodszky, S. Ferguson, J. Houck, and J. Tanis, 1998, Phys. Rev. A **57**, 2692.
Zerarka, A., 1997, Phys. Rev. A **55**, 1976.
Zouros, T., D. Schneider, and N. Stolterfoht, 1988, J. Phys. B **21**, L671.